RILEM State-of-the-Art Reports

Manfred N. Partl
Laurent Porot
Hervé Di Benedetto
Francesco Canestrari
Paul Marsac
Gabriele Tebaldi *Editors*

Testing and Characterization of Sustainable Innovative Bituminous Materials and Systems

State-of-the-Art Report of the RILEM Technical Committee 237-SIB

Springer

RILEM State-of-the-Art Reports

RILEM STATE-OF-THE-ART REPORTS
Volume 24

RILEM, The International Union of Laboratories and Experts in Construction Materials, Systems and Structures, founded in 1947, is a non-governmental scientific association whose goal is to contribute to progress in the construction sciences, techniques and industries, essentially by means of the communication it fosters between research and practice. RILEM's focus is on construction materials and their use in building and civil engineering structures, covering all phases of the building process from manufacture to use and recycling of materials. More information on RILEM and its previous publications can be found on www.RILEM.net.

The RILEM State-of-the-Art Reports (STAR) are produced by the Technical Committees. They represent one of the most important outputs that RILEM generates – high level scientific and engineering reports that provide cutting edge knowledge in a given field. The work of the TCs is one of RILEM's key functions.

Members of a TC are experts in their field and give their time freely to share their expertise. As a result, the broader scientific community benefits greatly from RILEM's activities.

RILEM's stated objective is to disseminate this information as widely as possible to the scientific community. RILEM therefore considers the STAR reports of its TCs as of highest importance, and encourages their publication whenever possible.

The information in this and similar reports is mostly pre-normative in the sense that it provides the underlying scientific fundamentals on which standards and codes of practice are based. Without such a solid scientific basis, construction practice will be less than efficient or economical.

It is RILEM's hope that this information will be of wide use to the scientific community.

More information about this series at http://www.springer.com/series/8780

Manfred N. Partl · Laurent Porot
Hervé Di Benedetto · Francesco Canestrari
Paul Marsac · Gabriele Tebaldi
Editors

Testing and Characterization of Sustainable Innovative Bituminous Materials and Systems

State-of-the-Art Report of the RILEM Technical Committee 237-SIB

Springer

Editors
Manfred N. Partl
Road Engineering/Sealing Components
Empa
Dübendorf
Switzerland

Laurent Porot
Arizona Chemical
Almere
The Netherlands

Hervé Di Benedetto
Génie Civil et Bâtiment
University of Lyon
Vaulx-en-Velin, Lyon
France

Francesco Canestrari
Dipartimento ICEA
Università Politecnica delle Marche
Ancona
Italy

Paul Marsac
IFSTTAR
Bouguenais
France

Gabriele Tebaldi
Department of Civil & Environmental Engineering and Architecture
University of Parma
Parma
Italy

ISSN 2213-204X ISSN 2213-2031 (electronic)
RILEM State-of-the-Art Reports
ISBN 978-3-319-71022-8 ISBN 978-3-319-71023-5 (eBook)
https://doi.org/10.1007/978-3-319-71023-5

Library of Congress Control Number: 2017959159

Printed on acid-free paper

This Springer imprint is published by Springer Nature
The registered company is Springer International Publishing AG
The registered company address is: Gewerbestrasse 11, 6330 Cham, Switzerland

Preface

The *International Union for Testing and Research Laboratories for Materials testing and Structures* (Rilem) has supported the development and application of bituminous pavement materials over decades with different Technical Committees (TCs) working on specific material-related questions regarding characterization and performance testing of bituminous binders, mixtures, and pavement structures.

The first TC on bituminous materials is reported back to the 60s of the last century. About 20 years later, it became clear that the subject was too complex and fascinating for being treated by only one expert group and two major parallel follow-up lines for successive TCs emerged. The first one was basically dealing with testing and characterization of bituminous materials under the aspect of time–temperature-dependent properties and the great variety of bituminous binders and mixtures; the second line of TCs was driven by the phenomena of crack formation in bituminous pavements. Yet, it took another 20 years until the creation of even more parallel working TCs started which is why we are now in the situation of having four to five TCs dealing with materials, tendency increasing.

Main objective of all these TCs was and still is the fundamental improvement and comparison of test methods in the sense of pre-standardization together with the elaboration of tools and recommendations for meaningful characterization and quality assessment of asphalt pavement materials. This objective also calls for advanced chemo-physical understanding of material behavior and pavement systems based on fundamental material properties and suitable models for describing and predicting the intrinsic mechanisms that determine the material behavior not only under idealized laboratory conditions but also under complex performance-related situations, e.g., when testing whole structures or subsystems of pavements with full scale, accelerated loading and real 1:1 field setups.

This report presents in detail the results of the activities of five task groups of the RILEM TC 237-SIB on *Testing and Characterization of Sustainable Innovative Bituminous Materials and Systems,* which has been installed in autumn 2010. It concentrates on specific new topics in asphalt binder and mixture testing based on previous TC work and on accomplishing some interlaboratory activities that were initiated by the earlier TC 206-ATB on *Advanced Testing and Characterization of*

Bituminous Materials. It deals with new developments in asphalt testing, in particular also in view of new innovative bituminous materials, such as hot and cold recycled mixtures, grid-reinforced pavements, and recycled Reclaimed Asphalt Pavements (RAP), where test methods developed for traditional asphalt concrete are not a priori applicable. The TC 237-SIB (Chair: Manfred N. Partl, EMPA, Switzerland; Secretary, Emmanuel Chailleux, IFSTTAR, France) relied on more than 60 members from 20 countries who were involved in Task Groups with the following goals:

Binders

(Convenor: Dariusz Sybilski, IBDIM Poland, followed by Laurent Porot, Arizona Chemical, The Netherlands):
Evaluate binder properties with respect to durability, relevant to distress accumulation performance and application, such as moisture-induced stripping. It focuses on polymer-modified binders and other new binders primarily with respect to adhesion, i.e., the interaction between binder and aggregates.

Mechanical Testing of Mixtures

(Convenor: Herve Di Benedetto, ENTPE, France):
Study three-dimensional linear viscoelastic cyclic behavior of asphalt mixtures considering the Poisson's ratio which is a complex viscoelastic parameter that is important to be determined experimentally.

Pavement Multilayer System Testing

(Convenor: Francesco Canestrari, Univ. Politecnica delle Marche, Italy):
Consolidate research done by TC 206 ATB on the evaluation of geogrids in asphalt pavement, also performing new work on interface testing and characterization taking into account different material configurations.

Recycling

(Convenor: Paul Marsac, IFSTTAR, France):
Evaluate test and mix design methods for the use of materials with bituminous materials from the road, also include methodologies to reproduce Reclaimed Asphalt Pavement (RAP) in the lab by comparing accelerated aging procedures as initiated in TC 206-ATB.

Cold Recycling

(Convenor: Gabriele Tebaldi, Univ. Parma, Italy):
Evaluate test and mix design methods for the use of materials with RAP from the road, focusing on cold mix recycling in case of high % RAP with emulsion and with foam bitumen, by proposing guidelines on how to characterize and define RAP in order to conduct comparable interlaboratory tests on evaluation and test methods for cold recycling mixtures.

Due to the fact that all work performed within this TC 237-SIB was conducted as purely voluntary work by its members, driven by their individual interest in the subject and their understanding that open discussion between experts with different

point of views is mandatory for making both reasonable progress and sustainable impact to the technical community, it was clear from the very beginning that not all goals could be achieved as originally expected at the beginning of the TC.

Nevertheless, it is hoped that the book at hand will be a valuable source for experts, practitioners, researchers, road authorities, and students to handle the challenges and opportunities that new sustainable bituminous materials may offer not only now but also in the future.

Rilem Members of TC 237-SIB 2010–2017 (Fluctuating over the years):

Gordon Airey (UK), Alex Apeagyei (UK), Ignacio Artamendi (UK), Hassan Baaj (Canada), Hussain U. Bahia (USA), Wojciech Bankowski (Poland), Davide Broere (The Netherlands), Yves Brosseaud (France), Willam G. Buttlar (USA), Francesco Canestrari (Italy), Armelle Chabot (France), Emmanuel Chailleux (France), Eshan Dave (USA), Joëlle De Visscher, (Belgium), Hervé Di Benedetto (France), Tomas Gabet (France), Marcin Gajewski (Poland), Vincent Gaudefroy (France), Gilda Ferrotti (Italy),William Grady (The Netherlands), Andrea Graziani (Italy), James Grenfell (UK), Ferhat Hammoum (France), Bernhard Hofko (Austria), Martin Hugener (Switzerland), Illan Ishai (Israel), Nicole Kringos (Sweden), Greet A. Leegwater (The Netherlands), Eyal Levenberg (Israel), Andreas Loizos (Greece), Xiaohu Lu (Sweden), Paul Marsac (France), Anne Millien (France), Konrad Mollenhauer (Germany), Francisco Morea (Argentina), Virginie Mouillet (France), Patrick Muraya (Norway), Manfred N. Partl (Switzerland), Daniel Perraton (Canada), Christophe Petit (France), Katherine Petros (USA), Laurent Porot (The Netherlands), Simon Pouget (France), Lily D. Poulikakos (Switzerland), Christiane Raab (Switzerland), Safwat Said (Sweden), Cesare Sangiorgi (Italy), Cédric Sauzéat (France), Tom Scarpas (The Netherlands), Hilde Soenen (Belgium), Dariusz Sybilsky (Poland), Gabriele Tebaldi (Italy), Ann Vanelstraete (Belgium), Michael Wistuba (Germany), Ludo Zanzotto (Canada), and Adam Zofka (Poland).

Dübendorf, Switzerland — Manfred N. Partl
Almere, The Netherlands — Laurent Porot
Vaulx-en-Velin, Lyon, France — Hervé di Benedetto
Ancona, Italy — Francesco Canestrari
Bouguenais, France — Paul Marsac
Parma, Italy — Gabriele Tebaldi

Acknowledgements

In order to compose this book and the huge data set behind it, many experts and laboratories provided their valuable input either through data analysis or performing tests at their own expense. This extensive voluntary work by technical, industrial, and academic experts from all over the world deserves acknowledgement and recognition.

As for the different task groups, the following individuals were active as members or as experts and deserve recognition for their immense contribution and devotion:

Binders

(Convenor: Dariusz Sybilski, IBDIM Poland, followed by Laurent Porot, Arizona Chemical, The Netherlands):

Apeagyei, A., Artamendi, I., Barcelo Martinez, F., Besamusca, J., Canestrari, F., Chailleux, E., Chaturabong, P., Gaudefroy, V., Grenfell, J., Hauser, E., Partl, M. N., Porot, L., Said, S., Soenen, H., Sybilski, D., Tozzo, C., Vansteenkiste, S., and Wistuba, M.

Mechanical Testing of Mixtures

(Convenor: Herve Di Benedetto, ENTPE, France):

Cannone Falchetto, A., Di Benedetto, H., Graziani, A., Grenfell, J., Hofko, B., Nguyen, Q.T., Perraton, Petit, C. D., Pouget, S., Poulikakos, L. D., Sauzéat, C., Tapsoba, N., and Wistuba, M.

Pavement Multilayer System Testing

(Convenor: Francesco Canestrari, Univ. Politecnica delle Marche, Italy):

Canestrari, F., D'Andrea, A., Ferrotti, G., Graziani, A., Partl, M. N., Petit, C., Raab, C., and Sangiorgi, C.

Recycling

(Convenor: Paul Marsac, IFSTTAR, France):

Farcas, F., Gabet, T., Grenfell, J., Marsac, P., Mouillet, V., Perez Martinez, M., Piérard, N., Porot, L., and Van den Bergh, W.

Cold Recycling

(Convenor: Gabriele Tebaldi, Univ. Parma, Italy):

Apeagyei, A., Bocci, M., Cannone Falchetto, A., Dave, E.V., Grenfell, J., Grilli, A., Hugener, M., Jenkins, K., Loizos, A., Lo Presti, D., Muraya, P., Pasetto, M., Perraton, D., and Tebaldi, G.

The different laboratories that took part in the interlaboratory tests will be mentioned in the individual chapters of this report and are here globally acknowledged. Without their help and determination, the work of this TC would not have been possible.

Finally, the authors and editors are grateful to the RILEM General Secretary Pascale Ducornet with her assistant Anne Griffoin who were both very supportive in getting the book printed by Springer.

RILEM Publications

The following list is presenting the global offer of RILEM Publications, sorted by series. Each publication is available in printed version and/or in online version.

RILEM Proceedings (PRO)

PRO 1: Durability of High Performance Concrete (ISBN: 2-912143-03-9; e-ISBN: 2-351580-12-5; e-ISBN: 2351580125); *Ed. H. Sommer*

PRO 2: Chloride Penetration into Concrete (ISBN: 2-912143-00-04; e-ISBN: 2912143454); *Eds. L.-O. Nilsson and J.-P. Ollivier*

PRO 3: Evaluation and Strengthening of Existing Masonry Structures (ISBN: 2-912143-02-0; e-ISBN: 2351580141); *Eds. L. Binda and C. Modena*

PRO 4: Concrete: From Material to Structure (ISBN: 2-912143-04-7; e-ISBN: 2351580206); *Eds. J.-P. Bournazel and Y. Malier*

PRO 5: The Role of Admixtures in High Performance Concrete (ISBN: 2-912143-05-5; e-ISBN: 2351580214); *Eds. J. G. Cabrera and R. Rivera-Villarreal*

PRO 6: High Performance Fiber Reinforced Cement Composites—HPFRCC 3 (ISBN: 2-912143-06-3; e-ISBN: 2351580222); *Eds. H. W. Reinhardt and A. E. Naaman*

PRO 7: 1st International RILEM Symposium on Self-Compacting Concrete (ISBN: 2-912143-09-8; e-ISBN: 2912143721); *Eds. Å. Skarendahl and Ö. Petersson*

PRO 8: International RILEM Symposium on Timber Engineering (ISBN: 2-912143-10-1; e-ISBN: 2351580230); *Ed. L. Boström*

PRO 9: 2nd International RILEM Symposium on Adhesion between Polymers and Concrete ISAP '99 (ISBN: 2-912143-11-X; e-ISBN: 2351580249); *Eds. Y. Ohama and M. Puterman*

PRO 10: 3rd International RILEM Symposium on Durability of Building and Construction Sealants (ISBN: 2-912143-13-6; e-ISBN: 2351580257); *Eds. A. T. Wolf*

PRO 11: 4th International RILEM Conference on Reflective Cracking in Pavements (ISBN: 2-912143-14-4; e-ISBN: 2351580265); *Eds. A. O. Abd El Halim, D. A. Taylor and El H. H. Mohamed*

PRO 12: International RILEM Workshop on Historic Mortars: Characteristics and Tests (ISBN: 2-912143-15-2; e-ISBN: 2351580273); *Eds. P. Bartos, C. Groot and J. J. Hughes*

PRO 13: 2nd International RILEM Symposium on Hydration and Setting (ISBN: 2-912143-16-0; e-ISBN: 2351580281); *Ed. A. Nonat*

PRO 14: Integrated Life-Cycle Design of Materials and Structures - ILCDES 2000 (ISBN: 951-758-408-3; e-ISBN: 235158029X); (ISSN: 0356-9403); *Ed. S. Sarja*

PRO 15: Fifth RILEM Symposium on Fibre-Reinforced Concretes (FRC)—BEFIB'2000 (ISBN: 2-912143-18-7; e-ISBN: 291214373X); *Eds. P. Rossi and G. Chanvillard*

PRO 16: Life Prediction and Management of Concrete Structures (ISBN: 2-912143-19-5; e-ISBN: 2351580303); *Ed. D. Naus*

PRO 17: Shrinkage of Concrete—Shrinkage 2000 (ISBN: 2-912143-20-9; e-ISBN: 2351580311); *Eds. V. Baroghel-Bouny and P.-C. Aïtcin*

PRO 18: Measurement and Interpretation of the On-Site Corrosion Rate (ISBN: 2-912143-21-7; e-ISBN: 235158032X); *Eds. C. Andrade, C. Alonso, J. Fullea, J. Polimon and J. Rodriguez*

PRO 19: Testing and Modelling the Chloride Ingress into Concrete (ISBN: 2-912143-22-5; e-ISBN: 2351580338); *Eds. C. Andrade and J. Kropp*

PRO 20: 1st International RILEM Workshop on Microbial Impacts on Building Materials (CD 02) (e-ISBN 978-2-35158-013-4); *Ed. M. Ribas Silva*

PRO 21: International RILEM Symposium on Connections between Steel and Concrete (ISBN: 2-912143-25-X; e-ISBN: 2351580346); *Ed. R. Eligehausen*

PRO 22: International RILEM Symposium on Joints in Timber Structures (ISBN: 2-912143-28-4; e-ISBN: 2351580354); *Eds. S. Aicher and H.-W. Reinhardt*

PRO 23: International RILEM Conference on Early Age Cracking in Cementitious Systems (ISBN: 2-912143-29-2; e-ISBN: 2351580362); *Eds. K. Kovler and A. Bentur*

PRO 24: 2nd International RILEM Workshop on Frost Resistance of Concrete (ISBN: 2-912143-30-6; e-ISBN: 2351580370); *Eds. M. J. Setzer, R. Auberg and H.-J. Keck*

PRO 25: International RILEM Workshop on Frost Damage in Concrete (ISBN: 2-912143-31-4; e-ISBN: 2351580389); *Eds. D. J. Janssen, M. J. Setzer and M. B. Snyder*

PRO 26: International RILEM Workshop on On-Site Control and Evaluation of Masonry Structures (ISBN: 2-912143-34-9; e-ISBN: 2351580141); *Eds. L. Binda and R. C. de Vekey*

PRO 27: International RILEM Symposium on Building Joint Sealants (CD03; e-ISBN: 235158015X); *Ed. A. T. Wolf*

PRO 28: 6th International RILEM Symposium on Performance Testing and Evaluation of Bituminous Materials—PTEBM'03 (ISBN: 2-912143-35-7; e-ISBN: 978-2-912143-77-8); *Ed. M. N. Partl*

PRO 29: 2nd International RILEM Workshop on Life Prediction and Ageing Management of Concrete Structures (ISBN: 2-912143-36-5; e-ISBN: 2912143780); *Ed. D. J. Naus*

PRO 30: 4th International RILEM Workshop on High Performance Fiber Reinforced Cement Composites—HPFRCC 4 (ISBN: 2-912143-37-3; e-ISBN: 2912143799); *Eds. A. E. Naaman and H. W. Reinhardt*

PRO 31: International RILEM Workshop on Test and Design Methods for Steel Fibre Reinforced Concrete: Background and Experiences (ISBN: 2-912143-38-1; e-ISBN: 2351580168); *Eds. B. Schnütgen and L. Vandewalle*

PRO 32: International Conference on Advances in Concrete and Structures 2 vol. (ISBN (set): 2-912143-41-1; e-ISBN: 2351580176); *Eds. Ying-shu Yuan, Surendra P. Shah and Heng-lin Lü*

PRO 33: 3rd International Symposium on Self-Compacting Concrete (ISBN: 2-912143-42-X; e-ISBN: 2912143713); *Eds. Ó. Wallevik and I. Nielsson*

PRO 34: International RILEM Conference on Microbial Impact on Building Materials (ISBN: 2-912143-43-8; e-ISBN: 2351580184); *Ed. M. Ribas Silva*

PRO 35: International RILEM TC 186-ISA on Internal Sulfate Attack and Delayed Ettringite Formation (ISBN: 2-912143-44-6; e-ISBN: 2912143802); *Eds. K. Scrivener and J. Skalny*

PRO 36: International RILEM Symposium on Concrete Science and Engineering—A Tribute to Arnon Bentur (ISBN: 2-912143-46-2; e-ISBN: 2912143586); *Eds. K. Kovler, J. Marchand, S. Mindess and J. Weiss*

PRO 37: 5th International RILEM Conference on Cracking in Pavements—Mitigation, Risk Assessment and Prevention (ISBN: 2-912143-47-0; e-ISBN: 2912143764); *Eds. C. Petit, I. Al-Qadi and A. Millien*

PRO 38: 3rd International RILEM Workshop on Testing and Modelling the Chloride Ingress into Concrete (ISBN: 2-912143-48-9; e-ISBN: 2912143578); *Eds. C. Andrade and J. Kropp*

PRO 39: 6th International RILEM Symposium on Fibre-Reinforced Concretes - BEFIB 2004 (ISBN: 2-912143-51-9; e-ISBN: 2912143748); *Eds. M. Di Prisco, R. Felicetti and G. A. Plizzari*

PRO 40: International RILEM Conference on the Use of Recycled Materials in Buildings and Structures (ISBN: 2-912143-52-7; e-ISBN: 2912143756); *Eds. E. Vázquez, Ch. F. Hendriks and G. M. T. Janssen*

PRO 41: RILEM International Symposium on Environment-Conscious Materials and Systems for Sustainable Development (ISBN: 2-912143-55-1; e-ISBN: 2912143640); *Eds. N. Kashino and Y. Ohama*

PRO 42: SCC'2005—China: 1st International Symposium on Design, Performance and Use of Self-Consolidating Concrete (ISBN: 2-912143-61-6;

e-ISBN: 2912143624); *Eds. Zhiwu Yu, Caijun Shi, Kamal Henri Khayat and Youjun Xie*

PRO 43: International RILEM Workshop on Bonded Concrete Overlays (e-ISBN: 2-912143-83-7); *Eds. J. L. Granju and J. Silfwerbrand*

PRO 44: 2nd International RILEM Workshop on Microbial Impacts on Building Materials (CD11) (e-ISBN: 2-912143-84-5); *Ed. M. Ribas Silva*

PRO 45: 2nd International Symposium on Nanotechnology in Construction, Bilbao (ISBN: 2-912143-87-X; e-ISBN: 2912143888); *Eds. Peter J. M. Bartos, Yolanda de Miguel and Antonio Porro*

PRO 46: ConcreteLife'06—International RILEM-JCI Seminar on Concrete Durability and Service Life Planning: Curing, Crack Control, Performance in Harsh Environments (ISBN: 2-912143-89-6; e-ISBN: 291214390X); *Ed. K. Kovler*

PRO 47: International RILEM Workshop on Performance Based Evaluation and Indicators for Concrete Durability (ISBN: 978-2-912143-95-2; e-ISBN: 9782912143969); *Eds. V. Baroghel-Bouny, C. Andrade, R. Torrent and K. Scrivener*

PRO 48: 1st International RILEM Symposium on Advances in Concrete through Science and Engineering (e-ISBN: 2-912143-92-6); *Eds. J. Weiss, K. Kovler, J. Marchand, and S. Mindess*

PRO 49: International RILEM Workshop on High Performance Fiber Reinforced Cementitious Composites in Structural Applications (ISBN: 2-912143-93-4; e-ISBN: 2912143942); *Eds. G. Fischer and V.C. Li*

PRO 50: 1st International RILEM Symposium on Textile Reinforced Concrete (ISBN: 2-912143-97-7; e-ISBN: 2351580087); *Eds. Josef Hegger, Wolfgang Brameshuber and Norbert Will*

PRO 51: 2nd International Symposium on Advances in Concrete through Science and Engineering (ISBN: 2-35158-003-6; e-ISBN: 2-35158-002-8); *Eds. J. Marchand, B. Bissonnette, R. Gagné, M. Jolin and F. Paradis*

PRO 52: Volume Changes of Hardening Concrete: Testing and Mitigation (ISBN: 2-35158-004-4; e-ISBN: 2-35158-005-2); *Eds. O. M. Jensen, P. Lura and K. Kovler*

PRO 53: High Performance Fiber Reinforced Cement Composites—HPFRCC5 (ISBN: 978-2-35158-046-2; e-ISBN: 978-2-35158-089-9); *Eds. H. W. Reinhardt and A. E. Naaman*

PRO 54: 5th International RILEM Symposium on Self-Compacting Concrete (ISBN: 978-2-35158-047-9; e-ISBN: 978-2-35158-088-2); *Eds. G. De Schutter and V. Boel*

PRO 55: International RILEM Symposium Photocatalysis, Environment and Construction Materials (ISBN: 978-2-35158-056-1; e-ISBN: 978-2-35158-057-8); *Eds. P. Baglioni and L. Cassar*

PRO 56: International RILEM Workshop on Integral Service Life Modelling of Concrete Structures (ISBN 978-2-35158-058-5; e-ISBN: 978-2-35158-090-5); *Eds. R. M. Ferreira, J. Gulikers and C. Andrade*

PRO 57: RILEM Workshop on Performance of cement-based materials in aggressive aqueous environments (e-ISBN: 978-2-35158-059-2); *Ed. N. De Belie*

PRO 58: International RILEM Symposium on Concrete Modelling—CONMOD'08 (ISBN: 978-2-35158-060-8; e-ISBN: 978-2-35158-076-9); *Eds. E. Schlangen and G. De Schutter*

PRO 59: International RILEM Conference on On Site Assessment of Concrete, Masonry and Timber Structures—SACoMaTiS 2008 (ISBN set: 978-2-35158-061-5; e-ISBN: 978-2-35158-075-2); *Eds. L. Binda, M. di Prisco and R. Felicetti*

PRO 60: Seventh RILEM International Symposium on Fibre Reinforced Concrete: Design and Applications—BEFIB 2008 (ISBN: 978-2-35158-064-6; e-ISBN: 978-2-35158-086-8); *Ed. R. Gettu*

PRO 61: 1st International Conference on Microstructure Related Durability of Cementitious Composites 2 vol., (ISBN: 978-2-35158-065-3; e-ISBN: 978-2-35158-084-4); *Eds. W. Sun, K. van Breugel, C. Miao, G. Ye and H. Chen*

PRO 62: NSF/ RILEM Workshop: In-situ Evaluation of Historic Wood and Masonry Structures (e-ISBN: 978-2-35158-068-4); *Eds. B. Kasal, R. Anthony and M. Drdácký*

PRO 63: Concrete in Aggressive Aqueous Environments: Performance, Testing and Modelling, 2 vol., (ISBN: 978-2-35158-071-4; e-ISBN: 978-2-35158-082-0); *Eds. M. G. Alexander and A. Bertron*

PRO 64: Long Term Performance of Cementitious Barriers and Reinforced Concrete in Nuclear Power Plants and Waste Management - NUCPERF 2009 (ISBN: 978-2-35158-072-1; e-ISBN: 978-2-35158-087-5); *Eds. V. L'Hostis, R. Gens, C. Gallé*

PRO 65: Design Performance and Use of Self-consolidating Concrete—SCC'2009 (ISBN: 978-2-35158-073-8; e-ISBN: 978-2-35158-093-6); *Eds. C. Shi, Z. Yu, K. H. Khayat and P. Yan*

PRO 66: 2nd International RILEM Workshop on Concrete Durability and Service Life Planning—ConcreteLife'09 (ISBN: 978-2-35158-074-5; ISBN: 978-2-35158-074-5); *Ed. K. Kovler*

PRO 67: Repairs Mortars for Historic Masonry (e-ISBN: 978-2-35158-083-7); *Ed. C. Groot*

PRO 68: Proceedings of the 3rd International RILEM Symposium on 'Rheology of Cement Suspensions' such as Fresh Concrete (ISBN 978-2-35158-091-2; e-ISBN: 978-2-35158-092-9); *Eds. O. H. Wallevik, S. Kubens and S. Oesterheld*

PRO 69: 3rd International PhD Student Workshop on 'Modelling the Durability of Reinforced Concrete (ISBN: 978-2-35158-095-0); *Eds. R. M. Ferreira, J. Gulikers and C. Andrade*

PRO 70: 2nd International Conference on 'Service Life Design for Infrastructure' (ISBN set: 978-2-35158-096-7, e-ISBN: 978-2-35158-097-4); *Ed. K. van Breugel, G. Ye and Y. Yuan*

PRO 71: Advances in Civil Engineering Materials—The 50-year Teaching Anniversary of Prof. Sun Wei' (ISBN: 978-2-35158-098-1; e-ISBN: 978-2-35158-099-8); *Eds. C. Miao, G. Ye, and H. Chen*

PRO 72: First International Conference on 'Advances in Chemically-Activated Materials—CAM'2010' (2010), 264 p, (ISBN: 978-2-35158-101-8; e-ISBN: 978-2-35158-115-5); *Eds. Caijun Shi and Xiaodong Shen*

PRO 73: 2nd International Conference on 'Waste Engineering and Management —ICWEM 2010' (2010), 894 p, (ISBN: 978-2-35158-102-5; e-ISBN: 978-2-35158-103-2); *Eds. J. Zh. Xiao, Y. Zhang, M. S. Cheung and R. Chu*

PRO 74: International RILEM Conference on 'Use of Superabsorsorbent Polymers and Other New Addditives in Concrete' (2010), 374 p, (ISBN: 978-2-35158-104-9; e-ISBN: 978-2-35158-105-6); *Eds. O.M. Jensen, M.T. Hasholt, and S. Laustsen*

PRO 75: International Conference on 'Material Science—2nd ICTRC—Textile Reinforced Concrete—Theme 1' (2010) 436 p, ISBN: 978-2-35158-106-3; e-ISBN: 978-2-35158-107-0; *Ed. W. Brameshuber*

PRO 76: International Conference on 'Material Science—HetMat—Modelling of Heterogeneous Materials—Theme 2' (2010) 255 p, ISBN: 978-2-35158-108-7; e-ISBN: 978-2-35158-109-4; *Ed. W. Brameshuber*

PRO 77: International Conference on 'Material Science—AdIPoC—Additions Improving Properties of Concrete—Theme 3' (2010) 459 p, ISBN: 978-2-35158-110-0; e-ISBN: 978-2-35158-111-7; *Ed. W. Brameshuber*

PRO 78: 2nd Historic Mortars Conference and RILEM TC 203-RHM Final Workshop—HMC2010 (2010) 1416 p, e-ISBN: 978-2-35158-112-4; *Eds J. Válek, C. Groot, and J. J. Hughes*

PRO 79: International RILEM Conference on Advances in Construction Materials Through Science and Engineering (2011) 213 p, ISBN: 978-2-35158-116-2, e-ISBN: 978-2-35158-117-9; *Eds Christopher Leung and K.T. Wan*

PRO 80: 2nd International RILEM Conference on Concrete Spalling due to Fire Exposure (2011) 453 p, ISBN: 978-2-35158-118-6, e-ISBN: 978-2-35158-119-3; *Eds E.A.B. Koenders and F. Dehn*

PRO 81: 2nd International RILEM Conference on Strain Hardening Cementitious Composites (SHCC2-Rio) (2011) 451 p, ISBN: 978-2-35158-120-9, e-ISBN: 978-2-35158-121-6; *Eds R.D. Toledo Filho, F.A. Silva, E.A.B. Koenders and E.M.R. Fairbairn*

PRO 82: 2nd International RILEM Conference on Progress of Recycling in the Built Environment (2011) 507 p, e-ISBN: 978-2-35158-122-3; *Eds V.M. John, E. Vazquez, S.C. Angulo and C. Ulsen*

PRO 83: 2nd International Conference on Microstructural-related Durability of Cementitious Composites (2012) 250 p, ISBN: 978-2-35158-129-2; e-ISBN: 978-2-35158-123-0; *Eds G. Ye, K. van Breugel, W. Sun and C. Miao*

PRO 84: CONSEC13—Seventh International Conference on Concrete under Severe Conditions—Environment and Loading (2013) 1930 p, ISBN: 978-2-35158-124-7; e-ISBN: 978-2- 35158-134-6; *Eds Z.J. Li, W. Sun, C.W. Miao, K. Sakai, O.E. Gjorv & N. Banthia*

PRO 85: RILEM-JCI International Workshop on Crack Control of Mass Concrete and Related issues concerning Early-Age of Concrete Structures—

ConCrack 3—Control of Cracking in Concrete Structures 3 (2012) 237 p, ISBN: 978-2-35158-125-4; e-ISBN: 978-2-35158-126-1; *Eds F. Toutlemonde and J.-M. Torrenti*

PRO 86: International Symposium on Life Cycle Assessment and Construction (2012) 414 p, ISBN: 978-2-35158-127-8, e-ISBN: 978-2-35158-128-5; *Eds A. Ventura and C. de la Roche*

PRO 87: UHPFRC 2013—RILEM-fib-AFGC International Symposium on Ultra-High Performance Fibre-Reinforced Concrete (2013), ISBN: 978-2-35158-130-8, e-ISBN: 978-2-35158-131-5; *Eds F. Toutlemonde*

PRO 88: 8th RILEM International Symposium on Fibre Reinforced Concrete (2012) 344 p, ISBN: 978-2-35158-132-2, e-ISBN: 978-2-35158-133-9; *Eds Joaquim A.O. Barros*

PRO 89: RILEM International workshop on performance-based specification and control of concrete durability (2014) 678 pp, ISBN: 978-2-35158-135-3, e-ISBN: 978-2-35158-136-0; *Eds. D. Bjegović, H. Beushausen and M. Serdar*

PRO 90: 7th RILEM International Conference on Self-Compacting Concrete and of the 1st RILEM International Conference on Rheology and Processing of Construction Materials (2013) 396 p, ISBN: 978-2-35158-137-7, e-ISBN: 978-2-35158-138-4; *Eds. Nicolas Roussel and Hela Bessaies-Bey*

PRO 91: CONMOD 2014—RILEM International Symposium on Concrete Modelling (2014), ISBN: 978-2-35158-139-1; e-ISBN: 978-2-35158-140-7; *Eds. Kefei Li, Peiyu Yan and Rongwei Yang*

PRO 92: CAM 2014—2nd International Conference on advances in chemically-activated materials (2014) 392 p, ISBN: 978-2-35158-141-4; e-ISBN: 978-2-35158-142-1; *Eds. Caijun Shi and Xiadong Shen*

PRO 93: SCC 2014—3rd International Symposium on Design, Performance and Use of Self-Consolidating Concrete (2014) 438 p, ISBN: 978-2-35158-143-8; e-ISBN: 978-2-35158-144-5; *Eds. Caijun Shi, Zhihua Ou, Kamal H. Khayat*

PRO 94 (online version): HPFRCC-7—7th RILEM conference on High performance fiber reinforced cement composites (2015), e-ISBN: 978-2-35158-146-9; *Eds. H.W. Reinhardt, G.J. Parra-Montesinos, H. Garrecht*

PRO 95: International RILEM Conference on Application of superabsorbent polymers and other new admixtures in concrete construction (2014), ISBN: 978-2-35158-147-6; e-ISBN: 978-2-35158-148-3; *Eds. Viktor Mechtcherine, Christof Schroefl*

PRO 96 (online version): XIII DBMC: XIII International Conference on Durability of Building Materials and Components (2015), e-ISBN: 978-2-35158-149-0; *Eds. M. Quattrone, V.M. John*

PRO 97: SHCC3—3rd International RILEM Conference on Strain Hardening Cementitious Composites (2014), ISBN: 978-2-35158-150-6; e-ISBN: 978-2-35158-151-3; *Eds. E. Schlangen, M.G. Sierra Beltran, M. Lukovic, G. Ye*

PRO 98: FERRO-11—11th International Symposium on Ferrocement and 3rd ICTRC - International Conference on Textile Reinforced Concrete (2015), ISBN: 978-2-35158-152-0; e-ISBN: 978-2-35158-153-7; *Ed. W. Brameshuber*

PRO 99 (online version): ICBBM 2015—1st International Conference on Bio-Based Building Materials (2015), e-ISBN: 978-2-35158-154-4; *Eds. S. Amziane, M. Sonebi*

PRO 100: SCC16—RILEM Self-Consolidating Concrete Conference (2016), ISBN: 978-2-35158-156-8; e-ISBN: 978-2-35158-157-5; *Ed. Kamal H. Kayat*

PRO 101 (online version): III Progress of Recycling in the Built Environment (2015), e-ISBN: 978-2-35158-158-2; *Eds I. Martins, C. Ulsen and S. C. Angulo*

PRO 102 (online version): RILEM Conference on Microorganisms-Cementitious Materials Interactions (2016), e-ISBN: 978-2-35158-160-5; *Eds. Alexandra Bertron, Henk Jonkers, Virginie Wiktor*

PRO 103 (online version): ACESC'16—Advances in Civil Engineering and Sustainable Construction (2016), e-ISBN: 978-2-35158-161-2; *Eds. T.Ch. Madhavi, G. Prabhakar, Santhosh Ram and P.M. Rameshwaran*

PRO 104 (online version): SSCS'2015—Numerical Modeling—Strategies for Sustainable Concrete Structures (2015), e-ISBN: 978-2-35158-162-9

PRO 105: 1st International Conference on UHPC Materials and Structures (2016), ISBN: 978-2-35158-164-3, e-ISBN: 978-2-35158-165-0

PRO 106: AFGC-ACI-fib-RILEM International Conference on Ultra-High-Performance Fibre-Reinforced Concrete—UHPFRC 2017 (2017), ISBN: 978-2-35158-166-7, e-ISBN: 978-2-35158-167-4; *Eds. François Toutlemonde & Jacques Resplendino*

PRO 107 (online version): XIV DBMC—14th International Conference on Durability of Building Materials and Components (2017), e-ISBN: 978-2-35158-159-9; *Eds. Geert De Schutter, Nele De Belie, Arnold Janssens, Nathan Van Den Bossche*

PRO 108: MSSCE 2016—Innovation of Teaching in Materials and Structures (2016), ISBN: 978-2-35158-178-0, e-ISBN: 978-2-35158-179-7; *Ed. Per Goltermann*

PRO 109 (2 volumes): MSSCE 2016—Service Life of Cement-Based Materials and Structures (2016), ISBN Vol. 1: 978-2-35158-170-4, Vol. 2: 978-2-35158-171-4, Set Vol. 1&2: 978-2-35158-172-8, e-ISBN : 978-2-35158-173-5; *Eds. Miguel Azenha, Ivan Gabrijel, Dirk Schlicke, Terje Kanstad and Ole Mejlhede Jensen*

PRO 110: MSSCE 2016—Historical Masonry (2016), ISBN: 978-2-35158-178-0, e-ISBN: 978-2-35158-179-7; *Eds. Inge Rörig-Dalgaard and Ioannis Ioannou*

PRO 111: MSSCE 2016—Electrochemistry in Civil Engineering (2016), ISBN: 978-2-35158-176-6, e-ISBN: 978-2-35158-177-3; *Ed. Lisbeth M. Ottosen*

PRO 112: MSSCE 2016—Moisture in Materials and Structures (2016), ISBN: 978-2-35158-178-0, e-ISBN: 978-2-35158-179-7; *Eds. Kurt Kielsgaard Hansen, Carsten Rode and Lars-Olof Nilsson*

PRO 113: MSSCE 2016—Concrete with Supplementary Cementitious Materials (2016), ISBN: 978-2-35158-178-0, e-ISBN: 978-2-35158-179-7; *Eds. Ole Mejlhede Jensen, Konstantin Kovler and Nele De Belie*

PRO 114: MSSCE 2016—Frost Action in Concrete (2016), ISBN: 978-2-35158-182-7, e-ISBN: 978-2-35158-183-4; *Eds. Marianne Tange Hasholt, Katja Fridh and R. Doug Hooton*

PRO 115: MSSCE 2016—Fresh Concrete (2016), ISBN: 978-2-35158-184-1, e-ISBN: 978-2-35158-185-8; *Eds. Lars N. Thrane, Claus Pade, Oldrich Svec and Nicolas Roussel*

PRO 116: BEFIB 2016—9th RILEM International Symposium on Fiber Reinforced Concrete (2016), ISBN: 978-2-35158-187-2, e-ISBN: 978-2-35158-186-5; *Eds. N. Banthia, M. di Prisco and S. Soleimani-Dashtaki*

PRO 117: 3rd International RILEM Conference on Microstructure Related Durability of Cementitious Composites (2016), ISBN: 978-2-35158-188-9, e-ISBN: 978-2-35158-189-6; *Eds. Changwen Miao, Wei Sun, Jiaping Liu, Huisu Chen, Guang Ye and Klaas van Breugel*

PRO 118 (4 volumes): International Conference on Advances in Construction Materials and Systems (2017), ISBN Set: 978-2-35158-190-2, Vol. 1: 978-2-35158-193-3, Vol. 2: 978-2-35158-194-0, Vol. 3: ISBN:978-2-35158-195-7, Vol. 4: ISBN:978-2-35158-196-4, e-ISBN: 978-2-35158-191-9; *Ed. Manu Santhanam*

PRO 119 (online version): ICBBM 2017—Second International RILEM Conference on Bio-based Building Materials, (2017), e-ISBN: 978-2-35158-192-6; *Ed. Sofiane Amziane*

PRO 120: 2nd International RILEM/COST Conference on Early Age Cracking and Serviceability in Cement-based Materials and Structures (EAC-02), 2017, ISBN: 978-2-35158-197-1, e-ISBN: 978-2-35158-198-8; *Eds. Dimitrios Aggelis and Stéphanie Staquet*

RILEM REPORTS (REP)

Report 19: Considerations for Use in Managing the Aging of Nuclear Power Plant Concrete Structures (ISBN: 2-912143-07-1); *Ed. D. J. Naus*

Report 20: Engineering and Transport Properties of the Interfacial Transition Zone in Cementitious Composites (ISBN: 2-912143-08-X); *Eds. M. G. Alexander, G. Arliguie, G. Ballivy, A. Bentur and J. Marchand*

Report 21: Durability of Building Sealants (ISBN: 2-912143-12-8); *Ed. A. T. Wolf*

Report 22: Sustainable Raw Materials—Construction and Demolition Waste (ISBN: 2-912143-17-9); *Eds. C. F. Hendriks and H. S. Pietersen*

Report 23: Self-Compacting Concrete state-of-the-art report (ISBN: 2-912143-23-3); *Eds. Å. Skarendahl and Ö. Petersson*

Report 24: Workability and Rheology of Fresh Concrete: Compendium of Tests (ISBN: 2-912143-32-2); *Eds. P. J. M. Bartos, M. Sonebi and A. K. Tamimi*

Report 25: Early Age Cracking in Cementitious Systems (ISBN: 2-912143-33-0); *Ed. A. Bentur*

Report 26: Towards Sustainable Roofing (Joint Committee CIB/RILEM) (CD 07) (e-ISBN 978-2-912143-65-5); *Eds. Thomas W. Hutchinson and Keith Roberts*

Report 27: Condition Assessment of Roofs (Joint Committee CIB/RILEM) (CD 08) (e-ISBN 978-2-912143-66-2); *Ed. CIB W 83/RILEM TC166-RMS*

Report 28: Final report of RILEM TC 167-COM 'Characterisation of Old Mortars with Respect to Their Repair' (ISBN: 978-2-912143-56-3); *Eds. C. Groot, G. Ashall and J. Hughes*

Report 29: Pavement Performance Prediction and Evaluation (PPPE): Interlaboratory Tests (e-ISBN: 2-912143-68-3); *Eds. M. Partl and H. Piber*

Report 30: Final Report of RILEM TC 198-URM 'Use of Recycled Materials' (ISBN: 2-912143-82-9; e-ISBN: 2-912143-69-1); *Eds. Ch. F. Hendriks, G. M. T. Janssen and E. Vázquez*

Report 31: Final Report of RILEM TC 185-ATC 'Advanced testing of cement-based materials during setting and hardening' (ISBN: 2-912143-81-0; e-ISBN: 2-912143-70-5); *Eds. H. W. Reinhardt and C. U. Grosse*

Report 32: Probabilistic Assessment of Existing Structures. A JCSS publication (ISBN 2-912143-24-1); *Ed. D. Diamantidis*

Report 33: State-of-the-Art Report of RILEM Technical Committee TC 184-IFE 'Industrial Floors' (ISBN 2-35158-006-0); *Ed. P. Seidler*

Report 34: Report of RILEM Technical Committee TC 147-FMB 'Fracture mechanics applications to anchorage and bond' Tension of Reinforced Concrete Prisms—Round Robin Analysis and Tests on Bond (e-ISBN 2-912143-91-8); *Eds. L. Elfgren and K. Noghabai*

Report 35: Final Report of RILEM Technical Committee TC 188-CSC 'Casting of Self Compacting Concrete' (ISBN 2-35158-001-X; e-ISBN: 2-912143-98-5); *Eds. Å. Skarendahl and P. Billberg*

Report 36: State-of-the-Art Report of RILEM Technical Committee TC 201-TRC 'Textile Reinforced Concrete' (ISBN 2-912143-99-3); *Ed. W. Brameshuber*

Report 37: State-of-the-Art Report of RILEM Technical Committee TC 192-ECM 'Environment-conscious construction materials and systems' (ISBN: 978-2-35158-053-0); *Eds. N. Kashino, D. Van Gemert and K. Imamoto*

Report 38: State-of-the-Art Report of RILEM Technical Committee TC 205-DSC 'Durability of Self-Compacting Concrete' (ISBN: 978-2-35158-048-6); *Eds. G. De Schutter and K. Audenaert*

Report 39: Final Report of RILEM Technical Committee TC 187-SOC 'Experimental determination of the stress-crack opening curve for concrete in tension' (ISBN 978-2-35158-049-3); *Ed. J. Planas*

Report 40: State-of-the-Art Report of RILEM Technical Committee TC 189-NEC 'Non-Destructive Evaluation of the Penetrability and Thickness of the Concrete Cover' (ISBN 978-2-35158-054-7); *Eds. R. Torrent and L. Fernández Luco*

Report 41: State-of-the-Art Report of RILEM Technical Committee TC 196-ICC 'Internal Curing of Concrete' (ISBN 978-2-35158-009-7); *Eds. K. Kovler and O. M. Jensen*

Report 42: 'Acoustic Emission and Related Non-destructive Evaluation Techniques for Crack Detection and Damage Evaluation in Concrete' - Final Report of RILEM Technical Committee 212-ACD (e-ISBN: 978-2-35158-100-1); *Ed. M. Ohtsu*

Report 45: Repair Mortars for Historic Masonry - State-of-the-Art Report of RILEM Technical Committee TC 203-RHM (e-ISBN: 978-2-35158-163-6); *Eds. Paul Maurenbrecher and Caspar Groot*

Contents

Chapter 1
Introduction

Manfred N. Partl

Abstract An overview on the background and motivation for this report on the achievements of the technical committee RILEM TC 237-SIB on *Testing and Characterization of Sustainable Innovative Bituminous Materials and Systems* is presented, together with a short summary on the scope of this voluntary international team effort. Challenges and key research paths towards modern "green" asphalt pavements are addressed, focusing on general aspects associated with the increasing variety of approaches and their implication on testing and characterization of innovative asphalt pavement materials. As example for the complexity of the experimental challenges and the potential necessity to break free from traditional testing patterns, selected specific aspects of reinforced asphalt pavements are considered and discussed. It is emphasized that testing must be consistent with the purpose of the reinforcement, answering the key questions in what respect, under what conditions and in what loading direction reinforcement should be achieved and tested. This "garbage-in-garbage-out" awareness is also valid for all other fields dealing with testing and characterization of innovative bituminous materials and systems, of course.

Keywords Sustainability · Aging · Maturing · Healing · Green asphalt
Asphalt structure · Reinforcement

M. N. Partl (✉)
Empa, Swiss Federal Laboratories for Materials Science and Technology, CH-8600 Duebendorf, Switzerland
e-mail: manfred.partl@empa.ch

M. N. Partl
KTH, S-10044 Stockholm, Sweden

M. N. Partl et al. (eds.), *Testing and Characterization of Sustainable Innovative Bituminous Materials and Systems*, RILEM State-of-the-Art Reports 24,
https://doi.org/10.1007/978-3-319-71023-5_1

1.1 Background and Motivation

1.1.1 Challenge and Role of Modern Bituminous Pavement Materials

The use of bituminous pavement materials for roads has a long tradition and is a success story that started early in ancient times before progressively growing to global dimensions over centuries. Most of this development occurred on a technological try and error basis, leading to a wealth of practical knowledge and diverse experience that was not sustainable since much of it got lost whenever the experienced individuals professionally retired.

Re-inventing the wheel as well as sticking to traditional techniques and design rules was common until a few decades ago, when finally, triggered by the AASHO road test, scientific approaches and methodologies started sneaking into the field of asphalt technology, calling for in-depth understanding of the materials and its behavior, aiming at generalized fundamental standards and universal design tools. However, this process turned out to be very slow, often skeptically hampered by empirical and economical arguments and therefore not as straightforward as in other fields, like in steel or concrete technology.

This was partly due to the fact that failures of asphalt pavements are generally not classified as safety relevant catastrophes. Though, it is evident that poorly performing asphalt pavements are risky, in particular with respect to their safety relevant surfaces, but they cannot be considered as risky structures, like bridges that may collapse with high threat to life and health causing dramatic social and economic impact. Hence, simple try and error approaches for asphalt pavements appeared still acceptable for many years, with little risk and consequences for users, contractors and road authorities.

Another reason for the slow progress in asphalt pavement technology is the material itself, which is a thermo-rheological complex composite that is not easy to characterize and understand in its mechanical and chemo-physical behavior against the background of heavy stochastic traffic, weather induced loading and environmentally caused aging. The complexity is even amplified by the different field construction and maintenance processes resulting in a sometimes almost fatalistic awareness that the materials placed in the field cannot be considered identical to what was designed and tested in the laboratory. In fact, the gap between lab results and field experience is one of the major challenges in asphalt technology.

This gap is even increasing by the growing variety of materials and the recent boost of innovations in the field of asphalt pavement technology in general, which is not only restricted to bituminous pavement materials but applies also to innovative pavement structures that include reinforcing elements such as textiles and grids. Trigger and motor for these developments are new demands and challenges in terms of

- *Sustainable development*: Increase of durability, careful and efficient use of material resources, activation of self-healing capacities (crack-healing with induction,…), use of so-called rejuvenators, use of renewable energy…
- *Construction*: Cost reduction, energy saving, workability and compactability (fast pre-fabrication, automatization, all-weather, error tolerant,…), use of local and marginal materials…
- *Performance*: Higher bearing capacity, longer service life, reduction of maintenance, increase of driving safety and comfort, resilience against exceptional events (climate change, human action,…), adaptability (ice-repelling, self-luminous, temperature: proactive by stiffening in summer and softening in winter),…
- *Environmental Impact*: Energy consumption, noise reduction, use of potentially hazardous materials, pollution (CO_2 emission, particulates,…),…
- *Multifunctionality*: Energy harvesting, water retention and flood relieve, urban climate regulation (heat islands, evaporation,…), CO_2 storage, cleaning of environment (air, water)

With respect to sustainable development, it is important to keep in mind that materials are usually termed sustainable if they are not produced and used at cost of future generations, which clearly implies that durable materials are not necessarily sustainable.

Asphalt pavement materials, in particular, are durable thermoplastic materials with the potential of being re-used almost ad infinitum, since they can be melted easily and re-processed to virgin-like products. Hence, they may be classified as materials that are not only sustainable but even "supra-sustainable", i.e. more than just sustainable, because they are man-made upgraded materials not only without negative effect but with even potential benefit for future generations as valuable resource that will be available almost everywhere. However, asphalt pavement materials may only be supra-sustainable if our generation does not introduce negative components into the material (like tar in the past). In that sense our generation has a great responsibility.

For environmental reasons, intensive discussions and attempts are currently ongoing worldwide in order to reduce energy consumption for construction of asphalt pavements by promoting warm and cold mixture technology. This means a paradigm change in the sense that traditional management, design, construction and laboratory concepts for hot mixture technology are no longer a priori valid and that new material aspects have to be considered, such as environmentally driven curing (e.g. from climatic conditioning) and intrinsic maturing processes (e.g. from self-driven chemical reactions and physical restructuring), as schematically illustrated in Fig. 1.1.

As a result, the introduction of temperature-reduced asphalt mixtures has also changed the traditional understanding of phenomena like aging, which has generally been known as oxidation and temperature driven processes that change the

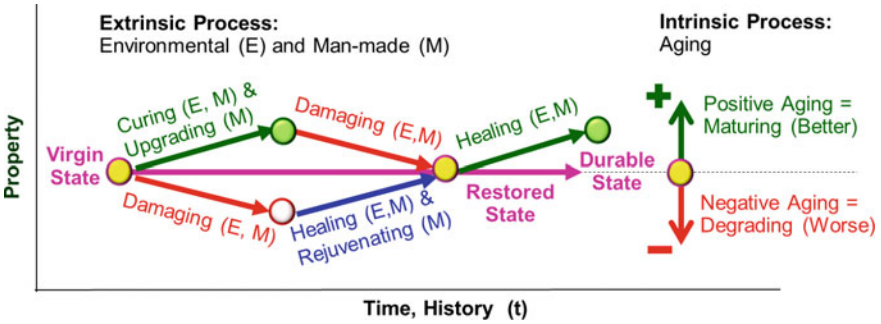

Fig. 1.1 Schematic illustration of the effect of extrinsic and intrinsic processes on the change of material properties over time

virgin material's constitution to the worse. Hence, aging is often taken as closely related to the process of degradation, causing unfavorable chemo-physical changes, such as embrittlement, that may lead to damage phenomena (e.g. cracks), thus influencing durability in a negative way. These negative aging effects may be mitigated or reversed by rejuvenation agents or healing measures.

However, as indicated in Fig. 1.1, asphalt aging must not only be understood as negative but also as positive process. In particular during curing phases, aging can also mean chemo-physical changes of virgin materials to the better, in the sense of maturing. This is, for instance, the case with pavements produced with foam bitumen or emulsions, where moisture loss during curing may improve mechanical properties over time.

Positive and negative aging can be influenced in different ways: Towards the positive side, upgrading of the mixture in an early stage as well as healing or rejuvenating measures after damaging and degradation may be conducted, whereas a reduction of environmental and man-made mechanical impact may be the way to go for influencing negative aging in favor of increasing durability.

1.1.2 Towards Green Asphalt Pavements

Nowadays, remarkable effort is devoted towards green asphalt pavements (GAP) that preserve material resources and consume the least amount of energy. Though considerable progress in energy reduction has been achieved in the field of hot, warm and cold mixture technology, performance and durability of GAP's are still not at the same level in most cases, let alone better than traditional hot mixed asphalt (HMA) pavements. Numerous concepts are actually proposed and studied under the general title of GAP:

- *Recycling of reclaimed asphalt pavements (RAP)*: i.e. re-use of old pavement material in newly placed pavement layers without down-cycling: The focus here has more and more shifted towards recycling of surface layers as closely to 100% as possible, since these climatically and mechanically most heavily loaded layers are losing their functionality first and must therefore be replaced first. At the same time the focus has also shifted towards energy saving temperature-reduced recycling techniques, relying on waxy additives and rejuvenators as well as the use of foam bitumen or emulsions.
- *Re-use of secondary materials*: Such as demolition waste, industrial by-products and post-consumer products without abusing pavements as linear landfills. Some of these post-user products have even shown positive effects on pavement performance, such as old tire rubber, which, depending of processing, may have positive effects on low temperature cracking resistance.
- *Marginal Materials*: i.e. easily available potential building materials of low quality that may require special treatment for up-grading. Typical marginal materials are mining or tunnel excavation residues, locally available poor quality mineral aggregates, such as lime stone, clay or schist, with unfavorable properties in terms of polishing, strength and petrographic characteristics, or local river sediments with unfavorable natural gradation. As long as no technologies exist for successfully using these easily available materials, expensive high quality components must still be hauled from far away.
- *Substitute materials and components*: Examples are organic resins and oils from non-food plants and algae that are renewable and that allow to replace traditional components, in particular bituminous binder. This may even result in partly or completely substituting bitumen by other suitable and environmental friendly polymeric binders.
- *Regenerative and upgrading materials*: They cover a wide and still quite unexplored field with a lot of innovative industrial potential that has produced a considerable quantity of patent protected products. This direction of GAP concepts may even comprise futuristic self-regenerating pavements materials, e.g. through microorganisms.

Nowadays regenerative materials are basically used as so-called rejuvenators, particularly in connection with RAP. Main focus is recovering selected properties of the bituminous binder that have been unfavorably changed through oxidative or thermal aging (in the sense of negative aging). However, claiming "rejuvenation" reflects more wishful thinking than a real process, because of the complexity of bitumen, which makes it practically impossible to recover the original virgin state in all aspects.

Modifying bitumen with all kinds of elastomeric or plastomeric polymers is one of the most common ways for upgrading GAPs. In addition, all kind of fibers, such as cellulose fibers from nano- to micro- size are considered as kind of reinforcing elements that influences thickness, viscosity, adhesion and low temperature fracture properties of bitumen. Homogeneous distribution, clustering and moisture susceptibility of fibers are only a few major challenges to overcome in that respect.

- *Crack-healing promotors*: Due to its viscous behavior, fine asphalt cracks may re-fill with bitumen internally seeping from the cracked pavement and heal to certain extent in summer due to elevated temperatures. This effect is often referred to as "self-healing" because it happens without any human action in spite of the fact that it is induced from outside, typically through sun radiation. However, this natural "self-healing" mechanism should not be over-rated, because, in order to avoid high temperature rutting, pavements are generally designed stiff enough to carry high traffic loads at summer temperatures without significant permanent deformations.

Hence, it may make sense to embed crack healing promoters into the asphalt, such as steel and nano particles which would allow stimulating healing artificially by externally activating the intrinsic healing potential (Liu et al. 2010). Adding healing promoters in asphalt mixtures may be considered as some kind of "vaccination" to support the "crack immune system" of the material by external stimulation through low frequency induction at 78 kHz (Garcia et al. 2014) or high frequency alternating magnetic fields at 285 kHz (Jeoffroy et al. 2016).

With this induced heating, bitumen can be melted locally such that it may flow into the cracks and fill them up. At the same time, thermal expansion would help to close the cracks to certain extent. However, the bitumen that has drained out locally from the pavement materials and is now filling the crack may be missing on its original location where the binder content has become lower. Hence, the healed material with locally slightly re-distributed binder is different from the original one as shown schematically in Fig. 1.2.

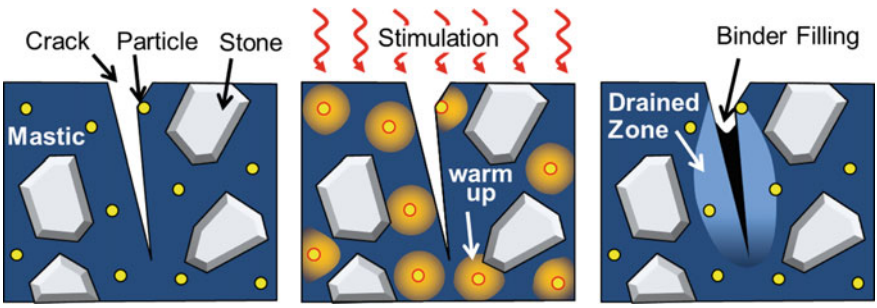

Fig. 1.2 Mechanism of stimulated crack-healing with embedded particles

These innovative "vaccination" techniques require special maintenance equipment and are only suitable for invisible micro cracks. They are still in an early stage of development with special problems to solve such as homogeneous distribution of the particles, prevention of local overheating of the binder as well as increase of efficiency in terms of time and activation depth.

1.2 Testing and Characterization

1.2.1 General Aspects

Due to the new challenges for asphalt pavement technology, the variety of products on the market develops almost progressively, thus accumulating uncertainty for customers and professionals who may not be able to rely on conclusive performance and test data. This situation increases the risk of failures and calls for intensive industrial empirical and scientifically driven multi-scale research that comprises the whole chain of knowledge from mega [dam…km], magno [dm…dam], meso [mm…dm], micro [µm…mm] even down to nano [nm…µm] scale, where simple stress-strain concepts start to fail and sophisticated analytic tools like atomic force microscopy AFM are used nowadays almost on a routine base. In fact, detecting "bee" or "3D-Toblerone®" structures on binder surfaces with AFM has recently created much excitement and discussion in the field of asphalt pavements (e.g. Dos Santos et al. 2016), proving that technology of asphalt pavement materials has finally successfully arrived in the scientific heaven with the challenge, of course, to keep its feet on the road.

Research in this scientific environment comprises advanced test methods such as Computed Tomography CT (Partl et al. 2003) for studying the inner aggregate and air void structure in compacted asphalt and neutron radiography with synchrotron light source for studying water uptake (Poulikakos et al. 2013) as well as refined tools for modelling either numerically or analytically. Besides of traditional numerical Finite Element Models FEM for small deformations, less common approaches, such as Discrete Elements Models DEM for large deformations (Ghafoori Roozbahany et al. 2015) or multiphase Lattice Boltzmann models LBM are used (Son et al. 2016).

The increasing variety of asphalt pavement materials means that many of the traditional test setups and empirical characterization methods for binders and mixtures are no longer a priori applicable and may even lead to erroneous conclusions. Penetration, for example, successfully used for classifying standard bitumen, is no longer meaningful in case of certain polymer modified bituminous binders. The same is true for the Marshall test which is not applicable for special asphalt mixtures, such as porous asphalt. In the Rilem state of the art report volume IX (Partl et al. 2013) it was made clear that test methods can only be applied in a general way if they are proven to be applicable for all three basic concepts of load carrying functions of asphalt mixtures as shown schematically in Fig. 1.3, i.e.

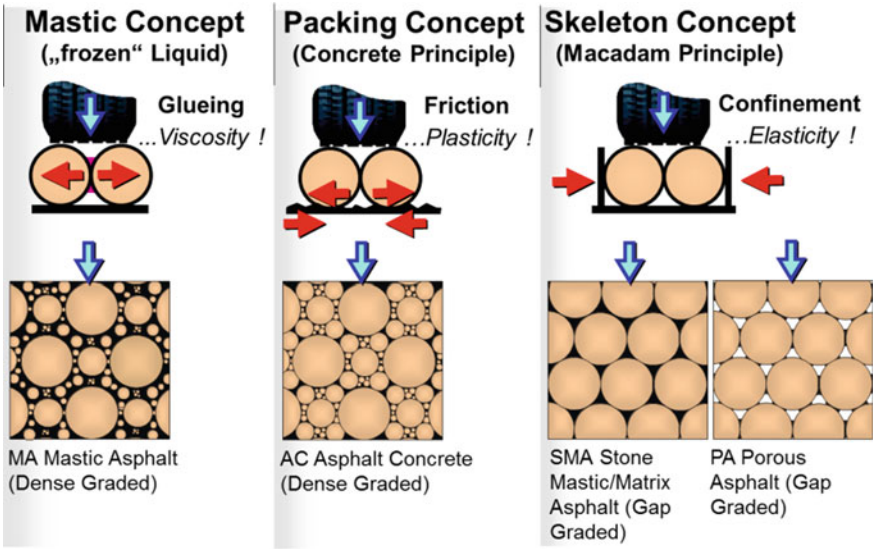

Fig. 1.3 Basic concepts for structural functioning of asphalt pavement mixtures (from Partl et al. 2013)

- **mastic concept** (frozen liquid principle),
  i.e. high binder content and virtually no air voids; aggregates “swim” in bituminous mortar matrix; load is mainly carried by the binder
- **packing concept** (concrete principle),
  i.e. densest packing of aggregates with minimal binder film thickness; load is carried by aggregates and binder
- **skeleton concept** (macadam principle),
  i.e. corn-to-corn contact and interlock of stones; load is primarily carried by aggregate skeleton; lateral support and confinement within layer is necessary.

In order to avoid that tests are used for cases other than developed for, and in order to support the development of new innovative bituminous pavement materials and systems, an almost uncountable number of test methods for individual material components, different asphalt mixtures and whole pavement systems were and are still developed. This creates lack of comparability, thus contributing to general confusion regarding the practical success of those innovations.

Moreover, there is also a lack of experience on long term behavior or on specific safety relevant questions, such as surface drying effects (e.g. Lal et al. 2016). This creates an increasing need for accelerated pavement testing with traffic load simulators for verifying new developments, based on the understanding that lab scale testing must be complemented by full-scale evaluation and validation, thus minimizing the risk of expensive development failures and for adapting the quality standards to constantly increasing needs and demands (Partl et al. 2015). However, since these

mechanical torture tests are generally quite expensive and time consuming they are often not conducted tempted by accepting the risk of failure in the field.

1.2.2 Testing of Reinforced Asphalt

Introducing reinforcing elements into asphalt pavement materials means that traditional test methods may be no longer applicable or meaningful and must therefore be adapted or complimented with new tests based on additional knowledge and newly developed equipment. Due to the character of the reinforcing elements (e.g. different densities and shapes), traditional mixture design methodologies may not be applicable and must be replaced (e.g. by volumetric instead of gravimetric material design or by discarding simple sieve size considerations) or complemented with design considerations for the pavement as multi-layered reinforced system. Hence, size effect questions as well as the search for the most representative test specimens are getting into new focus. This is particularly true in cases where the reinforcement elements are not only introduced into an asphalt matrix but in the interface between different pavement layers. In such cases, small-scale laboratory tests may have to be complemented by medium- scale or full-scale traffic load simulator tests. In any case, it is very important to be aware of the reinforcement mechanisms and the expected performance in practice before designing a test.

Reinforcing asphalt pavements is a subject that is particularly challenging due to their viscoelastic nature. At high temperatures, asphalt loses its elastic properties turning towards viscos behavior, whereas at low temperatures elastic properties become dominant. This means that at high temperatures creep deformations and stress relaxation have to be taken into account which are unfavourable for anchoring reinforcement elements and hamper durable load transfer between reinforcement and the surrounding asphalt matrix. In contrast, reinforcement at low temperatures is feasible.

When reinforcing, first, the key questions must be answered in what respect, under what conditions and in what loading direction reinforcement should be achieved. Should reinforcements serve for

- taking care of tension, compression, shear of bending mode,
- crack bridging, crack distribution or crack prevention,
- anisotropy induced load distribution (e.g. in case of rutting),
- reduction of stress concentrations (e.g. reflective racking),
- changing mechanical and thermal properties (in terms of strength deformability, modulus),
- providing new properties, e.g. healing?

Ignoring those questions often leads to confusions and misunderstandings in practice. As shown in Fig. 1.4a and b, for the general case of tension, reinforcement could mean stiffening by changing the modulus E, strengthening by boosting the

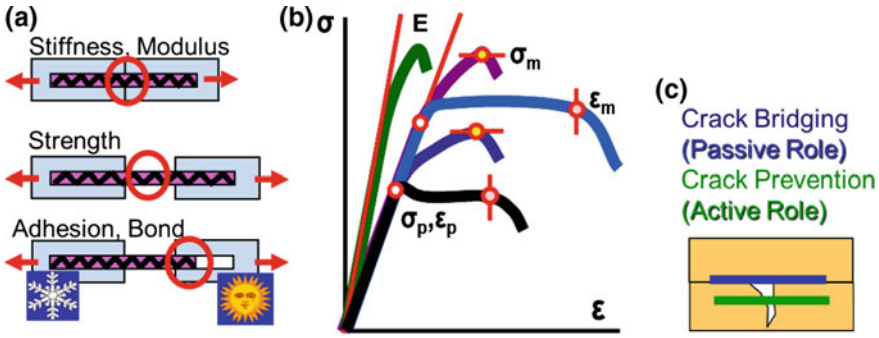

Fig. 1.4 Reinforcement strategies

maximum stress σ_m, increasing the stress and strain at the limit of proportionality σ_p, ε_p, extending (or reducing) maximum strain ε_m, etc.. Besides of stiffness and strength issues, anchoring or bond in the interface between reinforcement elements and the surrounding material must also be considered. This is particularly challenging with surrounding viscoelastic materials, where time and temperature dependent bonding may not only be affected by adhesion but also by strain jumps at the interface, when too extreme differences between moduli of the reinforcement and matrix materials occur. These effects are one reason why, in case of bituminous materials, the active role of reinforcement elements for crack prevention is often replaced by crack bridging mechanisms, where reinforcements take a passive role, such as in case of reflective cracking with crack propagation induced from the lower to the upper layer.

Fibers in bituminous materials are used in many variations, such as mineral, cellulose, carbon, polymer, glass and steel fibers in different dimensions, from millimeter down to micro- and nano- meter scale. They are claimed to have reinforcing properties by increasing fatigue, crack and aging resistance, stiffness, binder thickness, etc.. However, reinforcing asphalt with fibers is not discussed without controversy, because the mixing process may partly damage the fibers or lead to clusters and disorientation of fibers (Garcia et al. 2014). Those aspects must be taken into account by introducing new tests, such as CT.

Grids (or felts) are generally placed between two pavement layers and need testing within a representative part of the whole pavement system. Products available consist of steel, carbon, glass, polymer and basalt strings or fibers. For those reinforcing elements, bonding properties and mechanical effectiveness are crucial and must be tested according to their expected application. For example, flexible pavements suffering significant static or dynamic bending deformation must be constructed and tested with a reinforcement reasonably away from the neutral axis and fixed in the interlayer by a bonding mechanism, strong enough to resist delamination under infiltrating water or bottom-up crack induced stress fields. Figure 1.5 shows simple examples of possible performance related system test configurations in the laboratory. Shear bond (c) can be conducted in different ways,

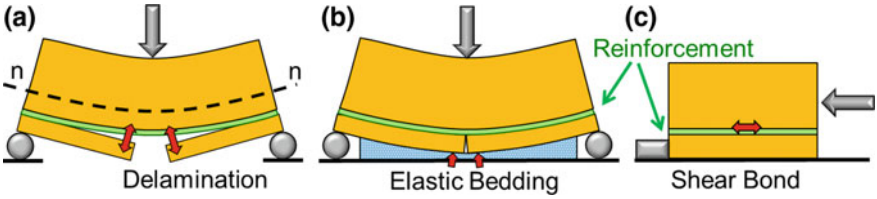

Fig. 1.5 Reinforcement testing

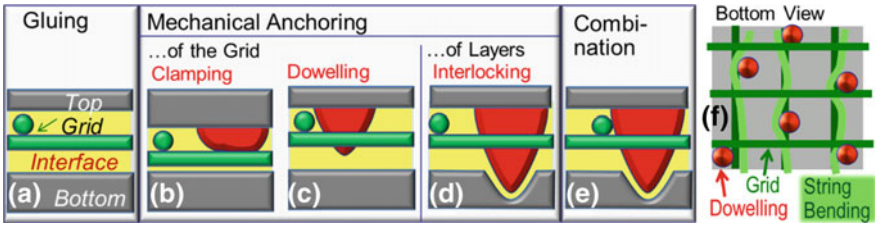

Fig. 1.6 Reinforcement mechanisms and strategies

such as direct, indirect and wedge splitting tests, whereas bending is possible with all kinds of vertical loading setups, from single load to moving wheel loads without (b) and with (c) elastic bedding (Raab et al. 2017). In the few practical cases, where delamination is of concern, direct, indirect tensile or peeling tests may also be justified, e.g. in case of blister formation (Hailesilassie et al. 2015).

Figure 1.6 provides an overview on principal interlayer bonding mechanisms that could serve for reinforcement strategies. On the one hand, one can completely rely on gluing the grid with a bond-coat into the interface between the top and bottom layer (a). With this approach all stresses and strains are transferred through the bond-coat, with the disadvantage that its viscoelastic properties are the critical functional key factors, but with the advantage that the different strings of the grid can be fully mobilized for transferring tension within the reinforcement grid in a straight way. On the other hand, one can consider complementing gluing by different kinds of mechanical anchoring, such as clamping (b) and dowelling (c) with aggregates or other suitable components added to the freshly applied and compacted top layer. This could mitigate the negative effects from gluing but increase the risk of disturbing the straight transfer of tension within the strings of the grid (d). With freshly applied bottom and top layers or appropriately grinded old bottom layers, mechanical interlocking of both layers with the reinforcement in addition to gluing may be possible. However, doweling and mechanical interlocking means that the strings of the grid perpendicular to the main reinforcing direction may be bent, thus compromising straight tension transfer in that direction (f).

1.3 Scope of This Book

Different environmental aspects and their relevance for testing, characterizing and understanding the mechanical behavior of modern asphalt pavement materials and systems are addressed. Emphasis is on aggregate-binder interaction, three-dimensional time-dependence of mixtures, characterization of reinforced asphalt layer interfaces, chemical and rheological aging characteristics of RAP-binder from HMA and, finally, on classification and characterization of cold recycled RAP. Tests are evaluated and discussed through comparative interlaboratory campaigns or round robin tests (RRT), following the principles for planning interlaboratory tests as outlined by Partl et al. (2013). These campaigns were all organized, performed and analyzed through voluntary effort, driven by the technical and scientific commitment of all participants and guided by their understanding that quality increase and new developments can only be successful with meaningful tests that include environmental aspects as key to sustainable application of bituminous materials and systems for roads. This enormous voluntary work deserves grateful recognition and acknowledgement from the asphalt community.

The first of the following Chapters concentrates on a comparative interlaboratory evaluation of different common test methods for estimating the affinity between aggregates and bituminous binder under the influence of water. It deals with simple technological, partly standardized test methods for assessing and characterizing resistance of asphalt against stripping. Thus, it addresses a subject crucial for long term durability of asphalt pavements under rainy conditions that depends on a wide range of influence factors, such as temperature and loading history as well as pavement and material structure and composition. Results of binder coating and bond strength interlaboratory tests with different binders and aggregates are presented and discussed in terms of repeatability and reproducibility.

The next Chapter is devoted to interlaboratory tests for measuring Poisson's ratio of compacted asphalt mixtures under uniaxial harmonic sinusoidal loading. Since it was not possible for all laboratories to perform the tests under exactly the same conditions, results are compared with reference to a three dimensional linear viscoelastic model, using successfully the same shift factor for both complex modulus and complex Poisson's ratio. It is shown that these results are in remarkably good agreement, but the scatter between the labs increases with low frequencies. Testing is reported to require special care, in particular regarding three-dimensional measurements, temperature monitoring, accuracy of measurements and setting-up of boundary condition. Nevertheless, it is shown that cyclic uniaxial tests appear promising for determining three-dimensional linear viscoelastic behavior of homogeneous bituminous mixtures.

The subsequent Chapter deals with bonding and horizontal shear transfer of grid reinforced asphalt layer interfaces. Interlaboratory tests with different types of grids are presented that were performed on double layered asphalt concrete specimens from field test sections and compared for their ranking potential and consistency with in-field performance of corresponding sensor equipped test sections under

heavy traffic. Interlayer shear tests, pull-off, static and dynamic bending tests, modified wheel tracking and the so-called tensile-bending test are discussed in terms of efficiency and functionality of grids for reinforcing asphalt concrete, taking into account temperature and speed effects. Discussions include interlayer debonding, the impact of grid reinforcement on flexural toughness and resistance against reflection cracking.

In the next Chapter four reliable ways of characterizing the aging of RAP from HMA are studied. Besides of the heterogeneity of RAP stockpiles, aging is one of the main issues, when recycling RAP in road structures. Work reported here refers to the database of an earlier interlaboratory effort on laboratory produced and plant mixtures that were subject to different aging conditions. It evaluates the results of a round robin test (RRT) for characterizing the chemical aging of recovered bitumen from these mixtures with fourier transform infrared spectroscopy (FTIR). This is done by determining different aging indexes and their relation to rheological parameters of a viscoelastic serial model composed of one Maxwell model and two nonlinear parabolic creep elements, as determined from DSR measurements.

The last Chapter focuses on cold recycling of RAP taking into account that significant differences to HMA technology have to be considered. It contains an extensive literature review on standards and methods for RAP mixtures with emulsions and foam bitumen, seeking a way for proposing steps towards an internationally recognized classification for RAP. Moreover, it discusses central topics such as specimen preparation and curing processes for cold RAP mixtures. In a round robin test, key elements for classification of RAP are validated, such as RAP particle size before and after bitumen extraction (i.e. “black” and “white” curve), characterization of particles and recovered binder, fragmentation resistance of aggregates against repeated shock or impact and, finally, cohesion with indirect tensile test (ITS) on compacted original RAP material.

References

Dos Santos S, Poulikakos LD, Partl MN (2016) Crystalline structures in tetracosane-asphaltene films. RSC Adv 6:41561–41567. https://doi.org/10.1039/C6RA03708A

Garcia A, Bueno M, Norambuena-Contreras J, Partl MN (2014) Influence of steel wool fibers on the mechanical, thermal and healing properties of dense asphalt concrete. J Test Eval 42(5):1–12. https://doi.org/10.1520/JTE20130197

Ghafoori Roozbahany E, Partl MN, Guarin A (2015) Particle flow during compaction of asphalt model materials. Constr Build Mater 100:273–284. https://doi.org/10.1016/j.conbuildmat.2015.09.061

Hailesilassie B, Hean S, Partl MN (2015) Testing of blister propagation and peeling of orthotropic bituminous waterproofing membranes. Mater Struct 48(4):1095–1108. https://doi.org/10.1617/s11527-013-0217-z

Jeoffroy E, Koulialias D, Yoon S, Partl MN, Studart AR (2016) Iron oxide nanoparticles for magnetically-triggered healing of bituminous materials. Constr Build Mater 112:497–505. https://doi.org/10.1016/j.conbuildmat.2016.02.159

Lal S, Moonen P, Poulikakos LD, Partl MN, Derome D, Carmeliet J (2016) Turbulent airflow above a full-scale macroporous material: boundary layer characterization and conditional statistical analysis. Exp Therm Fluid Sci 74:390–403. https://doi.org/10.1016/j.expthermflusci.2016.01.005

Liu Q, Schlangen E, García A, van de Ven M (2010) Induction heating of electrically conductive porous asphalt concrete. Constr Build Mater 24(7):1207–1213. https://doi.org/10.1016/j.conbuildmat.2009.12.019

Partl MN, Flisch A, Jönsson M (2003) Gyratory compaction analysis with computer tomography. J Road Mater Pavement Design 4:401–422. https://doi.org/10.1080/14680629.2003.9689956

Partl MN, Bahia H, Canestrari F, De la Roche C, Di Benedetto H, Piber H, Sybilsky D (2013) Advances in interlaboratory testing and evaluation of bituminous materials. RILEM State-of-the-Art Report 9:453. https://doi.org/10.1007/978-94-007-5104-0

Partl MN, Raab C, Arraigada M (2015) Innovative asphalt research using accelerated pavement testing. J Mar Sci Tech JMST 23(3):269–280. https://doi.org/10.6119/JMST-014-0326-1

Poulikakos LD, Sedighi Gilani M, Derome D, Jerjen I, Vontobel P (2013) Time resolved analysis of water drainage in porous asphalt concrete using neutron radiography. Appl Radiat Isot 77:5–13. https://doi.org/10.1016/j.apradiso.2013.01.040

Raab C, Arraigada M, Partl MN, Schiffmann F (2017) Cracking and interlayer bonding performance of reinforced asphalt pavements. Eur J Environ Civ Eng (EJECE). https://doi.org/10.1080/19648189.2017.1306462

Son S, Chen L, Kang Q, Derome D, Carmeliet J (2016) Contact angle effects on pore and corner arc menisci in polygonal capillary tubes studied with the pseudopotential multiphase lattice Boltzmann model. Computation 4(1):12. https://doi.org/10.3390/computation4010012

Chapter 2
Bituminous Binder

Laurent Porot, Hilde Soenen, Jeroen Besamusca, Alex Apeagyei, James Grenfell, Stefan Vansteenkiste, Emmanuel Chailleux, Vincent Gaudefroy, Preeda Chaturabong, Cristina Tozzo, Ignacio Artamendi, Darius Sybilski, Francisco Barcelo Martinez, Said Safwat, Manfred N. Partl, Francesco Canestrari, Elisabeth Hauser and Michael Wistuba

Abstract One of the most important aspects of asphalt pavement deterioration is the ingress of water in pavement which leads to loss of the material characteristics, even material integrity with loss of aggregates. Thus the behaviour of asphalt mixture under moisture conditions is one of the key parameter for specifications. It's a complex phenomenon which is influenced amongst other things by materials properties with wetting, cohesion and adhesion of bituminous binder and by environmental conditions with temperature, moisture, loading and layer type. It has been a research subject for a very long time and still not precisely described. A large

L. Porot (✉)
Kraton Chemical, Almere, The Netherlands
e-mail: laurent.porot@kraton.com

H. Soenen
Nynas, Machelen, Belgium

J. Besamusca
Kuwait Petroleum, The Hague, The Netherlands

A. Apeagyei · J. Grenfell
University of Nottingham, Nottingham, UK

S. Vansteenkiste
Belgium Road Research Center, Brussels, Belgium

E. Chailleux · V. Gaudefroy
LUNAM Université, IFSTTAR, Bouguenais, France

P. Chaturabong
Wisconsin University, Madison, USA

C. Tozzo
University Roma La Sapienza, Rome, Italy

I. Artamendi
Aggregates Industries, Coalville, UK

D. Sybilski
Road & Bridge Research Institute, Warsaw, Poland

M. N. Partl et al. (eds.), *Testing and Characterization of Sustainable Innovative Bituminous Materials and Systems*, RILEM State-of-the-Art Reports 24,
https://doi.org/10.1007/978-3-319-71023-5_2

number of test methods is available to estimate the affinity between aggregates and bituminous binders. These test methods can be subdivided in different ways; a first distinction can be based on the presence or absence of water during the test procedure. If water is present, the evaluation is in fact referred to as water sensitivity or moisture damage testing. Another distinction can be based on the type of sample that is evaluated. The test sample can be loose aggregates coated with a bituminous binder or a compacted asphalt mix sample. Lastly the individual components, bitumen and aggregate, can be tested separately through intrinsic properties. Furthermore, test results can also be based on the quantification of the test results, whether this is based on a qualitative or a quantitative evaluation. In RILEM TC 237 SIB, TG1 the main purpose was to evaluate common test methods, used to assess the affinity of bitumen to aggregate surfaces, to determine, if possible, the repeatability and reproducibility and to give recommendations for improvement. In this study both binders and aggregates have been considered. Three bituminous binders, two unmodified from different sources, one polymer modified binder, and four aggregate types, with different mineralogy, have been selected. The test methods considered in the study include the rolling bottle test, the boiling water stripping test and the bitumen bond strength test; also surface energy was investigated. This chapter presents the results of these tests and their accuracy.

Keywords Bituminous binder · Aggregate affinity · Round Robin test
Water sensitivity · Durability · Surface energy · Adhesion · Rolling bottle test
Boiling water test · Bitumen bond test

2.1 Introduction

One of the most important aspects of asphalt pavement deterioration is the ingress of water in pavement which leads to loss of the material characteristics, even integrity with loss of aggregates. Thus the behaviour of asphalt mixture under moisture conditions is one of the key parameters for specifications. The water

F. B. Martinez
Repsol, Madrid, Spain

S. Safwat
VTI, Linköping, Sweden

M. N. Partl
EMPA, Dübendorf, Switzerland

F. Canestrari
Universita Politecnica Delle Marche, Ancona, Italy

E. Hauser · M. Wistuba
ISBS Braunschweig University, Braunschweig, Germany

damage phenomenon is more than complex. The manufacturing of asphalt materials, the type of material with granular composition, void contents, the layer position in the pavement, the climate conditions with temperature and moisture, the loading case either with high shear or high/low speed certainly influence the end behaviour. For the bituminous binder its wetting ability, the cohesion and adhesion properties and to some extent the chemical composition are also parameters affecting the water sensitivity of asphalt materials.

A large number of test methods is available to estimate the affinity between aggregates and bituminous binders. These test methods can be subdivided in different ways; a first distinction can be based on the presence or absence of water during the test procedure. If water is present, the evaluation is in fact referred to as a water sensitivity or moisture damage test. Another distinction can be based on the type of sample that is evaluated and different levels towards moisture damage can be considered. Level 1 is for the individual components, stone and bitumen separately. Level 2 is testing loose mix or a coated stone. Level 3 is on compacted asphalt mixture. And level 4 is on the road itself. Each level adds a different degree of complexity, for example in the compacted asphalt mixture, void content is key; on the pavement, construction, in situ density, and traffic are influencing the end performances. Finally, test methods can also be based on the test results, whether a qualitative or a more quantitative evaluation is obtained.

In RILEM TC 237 SIB TG1, the main purpose was to evaluate common test methods, used to address the affinity of bitumen to aggregate surfaces, to determine, if possible, the repeatability and reproducibility and to give recommendations for improvement. The results obtained from different test methods were compared together.

Three bituminous binders have been selected, two unmodified from different sources and a polymer modified binder. And four aggregate types with different mineralogy have also been selected.

The test methods considered in this study so far included the rolling bottle test with eight laboratories, the boiling water stripping test with three laboratories and the bitumen bond strength test with three laboratories.

Furthermore, the results were compared with a more fundamental assessment of the intrinsic properties of bituminous binder and aggregates through surface energy measurement by two laboratories.

2.2 State of the Art

Adhesion of a bituminous binder onto aggregates is a quality criterion for the mixture performance and durability (Corte et al. 2004; Jakarni 2012). In particular, loss of adhesion can occur when water enters through the bitumen/mineral substrate interface (Bagampadde and Karlsson 2007). As the substrate presents more affinity for water, bitumen is displaced and the mixture's moisture resistance decreases (Hanz et al. 2007). Adhesion is described following several mechanisms (Tan and Guo 2013; Rychen et al. 2010):

- Mechanical adhesion, which causes strong bonding when the binder covers the asperities and fills the voids of the substrate;
- Chemical adhesion, which relates to the high affinity between the acid compounds of bitumen and the basic species from the aggregates;
- Surface free energy theory, which describes the surface energy evolution of the mineral when the binder wets the surface;
- Molecular orientation, which is explained by the orientation adsorption of polar molecules onto bitumen and substrate surfaces;
- Electrostatic adsorption, which indicates the affinity to each other for two materials having opposite charges.

In the dry state, adhesion strength of bituminous mixtures is mainly a function of the cohesive strength of the bitumen. In the presence of moisture, adhesion strength depends on substrate mineralogy (Zhang et al. 2015; Apeagyei et al. 2014, 2015). In road engineering, the bitumen/limestone combination exhibits strong adhesion even when exposed to moisture. However, siliceous aggregates are subject to stripping (Bourrel and Verzaro 1998) when exposed to moisture. Surface texture of the aggregate also plays an important role in adhesion (Yazgan 2003). Binder properties and operating conditions may also affect the wettability and the adhesion (Rychen et al. 2010; Some et al. 2013, 2014; Ziyani et al. 2016).

As adhesion is the bonding between two different materials, in any case of testing one needs two materials to investigate the adhesion phenomena. However each component, separately, have their intrinsic characteristics that can provide an estimation of combined adhesion. For example for the aggregates this could be based on the mineralogy or also the refractive index (Laurell Lyne et al. 2013a, b).

Finding an adhesion test for road applications has been a long search starting in the early 1900s. The Riedel and Weber test (1933) is a visual test that was published in 1933 and uses boiling water doped with increasing sodium carbonate concentration. Several other visual similar tests were introduced (Curtis 1990). Andersland and Goetz showed in (1955) that a sonic test can give information on the deterioration of asphalt mixes. An overview of different tests with pros and cons are published by Mathews et al. in (1965). In 1973 the interaction between bitumen and aggregate was investigated with the micro calorimetric method (Ensley 1973).

In the 80s and 90s during the Strategic Highway Research Program (SHRP) a huge amount of data was gathered, reviewed and published and made available on internet. Some reports combine molecular structures of bitumen components with aggregate components to identify possible adhesion and absorption (Jeon and Curtis 1992; Curtis et al. 1993; Lee et al. 1990; Tarrer and Wagh 1991). Other reports showed proof of test methods with road experience (Hicks and Finn 1994). Several literature sources concluded that binder or aggregate alone was not valid to rank but pairs are needed for ranking (Scholz et al. 1994; Terrel and Al-Swailmi 1994). The amount of papers concerning the adhesion over time was reviewed by Renken et al. (2003). He showed two different periods in time, around 1940 and around 1960. The concern on adhesion was high resulting in more published work on this topic.

Then it was end of 80s that new interest resulted in a state of the art report (NCAT 1988).

Recent studies followed different paths to identify adhesion. For example Chaudhury et al. (1992), Chaudhury (1996) and Chung and Chaudhury (2005) published, among other publications on adhesion and a Science review on the contact angle measurements in 1992. Several theses (Shah 2003; Hefer 2004; Bhasin 2006) and publications (Howson et al. 2011; Hirsch et al. 2009) relate the same topic to asphalt mix performance.

The adhesion between aggregate and binder was identified as one of the most important parameters influencing moisture sensitivity. The importance of anti-stripping material was one of the solutions for the problem (LTRC 1995). Congresses and workshops addressing only moisture sensitivity (Committee 2003) were organised to discuss the experience and way forward. The outcomes revealed that 78% of the US agencies tested asphalt mix for water sensitivity. Over 80% used the indirect tensile test to indicate resistance against loss of adhesion. Gubler et al. (2005) showed that actually the ITS-test is not the best method to be used and recommended the Coaxial Shear Test (CAST) instead. Wong et al. showed that the Asphalt Pavement Analyser (APA) can identify the influence of water on permanent deformation (Wong et al. 2004) while Castaneda introduced the use of the mechanical characteristics in a Cole-Cole plot (Castenada Et al. 2004). A new state of art was published by The Royal Institute of Technology of Stockholm (RIO Technology 2003) showing that the modified Lottman was the best test method available but careful selection of materials and good construction practice are essential.

The combined effort of the European Asphalt Pavement Association, EAPA, the Federal Highway Agencies, FEHRL, and the European Bitumen Association, Eurobitume, identified several bitumen properties related to asphalt properties. These were, except for adhesion where the conclusion was "In contrast to other tests, interfacial properties. Therefore, adhesion is possibly the most difficult one to conceive. It has to describe the suitability of binders to adhere to various pavement components such as aggregates, sand and fillers. Although a lot of interesting ideas are included in the tests already described in this chapter, the subject of adhesion still needs future research in order to establish well validated and performance-based specification" (BitVal 2006). In the European committee on standardisation, CEN, the technical committees on TC227 "Road materials" and TC336 "Bituminous binders" combined their effort to identify the current test methods used (Besamusca et al. 2012). They showed that most test methods are related to other aspects than adhesion resulting in ranking of products not related to adhesion and the influence of aggregate is bigger than the bitumen source. Bagampadde et al. also concluded (2006) that the influence of aggregate is more pronounced on adhesion properties than the influence of bitumen.

The adhesive-cohesive behaviour is simulated by the work of Kringos (Kringos et al. 2008) showing that surface energy alone is not enough to predict bitumen-aggregate interaction.

Jorgensen published in (2002) round robin results of the boiling water test based on a slightly modified protocol of the Texas boiling test, where the quantitative test result is obtained by visual evaluation of the residual percentage of coating, and the rolling bottle test. It was shown that the boiling water test, as used in this study, was valid to identify bad combinations of binder and aggregate but the rolling bottle test could rank combinations. Several publications (Grönniger et al. 2010; Källén et al. 2013; Morgenstern et al. 2010; Renken et al. 2010; Grönniger 2008) showed that the visual inspection is very subjective and is the main disadvantage of the method used. Introducing digital analysing techniques could improve the test (Lamperti et al. 2015).

Special attention should be given to the work of Ulmgren (2004). This publication investigated the bonding between mastic and aggregate while almost all other publications focus on binder and aggregates. The mastic-aggregate interaction is of special interest in case of porous asphalt pavement, and is most probably related to ravelling (Mo 2010).

In recent work from KTH and Nynas (Laurell Lyne et al. 2010, 2013) the adhesion between minerals and bituminous binders was estimated from the dispersive, non-polar van der Waal's interaction component of adhesion. In literature (van Oss et al. 1988), the dispersive component can be estimated using the refractive index. This approach was used and allowed ranking minerals and corresponding aggregates according to their degree of stripping; the stripping ranking was derived from literature (Cordon 1979). The study also indicated that aggregates with a refractive index higher than approximately 1.6 are expected to be less susceptible to stripping. And, it was also shown that the elemental composition of a mineral affects its refractive index and hence it's dispersive adhesion to bitumen. Especially the presence of alkali metals was seen as critical for obtaining a good resistance to moisture damage.

The recovery of oil and bitumen from sandstone reservoirs are similar with the research performed on asphalt mix adhesion, but contrary. The recovery from sandstone reservoirs are focussed on the release of oil and bitumen while asphalt mix research wants to increase the adhesion. Both researches aim for the understanding of the process and therefore it is worthwhile to look at the approach of several researchers (Dudásová et al. 2008; Chukwudeme and Hamouda 2009; Tu et al. 2005).

Still new test methods are introduced to gain understanding of the adhesion phenomenon. For example the proposal of the blister tests (Fini et al. 2008) to address the interfacial fracture energy. The fracture energy was also investigated by combining energy from a peeling test and X-ray measurements (Horgnies et al. 2011).

Recent publications combined visual tests with mechanical tests and surface energy (Grenfell et al. 2014; Liu et al. 2014) to find the best fit for roads and even more fundamental properties like van der Waal forces (Laurell Lyne et al. 2013) are investigated. Moisture ingress by diffusion was previously studied by Kassem et al. (2006) and recently by Apeagyei et al. (2014).

Considering the affinity between aggregates and bituminous binder, there are different test methods available. One of the most widely used tests in Europe is the rolling bottle test as described in the standard EN 12697-11. The boiling water stripping test is also part of the EN 12697-11 standard. And in recent years the Bitumen Bond Strength, BBS, test was introduced in the US with AASHTO TP91.

2.3 Organisation of the Round Robin Test

2.3.1 Participating Laboratories

In RILEM TC 237 SIB TG1, the initial intention is to further understand the fundamental mechanism of water interaction in asphalt mixtures, and to review the various test methods available, to identify which test is the most suitable. In these conditions, one main purpose is to evaluate the repeatability and reproducibility of common test methods used to evaluate the affinity of bituminous binder to aggregate surfaces, and to provide recommendations for improvement.

Within the round robin test from TG1, a total of 13 laboratories participated, running different test methods addressing the affinity between aggregates and bituminous binder as listed in Table 2.1. Results from all of these participants were received and further analysed.

2.3.2 Bituminous Binder

A total of three bituminous binders from two different suppliers were used for coating the aggregates. Two unmodified 50/70 paving grade bituminous binders according to EN 12591 and one polymer modified bitumen graded as 45/80-60 PmB according to EN 14023. The basic properties of the three binders are reported in Table 2.2 and were defined in terms of:

- Penetration value at 25 °C in accordance with EN 1426, which reflects the consistency of the bitumen at ambient temperature. The higher it is, the softer the bitumen is.
- Ring and ball temperature (softening point) in accordance with EN 1427, which reflects the consistency of the bitumen at high temperature. The higher it is, the more heat the bitumen needs in order to soften (or to flow).

The three bituminous binders had similar values in term of penetration values at 25 °C meaning that their consistency/viscosity at ambient temperature were in the same range of magnitude. Thus test run at ambient temperature should eventually not to be affected by the binder consistency. On the other hand, the softening point temperature for the polymer modified binder was higher around 60 °C, than those for the neat binders. Thus, the tests run at high temperature may be expected to have different results if viscosity is affecting the cohesion/adhesion of the bitumen with aggregates.

Table 2.1 List of the laboratories participating in the RRT and their tests

Institution	Country	Test method	Standard
IBDiM	Poland	Rolling bottle	EN 12697-11 clause 5
Nynas	Belgium	Rolling bottle	EN 12697-11 clause 5
University of Nottingham	UK	Rolling bottle	EN 12697-11 clauses 5
		Bitumen bond strength	ASTM D 4541
		Surface energy	In house method
Repsol	Spain	Rolling bottle	EN 12697-11 clause 5
IFSTTAR	France	Boiling water stripping	XP T66-043
		Angle contact between rock and binder	Specific device drop method
Arizona Chemical	The Netherlands	Rolling bottle	EN 12697-11 clause 5
BRRC	Belgium	Boiling water stripping	EN 12697-11 clause 7
University of Parma	Italy	Bitumen bond strength	ASTM D 4541
University of Ancona	Italy	Bitumen bond strength	ASTM D 4541
Wisconsin University	US	Bitumen bond strength	ASTM D 4541
VTI	Sweden	Rolling bottle	EN 12697-11 clause 5
		Boiling water stripping	EN 12697-11 clauses 7
TU Braunschweig	Germany	Rolling bottle	EN 12697-11 (A)
University Roma La Sapienza	Italy	Rolling bottle	EN 12697-11 clause 5

Table 2.2 Basic properties of the used bituminous binders

	Unit	Standard	Bit 1	Bit 2	Bit 3
Binder type			50/70	50/70	PmB 45/80-60
Penetration value at 25 °C	×0.1 mm	EN 1426	51	57	50
Softening point temperature	°C	EN 1427	51.2	50.8	65.4

2.3.3 Aggregates

The four aggregates (granite, basalt, greywacke and limestone) were all supplied by Aggregate Industries from different quarries located in the UK. These aggregate types were selected expecting a difference in moisture susceptibility based on the differences in mineralogy or composition.

Granite is an intrusive igneous rock composed of interlocking crystals. It is coarse grained, with similar sized individual crystals randomly arranged. Petrographic examination of the granite used in this study showed that the rock comprised mainly of quartz, feldspars (orthoclase), amphibole and biotite. Feldspars and amphibole grains are angular and coarse grains. Biotite grains, on the other hand, are elongated and smaller than the feldspars. X-ray Fluorescence, XRF, analysis of the granite indicated relatively high silica content of 64%. Silicates in this granite comprise of quartz, feldspars, amphibole and biotite. Quartz is composed of pure silica. Orthoclase feldspars are alumino-silicates containing potassium and are the main component in the granite (46%). Amphibole is an inosilicate or chain silicate containing iron and magnesium in its structure. It might also contain sodium and calcium. Biotite is a phyllosilicate (sheet silicate) mineral rich in iron and magnesium.

Basalt is a fine-grained igneous rock comprised primarily of plagioclase feldspars, pyroxene and quartz. Plagioclase feldspars are alumina-silicates with different percentages of sodium and calcium. Pyroxene, on the other hand, is an inosilicate mineral containing calcium, sodium, iron and magnesium. XRF analysis of the basalt indicated a silica content of 50% approximately.

Greywacke is a sedimentary rock belonging to the sandstone group. Petrographic examination showed that greywacke aggregate comprised of several mineral grains namely quartz, feldspars, chlorite and biotite. Quartz and feldspars grains are angular and relatively coarse grains. Chlorite and biotite mineral grains, on the other hand, are elongated and smaller in size. Moreover, in the greywacke coarse angular quartz and feldspar grains are cemented by the much finer matrix of chlorite and biotite minerals. XRF analysis of the greywacke indicates relatively high silica content (66%). The silica combines with the main oxides (iron, magnesium, calcium, sodium and potassium oxide) to form the silicates. In the greywacke theses silicates comprise of quartz, feldspars, chlorite and biotite. Quartz is composed of pure silica. Feldspars are alumina-silicates containing potassium, sodium and calcium. Chlorite and biotite are phyllosilicate minerals, i.e. with a tendency to split along defined crystallographic structural planes, rich in iron and magnesium.

Limestone is a sedimentary rock formed in a marine environment from the precipitation of calcium carbonate and compressed to form a solid rock. It is composed primarily of calcium carbonate ($CaCO_3$) in the form of calcite. Petrographic examination of the limestone used in the study showed an almost single mineral phase nature of the aggregate.

The aggregates can be ranked according to their degree of stripping as slight (greywacke), slight to moderate (limestone and basalt) and severe (granite)

(Hicks and Finn 1994). However, limestone, in particular if it consists almost exclusively of calcite, has been classified as having a good resistance to stripping (Laurell Lyne et al. 2013a). Therefore, it was expected that a reliable laboratory test should be able to distinguish between the mixtures based on the selected aggregates. The aggregates were supplied as crushed with nominal aggregate size expected of 8/11 mm. Bulk stones were also supplied for the bitumen bond strength test.

2.3.4 Experimental Procedure

2.3.4.1 Rolling Bottle

The Rolling Bottle Test (RBT) was conducted in accordance with EN 12697-11 clause 5 (EN 12697) with minor modifications based on each laboratory practice. It should be noted that the RBT is a subjective test in that affinity is expressed by visual estimation of the degree of bitumen coverage on un-compacted bitumen-coated mineral aggregate particles after the influence of mechanical stirring action in the presence of water (Fig. 2.1).

For the aggregates, only material retained between the 8 and 11 mm sieve was used for conducting the rolling bottle tests. To prepare samples for testing, dust-free aggregate samples weighing 510 g are dried in an oven at 110 ± 5 °C overnight to constant mass and then coated with about 17 g of hot bitumen (150 °C for the 50/70 pen and 180 °C for the 45/80 PmB) binder in a mixing bowl. The aggregate-binder mixture is then cooled loose at room temperature. The mixed material is stored at ambient temperature between 12 and 64 h before testing. Each of the test bottles is filled to about half their volume with cold (5 °C) deionised water, and about 150 g of the loose aggregate-mixture is placed in each bottle before topping the bottle with deionised water to the shoulder (about 2/3 full). The whole assembly

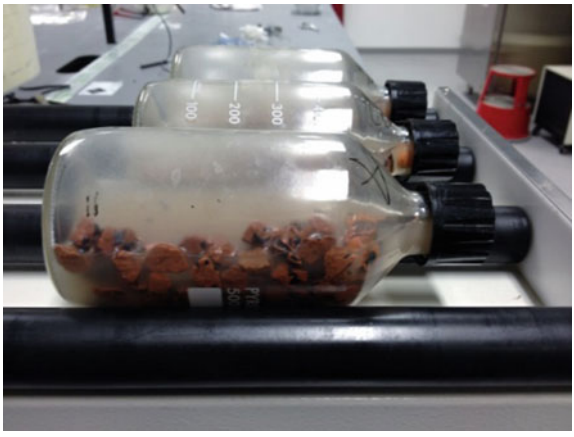

Fig. 2.1 Rolling bottle test equipment

is put in the bottle roller rotating at a speed of 60 rotations per minute for 6 h. The room temperature throughout the test has to be maintained between 15 and 25 °C. At the end of the 6 h period, the aggregate particles are emptied from the test bottle into a test bowl which is then filled with fresh, cold deionised water to a level just above the top of the surface of the particles. Subsequently, the test bowl is placed on a white surface. The purpose of adding fresh water is to allow for optimal visual determination of binder coverage on the aggregate particles. At least three replicates of each sample are tested.

At the end of the test, the degree of bitumen coverage of the aggregate particles is estimated by visual observation and recorded to the nearest 5% using the scale set in the standard EN 12697-11 as per Fig. 2.2. As during the test itself there is a polishing effect of the stone edges more or less important depending on the stone types, which makes difficult to use the variation of mass before and after the test to assess the degree of coating.

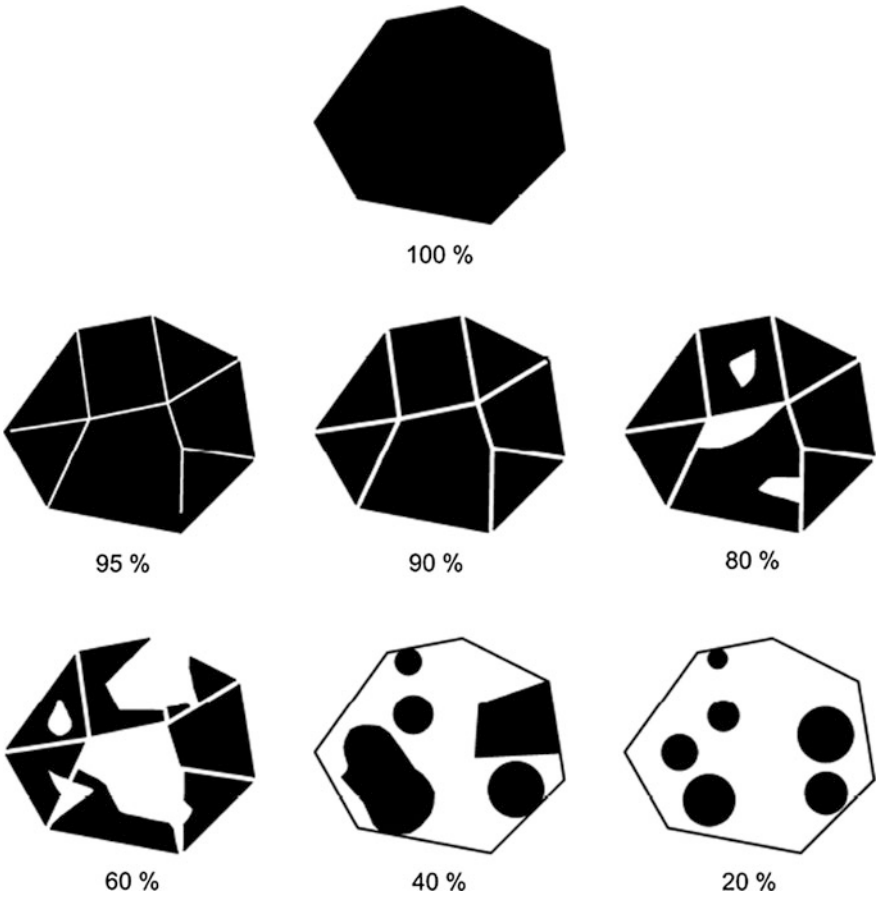

Fig. 2.2 Rolling bottle test scale for bitumen coating (from EN 12697-11)

The degree of binder coverage is defined as the average proportion of the surface area of the aggregate particles that are covered with the binder, expressed as a percentage, 100% being fully coated and 0% being totally uncoated. The degree of binder coverage on the aggregate particles is visually estimated by two experienced technicians independently. The procedure (i.e. rotation in the bottle roller and measuring of binder coverage) is repeated for another cycle up to 24 h and eventually two more cycles (up to 48 and 72 h) with the original fouled water. The degree of binder coverage is estimated as described previously. For each rolling duration (6, 24, 48 and 72 h), the mean value of each technician's recordings of the average degree of binder coverage obtained on the three samples (three bottles) is calculated to the nearest 5%, and the results are averaged to obtain the degree of binder coverage for a given mixture.

In the EN 12697-11 standard, there is not yet an officially established level of precision. It is estimated from normal practice with a coefficient of repeatability and reproducibility of respectively 20 and 30%.

2.3.4.2 Boiling Water Stripping Test

The Boiling Water Stripping (BWS) method, was carried out according to EN 12697-11 clause 7 (EN 12697) and for one laboratory also according to the French standard XP T 066-043 (066-043). The test determines, in a quantitative way, the affinity between any mineral aggregate and bituminous binder combinations in which the mineral is calcareous, silico-calcareous or siliceous by nature. As the percentage of stripping is measured by an acid/base titration while making use of a calibration curve, it is anticipated to be a more objective assessment of the affinity between a binder and aggregate as compared to the rolling bottle method.

More specifically, the procedure involves the coating of 1.5 kg of aggregate of an 8–11.2 mm fraction (basic set plus set 1) with 2.0% by mass of binder. The mixing temperature is equal to the reference temperature for mixtures as defined in EN 12697-35. For the 50/70 pen graded bitumen it is 150 °C. In a next step, a series of mixtures of uncoated (= bare) aggregates and coated aggregates are produced in well-defined proportions (corresponding to 0, 10, 20, 30, 50 and 100% of uncoated aggregate) and subjected to chemical attack of an acid for a predefined time to produce a calibration curve of acid consumption against the proportion of uncoated aggregates. The acid attacks any bare surface of the aggregates and therefore its consumption is proportional to the stripped surface area. The acid to be used is either hydrochloric acid (0.1 N) in case of calcareous aggregates (e.g. limestone) or, in case of aggregates of siliceous nature (e.g. igneous rock), the more reactive and concentrated hydrofluoric acid (1 N) is applied.

In a subsequent step, 200 g of the coated aggregate to be tested is boiled in 600 ml of de-mineralised water for 10 min, allowed to dry and subjected to an acid attack in order to calculate, while using the calibration curve, the degree of bitumen coverage and therefore the extent of stripping (the test result is the average of two individual values of stripping obtained).

In the EN 12697-11 standard a repeatability coefficient of variation of 15% of the determined value is stated (absolute precision threshold on the determination of the stripping of 2%). No reproducibility data have been established yet.

For the French XP T 66-043 standard (66-043), the test is carried out with the granular fraction 6–10 mm. Aggregates are firstly washed and dried in a ventilated oven for 12 h at 110 °C. Then, 100 g of aggregates are mixed with bitumen at the temperature defined in EN (12594), according to penetration grade. The bitumen content is 5% and the mixing time is 60 s. The mix is immersed in hot deionised water at 60 °C for 16 h. The percentage of uncoated aggregates is estimated by visual observation. Results are expressed as follows:

100: when no aggregate surfaces are uncoated
90: for 90% of the aggregate surfaces are coated with bitumen
75: between 75 and 90% of the aggregate surfaces are coated with bitumen
50: between 50 and 75% of the aggregate surfaces are coated with bitumen
<50: less than 50% of the aggregate surfaces are coated with bitumen
0: the binder does not coat the aggregates anymore.

Some examples of visual evaluation are given in Fig. 2.3.
The Table 2.3 compares both test methods.

Fig. 2.3 Example of coating class according to XP T 66-043

Table 2.3 Comparison of boiling water stripping methods

Method	EN 12697-11 clause 7	XP T 066-043
Aggregate	8/11.2 mm	6/10 mm
Weight	200 g	100 g
Binder content	2%	5%
Test temperature	Boiled water	60 °C
Test duration	10 min	16 h
Interpretation	Acid titration after calibration	Visual interpretation

2.3.4.3 Bitumen Bond Strength

Two different types of pull-off adhesion tests were used to characterise the aggregate-bitumen bond strength. They included the standard Bitumen Bond Strength (BBS) test also known as the PATTI test and the new pull-off test. The main advantage of the new pull-off test is the ability to control bitumen film thickness, control loading rate, and test asphalt mastics bonding capability on stone.

The Bitumen Bond Strength test, BBS, (AASHTO TP-91) test uses a Pneumatic Adhesion Tensile Testing Instrument, PATTI®, adapted from the paint and coatings industry (ASTM D4541) (Fig. 2.4).

The test device and procedure have been modified and developed in recent research (Youtcheff and Aurilio 1997 1997) to measure the moisture susceptibility of bituminous binders (Meng 2010; Moraes et al. 2011; Miller et al. 2010). The BBS test protocol requires a bond of an aggregate substrate with a binder under controlled conditions of temperature and humidity. The main components of the BBS equipment are the pressure hose, a portable pneumatic adhesion tester, a piston, the reaction plate and a metal pull-off stub (Fig. 2.5).

Before running a test, the piston is placed over the pull-off stub and the reaction plate screwed on it. Then, compressed air is introduced through the pressure hose to the piston. An upward pulling force on the specimen is applied by the pull-off stub. During the test, failure occurs when the applied pressure exceeds the cohesive strength of the asphalt binder or the adhesive strength of the binder-aggregate interface. The pressure at failure is recorded and the pull-off tensile strength (POTS) is calculated according to the following equation:

Fig. 2.4 PATTI® test equipment

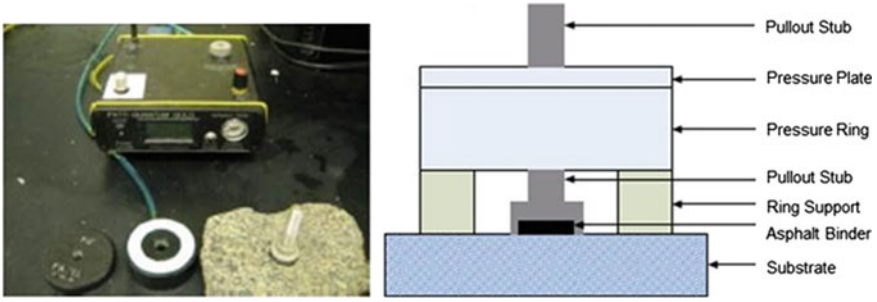

Fig. 2.5 Bitumen bond strength test

$$\text{POTS} = [(\text{BP} * \text{Ag}) - \text{C}]/\text{Aps}$$

where,

Ag contact area of gasket with reaction plate (mm^2)
BP burst pressure (kPa)
Aps area of pull stub (mm^2)
C piston constant

The pull-off stub has a rough surface that can prevent asphalt debonding from the stub surface by providing mechanical interlock and larger contact area between the asphalt binder and stub. The pull-off stub in the new pull-off BBS test has a diameter of 20 mm with a surrounding edge, used to control film thickness. The stub edge has a thickness of 800 μm, as shown in Fig. 2.6. This geometry and surface treatment was described in two extensive recent studies (Meng 2010; Canestrari et al. 2010) in an effort to improve repeatability of the testing system.

Aggregate plates were cut with a constant thickness and parallel top and bottom surfaces. The aggregate plates were then lapped on both sides using 280 grit

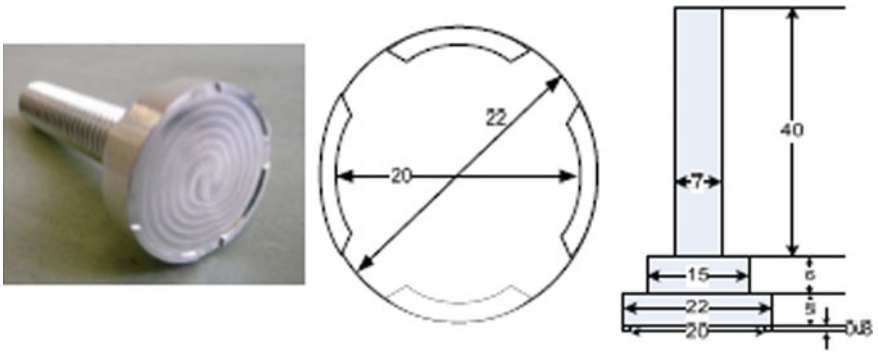

Fig. 2.6 Pull-off stub for the Bitumen bond strength test (BBS)

silicon carbide material after cutting. Lapping is to control the roughness of the surface. After cutting and lapping, aggregate plates are immersed in distilled water in an ultrasonic cleaner for 60 min at 60 °C to remove any residue from the cutting process and neutralise the surface of aggregate to its original condition.

Then the aggregate surface and pull-off stubs are cleaned with acetone to remove moisture and dust, which could affect adhesion. They are heated in an oven at 65 °C for a minimum of 30 min to remove absorbed water on the aggregate surface and provide a better bond between the bituminous binder and the aggregate. The bituminous binders are heated in an oven at 150 °C. The stubs are removed from the oven, and the bituminous binder sample is placed immediately on the surface of the stub for approximately 10 s. Then the aggregate plate is removed from the oven, and the stub with the binder is pressed firmly into the aggregate surface until the stub attaches the surface and no bituminous binder is observed to be flowing out from the bond. The stubs must be pushed down as straight as possible with uniform force, and twisting should be avoided to reduce the formation of trapped air bubbles inside the sample and to minimise stresses. Before testing, dry samples are cured at three temperatures (15, 22, 30 °C) in an environmental chamber for 24 h. For wet conditioning, samples are first cured at room temperature for 1 h to allow for the aggregate-binder-stub system to reach a stable temperature. Then, samples are immersed in a water tank at a specific temperature of 40 °C for the specified conditioning time of 20 h. When the conditioning time is completed, the samples are maintained at room temperature for 1 h before testing.

After testing, the maximum pull-off tension the failure type is recorded. If more than 50% of the aggregate surface is exposed, then failure is considered to be adhesive; otherwise, it is a cohesive failure.

A modified protocol for the new pull-off test was also used to determine bond strength between the aggregates and asphalt mastics as shown in Fig. 2.7

Asphalt mastics were fabricated for testing using a 40/60 pen bitumen, granite fine aggregate and mineral filler. The same mastic has been shown to produce

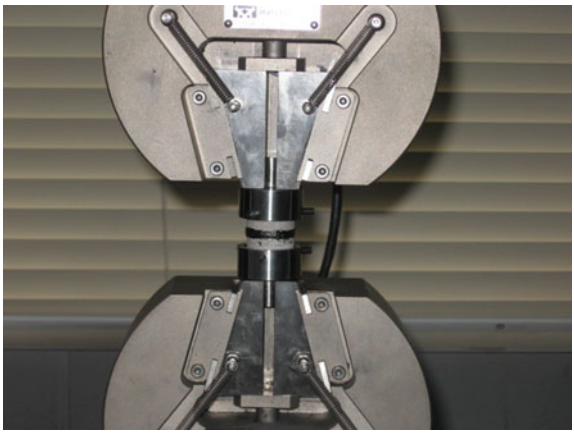

Fig. 2.7 New pull-off test

moisture susceptible bonds with certain aggregate types. Note that the granite used for producing the mastics came from a different source than the one used as substrates in the study. The proportion of the constituent components (fine aggregate, mineral filler, bitumen) of the mastics was 50:25:25 by weight of mixture and was chosen to mimic mastic mix design commonly used in open-graded friction courses. The mastics were produced by combining the dried aggregates and molten bitumen using a Hobart mechanical mixer at a mixing temperature of 185 °C.

The aggregate substrates measuring 20 mm diameter by 20 mm thick cores were obtained using carbide-tipped, electrically operated water-cooled core-drills. The top and bottom surfaces of the substrates were ground using No. 5 sandpaper, to remove all blemishes left by the sawing process, in order to get parallel surfaces to ensure complete adhesion of mastic to aggregate surfaces during the adhesion testing. The fabrication of the substrates was completed by washing the substrates in deionised water (25 °C) and then drying them in an oven at 70 °C for 48 h. For each testing condition (aggregate type, mastic type and moisture conditioning time), six substrates measuring 20 mm diameter by 20 mm thick were cored in order to fabricate three replicate aggregate-mastic butt joints.

The substrates and mastic were heated to a temperature of 140 °C. Small amounts of mastic were then poured into silicone moulds to form mastic films of dimensions approximately 3 mm thick and about 26 mm diameter. The mastic films were annealed to the 20 mm diameter hot (130 °C) aggregate substrates. A second aggregate substrate, also at 130 °C was annealed to the exposed face of the mastic to form a butt joint comprising the 3 mm thick mastic sandwiched between two aggregate substrates. Moisture conditioning was performed at 20 °C by partially submerging the substrate in water such that only about 1–2 mm of the bottom aggregate substrate was exposed to the open air. This arrangement ensured that the aggregate-mastic interface was completely dry at the beginning of a test and, therefore, moisture reached the aggregate/mastic bond only through the aggregate.

2.4 Results of the RRT for Aggregate, Bitumen Affinity

2.4.1 Rolling Bottle Test

A total of 8 laboratories conducted the rolling bottle test following EN 12697-11 clause 5. The test was performed for 6 and 24 h, three laboratories have run the test to 48 and 72 h as well. For these conditions for the three different bituminous binders, four different aggregates and two time periods for eight laboratories and additional two time periods for three laboratories a total of 264 pieces of data were generated and further analysed (Porot et al. 2015).

After each period of the test, the aggregate coating was reported as the percentage of residual binder covering the aggregates, 100% being fully coated and 0% being not

coated anymore. Table 2.4 displays the whole results for all laboratories with, after the 6 and 24 h period, the individual values, the average and standard deviation values. After 48 and 72 h, only the individual values and mean values are displayed.

The standard deviation after 6 h was between 4 and 19%, being lowest for limestone and highest for granite. After 24 h, the standard deviation was between 6 and 21%; still limestone was displaying the lowest value while the granite value was improved as the average value was very low or null. For an intermediate coating value, the standard deviation was high. The determination of

Table 2.4 Rolling bottle test results

	Granite			Basalt			Greywacke			Limestone		
	Bit 1 (%)	Bit 2 (%)	Bit 3 (%)	Bit 1 (%)	Bit 2 (%)	Bit 3 (%)	Bit 1 (%)	Bit 2 (%)	Bit 3 (%)	Bit 1 (%)	Bit 2 (%)	Bit 3 (%)
Rolling bottle results after 6 h												
Lab 1	25	25	35	50	60	75	85	80	80	95	90	95
Lab 2	65	60	70	65	65	65	80	75	85	80	80	85
Lab 3	70	70	75	70	80	90	85	85	95	85	85	90
Lab 4	50	30	70	60	60	75	85	85	85	90	90	95
Lab 5	55	70	70	70	75	80	80	80	80	85	85	85
Lab 6	30	30	70	90	90	100	80	80	95	95	90	95
Lab 10	35	40	50	80	90	95	50	60	70	90	90	90
Lab 13	65	65	70	85	75	90	65	65	85	85	85	85
Average	49	49	64	71	74	84	76	76	84	88	87	90
Std. dev.	17	19	14	13	12	12	12	9	8	5	4	5
Max	*70*	*70*	*75*	*90*	*90*	*100*	*85*	*85*	*95*	*95*	*90*	*95*
Min	*25*	*25*	*35*	*50*	*60*	*65*	*50*	*60*	*70*	*80*	*80*	*85*
Rolling bottle results after 24 h												
Lab 1	0	0	5	10	20	40	30	50	50	85	85	90
Lab 2	20	5	30	20	30	30	75	45	60	75	70	75
Lab 3	30	25	40	30	40	60	60	65	75	65	75	80
Lab 4	5	5	20	15	10	30	40	60	60	60	85	85
Lab 5	20	20	30	60	60	70	50	45	55	65	70	75
Lab 6	5	5	5	35	25	75	20	15	40	80	80	90
Lab 10	5	5	15	20	35	40	25	15	25	70	75	85
Lab 13	15	5	35	60	50	70	30	15	50	75	70	75
Average	13	9	23	31	34	52	41	39	52	72	76	82
Std. dev.	10	9	13	19	16	19	19	21	15	8	6	7
Max	*30*	*25*	*40*	*60*	*60*	*75*	*75*	*65*	*75*	*85*	*85*	*90*
Min	*0*	*0*	*5*	*10*	*10*	*30*	*20*	*15*	*25*	*60*	*70*	*75*

(continued)

Table 2.4 (continued)

	Granite			Basalt			Greywacke			Limestone		
	Bit 1 (%)	Bit 2 (%)	Bit 3 (%)	Bit 1 (%)	Bit 2 (%)	Bit 3 (%)	Bit 1 (%)	Bit 2 (%)	Bit 3 (%)	Bit 1 (%)	Bit 2 (%)	Bit 3 (%)
Rolling bottle results after 48 h												
Lab 2	10	5	5	10	20	15	55	35	35	55	55	70
Lab 4							15	40	35	50	75	80
Lab 10	0	0	5	5	30	30	15	5	10	50	65	80
Average	5	3	5	8	25	23	28	27	27	52	65	77
Rolling bottle results after 72 h												
Lab 2	0	0	0	0	20	15	55	25	25	55	55	65
Lab 4								15	20	50	70	80
Lab 10	0	0	0	0	30	30	5	0	5	40	50	70
Average	0	0	0	0	25	23	30	13	17	48	58	72

Reproducibility was difficult within this round robin test as the number of laboratories was not enough to determine a reliable statistical analysis. For a probability of 95%, this led to reject five values over 100, in other words it requires at least 20 data points to reject one. When considering a probability of 95% resulting in twice the standard deviation, the reproducibility could be assessed as follows (Table 2.5).

The graphs display the results after 6 and 24 h for each aggregate and each bituminous binder. The error bars provide the variability of the results and are equal to minimum and maximum values from the eight laboratories.

Figure 2.8 displays the result after 6 h. The scattering of the results between laboratories was high. Granite aggregates displayed the worst results with values between 25 and 75%. Limestone aggregates displayed good results with limited variability, between 80 and 95%. However it was not discriminating enough to clearly distinguish between basalt and greywacke with values between 50 and 100%. When considering the different binders, the polymer modified binder might display slightly better results, but it was still within the variability of the results.

Figure 2.9 displays the results after 24 h. The scattering of the results was still high but the outcomes become more selective between aggregates. The extreme results, bad results for granite and good results for limestone, were more pronounced. Intermediate aggregates, basalt and greywacke, had intermediate values with a high variation between 10 and 75%. And again the polymer modified binder might display better results but the variability overlaps that of the standard bitumen.

The results after 48 and 72 h were recorded by 3 laboratories and are relevant for the aggregates which remained coated after 24 h. Figure 2.10 presents the results.

Table 2.5 Assessment of the rolling bottle test reproducibility

Value	<25%	>25% < 75%	>75% < 90%	>90%
R	20%	40%	20%	10%

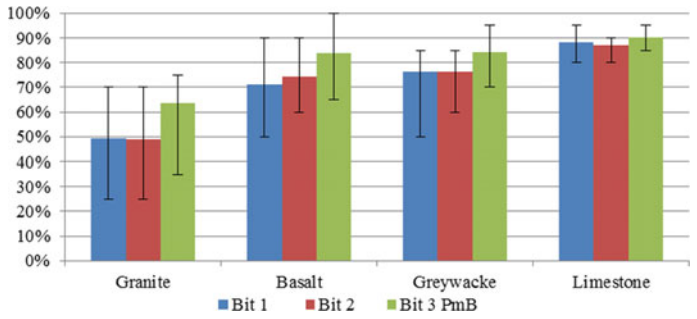

Fig. 2.8 Results of the rolling bottle test after 6 h

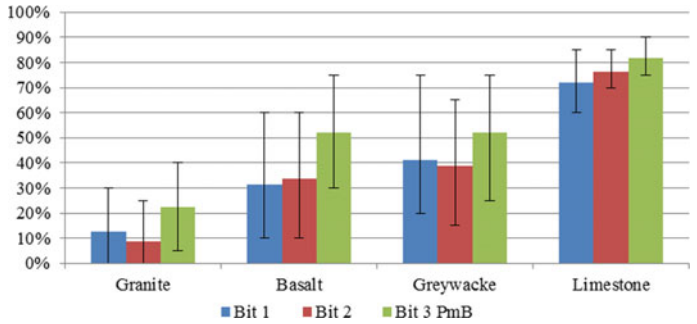

Fig. 2.9 Results of the rolling bottle test after 24 h

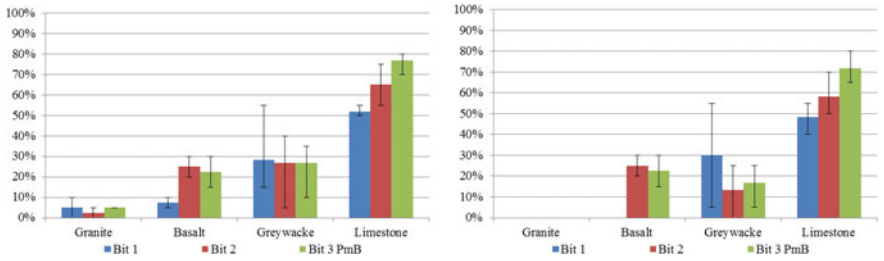

Fig. 2.10 Rolling bottle test results after 48 and 72 h

Each participant of this round robin test used the same standard test method. While the standard describes the different conditions to prepare the sample, to run the test and to interpret the results, there is still some freedom to conduct the test. Six laboratories over the eight reported precisely the test conditions, Table 2.6 summarises the main testing conditions that were reported.

Table 2.6 Rolling bottle test conditions

Laboratory	EN 12-697	Lab 3	Lab 4	Lab 5	Lab 6	Lab 10	Lab 13
Aggregate size	6/10 or 8/11	6/10	8/11	8/11	8/11	8/11	8/11
Washed or not	Washed	Washed		Washed	Washed	Washed	Washed
Factor for agg. density	Eventually	No	Yes	Yes	No	No	Yes
Mixing temperature	For 50/70, 150 °C					150 °C for 50/70 180 °C for PmB	140 °C for 50/70 180 °C for PmB
Waiting time before test	12–64 h at 20 °C					@ 18 h	
Rolling speed	60 rpm	60	40	40 50/70 60 PmB	60	60	60
Temperature at beginning	5 °C			5 °C		5 °C	5 °C
Test temperature	15–25 °C	17 °C		21 ± 2 °C	21 °C	21–25 °C	23 ± 2 °C

Aggregate size is either 6/10 or 8/11, most of laboratories used the 8/11 gradation, only one used the 6/10. In all cases, aggregates were washed before the test. One reported they removed the flat and elongated aggregates from basalt.

As the aggregate density may be different due to the petrographic nature of the stone, the standard advises to adjust the quantity of binder with a density factor, however only 3 laboratories reported they did so.

The mixing, temperature was in accordance with the one required by bitumen grade, 150 °C for the 50/70 pen grade bitumen and 180 °C for the PmB.

After mixing, the coated aggregates have to be kept between 12 and 64 h at 20 °C. However the exact time was not specifically reported by the laboratories.

The speed of the rolling bottle is adjustable according to the grade of the binder; the softer the bituminous binder, the lower the speed is. For the 50/70, only two laboratories used 40 rpm while the others used 60 rpm as recommended by the standard.

Finally the test temperature has to be between 15 and 25 °C. As the test is done at room temperature, there were some variations between laboratories but the temperature was reported between 17 and 23 °C with half of participants running the test at 21 °C.

2.4.2 Boiling Water Stripping Test

Only 2 laboratories conducted the boiling water stripping test according to EN 12697-11 clause 7 and one according to the French XP T 066-043 standard (066-043).

Table 2.7 displays the results for both test methods. The results of the test run according to EN 12697-11 are presented, with the corresponding average values, standard deviation and min/max values. Latter relative deviations permit a comparison with the precision data stated in the current European standard EN 12697-11 clause 7.8.

In this study, no repeated tests were carried out; consequently the determination of the repeatability is not possible. Moreover, as for the EN method, only two sets of data are available, a valid statistical analysis in order to assess the reproducibility of the test method by calculating R-values is also not conceivable (at present no reproducibility data are recorded in EN 12697-11 clause 7.8). Therefore, in order to evaluate the results summarised in Table 2.7, relative differences between the average values and individual laboratories were matched against the repeatability coefficient of variation of 15% as indicated in the European standard, although the latter criterion is based on results generated by one laboratory. However, by performing such an exercise, the limited data available can be discussed in terms of precision. The findings of the latter comparison include:

- All relative maximal differences between a test result obtained by one laboratory and the average result are smaller than 15%, except for one case (combination of granite and bitumen 2). Therefore, the results as reported by both laboratories are very consistent and consequently no differences in terms of ranking were observed.

Table 2.7 Results of the boiling water stripping tests

	Granite			Basalt			Greywacke			Limestone		
	Bit 1 (%)	Bit 2 (%)	Bit 3 (%)	Bit 1 (%)	Bit 2 (%)	Bit 3 (%)	Bit 1 (%)	Bit 2 (%)	Bit 3 (%)	Bit 1 (%)	Bit 2 (%)	Bit 3 (%)
Boiling water test according to EN 12697-11												
Lab 6	23	44	57	76	87	97	nd	81	77	91	85	91
Lab 7	23	17	44	94	92	96	49	66	82	85	86	96
Average	23	31	51	85	90	97	49	74	80	88	86	94
Std. dev.	0	19	9	13	4	1	–	11	4	4	1	4
Max	23	44	57	94	92	97		81	82	91	86	96
Min	23	17	44	76	87	96		66	77	85	85	91
Boiling water test according to XP T66-043												
Lab 11	0	0	<50	75	90	100	<50	<50	90	75	75	90

nd not determined

- It is worthwhile noting that for neither laboratory a difference between the test result (average of two runs) and an individual value exceeded 5% in absolute terms (data not shown).
- As anticipated, the scattering of test results increased in cases where aggregate was more prone to stripping and consequently the degree of bitumen coverage decreased (e.g. granite/bitumen combinations).

In Fig. 2.11 the average results of EN 12697-11 for the water boiling stripping test are plotted together with their spread. The error bars provide the variability of the results and are equal to minimum and maximum values from the two laboratories.

The granite displayed the worst results with residual equivalent coating between 20 and 50%, while both limestone and basalt have the best results above 80% coating. Greywacke had somewhat intermediate results between 50 and 80%. In the case of this test it is worth to notice a recordable difference between binders especially the neat unmodified bituminous binder when affinity is not above 80% coating. However, surprisingly the PmB, having a higher softening point than the neat binders, does not show significantly higher values.

The outcome of the boiling water stripping tests using the EN standard was compared to the result of the French test XP T66-043. Table 2.7 summarised the results for both test methods. As only one laboratory carried out this latter test, no statistical analysis could be done.

Although the test result of the French method XP T66-043 is expressed while making use of 6 different classes of residual coating, quantitative results are in correlation with the results obtained in the boiling water stripping test. Not only a similar ranking is observed, but for some cases the visual appreciation is very close to the quantitative result as obtained by titration according to EN 12697-11 clause 7 especially for limestone and basalt.

It should also be noted that by using a class <50% for all test results corresponding to a stripping percentage lower than 50%, the possible variability in the test result, as obtained by visual appreciation of the remaining area coated with bitumen, is, to some extent, strongly reduced. This approach is of particular interest

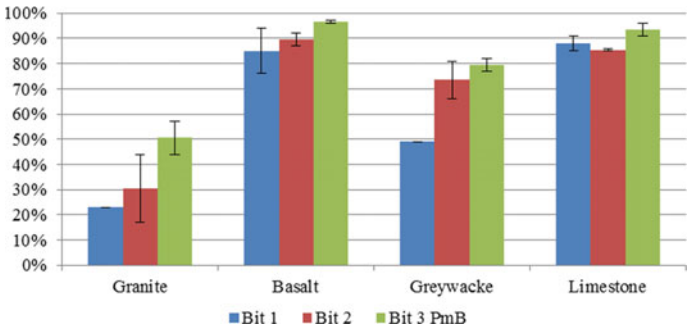

Fig. 2.11 Results of the boiling water stripping test

for aggregates showing a rather intermediate or even low affinity with bituminous binders in the presence of water such as granite. Applying such methodology also circumvents the high spread in test results as observed for instance in the rolling bottle test.

It is worth to notice that the softening point of the PmB was around 60 °C in the same magnitude of range as the test temperature, while for the unmodified binders the softening point was about 50 °C. A viscosity effect of the binders may be induced with better results for the PmB as can be seen systematically for the four different aggregate types.

2.4.3 Bitumen Bond Strength

For the bitumen bond strength, three laboratories performed the test, two using the same protocol, lab 8 and lab 9 and the third one, lab 10, using the developed protocol for mastic. For the conventional BBS test, the dry samples were tested first at temperatures of 15, 22 and 30 °C with the four different aggregate types (granite, basalt, greywacke and limestone), the same temperature range being used to evaluate early ravelling. Different moisture conditioning regimes (time and temperature conditioning) were used by the three laboratories.

2.4.3.1 BBS Results with Dry Strength Measurements

Table 2.8 provides the overall results for the standard BBS test, as performed by the two laboratories with calculated average and standard deviation values even if this latter value is not really meaningful as there were only two test results.

The graphs in Fig. 2.12 display the dry results at 15 °C, Fig. 2.13 at 22 °C and Fig. 2.14 at 30 °C. The average values are displayed while the error bars are for the two max and min values.

When considering the binder types, differences were within the variability of the measurements. For the aggregates types, except for granite displaying slightly lower strength, they all had the same values. The differences were even lower at 22 and 30 °C. The polymer modified binder showed lowest POTS in all temperatures and aggregate types relative to unmodified binders. It is also worth to notice that for both laboratories the failure was reported as cohesion failure and not adhesion failure.

Overall the dry bond strength decreased with increasing test temperature. At 15 °C, the strength was about 4–5 MPa, at 22 °C it decreased to 3 MPa and at 30 °C to 2 MPa. Results demonstrate the sensitivity of the pull-off tensile strength (POTs) parameters to test temperature and then to the bitumen stiffness.

This outcome is not unexpected as the stiffness of the bituminous binder changes significantly over this range of temperatures. Temperature susceptibility for all asphalt binder types was relatively close in the range of 50–63%. This observation

Table 2.8 Results of the bitumen bond test, dry measurements

	Granite			Basalt			Greywacke			Limestone		
	Bit 1	Bit 2	Bit 3	Bit 1	Bit 2	Bit 3	Bit 1	Bit 2	Bit 3	Bit 1	Bit 2	Bit 3
Bitumen bond strength (MPa), dry measurement at 15 °C												
Lab 8	4.08	4.94	4.54	4.80	4.51	5.16	5.21	5.11	3.51	4.58	4.62	4.24
Lab 9	3.73	4.83	4.94	4.61	3.87	4.47	4.58	3.94	4.06	4.04	4.22	4.21
Average	3.91	4.88	4.74	4.71	4.19	4.81	4.90	4.52	3.78	4.31	4.42	4.22
Std. dev.	0.25	0.08	0.28	0.13	0.45	0.49	0.44	0.83	0.39	0.38	0.28	0.02
Bitumen bond strength (MPa), dry measurement at 22 °C												
Lab 8	3.34	3.25	3.70	3.31	3.30	3.21	3.42	3.42	2.32	2.89	2.77	2.96
Lab 9	3.12	3.28	3.25	3.11	2.80	2.95	2.94	2.99	2.57	2.80	2.68	2.72
Average	3.23	3.27	3.47	3.21	3.05	3.08	3.18	3.20	2.45	2.85	2.73	2.84
Std. dev.	0.16	0.02	0.32	0.14	0.35	0.18	0.34	0.30	0.18	0.06	0.06	0.17
Bitumen bond strength (MPa), dry measurement at 30 °C												
Lab 8	1.94	2.31	2.36	1.84	2.17	2.45	2.41	2.15	1.83	2.30	2.29	2.15
Lab 9	1.85	1.76	2.13	1.98	1.85	1.68	2.04	1.68	1.68	1.66	1.79	1.66
Average	1.89	2.04	2.25	1.91	2.01	2.07	2.22	1.91	1.75	1.98	2.04	1.90
Std. dev.	0.06	0.39	0.16	0.10	0.23	0.54	0.26	0.33	0.11	0.45	0.36	0.35

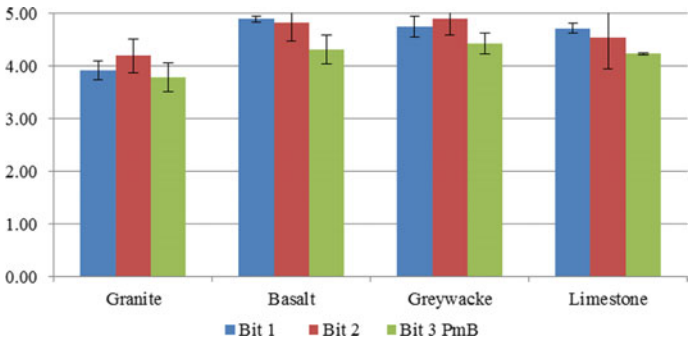

Fig. 2.12 Bitumen bond strength results at 15 °C in MPa

emphasises the significance of climatic conditions on asphalt binder selection to prevent in-service ravelling and justifies the use of three test temperatures to fully capture the bond strength vs. temperature relationship.

The dry strength is not able to address the differences in either binder or in aggregate types. For each temperature, the dry results had not statistically independent values towards aggregate types of binders. Thus the average calculation of the standard deviation is about 10% which provides an indication of the test accuracy.

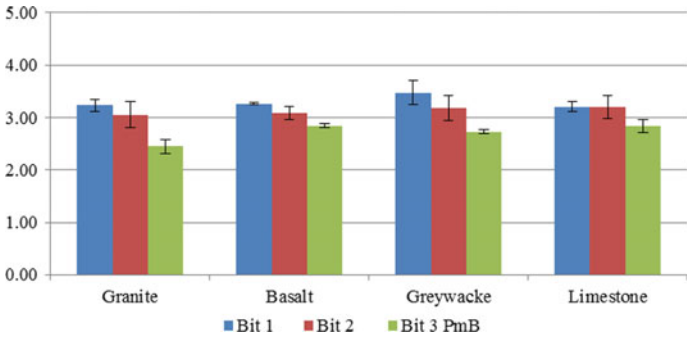

Fig. 2.13 Bitumen bond strength results at 22 °C in MPa

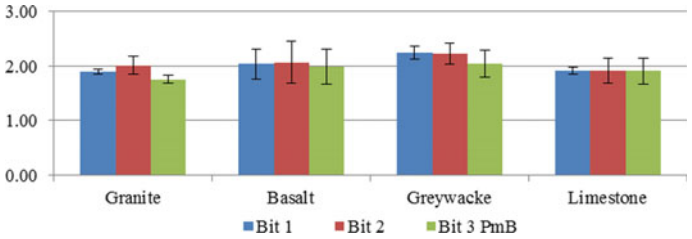

Fig. 2.14 Bitumen bond strength results at 30 °C in MPa

2.4.3.2 Results of Moisture Damage Evaluation

The moisture damage was evaluated using the Bond Strength Ratio (BSR) defined as the ratio between wet and dry bond strength at 22 °C. Table 2.9 provides the results of the wet bond strength at 22 °C and the calculated BSR. The failure mode is recorded as A for adhesion and C for cohesion.

It is worth to notice that except for granite which was adhesion failure, the failure mode was cohesion failure similarly to the dry results. This can either means that the water did not reach the binder aggregate bond and the failure is still cohesive or the water did reach the bond, but the adhesion is still stronger than the cohesion. Particularly for greywacke and limestone the difference between dry and wet strength is negligible and in the accuracy of the test.

Figure 2.15 displays the bitumen bond strength under wet conditions at 22 °C with average values and error bars being for the values of both laboratories. While for greywacke and limestone the measurements for both labs displayed a low variability, for granite and basalt, the variation was much higher. In addition for wet

Table 2.9 Results of the bitumen bond test, wet measurements

	Granite			Basalt			Greywacke			Limestone		
	Bit 1	Bit 2	Bit 3	Bit 1	Bit 2	Bit 3	Bit 1	Bit 2	Bit 3	Bit 1	Bit 2	Bit 3
Bitumen bond strength (MPa), wet measurement at 22 °C												
Lab 8	0.85	0.47	0.53	1.92	1.77	1.45	3.51	2.79	2.79	3.13	2.91	2.91
	A	A	A	C	C	C	C	C	C	C	C	C
Lab 9	1.82	1.33	1.30	2.90	1.27	2.46	3.17	2.90	2.80	3.07	2.67	2.52
	A	A	A	C	C	C	C	C	C	C	C	C
Average	1.34	0.90	0.92	2.41	1.52	1.96	3.34	2.85	2.80	3.10	2.79	2.72
Std. dev.	0.69	0.61	0.54	0.69	0.35	0.71	0.24	0.08	0.01	0.04	0.17	0.28
Bitumen bond strength ratio (at 22 °C)												
Lab 8	25	14	23	59	55	50	95	82	101	95	85	98
Lab 9	58	47	51	88	43	88	98	98	104	99	89	93
Average	42	31	37	74	49	69	96	90	103	97	87	96
Std. dev.	23	23	20	21	9	27	2	12	3	3	3	4

measurements, after water conditioning, the results were sensitive to the aggregate types with lower values for granite, around 1 MPa and also for basalt around 1.5–2 MPa. greywacke and limestone values were in the same range of magnitude as the dry measurements, around 3 MPa.

Considering binder types, there was a slight difference with Bitumen 1, unmodified bitumen having higher wet strength values compared to the others and even the modified binder did not show better values (Fig. 2.15).

Figure 2.16 displays the Bitumen Bond Strength Ratio (BSR) at 22 °C with average values while the error bars are for the two max and min values.

The results presented indicate a significant variation in resistance to moisture damage as measured by the bonding strength ratio due to changing asphalt binder and aggregate types. Results range from no moisture damage (BSR > 100%) to significant moisture damage (BSR < 50%). The BSR value can be considered to be similar to the wet to dry Tensile Strength Ratio (TSR) for hot mix asphalt, where a limiting value of 80% is commonly used to evaluate sensitivity. If a limiting BSR of 80% is used as a criterion to indicate failure, it appears that greywacke and limestone with BSR > 80% can be considered moisture resistant, while granite and basalt can be considered as moisture sensitive with BSR < 80%. Six combinations out of twelve will pass this criterion.

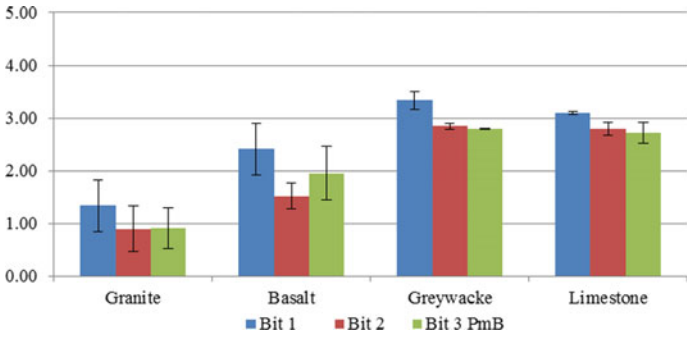

Fig. 2.15 Bitumen bond strength wet measurements at 22 °C (MPa)

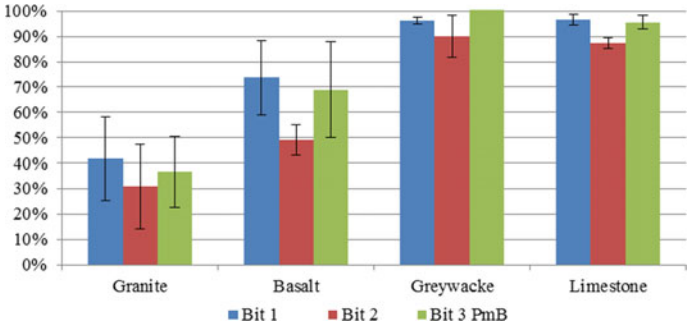

Fig. 2.16 Bitumen bond strength ratio at 22 °C (%)

Based on the BSR results, the BBS test is able to discriminate aggregate/bituminous binder combinations that are highly moisture sensitive such as granite. For the other case, as the failure is on cohesive bond, some other factors certainly affect the outcomes like water absorption of the stone, conditioning process or even size and shape of the sample.

2.4.3.3 Results of the New Pull-off Test

The effect of moisture for three different conditioning times (0, 3 and 7 days) on aggregate-mastic interfacial bond strength was determined by using a new pull-off test, called NOPTS (Zhang et al. 2015; Apeagyei et al. 2014). All the tensile tests were conducted at the same testing temperature of 25 °C using a constant cross-head speed of 20 mm/min. Three replicate specimens were tested. The results were used to estimate aggregate-mastic bond strength as a function of aggregate type and conditioning time. Some of the advantages of the NOPTS are the ability to precisely measure the loading rate, film thickness of both bitumen and mastics and simulate moisture diffusion at the aggregate-binder interface.

Due to lack of material and time only one binder, the Bit 2 50/70 pen bitumen was tested. The results for three replicate specimens conditioned in water and tested at 25 °C are summarised in Table 2.10 and Fig. 2.17.

The results showed that in the dry state, the difference between granite and limestone bond strength are not statistically significant. The effect of moisture was aggregate dependent. The effect of moisture on limestone bonds was not statistically significant even after 7 days of conditioning. However, significant degradation of strength can be seen in granite bonds as bond strength decreased after 7 days of moisture conditioning.

Table 2.10 New pull-off test results (MPa)

Conditioning time (days)		Granite	Basalt	Greywacke	Limestone
0 day	Mean value	2.18	4.71	4.20	3.43
	Std. dev.	0.64	0.62	1.01	0.48
3 days	Mean value	0.36	4.37	5.04	3.38
	Std. dev.	0.23	0.18	0.46	0.61
7 days	Mean value	0.22	5.32	4.56	3.96
	Std. dev.	0.16	1.02	0.61	0.48

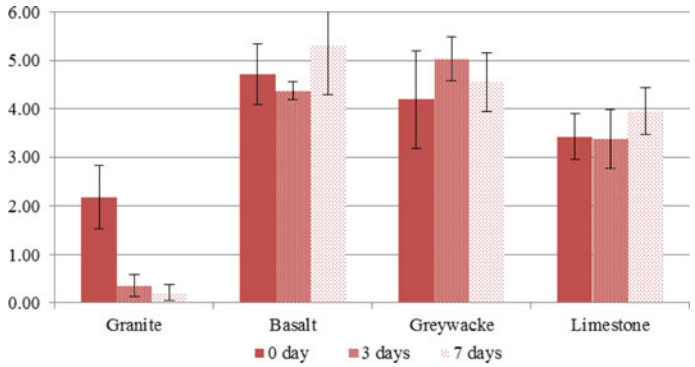

Fig. 2.17 NOPTS bond strength after 0, 3, 7 days water conditioning (MPa)

2.5 Surface and Adhesion Intrinsic Properties

2.5.1 Theoretical Background on Surface Properties

The surface free energy of a material is defined as the energy needed to create a new unit surface area of the material in a vacuum condition. The surface energies of bitumen and aggregate or a bitumen-aggregate system as in asphalt mixture are mainly comprised of an apolar (nonpolar) component and an acid-base component (Fowkes 1962; Good and van Oss 1991; Good 1992). Equation (2.1) is used to describe the total surface energy and its components:

$$\gamma = \gamma^{LW} + \gamma^{AB} \tag{2.1}$$

where

γ surface energy of bitumen or aggregate (mJ/m2);
γ_{LW} Dispersive part of Lifshitz–van der Waals interaction of the surface energy (mJ/m2); and
γ_{AB} Polar part of Lifshitz–van der Waals interaction and acid-base component of the surface energy (mJ/m^2).

The Lifshitz–van der Waals force contains at least three components: London dispersion forces, Debye induction forces, and Keesom orientation forces (Maugis 1999). The acid-base interaction includes all interactions of electron donor (proton acceptor)—electron acceptor (proton donor) type bonds including hydrogen bonding. To quantitatively predict and treat the acid-base interaction, Good and van Oss (Good and van Oss 1991) postulated a resolution of the acid-base term, γ^P into a Lewis acidic surface parameter and a Lewis basic surface parameter. The relationship between the γ^P and its components is shown in Eq. (2.2):

$$\gamma^{AB} = 2\sqrt{\gamma^{+}\gamma^{-}} \tag{2.2}$$

where

γ^{+} Lewis acid component of surface interaction, and
γ^{-} Lewis base component of surface interaction.

Surface tension is the work necessary to create a surface of a unit area. In terms of vocabulary, surface tension is referred to the liquid/vapour interface. For the solid/vapour interface, the term surface energy is used. The energy needed to separate two immiscible media is called interfacial tension.

Liquid surface tension and substrate surface energy can be divided into a polar γ_P and a dispersive component γ_D. This dispersive component corresponds to Van der Waals interactions and is present in every molecule (Miller et al. 2012). According to Good-Van Oss theory, the polar component can be separated into electron donor γ^{+} (Lewis acid) and electron acceptor γ^{-} (Lewis base) components (Miller et al. 2012). The overall surface energy or surface tension is:

$$\gamma = \gamma^{D} + \gamma^{P} = \gamma^{D} + 2\sqrt{\gamma^{+}\gamma^{-}} \tag{2.3}$$

Liquid/substrate adhesion work W_{adh} can be expressed as a function of the substrate surface energy γ_S, the liquid surface tension γ_L and the liquid/substrate interfacial tension γ_{SL}:

$$W_{adh} = \gamma_S + \gamma_L - \gamma_{SL} \tag{2.4}$$

W_{adh} can also be divided into two components to deduce the polar and non-polar interactions occurring at the interface:

$$W_{adh} = W_{adh}^{P} + W_{adh}^{D} \tag{2.5}$$

where W_{adh}^{P} and W_{adh}^{D} are the polar and the dispersive components of adhesion work respectively.

Surface energy of substrates and binder/substrate interfacial tension is strongly correlated to binder wetting. For a liquid drop deposition onto a solid surface, several wetting regimes can be observed:

- The liquid spreads completely; contact angle close to zero
- The liquid partially wets the surface. At equilibrium, the liquid presents a hemispherical shape and forms a contact angle θ with the surface; $0 < \theta < 180°$
- The liquid does not wet the solid. In this case, the contact angle is close to 180°.

In the partial wetting regime and at equilibrium, the summation of the forces applied at the liquid/solid contact line equals zero. Surface energy of the solid is then determined following Young's equation which is valid for pure liquids and

"ideal" surfaces, i.e. plane, rigid, smooth, chemically homogeneous and non-reactive surfaces (Beatty and Smith 2010):

$$\gamma_S = \gamma_{SL} + \gamma_L \cos\theta \tag{2.6}$$

The main objective for measuring surface energy of bitumen and aggregates is to be able to estimate the moisture sensitivity of asphalt mixtures using the principles of thermodynamics and physical adhesion. This objective was accomplished by using the surface energy properties of the aggregate and bitumen to calculate their interfacial adhesion work (dry bond strength) and the reduction in free energy of the system (work of debonding) when water displaces bitumen from the aggregate-bitumen interface (Eqs. 2.7 and 2.8). For an asphalt mixture to be durable and less sensitive to moisture, it is desirable that the adhesion work between the bitumen and the aggregate be as high as possible.

In addition to the two parameters: dry bond strength and debonding work, a third parameter, the cohesion of bitumen, can be calculated from the surface energy properties of bitumen. These three bond energy parameters (bitumen cohesion, dry bond strength, and debonding work) can then be used to assess the moisture sensitivity of an asphalt mixture. Bitumen cohesion is the cohesive bond strength of the material and is estimated as twice the total surface energy of the material. Dry bond strength $\left(W_{BA}^{a}\right)$ is defined as given in Eq. (2.7) as the interfacial adhesion work between the bitumen (B) and aggregate (A). A bigger value of dry bond strength suggests greater adhesion between the two materials and hence more resistance against debonding in the absence of moisture.

$$W_{BA}^{a} = 2\sqrt{\gamma_B^{LW}\gamma_A^{LW}} + 2\sqrt{\gamma_B^{+}\gamma_A^{-}} + 2\sqrt{\gamma_B^{-}\gamma_A^{+}} \tag{2.7}$$

Equation (2.8) gives the debonding work $\left(W_{BWA}^{a}\right)$ which is considered as the reduction in bond strength of a bitumen-aggregate system when water is introduced into the system or when water displaces the bitumen from the aggregate surface. A smaller value of this parameter for a given bitumen-aggregate system is indicative of a better moisture damage performance of that system.

$$\begin{aligned} W_{BWA}^{a} = &\left\{\left(\left(\sqrt{\gamma_A^{LW}} - 4.67\right)^2\right) + \left(2 \times \left(\sqrt{\gamma_A^{+}} - 5.05\right) \times \left(\sqrt{\gamma_A^{-}} - 5.05\right)\right)\right\} \\ &+ \left\{\left(\left(\sqrt{\gamma_B^{LW}} - 4.67\right)^2\right) + \left(2 \times \left(\sqrt{\gamma_B^{+}} - 5.05\right) \times \left(\sqrt{\gamma_B^{-}} - 5.05\right)\right)\right\} \\ &- \left\{\left(\left(\sqrt{\gamma_B^{LW}} - \sqrt{\gamma_A^{LW}}\right)^2\right) + \left(2 \times \left(\sqrt{\gamma_B^{+}} - \sqrt{\gamma_A^{+}}\right) \times \left(\sqrt{\gamma_B^{-}} - \sqrt{\gamma_A^{-}}\right)\right)\right\} \end{aligned} \tag{2.8}$$

The ratio (ER_1) between the adhesive bond energy values in the dry condition $\left(W_{BA}^{a}\right)$ and in the presence of water $\left(W_{BWA}^{a}\right)$ can be used to predict the moisture sensitivity of asphalt mixtures. A higher value of energy ratio indicates better resistance to moisture damage for that bitumen-aggregate combination. Bhasin et al. (2006) used Energy Ratio ER_1 to study different types of asphalt mixtures and concluded that asphalt mixtures with a ratio higher than 1.5 were more moisture resistant than the ones with ratios lower than 0.8.

$$ER_1 = \left|\frac{W_{BA}^{a}}{W_{BWA}^{a}}\right| \tag{2.9}$$

Aggregates with higher surface roughness and greater surface area are supposed to bond better with bitumen by providing more bond area and better interlocking. In order to accommodate this effect, a second bond energy parameter (ER1*SSA) obtained by multiplying the bond energy ratio ER_1 with specific surface area (SSA) has been proposed in addition to ER_1 to predict moisture sensitivity of asphalt mixtures.

Wetting/coating of an aggregate with bitumen is not only affected by the surface properties of the two materials; the viscosity or cohesion of the bitumen itself also plays a very important role. Bituminous binder with lesser cohesion and greater affinity for the aggregates will have a higher wettability and will coat the aggregate surface more than bitumen having less wettability characteristics. However, softer bituminous binder having lesser cohesion may be more prone to stripping (decrease in cohesion) in the presence of water. The effects of cohesion and wettability on moisture resistance can be accounted for by modifying the ER_1 parameter by replacing the bond strength in the dry condition $\left(W_{BA}^{a}\right)$ with a wettability relationship $\left(W_{BA}^{a} - W_{BB}\right)$. This new moisture sensitivity assessment parameter (ER_2) is given by Eq. (2.10). In order to accommodate the effects of aggregate micro-texture on the bitumen-aggregate bond strength in the presence of moisture, the bond parameter ER_2 can be multiplied by specific surface area of the aggregates to obtain a fourth bond energy parameter (ER_2*SSA).

$$ER_2 = \left|\frac{W_{BA}^{a} - W_{BB}}{W_{BWA}^{a}}\right| \tag{2.10}$$

where $\left(W_{BA}^{a}\right)$ and (W_{BB}) represent bitumen-aggregate dry bond strength and bitumen cohesion respectively.

These four bitumen-aggregate bond energy parameters (ER_1, ER_1*SSA, ER_2 and ER_2*SSA) can be used to assess the moisture susceptibility of the asphalt mixtures. In all cases, higher energy ratios are associated with mixtures with better moisture resistance (Grenfell et al. 2014).

2.5.2 Methods

Three experimental devices were used to determine the surface energy of the aggregate and bitumen samples. The devices included a Dynamic Contact Angle (DCA) analyser, a Dynamic Vapour Sorption (DVS) system and a Drop Shape Analyser (DSA). The DSA, a pendant drop method, was used to determine surface energy of both aggregates and binder at different temperatures while the DCA and DVS were used to determine surface energy of binder and aggregates, respectively, at room temperature. Carefully selected probe liquids (Table 2.11) were used depending on material and device type. A brief description of the procedures used for each device is provided next.

A Thermo Scientific CAHN Radian dynamic contact angle (DCA) analyser was used to determine the surface energy components of the binders. The DCA uses the Wilhemy plate method to determine surface energy of binders. Surface energy components of each binders was estimated using the contact angles that a set of three probe liquids with known surface energy components make with bitumen (in solid state) under dynamic conditions. The probe liquids used were water, glycerol and diiodomethane. The probe liquids were selected because of their purity, their low chemical interactions with bitumen and their known surface energy components. The results of the DCA test can be used to estimate the total surface energy of bitumen as well as its cohesive bond strength (Liu et al. 2014).

During the DCA test, a clean 40 mm × 24 mm × 0.45 mm No. 15 microscope glass slide is coated with bitumen and hung from the balance of the DCA equipment with the help of a crocodile clip. A beaker containing a probe liquid is placed on a movable stage positioned under the glass slide (Fig. 2.18). The bitumen-coated glass slide is then immersed up to a maximum depth of 5 mm (advancing) and then withdrawn (receding) from the liquid by moving the stage up and down, respectively, at a constant speed of 40 μm/s while continuously recording the change in

Table 2.11 Properties of probe liquids used for surface energy measurements

Probe liquid	γL (mN/m)	γLP (mN/m)	γL^{+} (mN/m)	γL^{-} (mN/m)	γLD (mN/m)	Device
Water	72.8	51.0	25.5	25.5	21.8	DCA
Glycerol	64.0	29.9	3.92	57.4	34.0	
Diiodomethane	50.8	0.0	0.00	0.00	50.8	
Octane	21.6	0.0	0.00	0.00	21.6	DVS
Ethyl Acetate	23.9	0.0	0.00	19.2	23.9	
Chloroform	27.2	0.0	3.80	0.00	27.2	
Water	72.8	51.0	25.5	25.5	21.8	DSA
Glycerol	64.0	29.9	3.92	57.4	34.0	
Ethylene glycol	47.7	16.8			30.9	

γL total surface energy; *γLP* polar component; *γLD* dispersive component

mass of the bitumen-coated slide with depth of immersion. The results are used to compute the contact angle between the bitumen and the probe liquid. All the DCA contact angle measurements were obtained at room temperature (23 ± 2 °C and 50 ± 5% relative humidity). Three replicates of each bitumen-probe liquid combination were tested.

The DCA approach for estimating surface energy of bitumen uses measured mass-depth relationships to estimate the forces acting on a bitumen-coated slide as it is being immersed or removed from a probe liquid to determine contact angles between the binder and at least three probe liquids. The contact angle results from the three probe liquids are used in Eq. (2.11) to obtain three simultaneous equations from which the three surface energy components (γ^D, γ^+, and γ^-) can be estimated. The estimated surface energy components are then used to determine the total surface energy $\left(\gamma_B^T\right)$ of the binders using Eq. (2.12) from which the cohesive bond strength (equal to twice γ_B^T) of the binder could also be obtained.

Fig. 2.18 Dynamic contact angle analyser test set-up

$$W_{BL} = \gamma_L(1 + \cos\theta) = 2\sqrt{\gamma_B^{LW}\gamma_L^{LW}} + 2\sqrt{\gamma_B^-\gamma_L^+} + 2\sqrt{\gamma_B^+\gamma_L^-} \tag{2.11}$$

where

W_{BL} adhesion work between the bitumen (B) and a probe liquid (L)
γ_L total surface energy of the probe liquid
θ contact angle between bitumen and probe liquid

$$\gamma_B^T = \gamma_B^{LW} + 2\sqrt{\gamma_B^-\gamma_B^+} \tag{2.12}$$

A DVS Advantage 2 system (Surface Measurement Systems, Middlesex, UK) was used to determine the surface energy components of the aggregates using sorption isotherms obtained at 25 °C as shown in Fig. 2.19.

The DVS tests were conducted using aggregates passing the 5 mm sieve and retained on the 2.36 mm sieve that had been cleaned with deionised water and dried in an oven at 115 °C to a constant mass. During the adsorption test, a pre-heating step was conducted combined with dry nitrogen run into the system for 800 min to ensure that any trace of moisture is removed from the sample surface. Three carefully

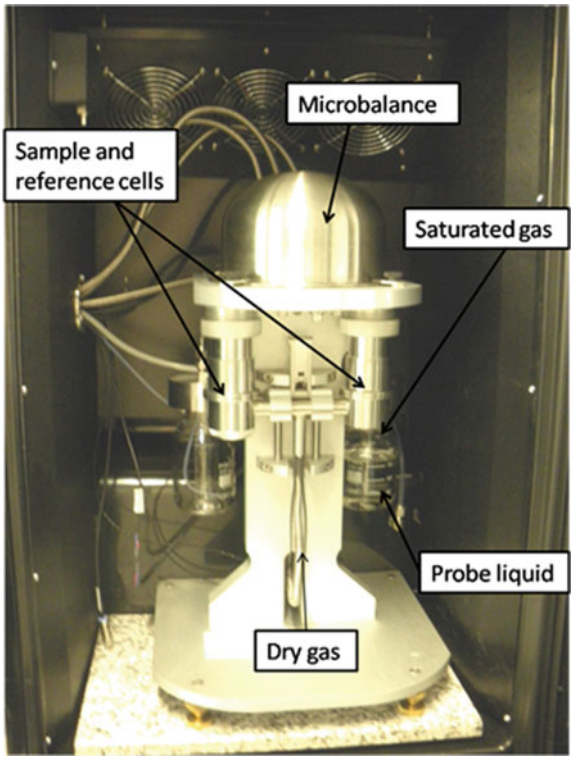

Fig. 2.19 Dynamic vapour sorption device (DVS Advantage 2)

selected probe liquids - octane, ethyl acetate, and chloroform were used. The probe liquids were selected because they have low chemical interactions with aggregates and because their surface energy components are known. The DVS approach for determining surface energy properties of aggregates involves measuring the weight gain of an aggregate sample (usually less than about 10 g in weight) kept in a sealed DVS sample chamber containing a probe liquid vapour (at partial pressures ranging from 0 to 95%). Only a single replicate of each aggregate-probe liquid combination was tested as each sorption isotherm took more than a day to complete. It is worth to notice that the instrument itself is more precise than the influence of the aggregates can have on the results. The device combines precise partial pressure control of probe liquid and unique real time vapour concentration monitoring with a high resolution (1 μg) microbalance to monitor aggregate weight gain.

For each aggregate-probe liquid combination, mass gain in the aggregates is monitored, using an ultra-sensitive balance, at 14 different partial pressures until equilibrium mass is reached at each partial pressure stage. The results (i.e. equilibrium mass) are plotted against partial pressure to generate sorption isotherms from which the SSA and spreading equilibrium pressures (Bhasin 2006) for each of the three probe liquids could be estimated. The results are then used to estimate the surface energy components of the aggregates as discussed below. Similar to Eq. (2.11) for determining surface energy of binders, Eq. (2.13) was used to generate three simultaneous equations which could be solved to obtain the three surface energy components by utilising the total surface energy and the spreading pressure of each probe liquid. The total surface energy of the aggregates is given by Eq. (2.14), using the surface energy components of the aggregates.

$$W_{AL} = 2\gamma_L + \prod_e = 2\sqrt{\gamma_B^{LW}\gamma_L^{LW}} + 2\sqrt{\gamma_B^{+}\gamma_L^{-}} + 2\sqrt{\gamma_B^{-}\gamma_L^{+}} \tag{2.13}$$

where

W_{AL} adhesion work between an aggregate (A) and a probe liquid (L)
γ_L total surface energy of the probe liquid
π_e spreading pressure of probe liquid aggregateAggregate

$$\gamma_A^T = \gamma_A^{LW} + 2\sqrt{\gamma_A^{-}\gamma_A^{+}} \tag{2.14}$$

The Drop Shape Analyser (DSA) was used for characterising the surface properties of materials and for assessment of bitumen/mineral substrate adhesion. Surface tension of the bituminous binder was assessed using a drop tensiometer (DSA 100, Krüss GmbH) via the pendant drop method. Binder was introduced in a brass syringe, itself placed in a dosing cell heated at the target temperature. Droplets were formed automatically using DSA software below the syringe. Figure 2.20 shows the DSA equipment.

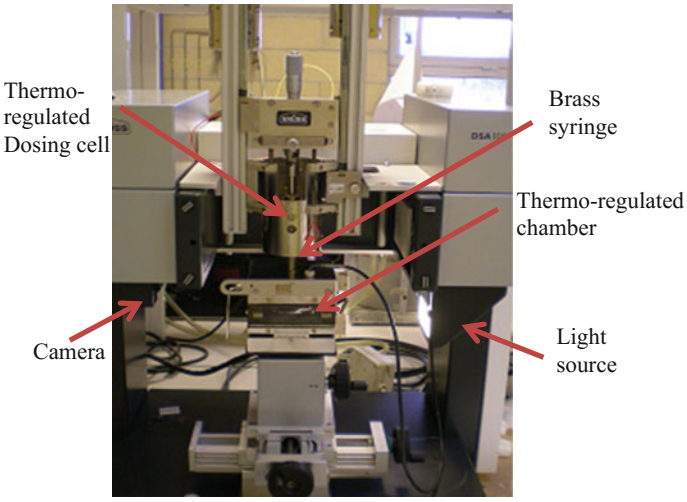

Fig. 2.20 The drop shape analyser (DSA)

The surface tension is the average value from five measurements. Surface tension, in the air, was performed at the same temperature, 120 °C, than the contact angle between the binder drop and the aggregate substrate. It is determined using equations taking into account the geometrical form of the droplet and the binder density. Dispersive and polar components of surface energy (γ_L^D and γ_L^P respectively) allow characterising the chemical interactions inside the binder. Both components are determined from a contact angle measurement of a bitumen drop on a PTFE substrate (pure dispersive material, γ_S = 20.5 mJ/m^2). They were calculated using the following Eqs. (2.15) and (2.16):

$$\gamma_L^D = \frac{\gamma_L^2(1+\cos\theta)^2}{4\,\gamma_S} \tag{2.15}$$

$$\gamma_L^P = \gamma_L - \gamma_L^D \tag{2.16}$$

The surface energy of substrates is assessed by measuring contact angles in hot conditions (at 120 °C in this study) using a thermoregulated syringe and chamber to heat binder and aggregates. Rocks were obtained from quarries and drilled to obtain 40 mm diameter cores. Then cores are sawn in water to have 5–15 mm thick slices which have been ground to low roughness. Samples are stored in a cool place away from dust six days before the contact angle tests. Concerning the contact angle measurements, three reference liquids with different polar properties are used. They include water, glycerol and ethylene glycol. Their surface properties are presented in Table 2.11.

Liquid droplets were created automatically using a multi-dosing cell. Contact angles are determined with the software, which fits the angle with an ellipsoidal

equation. The drop diameter on the slide was 3–8 mm. Contact angles are taken just after drop stabilisation. They are the average value of, at least, five measurements. The surface energy is deduced from the contact angle via the Owens-Wendt-Rabel-Kaelble:

$$\frac{\gamma_L(1+\cos\theta)}{2(\gamma_L^D)^{1/2}} = (\gamma_S^D)^{1/2} + (\gamma_S^P)^{1/2}\frac{(\gamma_L^P)^{1/2}}{(\gamma_L^D)^{1/2}} \tag{2.17}$$

γ_S^D and γ_S^P are the dispersive and the polar component of the mineral substrate respectively, γ_L^D and γ_L^P are the dispersive and the polar component of the reference liquid respectively, γ_L is the surface tension of the reference liquid, θ is the reference liquid/mineral substrate contact angle.

Finally, bitumen binder/mineral substrate adhesion work W_{adh} is theoretically determined using Eq. (2.18):

$$W_{adh} = 2\left[(\gamma_L^D\gamma_S^D)^{1/2} + (\gamma_L^P\gamma_S^P)^{1/2}\right] \tag{2.18}$$

According to contact angle measurements between binder droplets on mineral substrate, adhesion work W_{adh} could be also determined using the Dupre equation:

$$W_{adh} = \gamma_L(1+\cos\theta) \tag{2.19}$$

In this case, contact angle measurements are performed using a binder and a substrate heated at the same temperature.

2.5.3 *Results of Intrinsic Adhesion Properties*

2.5.3.1 Binders Surface Tension

Surface tension of the binders has been measured using the Dynamic Contact Angle (DCA) analyser with Wilhelmy plate and the Drop Shape analyser (DSA) in pendant drop configuration. Results are reported on Table 2.12. It has to be noted that the temperature of measurements are different, 23 °C for the DCA and 120 °C for the DSA.

Table 2.12 Surface tension of three binders by the DCA and the DSA method

Binder ID	Summary—SE components (mN/m)						
	DCA method (T = 23 °C)				DSA method (T = 120 °C)		
	γ^D	γ^+	γ^-	γT	γD	γP	γT
Bit 1	18.82	0.34	5.08	**21.44**	16.64	10.81	**27.46**
Bit 2	20.75	0.06	2.90	**21.57**	16.34	10.55	**26.89**
Bit 3	26.63	0.00	4.86	**26.64**	17.18	9.69	**26.87**

The same order of magnitude was found when considering the total surface tensions of the three binders using both methodologies, DCA and DSA. The values of Table 2.12 appear to be between 19 and 27 mN/m. Values generally reported in the literature (Lytton and Flumerfelt 1998; Shell et al. 1979; Saal 1933) are between 24 and 33 mN/m. Surface tensions from the DCA method on the unmodified binders appear, by consequence, lower than expected. However, DCA and DSA methods give the same values for the PmB binder (γ^T = 26.6 mN/m for DCA and γ^T = 26.9 mN/m for DSA).

Surface tension is generally found to be independent of binder nature. The DSA method agrees with this observation. Moreover, both methods show that bituminous binder surface tension is more dispersive than polar, while there is polar difference reported between DCA and DSA.

2.5.3.2 Aggregates Surface Energy

Surface energy of aggregates, measured with the Dynamic Vapour Sorption Test (DVS) and the Contact Angle Measurement (CAM), are reported on Table 2.13. Small particles (5–2.36 mm) are used for the DVS method whereas bulk and not polished flat samples are used for the CAM method.

Whatever the method, surface energy appears to be dependent on aggregate nature. Considering the total surface energy, both methods give the same value for the greywacke (71 mN/m). However, a difference of 10 mN/m is found for the granite while a difference of 20 mN/m is found for the limestone. What is very curious is the repartition between the polar and dispersive components. The DVS method always gives a dispersive component of the surface energy superior to the polar component. This is quite unexpected when comparing to literature values. On the contrary, the CAM method shows a polar component superior to the dispersive one, except for the limestone.

These total surface energies differences could be explained by the surface characteristic of the aggregates. In the DVS method, crushed particles are used whereas sawed blocks are used for the CAM method. It has to be noted that these differences between methods have already been observed during the NCHRP program (Little and Bhassin 2006).

Table 2.13 Surface energy of the four aggregates

Aggregate type	Summary—SE components (mJ/m^2)						
	Method 1 (DVS)			Method 2 (CAM)			
	γ_{LW}	γ^+	γ^-	γT	γD	γP	γT
Granite	56.4	0.28	12.7	**60.17**	9.30	59.88	**69.18**
Basalt	–	–	–	–	13.85	45.11	**58.96**
Greywacke	56.53	2.22	22.27	**70.58**	6.15	64.90	**71.05**
Limestone	56.74	0.39	14.78	**61.56**	24.07	16.87	**40.94**

2.5.3.3 Adhesion Work Between Aggregates and Binders

Adhesion work is calculated using two approaches. The first uses bitumen surface tension and aggregate surface energy measurements through a theoretical calculation: Eq. (2.7) (associated with DCA and DVS methods) and Eq. (2.18) (associated with DSA and CAM method). Results using this approach are reported in Table 2.14. It should be noted that Eqs. (2.7) and (2.18) are equivalent in theory and should therefore result in similar results. However, in practice, Eq. (2.7) has been found to be more accurate.

The second uses the contact angle measurements at 120 °C between bitumen and aggregate (CAM method) and the bitumen surface tension measurements (from DSA method) to calculate the work of adhesion of the binder on the aggregate and the interfacial tension at the interface. Results using this approach are reported in Table 2.15.

Concerning the first approach, whatever the method used, values of adhesion work were between 66 and 84 mJ/m^2. Obviously, differences between both methods reflect the observations made on the surface tension and surface energy measurements. By consequence, both methods give adhesion work values very sensitive to aggregate nature. If we consider only greywacke, granite and limestone, method 1 gives the greywacke as the best and granite as the worst aggregate; method 2 gives the granite as the best and the limestone as the worst aggregate.

Table 2.14 Calculated adhesion work (Wa_{th}) between aggregate and bitumen from measured dispersive and polar components of γ_L and γ_S

Aggregate ID	Summary Wa (mJ/m^2)					
	Method 1 (Eq. 2.7)			Method 2 (Eq. 2.18)		
	Bit 1	Bit 2	Bit 3	Bit 1	Bit 2	Bit 3
Granite	71.69	71.94	79.86	75.79	74.93	73.47
Basalt	–	–	–	74.55	73.73	72.68
Greywacke	77.44	75.86	84.20	73.23	72.39	70.72
Limestone	72.65	72.62	80.52	67.05	66.35	66.25

Table 2.15 Experimental method: Adhesion work (Wa_{exp}) between aggregate and bitumen and interfacial tension (γSL) from contact angle measurement (T = 120 °C)

	Bit 1			Bit 2			Bit 3		
	θ (°)	Wa_{exp} (mJ/m^2)	γ_{SL} (mN/m)	θ (°)	Wa_{exp} (mJ/m^2)	γ_{SL} (mN/m)	θ (°)	Wa_{exp} (mJ/m^2)	γ_{SL} (mN/m)
Granite	8.4	54.62	42.02	8.8	53.47	42.61	15.0	52.85	43.22
Basalt	10.1	54.49	31.94	9.4	53.43	32.44	15.3	52.81	33.04
Greywacke	10.1	54.49	44.02	9.1	53.45	44.50	11.9	53.18	44.76
Limestone	9.8	54.52	13.88	8.4	53.50	14.33	15.0	52.84	14.98

The highest adhesion works were found for Bit 3 using method 1. On the contrary, the lowest adhesion works were found for the Bit 3 using method 2.

The second approach, as shown in the Table 2.15, gives adhesion work (Wa_{exp}) between 53 and 55 mJ/m^2, being very insensitive to aggregate nature. Whatever the aggregates, the lowest adhesion works (associated with higher contact angle) were found for Bit 3, which is consistent with the semi-theoretical approach, method 2 (Table 2.14). The interfacial tension has also been calculated ($\gamma_{SL} = \gamma s + \gamma_L - Wa_{exp}$) and reported in Table 2.15. The interfacial tension appeared to be strongly influenced by the surface energy of the aggregate (γs). In comparison to other aggregates, a very low value of interfacial tension was found for the limestone. Considering the Wa_{exp}, they were similar for all aggregates; the interfacial tension could be interesting to rank aggregates. In this case, it would distinguish limestone as a good aggregate for binding according to the low interfacial tension value measured.

2.5.3.4 Debonding Work, Compatibility Ratio

Debonding work is considered as the reduction in bond strength of a binder-aggregate system when water is introduced into the system or when water displaces the binder from the aggregate surface. A smaller value of this parameter for a given binder-aggregate system is indicative of a better moisture damage performance of that system. Furthermore, in theory, a negative work of debonding between an aggregate and a bitumen bond may be indicative of spontaneous de-bonding in water. Debonding work was calculated from Eq. (2.3) using the dispersive part of the Lifshitz–van der Waals component of the surface energy (and tension) and Lewis acid and base components of surface energy (and tension), for aggregates (DVS method) and bitumen (DCA method). The results are reported in Table 2.16 where each aggregate-bitumen combination resulted in a positive work of debonding; even though work of debonding alone cannot be used to conclusively rank the moisture resistance of an asphalt mixture. In this case, however, as the work of debonding is positive, it means that energy is needed to break the bitumen aggregate bond in water. It also means that a higher value would relate to a stronger bond compared to a lower value. The preceding criterion (lower work of debonding is worse than higher work of debonding) can be used to rank the materials, i.e. aggregate ranking: Greywacke < Limestone < Granite; bitumen ranking: Bit 1 < Bit 2 = Bit 3 (Table 2.16).

Table 2.16 Debonding work of aggregate-binder bond in presence of water

Aggregate	Binder		
	Bit 1	Bit 2	Bit 3
Granite	36.7	43.9	43.5
Greywacke	21.0	26.4	26.4
Limestone	33.6	40.5	40.1

The ratio (ER_1) between the adhesive bond energy values in the dry condition, adhesion work, and in the presence of water, debonding work, can be used to predict the moisture sensitivity of asphalt mixtures. In addition to ER_1, three other parameters ER_2, ER_1*SSA and ER_2*SSA, as previously defined, could be used to quantify moisture sensitivity. A higher value of energy ratio indicates better resistance to moisture damage for that binder-aggregate combination. For example, Bhasin et al. (2006) applied the ratio ER_1 to study different types of asphalt mixtures and concluded that mixtures with a ratio higher than 0.8 were more moisture resistant than the ones with ratios lower than 0.8. In addition, mixtures with ER_2 greater than 0.5 performed better than those with ER_2 less than 0.5. However, it is questionable if these threshold values still hold if the work of debonding results in a positive value. Results using values from Table 2.14 (method 1) and Table 2.16 are shown in Tables 2.17 and 2.18. Following the criteria proposed by Bhasin et al., none of the aggregate-bitumen combinations considered in this study appears to be poor performing mixtures in terms of moisture sensitivity.

2.5.4 *Outcomes of Surface Energy Measurements*

Surface tension of the bituminous binders and surface energy of the aggregates has been measured using different methodologies. Both methods show more differences for aggregates than for binders. For binders, surface tension values from both methods are close to each other and highlight a more dispersive than polar behaviour. This finding is in line with usual data in the literature. For aggregates, even if the same value is found for the greywacke, other surface energy values appear to be significantly different. Moreover, the DVS method gives for all aggregates a more dispersive behaviour whereas the CAM gives a more polar behaviour (except for limestone). There is no explanation for this at the moment. This effect could be the

Table 2.17 Compatibility ratios, ER_1 and ER_2

Aggregate	ER_1			ER_2		
	Bit 1	Bit 2	Bit 3	Bit 1	Bit 2	Bit 3
Granite	1.95	1.64	1.84	0.79	0.66	0.61
Greywacke	3.68	2.87	3.18	1.64	1.24	1.17
Limestone	2.16	1.79	2.01	0.89	0.73	0.68

Table 2.18 Compatibility ratios ER_1*SSA and ER_2*SSA

Aggregate	SSA (m^2/g)	ER_1*SSA			ER_2*SSA		
		Bit 1	Bit 2	Bit 3	Bit 1	Bit 2	Bit 3
Granite	2.2812	4.46	3.74	4.19	1.79	1.50	1.39
Greywacke	1.3978	5.15	4.02	4.45	2.30	1.73	1.63
Limestone	0.6199	1.34	1.11	1.24	0.55	0.45	0.42

consequence of the geometrical surface properties of the bulk flat and not polished sample used in the CAM method.

Adhesion works between bitumen and aggregate are first calculated from the dispersive and polar component of surface energy and surface tension, from both methods (DVS and CAM). Obviously, differences between the two methods reflect the observations made on the surface tension and surface energy measurements. Regarding the DVS method, greywacke has the highest adhesion work and the granite and limestone has the lowest. Regarding the CAM method, granite, basalt and greywacke (very close values) have the highest adhesion work, limestone the lowest.

Adhesion works were also determined from a more direct method; the contact angle between binder and aggregate. There is no aggregate influence on the adhesion work from this direct method. There is a small influence of binder on the adhesion work; the PmB Bit 3 appeared to give the lowest values. It has to be noted that, in each case, the contact angle was quite low, between 8° and 15°, which is the consequence of good wettability.

Both methods, used to get the adhesion work, do not give the same results. The first, by calculation, is able to find differences between aggregates; the second appears to be more sensitive to the binder.

The compatibility ratio allows taking into account, theoretically, the water effect which leads to the debonding phenomena. It has been calculated using the binder surface tension from the DCA method and the aggregate surface energy (dispersive and polar component). This compatibility ratio is more sensitive to aggregate than to binder type. none of the aggregate-bitumen combinations considered in this study appears to be poor performing mixtures in terms of moisture sensitivity regarding Bhasin criteria.

Knowing the on field performance of the aggregates used in bituminous mixtures for pavement, adhesion work from surface energy measurements cannot be used alone as a criteria for moisture resistance. Indeed, low adhesion work was calculated for limestone whereas this aggregate is generally associated with a good resistance to debonding. The compatibility ratio appears to be a more accurate criterion and the interfacial tension calculated from the contact angle measurement could also be a good indicator and allows ranking aggregate-bitumen combinations.

In order to have a more accurate comparison of the surface energy and adhesion work from the different methods, a first recommendation could be to work on the same theoretical framework or model. For example, it could be interesting to re-calculate all data using the energy decomposition in Lifshitz–van der Waals and Lewis acid-base components of surface energy. Another recommendation is to assess the influence of the surface state; roughness and porosity in the CAM method and cleanliness of the aggregate in the DVS method. Finally, in order to increase the debonding phemonenon knowledge, it could be interesting to assess the contact angle evolution (CAM method) for aggregate-bitumen samples immerged in water.

2.6 Discussion and Recommendation

2.6.1 Discussion of the Rolling Bottle Test Results

Based on the raw results, the first outcomes are:

- the results are more discriminating after 24 h compared to 6 h
- the type of aggregates has a significant influence
- the type of bituminous binder has limited influence, with slightly better results for the polymer modified binder compared to the pen grade binders.

However, the overall results of this test do not appear really accurate and a lot of variability is observed from the different laboratories. The highest variation being for basalt and greywacke aggregates which displayed intermediate values, regardless the bituminous binder. To some extent this is aligned with the precision statement of the EN 12697-11. A reproducibility of 30% is given in the standard with the note: *"The obtainable precision may depend on the level of the result as determinations close to 0 or 100 are easier visually to determine than 'mid-range' results between 25 and 75%"*. Also it has to be noted that these aggregates were dark aggregates and it was difficult to qualify the remaining coating of bituminous binder.

Analysing in detail the results, the first thought explaining such a difference, was the visual interpretation of the coverage. The standard provides some reference scale to "quantify" the coating degree. The final value has to be an average of observation from at least two different technicians on three samples. Some laboratories provided the full observation. Mostly the variation between two observers and samples was no more than 10% coating. Some laboratories also provided pictures of samples. Examples are given in Fig. 2.21, for the granite aggregates with Bit 3, polymer modified bitumen after 24 h. As granite is a light coloured aggregate, the pictures are easier to interpret. One laboratory recorded only 5% remaining coating, another 20% and the other 40%. From the pictures, the difference is still recordable.

Both assumptions, of the variation between technicians and the visual interpretation cannot alone explain the variability of the results. So far, the test results are not always consistent within the same test method. The reproducibility is not as good, and does not seem to come fully from the visual observation, maybe there are some underlining reasons. Another possible reason could come from the test conditions themselves. The EN standard still leaves some freedom for the test conditions such as the test temperature, if the bottles are already used or are brand new etc. This certainly needs more attention.

(A) Pictures of granite aggregate with PmB after 24 h from lab1 with 5% coating

(B) Pictures of granite aggregate with PmB after 24 h from lab 4 with 20% coating

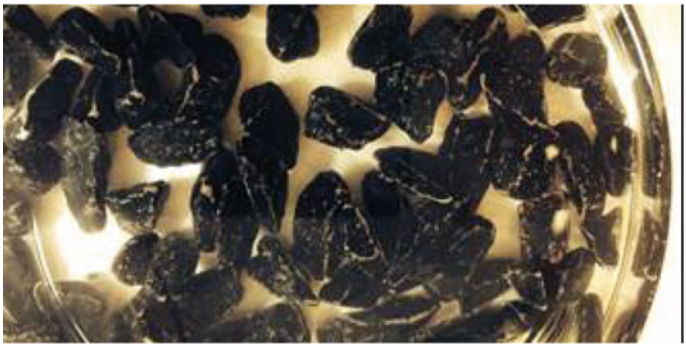

(C) Pictures of granite aggregate with PmB after 24 h from lab 3 with 40% coating

Fig. 2.21 Pictures of different rolling bottle test results

2.6.2 Blind Test for Visual Interpretation

For assessing the accuracy of visual inspection, a "blind test" was run using the pictures provided by one laboratory. The pictures came from the results of the boiling water stripping test according to XP T 066-043 test method. This method consists of bitumen coated aggregates left for 16 h in water maintained at 60 °C during the whole test duration.

The pictures from the combination of the four aggregates and the three bituminous binders were visually ranked by each experienced technician of the laboratories. Figure 2.22 displays the different pictures for each combination.

For Greywacke and Basalt, the darkness of the stone didn't help the visual interpretation. But clearly some differences are recordable between aggregate types. For bitumen type, differences are noticeable for the modified binder Bit 3 having a softening point temperature around the test temperature, while the other having lower softening point.

A total of 10 laboratories participated to this additional "blind test". The results are displayed in Table 2.19 and Fig. 2.23 with the mean values and the errors bars with the standard deviation.

The overall standard deviation across the different values is about 6% for 10 laboratories; this means a reproducibility of 12%. The variability of the measurements is lower for either very low or high values. While for intermediate values it is slightly higher variability.

The results are slightly different from the rolling bottle test but in line with the boiling water results. The interpretation is selective enough for aggregates. Granite gave the worst results and limestone was still good. However, basalt became one of the best regardless the binder. Regarding the different binders, there were significant differences with the modified binder, especially for the greywacke, displaying better results for the Bit 3 PmB.

2.6.3 Discussion Bitumen Bond Strength Results

In the field, ravelling can be the main problem in asphalt pavements. This failure needs to be taken into account to optimise the material used. Several factors are related to the deterioration of aggregate and bituminous binder resulting in ravelling. In the study, it focused on three main effects causing the bonding deterioration between aggregate and bituminous binder: temperature, binder and its modification and aggregate mineralogy. The samples were cured in dry conditions at different temperatures and were tested by BBS to determine the dry pull-off tensile strength. The dry results show a significant decrease in POTS with increasing temperature, however independent to bitumen types or aggregate types. This indicates that in-service temperature is important to control the bond strength of aggregate and asphalt binder.

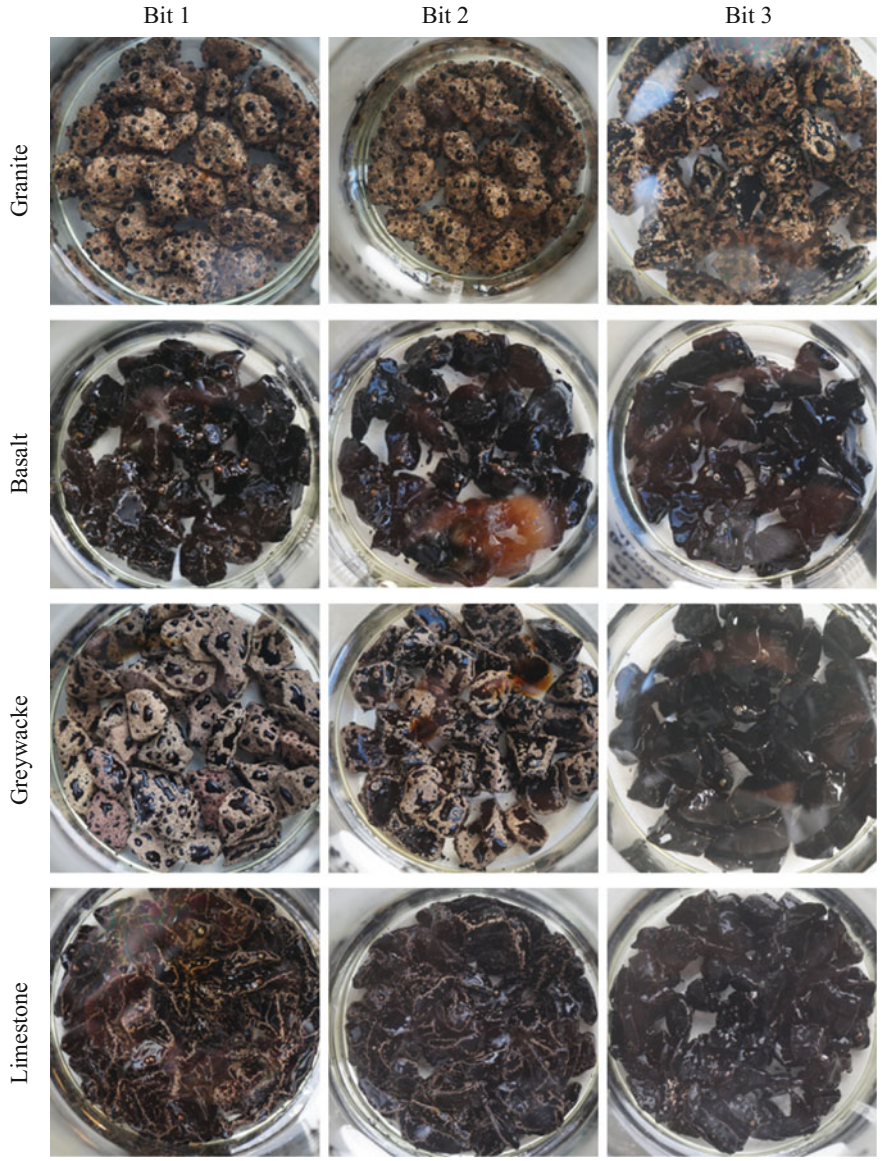

Fig. 2.22 Pictures for "blind test" addressing visual inspection reproducibility

The dry results had shown only significant different results for granite where the failure mode was in adhesion rather than cohesion. The failure mode is one predominant parameter to interpret the results.

For the polymer modified binder, the results show that in this case, where binders are selected with a similar penetration value at 25 °C and are tested under

Table 2.19 Assessment of the visual interpretation (% residual coating)

	Granite			Basalt			Greywacke			Limestone		
	Bit 1	Bit 2	Bit 3	Bit 1	Bit 2	Bit 3	Bit 1	Bit 2	Bit 3	Bit 1	Bit 2	Bit 3
Lab 2	10	10	35	95	100	100	15	60	100	85	90	100
Lab 3	10	10	25	85	95	100	15	50	95	75	85	95
Lab 4	10	10	20	90	90	100	15	30	100	80	80	95
Lab 5	20	20	35	85	90	100	30	40	95	55	70	90
Lab 6	10	10	30	85	95	100	15	40	100	75	85	95
Lab 7	15	20	50	90	85	95	25	40	100	80	85	90
Lab 10	15	15	30	85	85	95	15	30	95	50	60	95
Lab 11	10	10	25	95	95	100	20	60	100	85	90	95
Lab 13	20	15	25	80	90	95	25	35	95	65	80	85
Lab 14	20	20	40	80	90	100	30	40	100	65	80	90
Lab 15	10	10	25	95	100	100	15	35	100	85	85	100
Average	14	14	31	88	92	99	20	42	98	73	81	94
Std. dev.	5	5	9	6	5	2	6	11	3	12	9	5
Min	10	10	20	80	85	95	15	30	95	50	60	85
Max	20	20	50	95	100	100	30	60	100	85	90	100

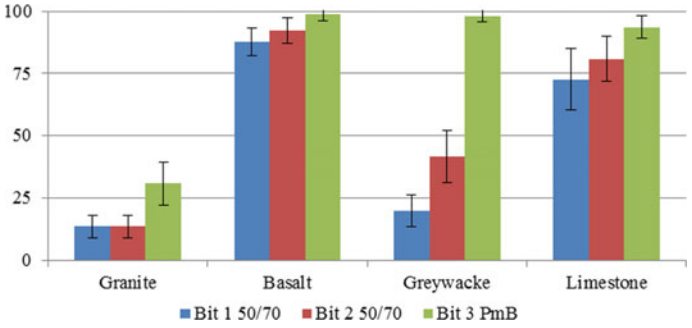

Fig. 2.23 Blind test results for residual coating

temperature and loading conditions similar to the penetration test, the modified binder did not show a difference in the cohesive strength of the material, which was the case when it was tested in the dry case.

The evaluation of bituminous binder moisture damage on BBS used the same criterion as for the Tensile Strength Ratio (TSR) used for asphalt mixture. If a value of a TSR ratio of 70% is used as a criterion to indicate failure, it appears that the same 70% criterion can be used with the BSR. This can rank the effect of combination of aggregate mineralogy and bituminous binder on moisture damage. Granite has the worst compatibility with the bituminous binder to prevent moisture

damage. Greywacke showed the greatest potential for aggregate use, in preventing moisture damage.

2.6.4 Comparison Between Test Methods

From the different test methods used, the rolling bottle test, the water boiling test or the bitumen bond strength, the results are mostly affected by aggregate type. The binder impacts the results significantly, mostly with the boiling water when the temperature is raised at least to the softening point level of the binder. In this condition, the modified binder, having higher softening point, shows better results than the unmodified binder. In this condition, it was of interest to make a ranking comparison of the different aggregates.

For the rolling bottle test, there is a clear trend that granite displays the worst results and limestone the best, but for greywacke and basalt the ranking is equally balanced between laboratories.

However, for the boiling water stripping test, the ranking is slightly different. The granite aggregates are still the worst, but the ranking changes with basalt being the best, then limestone and finally greywacke.

Finally for the bitumen bond strength, granite is still the worst followed by basalt, and limestone and greywacke being very similar.

From this comparison, it is not obvious to conclude that the three test methods are equal and provide similar results. They all discriminate granite to have the worst affinity with bituminous binder in presence of water. For limestone, considering the absolute values, they all rank it as having good results in terms of affinity. However for intermediate values, the ranking from test to test is not consistent and the absolute values are not comparable.

Table 2.20 summarises the results for the pen grade bitumen with 1 being the highest remaining coating and 4 the lowest.

The reasons for the different ranking should be discussed in relation to the specific properties that are tested and also to differences in how the water is affecting the adhesion. For example in the rolling bottle test and the water boiling the rough aggregate is used, while in the BBS it is controlled-polished; so one parameter, stone roughness is not included in the BBS while it is playing a role in the other two tests. Furthermore, in the rolling bottle and the boiling water test, the coated stones are immersed in water, while in the BBS test water needs to penetrate through the aggregate to reach the interface; this introduces at least one extra parameter. For aggregates that absorb water very slowly the bond may not be attached within the experimental set up in the BBS test. This effect is not playing a role in the two other tests. Moreover, in the BBS test the failure can take place in the bitumen film or at the interface, where a coating below 50% is used as the adhesive failure; in the rolling bottle test only adhesive failure occurring in the interface is counted. And in the boiling water test, finally, the temperature conditions are very different, so the binder viscosity may have a more pronounced effect.

Table 2.20 Ranking between laboratories for each test methods

	Granite	Basalt	Greywacke	Limestone
Rolling bottle test after 24 h				
Average coating	10%	30%	40%	75%
Lab 1	4	3	2	1
Lab 2	4	3	2	1
Lab 3	4	3	2	1
Lab 4	4	3	2	1
Lab 5	4	2	3	1
Lab 6	4	2	3	1
Lab 10	4	2	3	1
Lab 13	4	2	3	1
Average	4	2.5	2.5	1
Boiling water stripping test				
Average coating	0–25%	75%	50%	75–85%
Lab 6	4	1	3	2
Lab 7	4	1	3	2
Lab 11	4	1	3	2
Average	4	1	3	2
Bonding bond strength test				
BSR	30–40%	50–90%	100%	85–100%
Lab 8	4	3	1	2
Lab 9	4	3	1	2
Lab 10				
Average	4	3	1	2

Nevertheless, it is interesting to see that with all these differences, all labs found the same worst aggregate.

The test conditions, especially in the case of the boiling water test play an important role in the results. Thus, the choice of one test should depend on climate conditions and/or viscosity of the binder.

When comparing the surface energy of aggregates independently to binder types, as determined in Table 2.13, it is not obvious there is a good correlation. Even the debonding work of aggregate/binder in presence of water, as shown in 0 cannot explain the results from the other tests; limestone and granite having similar values compared to greywacke.

Another important topic is how to correlate these test conditions to field behaviour. As bituminous binder viscosity is temperature dependent, it automatically affects the adhesion/cohesion properties of the binder. There is still limited research at this point of time to understand how the temperature influences the affinity or adhesion. If lowering the temperature will affect the adhesion: is there a linear

relation or is there a temperature where the adhesion is worst? And finally this test is performed on fresh bituminous binder, while on the road the binder was already processed through the mix plant and is already aged. The behaviour could be influenced by ageing.

2.6.5 Recommendation

The activities around this Task Group were mostly focused on having a better understanding of the adhesion and cohesion between bituminous binder and aggregates especially in presence of water. The number of laboratories participating to this study clearly shows the interest of this subject as confirmed by the numerous bibliographies available. Even with 13 laboratories in total there were seven different test methods or deviations from standard test methods used. As stated in the introduction, the adhesion theme is more than complex and within the scientific community there is no or not yet consensus on how to address that in a unique way. The end results certainly depend on many different factors which will fit more with one test method rather than another one.

Considering ravelling as the ultimate visible effect of loss of adhesion for hot climates; the bitumen bond strength with dry strength will certainly address pavement degradation. When ravelling occurs, most likely during summer time in presence of water, like in tropical or hot oceanic climate, the boiling water test is more appropriate for addressing good combinations of aggregate and binder. And for temperate climate conditions, the rolling bottle test could give a good indication of good vs. bad aggregate affinity.

Despite the reasonably good level of participation, the number of final results was not enough to determine statically valid repeatability and reproducibility. However, some recommendations can be made to consider values in terms of class rather than absolute value. Typically, it can be suggested four different classes as described in Table 2.21.

Considering the rolling bottle test, the test can be run by many laboratories, requires limited equipment and is easy to run. The test conditions are multiple and certainly need to be more accurately used and recorded. The overall reproducibility can be assessed in the magnitude of 15%, maybe higher for intermediate values between classes 2 and 3. The results after 24 h are already discriminating for combinations of aggregates and binders. The aggregates are the affecting parameter towards adhesion at equi-penetration values. However softness of binder could certainly affect the results.

Table 2.21 Proposed classes for affinity between aggregate and binders

Class	1	2	3	4
Ratio	100–75%	75–50%	50–25%	25–0%

For the boiling water test, the method is more accurate and quick to run (10 min) provided the calibration curve is done. It is less used than the rolling bottle and may use aggressive acid. The French standard is maybe more aggressive due to longer test duration, but to some extent more relevant to the normal temperature conditions of a pavement. The reproducibility is relatively good and can be assessed in the range of 10–15%, but this would require more data points.

For both of the above tests, automatic image analysis can improve accuracy but the main variability of results still remains in the test conditions and the preparation and conditioning of the samples.

The bitumen bond test may be a promising test method although it requires significant preparation of the stone, using a bulk piece of stone that can be different from the aggregates used in the final asphalt mixture. The test provides a comprehensive set of information from dry conditions and in presence of water. Its use has become more common in North America and so far not yet implemented in Europe. Reproducibility is not yet straight forward. The new protocol including mastic combination is promising and could improve reproducibility while addressing better control of load and sample shape.

In terms of recommendation, to improve reproducibility, additional work and effort have to be made on accurately defining and recording the test conditions.

2.7 Conclusions

As water damage is one important part of asphalt pavement durability. RILEM TC 237-SIB, Task Group 1 (TG1) worked on the affinity between aggregates and bituminous binder especially in presence of water. A round robin test was conducted with 13 laboratories and various test methods using four different aggregate types and three bituminous binders.

Water damage is more than a complex phenomenon and involves, amongst other things, wetting effect, adhesion and cohesion of bituminous binder over various conditions of use with climate, materials composition and loading.

The rolling bottle test consists of recording the remaining percentage of bituminous binder coating aggregates after being rolled in a water bottle. Whilst the test is run for 6, 24, 48 and 72 h, the outcomes start to be really discriminating after 24 h.

The analysis of these results shows that the reproducibility of the rolling bottle test is to date rather fair; one reason may be related to the visual interpretation of the percentage of coating, but blind analysis has shown relatively good repeatability. Other possible causes are more on the test conditions and sample preparation. The reproducibility of the rolling bottle test with the limited data available depends on the degree of coating. For poor, <25%, and excellent values, >75%, the reproducibility is relatively good with 15% while for intermediate values it is only 40%.

The boiling water test consists of more accurately measuring remaining coated bitumen on aggregates after being left in boiling water for 10 min. The test results

are discriminating towards aggregate type and start to be dependent of bitumen type as far as there are differences in the softening point. The number of data was not enough to technically determine reproducibility, but can be estimated to be 10–15%, again depending of the absolute results.

The bitumen bond strength test consists of measuring the bonding strength of bitumen on a block of stone aggregate. Results in dry conditions made at different temperatures are independent to aggregates and binders. The bonding strength ratio of wet over dry strength values at 22 °C has been shown to be in the same range of interpretation as the tensile strength ratio as measured on asphalt mixtures. Again with a limited amount of laboratories the reproducibility is difficult to determine and absolute results have shown a wide variability between laboratories.

The final recommendations from this study are that the different tests display similar results for extreme values, worst or best combinations of aggregate binder. But for intermediate values, the correlation between tests is less obvious. While reproducibility was difficult to determine due to insufficient data sets, it is in line with what is reported in the literature and the current standard. In order to better improve the accuracy of the results, it is suggested to provide results within four classes; from class 1 being best results to class 4 being the worst results.

When comparing rankings as obtained by each participant, the results are much more consistent. Most of the results have ranked the limestone aggregate as the best and granite the worst; the intermediate greywacke and basalt are more difficult to distinguish. The ranking of the stone types is rather independent of the binder type. Regarding the binders, the polymer modified binder ranks slightly better for all stone types, compared to the two unmodified binders, which perform similarly especially at high temperature test conditions.

In order to validate the affinity test method to experience from field behaviour; the effect of the variations in the field temperature and the effect of aged binder need to be taken into account.

Glossary

RILEM Réunion internationale des laboratoires et experts en matériaux

SIB Testing and characterization of sustainable innovative bituminous materials and systems

TG1 Task group 1

SHRP Strategic highway research program

ITS Indirect tensile strength

ITSR Indirect tensile strength ratio

CAST Coaxial shear test

APA Asphalt pavement analyser

EAPA European asphalt pavement association

FEHRL Federal highway agencies

CEN European committee on standardization

BBS Bitumen bond strength

AASHTO American association of state highway and transportation officials

RRT Round robin test

IFSTTAR Institut français des sciences et technologies des transports, de l'aménagement et des réseaux

NTEC Nottingham transportation engineering centre

XRF X-ray fluorescence

RBT Rolling bottle test

PmB Polymer modified bitumen

PATTI® Pneumatic adhesion tensile testing instrument

POTS Pull-off tensile strength

Ag Contact area of gasket with reaction plate (mm^2)

BP Burst pressure (kPa)

Aps Area of pull stub (mm^2)

C Piston constant

BSR Bond strength ratio

NOPTS New pull-off test

γ surface energy of bitumen or aggregate (mJ/m^2)

γ_{LW} Dispersive part of Lifshitz–van der Waals interaction of the surface energy (mJ/m^2)

γ_{AB} Polar part of Lifshitz–van der Waals interaction and acid-base component of the surface energy (mJ/m^2)

$\gamma+$ Lewis acid component of surface interaction

$\gamma-$ Lewis base component of surface interaction

γ_P Polar component of surface tension energy

γ_D Dispersive component of surface tension energy

γ_S Substrate surface energy

γ_L Liquid surface tension

γ_{SL} Liquid/substrate interfacial tension

W_{adh} Adhesion work

W_{adh}^{P} Polar components of adhesion work

W_{adh}^{D} Dispersive component of adhesion work

W_{BA}^{a} Dry bond strength, interfacial adhesion work between the bitumen (B) and aggregate (A)

W_{BWA}^{a} Interfacial adhesion work between the bitumen (B) and aggregate (A) in presence of water

W_{BB} Bitumen cohesion

W_{BL} Adhesion work between bitumen (B) and a probe liquid (L)

DCA Dynamic contact angle

DVS Dynamic vapour sorption

DSA Drop shape analyser

CAM Contact angle measurement

SSA Specific surface area

References

Andersland OB, Goetz WH (1955) Sonic test for the evaluation of stripping resistance in compacted bituminous mixtures. AAPT 25:p148

Apeagyei AK, Grenfell JA, Airey GD (2014a) Moisture-induced strength degradation of aggregate–asphalt mastic bonds. Road Mater Pavement Design 15(1):239–262

Apeagyei AK, Grenfell JA, Airey GD (2014b) Application of fickian and non-fickian diffusion models to study moisture diffusion in asphalt mastics. Mater Struct. https://doi.org/10.1617/s11527-014-0246-2

Apeagyei A, Grenfell J, Airey G (2015) Influence of aggregate absorption and diffusion properties on moisture damage in asphalt mixtures. Road Mater Pavement Design 16:404–422

Bagampadde U, Karlsson R (2007) Laboratory studies on stripping at bitumen/substrate interfaces using FTIR-ATR. J Mater Sci 42:3197–3206

Bagampadde U, Isacsson I, Kiggundu BM (2006) Impact of bitumen and aggregate composition on stripping in bituminous mixtures. Mater Struct 39:303–315

Beatty S, Smith J (2010) Fractional wettability and contact angle dynamics in burned water repellent soils. J Hydrol 391:97–108

Besamusca J, Rooijen van R, Robertus C, Beuving E (2012) The search for simple test to assess the complex of adhesion and durability of adhesion. In: 5th Eurasphalt and Eurobitume congress

Bhasin A (2006) Development of methods to quantify bitumen–aggregate adhesion and loss of adhesion due to water. Ph.D. dissertation, Texas A&M University, College Station

Bhasin A, Masad E, Little D, Lytton R (2006) Limits on adhesive bond energy for improved resistance of hot-mix asphalt to moisture damage. Transp Res Record: J Transp Res Board 1970:3–13

BitVal (2006) Analysis of available data for validation of bitumen tests. Report on phase 1 of the BitVal project

Bourrel M, Verzaro F (1998) Contrôle de la rupture des émulsions de bitume dans les applications routières. Revue Generale des Routes et Aerodromes 761:58–63

Canestrari F, Cardone F, Graziani A, Santagata F, Bahia H (2010) Adhesive and cohesive properties of asphalt-aggregate systems subjected to moisture damage. Road Mater Pavement Design 11:11–32

Castenada E, Such C, Hammoum F (2004) Towards a better understanding of moisture damage of hot mix asphalt using the complex modulus. In: 3rd Euroasphalt and Eurobitume Congress, paper 211, Vienna

Chaudhury MK (1996) Interfacial interaction between low-energy surfaces. Rep: A Rev J Mat Sci Eng R16:97–159

Chaudhury K, Whitesides G (1992) Correlation between surface free energy and surface constitution. Science 255(5049)

Chukwudeme EA, Hamouda AA (2009) Oil recovery from polar components (asphaltene and SA) treated chalk rocks by low salinity water and water containing SO_4^{2-} and Mg^{2+} at different temperatures, colloid and surfaces A. Physicochem Eng Aspects 336:174–182

Chung JY, Chaudhury MK (2005) Soft and hard adhesion. J Adhes 81:1119–1145

Cordon W (1979) Properties, evaluation and control of engineering materials. McGraw-Hill, NY

Corte J-F, Di Benedetto H (2004) Matériaux routiers bitumineux 1: description et propriétés des mélanges, Hermès science publications

Curtis C (1990) A literature review of liquid antistripping and tests for measuring stripping. SHRP-A/UIR-90-016

Curtis CW, Ensley K, Epps J (1993) Fundamental properties of asphalt–aggregate interactions including adhesion and absorption. SHRP-A-341

Dudásová D, Simon S, Hemmingsen PV, Sjöblom J (2008) Study of asphaltenes adsorption onto different minerals and clays part 1: experimental adsorption with UV depletion detection colloid and surfaces A. Physicochem Eng Aspects 317:1–9

EN 12594. Bitumen and bituminous binders, preparation of test samples. EN 12594

EN 12697-11. bituminous mixtures—test methods for hot mix asphalt—part 11: determination of the affinity between aggregate and bitumen. EN 12697-11

Ensley K (1973) A study of asphalt–aggregate interactions and asphalt molecular interactions by microcalorimetric methods: postulated Interaction Mechanism. J Inst Petr 59(570)

Fini EH, Al-Qadi IL, Masson JF, McGhee KK (2008) Interfacial fracture energy: an indicator of bituminous material adhesion. AAPT, vol 77

Fowkes F (1962) Determination of interfacial tensions, contact angles, and dispersion forces in surfaces by assuming additivity of intermolecular interactions in surfaces. J Phys Chem 382:66

Good R (1992) Contact angle, wetting and adhesion: a critical review. J Adhes Sci Technol 6:1269–1302

Good R, van Oss C (1991) The modern theory of contact angles and the hydrogen bond components of surface energies, modern approach to wettability: theory and application. Plenum Press, New York

Grenfell J, Ahmad NB, Liu Y, Apeagyei A, Large D, Airey G (2014) Assessing asphalt mixture moisture susceptibility through intrinsic adhesion, bitumen stripping and mechanical damage. Road Mater Pavement Design 15(1):132

Grönniger J (2008) Computergestuetzte Auswertung von rolling-bottle-tests/ computer aided analysis of rolling-bottle-tests. Strasse Und Autobahn 59(7):415–419

Grönniger J, Wistuba M, Renken P (2010) Adhesion in bitumen-aggregate-systems: new technique for automated interpretation of rolling bottle tests. Road Mater Pavement Design 11(4):881–898

Gubler R, Partl MN, Canestrari F, Grilli A (2005) Influence of water and temperature on mechanical properties of selected asphalt pavements. Mater Struct 38:523–532

Hanz A, Bahia H, Wen H (2007) Test method to determine aggregate/asphalt adhesion properties and potential moisture damage. WHRP 07–02

Hefer AW (2004) Adhesion in bitumen–aggregate systems and quantification of the effects of water on the adhesive bond. Thesis University of Pretoria, Dec 2004

Hicks RG, Finn FN (1994) Validation of the relationship between asphalt properties and asphalt–aggregate mix performance. SHRP-A-398, Stage 1

Hirsch V, Friemel-Goettlich B (2009) Bestimmung des adhaesiven Potentials von Bitumen und Gesteinsoberflaechen mit Hilfe der Kontaktwinkelmessmethode. Berichte der Bundesanstalt für Straßenwesen unterreihte Straßenbau, Issue 59, 2009

Horgnies M, Darque-Ceretti E, Fezai H, Felder E (2011) Influence of the interfacial composition on the adhesion between aggregates and bitumen: Investigations by EDX, XPS and peel test. Int J Adhes Adhes 31:238–247

Howson J, Masad E, Bhasin A, Little D, Lytton R (2011) Comprehensive analysis of the surface free energy of asphalt and aggregates and the effects of changes in pH. Constr Build Mater 25:2554–2564

Jakarni FM (2012) Adhesion of asphalt mixtures. Ph.D. dissertation, University of Nottingham, Nottingham

Jeon YW, Curtis CW (1992) A literature review of the adsorption of asphalt functionalities on aggregate surfaces. SHRP-A-3131992

Jorgensen T (2002) Testing adhesion between bitumen and aggregate with the rolling bottle test and the boiling test. In: 6th International conference on bearing capacity of roads and airfields, Lisbon, Portugal

Källén HA, Heyden AA, Lindh PB (2013) Measuring bitumen coverage of stones using a turntable and specular reflections. In: VISAPP, proceedings of the international conference on computer vision theory and applications, vol 1, pp 333–337

Kassem E, Masad E, Bulut R, Lytton R (2006) Measurements of moisture suction and diffusion coefficient in hot mix asphalt and their relationship to moisture damage. In: Annual meeting transportation research board, Washington, D.C.

Kringos N, Scarpas A, Bondt de A (2008) Determination of moisture susceptibility of mastic-stone bond strength and comparison to thermodynamical properties. Annual meeting AAPT, Philadelphia

Lamperti R, Lantieri V, Sangiorgi C, Bitelli G, Simone A (2015) Semi-automatic evaluation of the degree of bitumen coverage on bitumen-coated aggregates. In Rilem SIB symposium, Ancona

Laurell Lyne A, Birgisson B, Redelius P (2010) Interaction forces between mineral aggregates and bitumen calculated using the Hamaker Constant. Road Mater Pavement Design 11:305–323 (Special issue on asphalt technology EATA 2010)

Laurell Lyne A, Redelius P, Collin M, Birgisson (2013) Characterisation of stripping properties of stone material in asphalt. Mater Structu 46(1):47–61

Laurell Lyne A, Krivosheeva O, Birgisson B (2013) Adhesion between bitumen and aggregate: implementation of spectroscopic ellipsometry characterisation and estimation of Hamaker's constant. Mater Struct 46(10)

Lee DL, Guinn JA, Khandhal PS, Dunning RL (1990) Absorption of asphalt into porous aggregates. SHRP-A/UIR-90-009

Little D, Bhassin A (2006) Using surface energy measurement to select materials for asphalt pavement. NCHRP project 9-37

Liu Y, Apeagyei A, Ahmad N, Grenfell J, Airey G (2014) Examination of moisture sensitivity of aggregate-bitumen bonding strength using loose asphalt mixture and physico-chemical surface energy property tests. Int J Pavement Eng 15(7):657–670

LTRC (1995) Compatibility of aggregate, asphalt cement and antistripping materials. LTRC report no 292

Lytton R, Flumerfelt R (1998) Report to foundation CROW the Netherlands from the Texas Engineering Experiment Station. Texas A&M University

Mathews DH, Colwill DM, Yüce R (1965) Adhesion tests for bituminous materials. J Appl Chem
Maugis D (1999) Contact, adhesion and rupture of elastic solids. Springer, New York
Meng J (2010) Affinity of asphalt to mineral aggregate: pull-off test evaluation. M.S. thesis, University of Wisconsin-Madison, Madison
Miller T, Arega Z, Bahia H (2010) Correlating rheological properties of emulsion residue to early chip seal performance. J Transp Res Board 2179:66–74
Miller C, Little D, Bhasin A, Gardner N, Herbert B (2012) Surface energy characteristics of natural minerals and their impact of aggregate–bitumen bond strengths and asphalt mixture durability. In: TRB annual meeting, Washington
Mo L (2010) Damage at the interface of interlayers and mastic of open grade porous asphalt. Thesis University Delft
Moraes R, Velasquez R, Bahia H (2011) Measuring effect of moisture on asphalt-aggregate bond with the bitumen bond strength test. J Transp Res Board 9:70–81
Morgenstern A, Sschulze C, Marschke L (2010) Verbesserung der Praezision der Pruefung zur Bestimmung des Haftverhaltens zwischen groben Gesteinskoernungen und Bitumen/ Improved test methods for the determination of the affinity between aggregate and bitumen. Strasse Und Autobahn 61(12):879–884
NCAT (1988) Stripping in HMA mixtures: state-of-the-art and critical review of test methods. NCAT report no 88-02
Porot L, Soenen H, Besamusca J, Apeagyei A, Grenfell J, Sylbilski D (2015) Bitumen/aggregate affinity—rilem round robin test on rolling bottle test. In: RILEM SIB Symposium, Ancona
Renken P (2003) Haftung zwischen Bitumen und Gesteinskörnungen—ein Statusbericht. Bitumen, 65 Jahrgang, Heft 1, March
Renken P, Wistuba M, Grönniger J, Schindler K (2010) Adhesion von Bitumen am Gestein: Verfahren der quantitativen Bestimmung auf Grundlage der Europaeischen Normung. Forschung Strassenbau und Strassenverkehrstechnik, Issue 1043, 2010
Rieder W, Weber H (1933) Adhesion of bituminous binders to stone. Asph.u. Teer, 37–41
Rychen P, Pittet M, Dumont A-G (2010) Determination of the presence and efficiency of adhesion agent in asphalt concrete. EPFL report 153410, Swiss Federal Roads
Saal R (1933) Bitumen
Scholz TV, Terrel RL, Al-Joaib A, Bea J (1994) Water sensitivity: binder validation. SHRP-A-402
Shah BD (2003) Evaluation of moisture damage within asphalt concrete mixes. Thesis Texas A&M University
Shell (1979) Bitumes, techniques et utilisations, Shell France
Some S, Delaunay D, Gaudefroy V (2013) Comparison and validation of thermal contact resistance models at solid-liquid interface taking into account the wettability parameters. Appl Therm Eng 61:513–540
Some S, Gaudefroy V, Delaunay D (2014) A new laboratory method to evaluate the influence of aggregate temperature on the binder-aggregate bonding: first results. Mater Struct 47:963–976
T. Committee (2003) Moisture sensitivity of asphalt pavements. A national seminar, San Diego, 4–6 Feb 2003
Tan Y, Guo M (2013) Using surface free energy method to study the cohesion and adhesion or asphalt mastic. Constr Build Mater 47:254–260
Tarrer AR, Wagh V (1991) The effect of the physical and chemical characterization of the aggregate on bonding. SHRP-A/UIR-91-507
RIO Technology (2003) Fundamentals of stripping in bituminous pavements. Div. of Highway Engineering, VT AR 03:01 Research, Stockholm
Terrel RL, Al-Swailmi S (1994) Water sensitivity of asphalt–aggregate mixes: test sections. SHRP-A-403
Tu Y, O'Carroll JB, Kotlyar LS, Sparks B (2005) Recovery of bitumen from oilsands: gelation of ultra-fine clay in the primary separation vessel. Fuel 84:653–660
Ulmgren N (2004) The influence of the mastic on the durability of asphalt pavements as studied by the shaking abrasion test. In: 3rd Eurasphalt and Eurobitume congress, vol 2, pp 1464–1475

van Oss C, Chaudhury M, Good R (1988) Interfacial Lifshitz–van der Waals and polar interactions in macroscopic systems. Chem Rev 88(6):927–941

Wong WG, Han HF, He GP, Qiu X, Wang K (2004) Effects of water on permanent deformation potential of asphalt concrete mixtures. Mater Struct 37:532–538

XP T 066-043. Essai d'adhésivité passive des liants anhydres en présence d'eau. Norme Francaise

Yazgan B (2003) A new testing protocol for seal coat (chip seal) aggregate binder compatibility. Master's degree dissertation, Texas Technical University, Texas

Youtcheff J, Aurilio V (1997) Moisture sensitivity of asphalt binders: evaluation and modeling of the pneumatic Adhhsion test results. In: 42nd annual conference of Canadian Technical Asphalt Association, pp 180–200

Zhang J, Apeagyei A, Airey G, Grenfell J (2015) Influence of aggregate mineralogical composition on water resistance of aggregate–bitumen adhesion. Int J Adhes Adhes 62:45–54

Ziyani L, Gaudefroy V, Ferber V, Hammoum F (2016) A predictive and experimental method to assess bitumen emulsion wetting on mineral substrates, colloids and surfaces a: physicochem. Eng Aspects 489:322–335

Chapter 3
Three-Dimensional Characterisation of Linear Viscoelastic Properties of Bituminous Mixtures

A. Graziani, H. Di Benedetto, D. Perraton, C. Sauzéat, B. Hofko, Q. T. Nguyen, S. Pouget, L. D. Poulikakos, N. Tapsoba, J. Grenfell, A. Cannone Falchetto, M. Wistuba and C. Petit

Abstract This chapter focuses on the three-dimensional linear viscoelastic (3D-LVE) behaviour of bituminous mixtures and in particular on the measurement and modelling of the complex Young's modulus and Poisson's ratio (PR). In the first part of the chapter, the LVE definition of PR is reviewed and experimental measurements of the LVE PR carried out over the last 40 years are summarised. The second part of the chapter is devoted to the description of a RILEM round robin test (RRT) organized by Task Group 3 (TG3) "Mechanical testing of bituminous

A. Graziani (✉)
Università Politecnica delle Marche, Ancona, Italy
e-mail: a.graziani@univpm.it

H. Di Benedetto · C. Sauzéat · N. Tapsoba
University of Lyon, ENTPE – LTDS (UMR CNRS 5513), Vaulx-en-Velin, France

D. Perraton
University of Québec, ETS, 1100 Notre-Dame Ouest, Montreal, QC, Canada

B. Hofko
Vienna University of Technology, Vienna, Austria

Q. T. Nguyen
University of Transport and Communications, Hanoi, Vietnam

S. Pouget
EIFFAGE Infrastructures, Lyon, France

L. D. Poulikakos
Empa, Swiss Federal Laboratories for Materials Science and Technology, Dübendorf, Switzerland

J. Grenfell
ARRB, 500 Burwood Highway, Vermont South, VIC 3133, Australia

A. Cannone Falchetto · M. Wistuba
Technische Universitat Braunschweig, Braunschweig, Germany

C. Petit
Universite de Limoges, Equipe Génie Civil et Durabilité, Limoges, France

M. N. Partl et al. (eds.), *Testing and Characterization of Sustainable Innovative Bituminous Materials and Systems*, RILEM State-of-the-Art Reports 24,
https://doi.org/10.1007/978-3-319-71023-5_3

mixtures" of RILEM TC 237-SIB. Within the RRT uniaxial cyclic (sinusoidal tension/compression or haversine compression) tests at different temperatures and frequencies were carried out on cylindrical specimens cored from laboratory compacted slabs. Two types of bituminous mixtures, GB3 (continuously graded) and GB5® (gap-graded), were analysed. Five laboratories participated in the RRT, each laboratory measured axial and transverse (or diametral) strains using different sensors and configurations. In particular, transverse strain was measured along two orthogonal directions in order to evaluate the effect of compaction-induced anisotropy on PR. Results confirmed that PR of bituminous mixtures is a complex function of temperature and frequency and that the time-temperature superposition principle can be applied (for absolute value and phase angle). For the studied mixtures the norm of the complex PR ranged between 0.22 (low temperatures/high frequencies) and 0.60 (high temperatures/low frequencies) whereas the phase angle was less than 6°. A small difference (less than 0.05) was found between measurements carried out in two orthogonal directions. This small difference is probably related to measurement accuracy and not to the anisotropic behaviour of the material. Comparison of data between the different laboratories, which could not be performed at exactly the same temperatures and frequencies, was performed using a common reference given by the 3-dimensional formulation of the 2S2P1D linear viscoelastic model. This model provides a good simulation of experimental data. Based on close results from all participating laboratories, it is possible to conclude that cyclic uniaxial test could be a good candidate to become a standard test for evaluating the 3D-LVE behaviour of bituminous mixtures.

Keywords Bituminous mixtures · Linear viscoelastic behaviour
Complex Poisson's ratio · Three-dimensional characterization ·
Thermo-rheological modelling

List of Symbols

Roman Letters

a_{Tref}	Temperature shift factors with respect to T_{ref}
C_1, C_2	WLF constants
E	Young's modulus
E_0	Absolute value (norm) of complex Young's modulus
E_1	Real (storage) component of complex Young's modulus
E_2	Imaginary (loss) component of complex Young's modulus
E^*	Complex Young's modulus
f, f_t	Testing frequency
f_{eq}	Equivalent frequency
G	Shear modulus
G_{ij}	Shear moduli in plane ij
K	Bulk modulus
T^*	Complex transverse modulus
T_{ref}	Reference temperature

Greek Letters

ε_i	Normal strain in direction i
ε_i^*	Phasor of normal strain in direction i
ε_{0i}	Amplitude of sinusoidal strain in direction i
φ	Phase angle
φ_E	Phase (or loss) angle of complex Young's modulus
φ_{vi}	Phase angle of complex Poisson's ratio in direction i
$\varphi_{\sigma 1}$	Phase angle of sinusoidal stress in direction 1
$\varphi_{\varepsilon i}$	Phase angle of sinusoidal strain in direction i
ν	Poisson's ratio
ν^*	Complex Poisson's ratio
ν_i^*	Complex Poisson's ratio in direction i
$\nu_{0i}{}^*$	Absolute value (norm) of complex Poisson's ratio in direction i
ν_{1i}	Real component of complex Poisson's ratio in direction i
ν_{2i}	Imaginary component of complex Poisson's ratio in direction i
ν_{ij}	Elastic Poisson's ratio in plane ij
σ_1^*	Phasor of normal stress in direction 1
σ_{01}	Amplitude of sinusoidal stress in direction 1
ω	Pulsation (angular frequency)
τ_E, τ_v	Characteristic time for Young's modulus and Poisson's ratio rheological modelling

List of Abbreviations

1D	One-Dimensional
2D	Two-Dimensional
2S2P1D	2 Springs, 2 Parabolic (elements) 1 (linear) Dashpot
3D	Three-Dimensional
AASHTO	American Association of State Highway and Transportation Officials
DSR	Dynamic Shear Rheometer
ENTPE	Ecole Nationale des Travaux Publics de l'Etat
EVCP	Elastic Viscoelastic Correspondence Principle
GB	Grave Bitume
HMA	Hot Mix Asphalt
IDT	Indirect Tension
LE	Linear Elastic
LVDT	Linear Variable Differential Transformer
LVE	Linear Viscoelastic
MEPDG	Mechanistic-Empirical Pavement Design Guide
NCHRP	National Cooperative Highway Research Program
PR	Poisson's Ratio
RILEM	International Union of Laboratories and Experts in Construction Materials, Systems and Structures
RRT	Round Robin Test

TG3	Task Group 3
TTSP	Time-Temperature Superposition Principle
WLF	Williams-Landel-Ferry

3.1 Introduction

3.1.1 Three-Dimensional Characterisation of Bituminous Mixtures

Stress and deformation analyses involving pavement structures require a three-dimensional (3D) approach. In the analytical models employed to perform such analyses, the layer response is generally considered isotropic and characterized using the two material properties derived from the linear elastic (LE) theory: the axial (or Young's) modulus E and the Poisson's ratio (PR) ν.

As far as bituminous mixtures are concerned, characterisation of the deformation response is based on the linear viscoelasticity (LVE) theory and on the time-temperature superposition principle (TTSP) (Di Benedetto and De la Roche 1998). In particular, stiffness properties can be evaluated in small deformation (less than 10^{-4} m/m) using the complex Young's modulus E^* (Di Benedetto et al. 2001). Measurement and modeling of E^* has been a central topic in pavement engineering since its very beginning (Papazian 1963; Huet 1963; Sayegh 1965). Consequently, several test methods have been standardized and various predictive (i.e. composition-based) or thermo-rheological models are currently available for E^* (Di Benedetto and De la Roche 1998; Kim 2008; Olard and Di Benedetto 2003).

Measurement and modeling of the PR of bituminous mixtures is not a new research issue. In particular, its dependence on temperature and time (or frequency) was highlighted since the beginning of the '60s (Papazian 1963; Sayegh 1968). However, for pavement analysis and design, such variability is generally overlooked and a constant value (e.g. $\nu = 0.35$) is assumed in both LE and LVE response models (Huang 2004; Chabot et al. 2010). Such a simplified approach has been partly improved in the AASHTO Mechanistic-Empirical Pavement Design Guide (MEPDG) (NCHRP 2009), which allowed the use of a variable PR for hot-mix asphalt (HMA) mixtures. Sensitivity analyses carried out on the MEPDG design inputs, confirmed the importance of an accurate estimation of the PR of HMA and its impact on flexible pavement performance prediction (Maher and Bennert 2008; Schwartz et al. 2013).

Under the hypothesis of isotropy, the 3D characterisation of a LVE body requires the simultaneous measurement of two independent material functions (Hilton 2001; Tschoegl et al. 2002). For HMA this can be practically achieved by the simultaneous measurement of the complex Young's modulus E^* and the

complex PR v^*. Though apparently straightforward, such an approach raises various practical and theoretical issues.

From a practical point of view, the simultaneous measurement of two perpendicular strains during the same experiment is required. This clearly requires an experimental setup which is more complicated with respect to the ones routinely used to measure only 1D properties like the Young's modulus (Di Benedetto et al. 2007a, b). In addition, such strain measurements must be extremely accurate because, under specific test conditions (i.e. lower PR values), the transverse strain is almost one order of magnitude smaller than the longitudinal strain.

From a theoretical point of view, it should be highlighted that the LVE PR can be defined in different ways (Hilton 2001). Several authors pointed out the ambiguities of some of these definitions, highlighting that the PR is not a fundamental material property such as relaxation moduli or creep compliances (Lakes and Wineman 2006; Hilton 2011). In fact, it can be shown that complex PR, as defined further in this section, is in relation (Carson transform at point $j\omega$) of the time domain PR (that can be obtained easily for specific loading condition corresponding to relaxation). These two PR are fundamental material properties.

In addition, although in pavement design methods HMA is considered to behave as an isotropic material, the laying and compaction process could lead to a preferential orientation of the aggregate particles, thus inducing an anisotropic behavior. In particular, the following three preferential directions can be recognized in a pavement structure:

- direction 1 (dir1): horizontal longitudinal direction, parallel to the roller compactor movement;
- direction 2 (dir2): vertical direction along which densification occurs;
- direction 3 (dir3): transverse horizontal direction.

To reproduce the roller compactor effect on the structural arrangement of an asphalt material placed on the road, different types of compactors were developed to produce HMA slabs in the laboratory. Often, samples used for mechanical investigations are cored in the direction of the compactor wheel movement (dir1) to determine the complex Young's modulus. In order to evaluate whether the Poisson's ratio can be considered as an isotropic property, under axial loading (dir1) both transvers strains (i.e. in dir2 and dir3) must be measured.

In this context, Task Group 3 (TG3) "Mechanical Testing of Mixtures" of the RILEM Technical Committee 237-SIB "Testing and characterisation of sustainable innovative bituminous materials and systems" decided to study, between 2012 and 2015, the 3D-LVE response of bituminous mixtures through the measurement of E^* and v^*. To this aim, a round robin test (RRT) was organized in order to compare different measurement techniques and evaluate the possible effect of compaction-induced mixture anisotropy on the tested specimens.

3.1.2 Presentation of the Chapter

This chapter summarizes the efforts of active TG3 members and is organized as follows. Section 3.2 is devoted to a literature review and is divided into two main parts. First, the definition of Poisson's ratio in LVE is reviewed, and then available experimental data regarding the Poisson's ratio of bituminous materials are summarized. Section 3.3 illustrates the organization and the results of the Rilem RRT. This section includes the description of the test principle, the tested mixture and of the experimental setup adopted by the participating laboratories. Experimental results i.e. the complex Young's modulus and complex PR obtained by the participating laboratories are presented and analyzed. Conclusions and recommendations are reported in Sect. 3.4.

3.2 Literature Review

3.2.1 Poisson's Ratio

3.2.1.1 Poisson's Ratio Definition in Linear Elasticity

The 3D LE response of an isotropic medium can be characterized using two constants. The shear modulus G and the bulk modulus K are usually considered fundamental elastic constants since they can be used to separate the infinitesimal deformation into changes of shape and volume, respectively. However, the Young's modulus E and Poisson's ratio ν are the most frequently used constants in engineering practice, because their direct experimental determination is readily understood.

In particular, considering a uniaxial (1D) stress state ($\sigma_1 \neq 0$; $\sigma_2 = \sigma_3 = 0$), the PR is obtained as the ratio between the opposite of the transverse strain $\varepsilon_2 = \varepsilon_3$ and the axial strain ε_1:

$$\nu = -\frac{\varepsilon_2}{\varepsilon_1} \tag{3.1}$$

It is remarked that, for deformation energy to be non negative, the PR must be in the range $-1 < \nu < 0.5$. The value $\nu = 0.5$ identifies a deformation mode with no volume change, and is often assumed for bitumens (Van Der Poel 1954), whereas negative values of ν characterize the so-called auxetic materials (Lakes 1987).

Generalized definitions of G, E and ν are also used to write LE constitutive relations for anisotropic bodies. For example, the response of orthotropic materials (three planes of symmetry), can be described using nine elastic constants if the rheological tensor is symmetrical (case of hyper-elastic behavior type): three Young's moduli (E_{11}, E_{22}, E_{33}), three shear moduli (G_{12}, G_{23}, G_{31}) and three

Poisson's ratios (v_{12}, v_{23}, v_{31}) (Lekhnitskii 1977). Analogously, for transversely isotropic (hyper-elastic) materials (one axis of symmetry), five elastic constants are necessary: the longitudinal Young's modulus (E_{11}), the transverse Young's modulus (E_{22}), the shear modulus (G_{12}) and the Poisson's ratios v_{22} and v_{12}.

3.2.1.2 Poisson's Ratio Definition in Isotropic Linear Viscoelasticity

Similar to any other LVE material function, the functional form of the viscoelastic PR depends on the form of the excitation which is applied to elicit the material response. Considering a 1D loading history corresponding to relaxation in direction 1 ($\varepsilon_1(t) = \varepsilon_{01}$ constant, $\sigma_2 = \sigma_3 = 0$) the viscoelastic PR is obtained by Eq. 3.2 similar to Eq. 3.1.

$$v(t) = -\frac{\varepsilon_2(t)}{\varepsilon_{01}} \tag{3.2}$$

If 1D sinusoidal excitation of pulsation ω is applied in direction 1 ($\varepsilon_1(t)$ or $\sigma_1(t)$, $\sigma_2 = \sigma_3 = 0$) the Fourier transform can be used to define a complex, frequency-domain PR, according to Eq. 3.3

$$\overline{\overline{v}}(\omega) = -\frac{\overline{\overline{\varepsilon_2}}(\omega)}{\overline{\overline{\varepsilon_1}}(\omega)} \tag{3.3}$$

where $\overline{\overline{f}}(\omega)$ is the Fourier transform of $f(t)$.

3.2.2 *Poisson's Ratio of Bituminous Mixes in the Linear Domain*

3.2.2.1 General Considerations

There are no standard test configurations or procedures for the experimental measurement of PR of bituminous mixes; therefore published values generally show a great dispersion, sometimes exceeding the upper LE limit for isotropic materials of 0.5. Besides test procedures, the main reason for this dispersion and "apparently" unrealistic values is that often tests are carried out at stress and strain levels that exceed the linearity limit (Kim 2008). An additional source of uncertainty may derive from the anisotropy of material response. For these reasons, when comparing experimental values of the PR, the importance of test type, loading mode, deformation level and specimen preparation procedure cannot be overemphasized.

The literature review presented in this section focuses on studies carried out within the LVE domain, which are characterized by the application of an "infinitesimal"

strain field. For bituminous mixtures the linearity limit is generally less than 100 μm/m. It is emphasized that this limit refers to axial strain and was established for complex Young's modulus (Di Benedetto et al. 2001; Airey et al. 2003).

As regards the test type, the PR has been measured using both axial tests on cylindrical specimens and indirect tension (IDT) testing. The first configuration is of homogeneous type and hence allows the direct calculation of PR through the comparison of longitudinal and transverse or diametral strains. On the other hand, the IDT is non-homogeneous because it requires the solution of a 2D stress-strain problem in order to obtain both Young's modulus and PR. For this reason, the use of IDT also calls for the validity of the EVCP (elastic viscoelastic correspondence principle).

As regards the loading mode, both harmonic tests (i.e. frequency mode) and monotonic tests (i.e. time mode) have been adopted. In the first case, both controlled axial stress and controlled axial strain[1] procedures have been used. In the second case, creep (which does not provide PR directly from strain ratio) or relaxation tests have been adopted.

As regards to specimen preparation, the effect of compaction-induced anisotropy should be considered. To reproduce the three preferential directions (orthotropic structure) of field compaction, laboratory wheel compactors can be employed (Clec'h et al. 2010). However, laboratory samples are often prepared using gyratory compactors, producing an internal structure characterized by an axis of symmetry (transverse isotropy structure).

In principle, the PR can also be obtained indirectly, from two other LVE response functions. This approach is clearly based on the validity of the EVCP and on the isotropy hypothesis. It was underlined that, in this case, the two source functions must be measured simultaneously, on the same specimen, with high accuracy and precision (Tschoegl et al. 2002).

3.2.2.2 Frequency-Domain Characterisation

Papazian (1963) first proposed a methodology to characterize the isotropic 3D LVE response of HMA by means of sinusoidal-stress loading tests and constant-stress static tests. Both types of test were performed on cylindrical specimens (Fig. 3.1a), measuring axial and circumferential strain (Fig. 3.1b) by means of bonded strain gauges. Two independent complex-domain response functions were calculated from experimental data: the complex Young's Modulus E^* and the complex transverse modulus T^*, the latter being the ratio of axial stress and transverse strain. Then, the complex PR v^* was mathematically defined as the ratio between E^* and T^*, which leads to the same definition given by Eq. 3.3. Papazian focused on the magnitude (i.e. the absolute value or the norm) of the response functions T^* and v^* and did not report any phase difference between the transverse and the axial strain response.

[1]Most test equipment (e.g. hydraulic or pneumatic press) actually simulates a control strain procedure by controlling the load level with a closed loop control system.

Sayegh (1968) measured the complex PR of bituminous mixtures using an experimental setup similar to that proposed by Papazian, i.e. comparing longitudinal and transverse strains of cylindrical bars subjected to harmonic longitudinal vibrations (Fig. 3.2a). Tests were carried out at temperatures from −5 to 40 °C and frequencies from 4 to 100 Hz, on a continuously graded mixture. Though a phase difference between transverse and longitudinal strain was clearly expected (Fig. 3.2a), the PR was found to be real number, monotonically increasing from 0.1 at high frequencies and low temperatures to 0.5 for low frequencies and high temperatures. The TTSP was applied to obtain an apparent master curve for the PR according to the following equation

$$\nu = 0.3 - 0.127 \arctan[0.94(a_{15}f - 2)] \tag{3.4}$$

where f is the loading frequency and a_{15} is the shift factor (reference temperature was 15 °C).

Following the pioneer studies by Papazian and Sayegh, direct measurements of the complex PR of bituminous mixtures have been carried out in the US (Stephenson and Manke 1972) and in France (Charif 1991; Doubbaneh 1995). Results confirmed that the norm of ν^* varies between 0.3 and the theoretical LE limit for isotropic materials of 0.50, depending on temperature and frequency. Moreover its imaginary part was found to be very small, indicating that, for pavement analysis purposes, it could be treated as a real number.

Starting from the end of the '90s the PR of HMA mixtures was investigated within the framework of the NCHRP Project 1-37A. Witczak and Mirza (1999) developed a regression equation to estimate the numerical value of the PR of HMA as a function of temperature. In the current version of the AASHTO mechanistic-empirical pavement design guide (MEPDG), the PR can be estimated from the resilient modulus (ARA 2004). In both cases, a sigmoidal function has been adopted:

$$\nu = 0.15 + \frac{0.35}{1 + \exp[3.1849 - 0.04233 \cdot T]} \tag{3.5a}$$

$$\nu = 0.15 + \frac{0.35}{1 + \exp[a + bE_{AC}]} \tag{3.5b}$$

where T is the temperature in °F and E_{AC} is the resilient modulus of HMA in psi. The default values of coefficients a and b suggested by the MEPDG for dense graded asphalt mixtures are −1.63 and 3.84×10^{-6}, respectively; these values were estimated from IDT tests (Maher and Bennert 2008). As it can be observed, in both Eqs. 3.5a and 3.5b, the PR monotonically increases starting from 0.15 at low temperatures (high frequencies) and approaches 0.5 at high temperatures (low frequencies).

Equation 3.5b was later verified by testing laboratory mixes, plant mixes and field cores (Maher and Bennert 2008). Modulus and PR values were measured

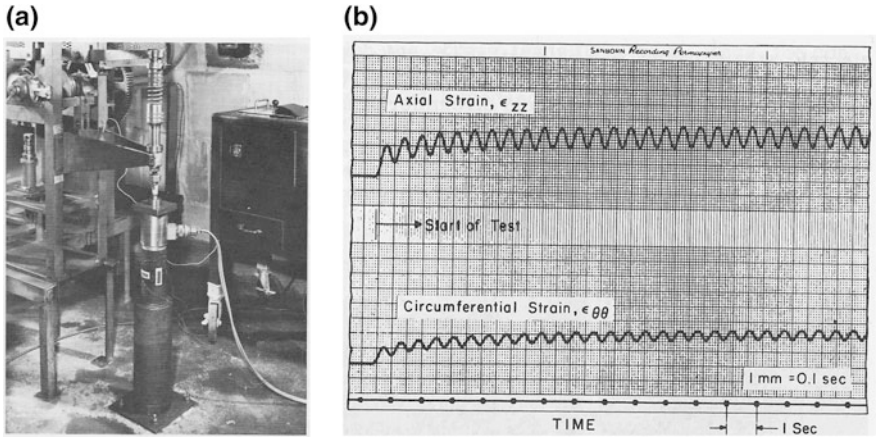

Fig. 3.1 Uniaxial harmonic test on cylindrical specimen reported by Papazian (1963); **a** tests setup; **b** measured strains

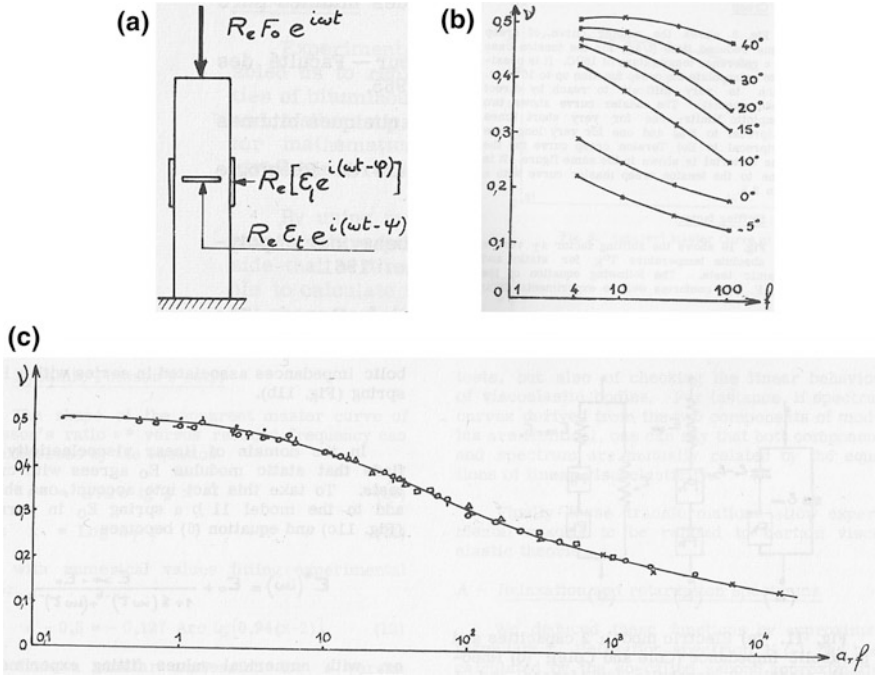

Fig. 3.2 Complex PR measurements reported by Sayegh (1968): **a** test setup; **b** isothermal curves; **c** master curve at 15 °C

using sinusoidal compression tests on cylindrical specimens (AASHTO TP62) at temperatures from −12 to 54 °C and frequencies from 0.1 to 25 Hz. Axial and transverse strains were measured using LVDT transducers (Fig. 3.3a). An example of the measured data (PR versus dynamic modulus) is reported in Fig. 3.3b. As it can be observed, values measured in this study did not follow a sigmoidal trend and were consistently lower than those predicted by Eq. 3.5b.

The PR was measured using sinusoidal IDT tests by Kim et al. (2004) and by Islam et al. (2015). In the fist study, tests were carried out on a wide range of laboratory specimens prepared using the gyratory compactor, at temperatures from −10 to 35 °C and frequencies from 0.01 to 25 Hz. In the second study, tests were carried out on field cores at temperatures from −15 to 54 °C and frequencies from 0.1 to 1 Hz. Two LVDTs were used to measure the vertical and the horizontal strain on one side of the specimen (Fig. 3.4).

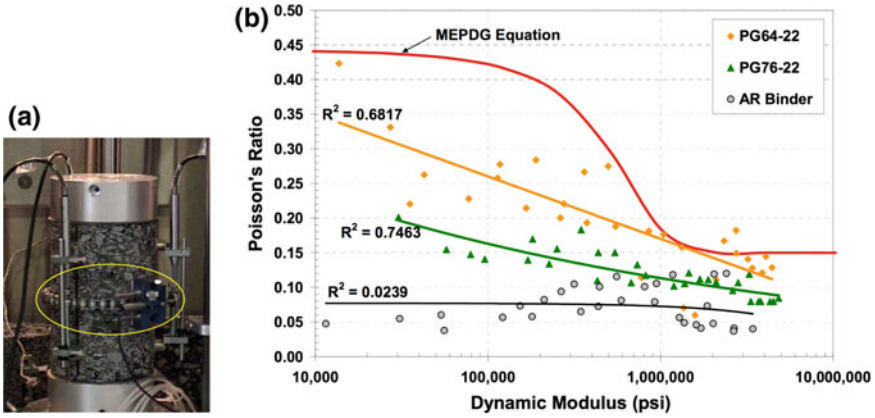

Fig. 3.3 PR measurements at Rutgers University (Maher and Bennert 2008): **a** tests setup; **b** measured PR values

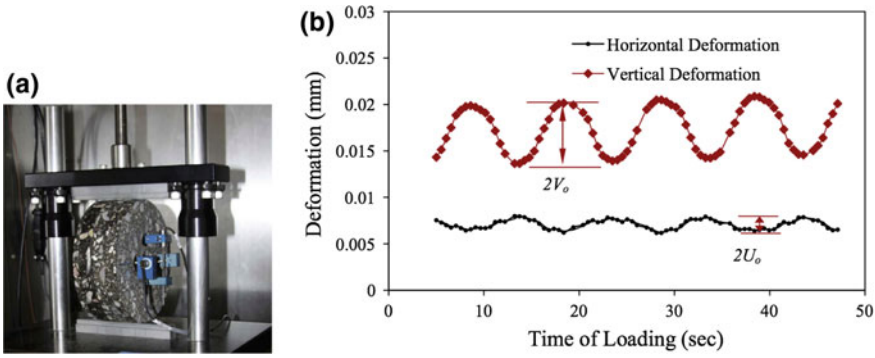

Fig. 3.4 PR measurements in IDT tests (Islam et al. 2015): **a** tests setup; **b** measured horizontal and vertical deformation

In both studies the reported values of PR monotonically increased from 0.15 at low temperatures (high frequencies) to 0.5 at high temperatures (low frequencies). The data reported by Islam et al. (2015) also confirmed the validity of the sigmoidal trend described by Eq. 3.5b, though different regression coefficients were obtained.

The 3D LVE response of bituminous mixtures has been deeply investigated at University of Lyon/Ecole Nationale des Travaux Publics de l'Etat (ENTPE) (Di Benedetto et al. 2007a; Nguyen et al. 2009; Di Benedetto et al. 2009; Pouget et al. 2010, 2012a, b; Mounier et al. 2012; Nguyen et al. 2015). Tests have been carried out on cylindrical specimens using sinusoidal tension-compression and compression loading. Axial and radial strains were deduced using extensometers and non-contact measurements (details on tests equipment and procedures are presented in Sect. 3.3.2.5). Test conditions included a wide range of temperatures (from −30 to 50°C) and frequencies (from 0.01 to 10 Hz). Experimental results confirmed that the norm of the complex PR depends on both frequency and temperature; specifically it increases if frequency decreases and temperature increases (Fig. 3.5a–c). Reported values of the PR norm ranged from 0.10 at low temperatures (high frequencies) to 0.5 at high temperatures (low frequencies). It was also observed that the phase angle of PR is not null, even though its absolute value is small (below 5°). Validity of the TTSP was verified and master curves were obtained for both the norm and phase angle of PR. Experimental results showed that at low and intermediate temperatures transverse strain lagged axial strain. However, at higher temperature and low frequencies this behavior is reversed, resulting in a change of sign for the PR phase angle (Fig. 3.5d); in such a case the PR norm shows a maximum, and therefore its master curve is not monotonic (Fig. 3.5c).

Extensive work on the modeling of both E^* and ν^* allowed to develop a general 3D LVE model with a continuous spectrum called 2S2P1D (details on the 2S2P1D model is presented in Sect. 3.3.3.5). From Eqs. 3.18 and 3.19, if it is considered that $\tau_E = \tau_\nu = \tau$, the obtained complex PR is as follows:

$$\nu^*(\omega) = \nu_{00} + (\nu_0 - \nu_{00}) + \frac{E^*_{2S2P1D}(\omega) - E_{00}}{E_0 - E_{00}} \tag{3.6}$$

where ν_{00}, E_{00} denote the static values ($\omega \to 0$), ν_0, E_0 denote the glassy values ($\omega \to \infty$) and $E^*_{2S2P1D}(\omega)$ is the 2S2P1D expression for the complex Young's modulus (Di Benedetto et al. 2007b). Using this modeling approach the E^* and ν^* master curves are characterized by the same shape parameters and the same shift factors can be used for their construction (see Sect. 3.3.3.5).

The 3D LVE characterisation of asphalt mixtures with different void levels and of epoxy asphalt concrete mixes, has been carried out by Graziani et al. (2014a) and by Bocci et al. (2015). Cylindrical specimens prepared using gyratory compaction were tested in both cyclic compression and tension compression. Test temperatures varied from 0 to 40 °C and frequencies varied from 0.1 to 12 Hz. Axial and transverse strains were measured using bonded strain gauges (Fig. 3.6a). Results confirmed that the PR is a complex number, with very low phase angle (less than 6°). Unique curves identified the material behavior in the Cole-Cole and Black

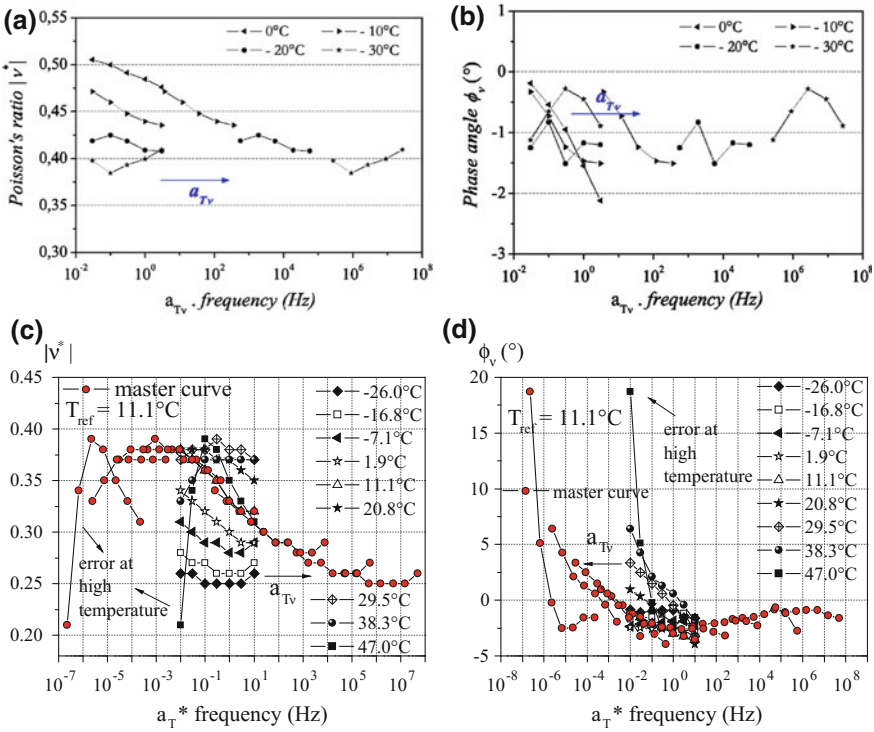

Fig. 3.5 Complex PR measurements (norm $|\nu^*|$ and phase angle ϕ_ν) in tension-compression tests: **a**, **b** data for 50/70 bitumen, from Di Benedetto et al. (2007a, b); **c**, **d** data for bituminous mixture, from Nguyen et al. (2015)

diagrams (Fig. 3.6b), confirming that the TTSP can be applied to both absolute value and phase angle of PR. Moreover, the authors showed that, under the hypothesis of isotropy, the same test results can be used to directly calculate the complex bulk modulus K^* and the complex shear modulus G^* (Graziani et al. 2014b).

3.2.2.3 Time-Domain Characterisation

Lee and Kim (2009) carried out IDT tests on field cores at 10 °C in order to measure the complex Young's modulus and the creep compliance. The viscoelastic PR was then obtained from both test modalities through the application of the EVCP. Interconversion from the frequency domain to the time domain was carried out using Prony series. Similar values were obtained from both test modalities.

Kassem et al. (2011) measured the viscoelastic PR of asphalt concrete specimens prepared with a Superpave gyratory compactor. Uniaxial tests were carried out at

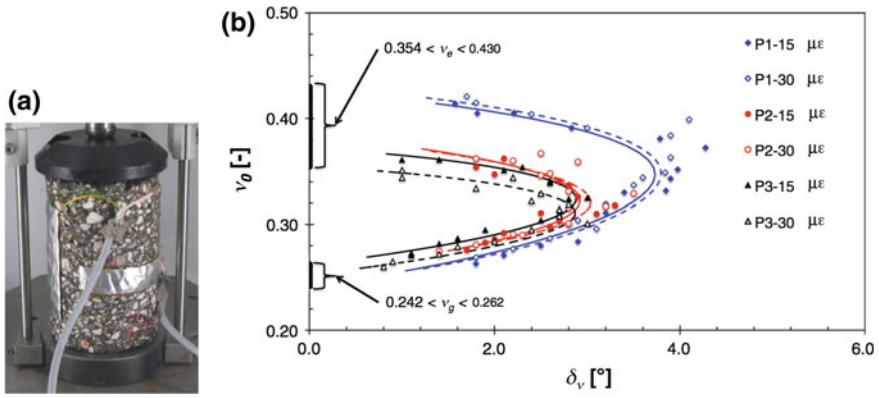

Fig. 3.6 Complex PR measurements in cyclic compression tests (Graziani et al. 2014a, b); **a** tests setup; **b** black diagram

20 °C using three loading modes: tensile relaxation, compressive relaxation and tensile constant rate of strain. Results showed that in the three loading modes the viscoelastic PR increased with times. However different values and time dependencies were obtained. The difference in the time dependency of the PR between tension and compression loadings was explained by the effect of the aggregate skeleton.

The time-dependent PR was also measured by Islam et al. (2015). Relaxation tests carried out using the IDT configuration showed that the PR increased with time (up to 240 s) and temperature (from −15 to 54 °C).

3.3 Round Robin Test on Poisson's Ratio Measurement

3.3.1 Introduction

3.3.1.1 Overview

As discussed in Sect. 3.2, the characterisation of the 3D LVE behavior of bituminous mixtures, in particular measurement and modeling of the complex PR, has recently attracted increasing interest. In this context, Task Group 3 (TG3) "Mechanical Testing of Mixtures" of RILEM Technical Committee 237-SIB "Testing and characterisation of sustainable and innovative bituminous materials and systems" organized a RRT focused on the simultaneous measurements of E^* and ν^* by means of uniaxial tests on cylindrical specimens.

The tests were carried out on two dense-graded bituminous mixtures, normally used for base construction in France. Slab samples were compacted in the laboratory and shipped to the participating laboratories for coring and testing.

Sinusoidal tension-compression or haversine compression tests were performed at a reference axial strain level of 50 μm/m. Two transverse (or circumferential) strains were measured in order to verify the effect of compaction-induced anisotropy on PR.

3.3.1.2 Participating Laboratories

Eleven laboratories participating on a voluntary basis received the slabs:

1. University of Lyon/ENTPE, France;
2. Polytechnic University of Marche, Italy;
3. University of Québec/ETS, Canada;
4. Vienna University of Technology, Austria;
5. Empa, Switzerland;
6. Technical University of Braunschweig, Germany;
7. IFSTTAR, France;
8. EIFFAGE Travaux Publics Company, France;
9. University of Nottingham, UK;
10. University of Limoges, France;
11. Technion, Israel.

Results from the first five laboratories are included in the present report. The paper from Perraton et al. (2016), also gives some results of this RILEM RRT.

3.3.2 Experimental Program

3.3.2.1 Test Description

The 3D LVE characterisation of bituminous mixtures in the complex domain was carried out by means of uniaxial harmonic (sinusoidal) tests on cylindrical specimens. This test configuration allows the simultaneous measurement of E^* and ν^*.

According to the specimen configuration represented in Fig. 3.7a, stress is applied only in direction 1 ($\sigma_1(t) \neq 0$, $\sigma_2(t) = \sigma_3(t) = 0$), whereas the deformation response is characterized by the three strains $\varepsilon_1(t)$, $\varepsilon_2(t)$ and $\varepsilon_3(t)$. Measurement of $\varepsilon_2(t)$ and $\varepsilon_3(t)$ allows to check if the material response is transversely isotropic. In that case $\varepsilon_2(t) = \varepsilon_3(t)$.

Steady-state stress and strain signals (time-histories) may be written as follows:

$$\sigma_1(t) = \sigma_{01} \sin(\omega t + \varphi_{\sigma 1}) \tag{3.7a}$$

$$\varepsilon_{\mathrm{i}}(t) = \varepsilon_{0\mathrm{i}} \sin(\omega t + \varphi_{\varepsilon \mathrm{i}}) \quad \mathrm{i} = 1, 2, 3 \tag{3.7b}$$

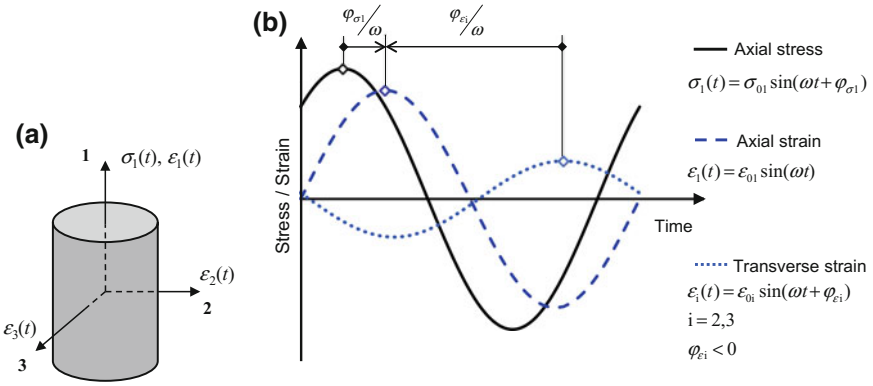

Fig. 3.7 Uniaxial harmonic test on cylindrical specimen: **a** identification of principal axes; **b** time-domain representation of stress and strain signals

where σ_{01}, ε_{0i} are the amplitudes of the sinusoidal signals, $\varphi_{\sigma 1}, \varphi_{\varepsilon i}$ are their phase angles, $\omega = 2\pi/T$ is the angular frequency or pulsation and T is the period of the oscillations. Index i takes the values: 1, 2 and 3. Linearity implies that stress and strains have the same frequency, whereas viscous damping implies that axial strain lags axial stress ($\varphi_{\sigma 1} - \varphi_{\varepsilon 1} > 0$). It is highlighted that phase angles actually represent time shifts between signals ($\varphi = \omega \Delta t$) and, therefore, are relative quantities. As a consequence, without loss of generality, it can be assumed that $\varphi_{\varepsilon 1} = 0$ and hence $\varphi_{\sigma 1} > 0$ (Fig. 3.7b).

As far as bituminous mixes are concerned, contraction/expansion in the axial direction is accompanied by expansion/contraction in the transverse directions. As highlighted in Sect. 3.2.2.2, various experimental studies showed that $\varepsilon_2(t)$ and $\varepsilon_3(t)$ are approximately in counter-phase with respect to $\varepsilon_1(t)$. In addition, it was generally observed that axial contraction/expansion reaches its maximum value before transverse expansion/contraction. With the notation adopted in Eqs. 3.7, this is indicated as $\varphi_{\varepsilon i} < -\pi$, or, equivalently $-\varphi_{\varepsilon i}/\omega > T/2$. However, the latter is only a heuristic assumption, which is subjected to experimental verification (Tschoegl 1989).

The sinusoidal signals described by Eqs. 3.7 can be represented by the complex exponentials:

$$\sigma_1^*(\omega) = \sigma_{01} \exp[\mathrm{j}(\omega t + \varphi_{\sigma 1})] \tag{3.8a}$$

$$\varepsilon_i^*(\omega) = \varepsilon_{0i} \exp[\mathrm{j}(\omega t + \varphi_{\varepsilon i})], \quad i = 1, 2, 3 \tag{3.8b}$$

where j is the imaginary unit. The complex signals described by Eqs. 3.8 are represented as phase vectors or phasors in Fig. 3.8.

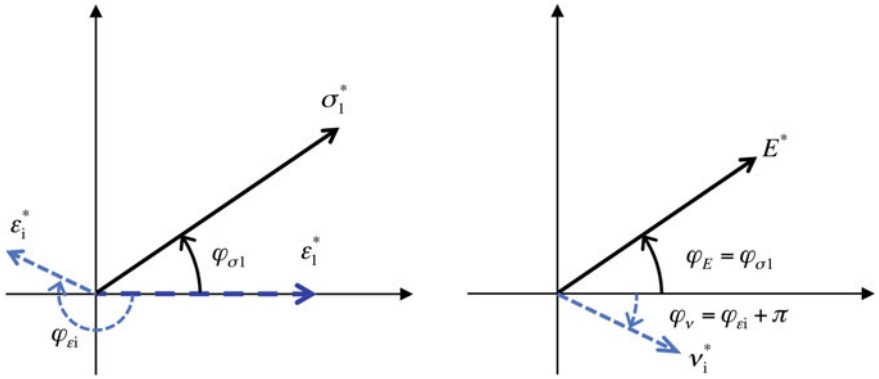

Fig. 3.8 Complex plane representations of stress-strain signals (left) and complex response functions (right)

The complex Young's modulus E^* is defined as

$$E^*(\omega) = \frac{\sigma^*}{\varepsilon^*} = E_0(\omega)\exp[\mathrm{j}\varphi_\mathrm{E}(\omega)] \tag{3.9}$$

where $E_0 = \sigma_{01}/\varepsilon_{01}$ is the absolute value (norm) and $\varphi_\mathrm{E} = \varphi_{\sigma 1}$ is the phase angle. Analogously, the complex PR in direction i (i = 2, 3) may be defined as follows:

$$v_\mathrm{i}^*(\omega) = -\frac{\varepsilon_\mathrm{i}^*}{\varepsilon_1^*} = -v_{0\mathrm{i}}(\omega)\exp[\mathrm{j}\phi_{\varepsilon\mathrm{i}}(\omega)] = v_{0\mathrm{i}}(\omega)\exp[\mathrm{j}\phi_{v\mathrm{i}}(\omega)] \tag{3.10}$$

where $v_{0\mathrm{i}} = \varepsilon_{0\mathrm{i}}/\varepsilon_{01}$ (i = 2, 3) are the absolute values and $\phi_{v\mathrm{i}}$ are the phase angles, with $\phi_{v\mathrm{i}} = \phi_{\varepsilon\mathrm{i}} \pm \pi$, because the "−" sign can be converted into a π rotation in the complex plane (Fig. 3.8). It can be seen that according to the phase angle sign notation introduced by Eq. 3.7, if transverse contraction/dilation lags behind axial dilation/contraction $\phi_{v\mathrm{i}}$ is negative. Clearly the definition given by Eq. 3.10 can be considered as equivalent to Eq. 3.3.

As the real and imaginary parts of E^* are related to energy storage and energy loss at each cycle, the storage and loss moduli are defined respectively:

$$E_1 = E_0\cos\varphi_E, \quad E_2 = E_0\sin\varphi_E \ \text{ and } \ E_0 = E_1 + \mathrm{j}E_2 \tag{3.11}$$

Analogously, the real and imaginary parts can be calculated for v^*:

$$v_{1\mathrm{i}} = v_{0\mathrm{i}}\cos\varphi_{vi}, \quad v_{2\mathrm{i}} = v_{0\mathrm{i}}\sin\varphi_{vi} \ \text{ and } \ v_\mathrm{i}^* = v_{1\mathrm{i}} + \mathrm{j}v_{2\mathrm{i}} \tag{3.12}$$

When experimental data are analyzed using the complex-domain approach, Eqs. 3.7 must be fitted to experimental data. The quality of results, i.e. the values of E^* and v^*, will necessarily depend on the quality of such a fitting. Since purely sinusoidal stress and strain signals need to be considered in the analysis, tension/

compression (T/C) tests should be the optimal choice. However, haversine compression (or tension) tests can also be employed. In such cases, a creep component in compression (or tension) is superposed to the sinusoidal component, for both excitation and response. This component should be removed during data analysis. In either case, in order to avoid an excessive impact of creep deformation on the results, the test should not be too long.

On the other hand, in order to approximate a steady-state response, the transient response due to the initial test conditions needs to become negligible. This requires the application of a certain number of test cycles, depending on the damping characteristics of the material (Gayte et al. 2015). Therefore, for bituminous mixtures, the test duration should be tailored to temperature and loading frequency.

As only the steady-state material response needs to be considered, the test may be carried out in controlled stress or controlled strain mode. In either case, the excitation should be as close as possible to a sinusoid. Hence, non-cyclic effects due to measurement noise, temperature variations or small non-linearities should be removed from the measured signals.

3.3.2.2 Materials

Two bituminous mixes, called GB3 and GB5® (GB stands for "Grave Bitume" in French), were produced in laboratory by EIFFAGE Travaux Publics Company, in accordance with the EN 12697-35 standard. The same pure bitumen 35/50 pen grade was used. The bitumen content of both GB3 and GB5® was 4.5% by weight of aggregate. High quality fully-crushed aggregates were used (diorite from "La Noubleau" quarry, France). The 0/14 mm grading curve (Fig. 3.9) is either continuous (GB3) or gap-graded (GB5®) and the maximum density of the mixes was 2670 and 2654 kg/m^3, respectively.

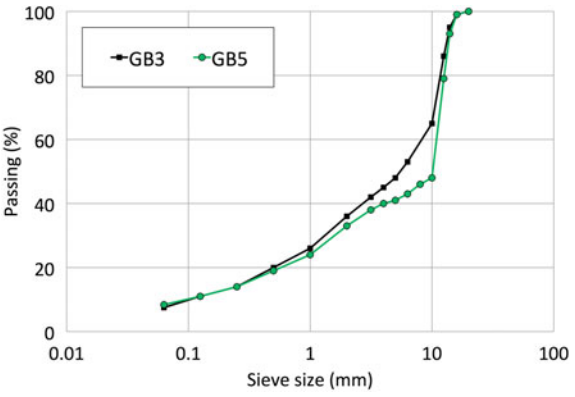

Fig. 3.9 Grading curves of the tested GB3 and GB5® mixtures

3.3.2.3 Sample Preparation

Immediately following laboratory mixing at 160 °C in a thermo-regulated mixer, the full batch was transferred from the mixer into a steel pan, covered and placed in a preheated oven at 145 °C. After a curing time of 2 h, the material was manually homogenized prior to compaction with a French LPC (Laboratoire des Ponts et Chaussées) wheel compactor (Fig. 3.10b), according to the European standard [EN 12697-33:2003+A1:2007].

After a rest period of 24–48 h, compacted slabs were removed from the mold and cut into two parts, then, a half slab was shipped to each laboratory for testing.

Cylindrical specimens were cored (Fig. 3.10a) from the provided slab section by each local laboratory staff. Core samples were then trimmed to the target height in accordance with the specific setup of each laboratory. Prior to coring the samples in the provided slab section, each laboratory marked the cored section in order to identify the location of directions 2 and 3 on the plane surface of the core sample for testing. The preferential material directions (1, 2 and 3) are indicated in Fig. 3.10a.

The geometric and volumetric characteristics of the tested specimens are reported in Table 3.1. It is remarked that the air void content of the studied GB3 and GB5® mixes do not strictly correspond to in situ values. Indeed, the typical air void content of GB3 (resp. GB5®) is between 6 and 9% (resp. 3 and 6%) (Olard 2012).

3.3.2.4 Complex Modulus Test on Binder

The complex modulus tests on bituminous binder were conducted by EIFFAGE Travaux Publics company, using the dynamic shear rheometer (DSR) and Métravib devices (Nguyen et al. 2013).

Complex shear modulus G^* was measured using the DSR apparatus in a 8 mm diameter plate-plate configuration (2 mm gap). Temperatures ranging from 10 to 70 °C and frequencies ranging from 0.01 to 30 Hz were applied. Complex Young's modulus E^* was calculated by applying an arbitrary PR equal to 0.5 ($E^* = 3G^*$).

Complex Young's modulus E^* was measured using the Métravib apparatus by means of tension-compression tests. The cylindrical specimen is 20 mm long and 10 mm diameter. The sample was loaded at temperatures ranging from −30 to 10 °C and at frequencies ranging from 0.01 to 30 Hz.

Test results are presented in Fig. 3.11a (Black diagram). Since the Black curve is unique that means the TTSP is verified. The norm of E^* master curve is built in Fig. 3.11b. The experimental results are fitted using the 2S2P1D model (see Sect. 3.3.3.2).

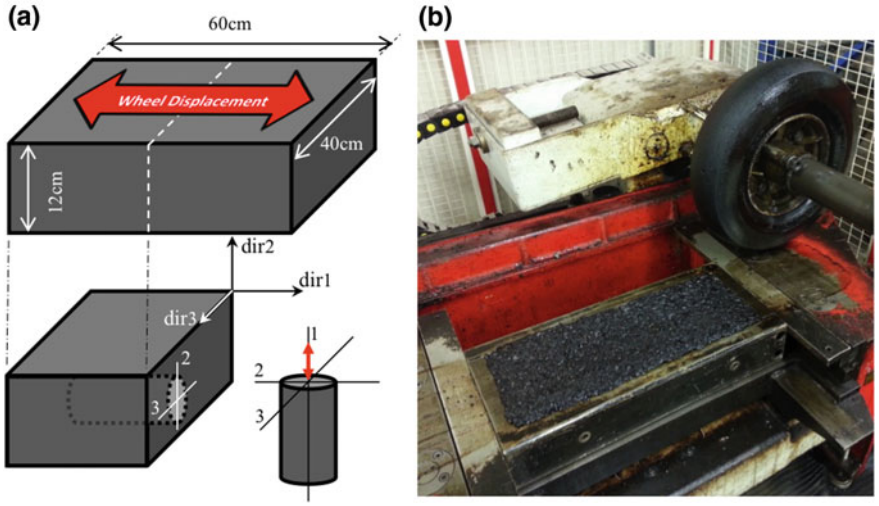

Fig. 3.10 Schematic representation of the production of a mechanical test sample: **a** sketch of the bituminous mixture specimen obtained from slab; **b** picture of the French LPC compactor used to produce asphalt bituminous mixture slab

Table 3.1 Geometrical characteristics of tested GB3 and GB5® specimens

Mix	Name	Mass (g)	Diameter (mm)	Length (mm)	Density (kg/m^3)	Air voids (%)
GB3	Lab1_sp1	1572	73.8	140.9	2610	2.3
	Lab1_sp2	1564	73.7	140.1	2614	2.1
	Lab2_sp1	3028	92.0	175.0	2603	2.5
	Lab3_sp1	1375	74.0	123.0	2615	1.5
	Lab4_sp1	3955	99.7	198.0	2593	2.9
	Lab5_sp1	3986	99.0	201.1	2594	2.9
GB5	Lab1_sp1	1581	73.8	140.5	2630	0.8
	Lab2_sp1	2192	93.0	118.0	2641	0.46
	Lab3_sp1	1425	74.0	125.9	2644	0.7
	Lab4_sp1	4061	99.6	200.5	2631	0.9
	Lab5_sp1	3721	98.8	185.0	2645	0.34

3.3.2.5 Test Equipment and Procedures for Tests on Bituminous Mixtures

Laboratories involved in the RRT used their own setup and instrumentation to determine the stresses and strains applied to the samples during testing. All cylindrical specimens were cored and loaded in dir1 (Fig. 3.10a). Tests were carried out in both tension-compression (sinusoidal loading) and compression (haversine

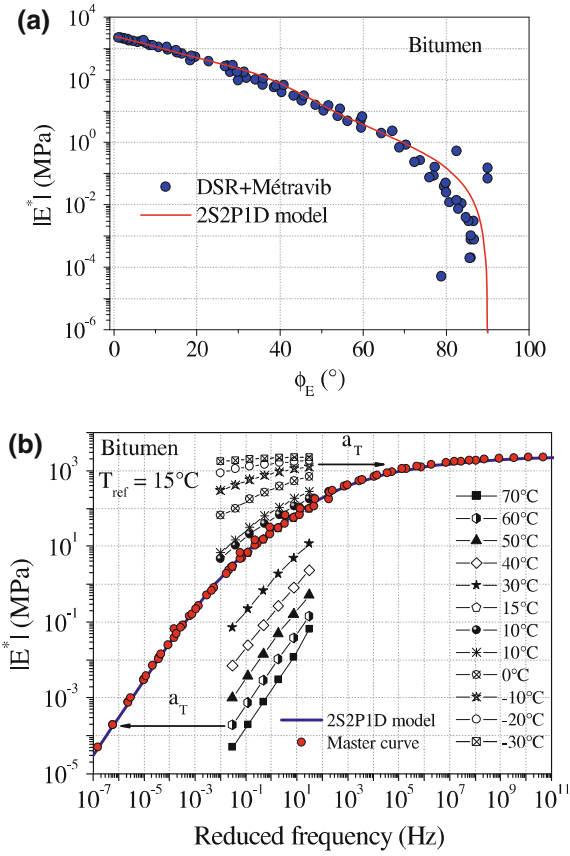

Fig. 3.11 Values of E^* of bitumen: **a** black diagram; **b** master curve of $|E^*|$ at the reference temperature T_{ref} = 15 °C

loading). Axial strain was measured using three types of sensors (extensometer, LVDT and strain gauge). All laboratories, except Lab1, measured the transverse (circumferential) strain using strain gauges. Lab1 used non-contact sensors to measure diametral deformation. The measured data were fitted with sinusoidal functions whose amplitude and phase was used to calculate E^* and ν_2^* (and/or ν_3^*) according Eqs. 3.9, 3.10.

In the following sections, the setup and procedure used by each laboratory are explained. Testing conditions are further summarized in Table 3.2.

Lab1 (France)

Sinusoidal loading in tension-compression (strain controlled) was applied to the glued specimen using a hydraulic press having a maximum load capacity of ±25 kN and a ± 50 mm axial stroke. A thermal chamber was used to control the temperature of the specimen during the test. The temperature was measured with a

Table 3.2 Summary of testing conditions applied by each laboratory

Lab	Loading conditions under testing						Measurements				
	Type[a]	Control mode	Set amplitude	T (°C)	Fr (Hz)	Connection	Strain			Temperature	
							dir1	dir2	dir3	Location	Gauge type
1	T/C	Strain dir1	50 μm/m	38.9; 29.9; 21.2; 16.9; 12.5; 3.6; −5.4; −14.5; −23.5	0.03; 0.1; 0.3; 1; 3; 10	Glued	3 extensometers 75 mm in length at 120°	2 non-contact sensors at 180°	2 non-contact sensors at 180°	At the testing sample surface, at mid height	PT100-rubber coat
2	T/C	Stress dir1	σ_0 is set to get 45 μm/m on ε_{01}	0; 10; 20; 30; 40	0.1; 0.25; 1; 3; 4; 12	Glued	3 strain gauges 60 mm in length at 120°	1 strain gauges of 60 mm length	1 strain gauges of 60 mm length	Inside dummy specimen[b]	K-type thermo-couple
3	T/C	Strain dir1	50 μm/m	0.1; 14.5; 30.5	0.03; 0.1; 0.3; 1; 3; 10	Glued	3 extensometers 50 mm in length at 120°	2 strain gauges of 51 mm length at 180°	2 strain gauges of 51 mm length at 180°	At the testing sample surface, at mid height	PT100 Not coated
4	C	Stress dir1	σ_0 is set to get 50 μm/m on ε_{01}	0.7; 15.5; 30.5	0.03; 0.1; 0.3; 1; 3; 10	Not glued	2 LVDT of ±2.5 mm length at 180°	2 strain gauges of 100 mm length at 180°	–	Inside dummy specimen[b]	PT100
5	C	Stress dir1	σ_0 is set to get 50 μm/m on ε_{01}	0.6; 14.9; 29.3	0.03; 0.1; 0.3; 1; 3; 10	Not glued	2 LVDT 100 mm in length at 180°	–	2 strain gauges of 100 mm length at 180°	Top/side spec. Inside/outside dummy specimen[b]	K-type thermo-couple

[a]T/C = Tension/compression; C = Compression

[b]The dummy specimen is placed in the thermal chamber during the test

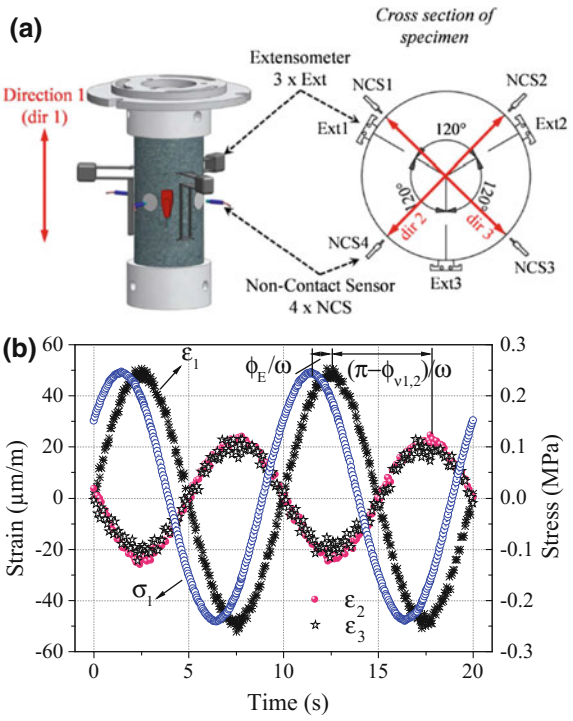

Fig. 3.12 Setup used by lab1: **a** specimen and measurement system; **b** example of stress and strain measurements (2 cycles at f = 0.1 Hz and T = 11.9 °C)

thermal gauge (PT100 surface temperature probe) glued on the specimen surface. The dimensions of the specimen were 75 mm in diameter and 140 mm in length.

The axial strain was measured on the middle part of the specimen using three extensometers (Fig. 3.12) located at 120° around the specimen, with an initial length of 75 mm. Radial strains were measured in dir2 and dir3 using 4 non-contact sensors (NCS). For each direction, two non-contact sensors were set in opposite directions on a sample diameter and aimed at two aluminum targets glued on the sample (Fig. 3.12).

Tests were carried out at 6 frequencies (0.03–10 Hz) and 9 temperatures (-25 to 40 °C). The sinusoidal axial strain (average of three extensometers) was used for monitoring of the amplitude of axial strain during cyclic loading to assure it was 50 μm/m. The number of cycles applied at each frequency was small (less than 100), and, as a result, the effect of heating due to viscous dissipation (Di Benedetto et al. 2011; Nguyen et al. 2012) was negligible. The axial stress was obtained from the load cell signal and radial strains were deduced from the two pairs of non-contact transducers (Fig. 3.12b).

Sinusoidal curves of strain and stress were fitted to the experimental data. As three extensometers were used for axial strain measurement, sinusoidal strains were first fitted to data for all single extensometers, and mean values of axial amplitudes and phase angles were used as ε_{01} and $\varphi_{\varepsilon 1}$ in all calculations. The same experimental device is used in Pham et al. (2015a, b).

Lab2 (Italy)

Sinusoidal loading in tension-compression (force controlled) was applied to the glued specimen using a hydraulic press with ±50 mm axial stroke, equipped with a ± 20 kN force transducer. A thermal chamber was used to control the temperature of the specimen during the test. The temperature was measured with a K-type thermocouple positioned inside an additional dummy specimen (Fig. 3.13a). The dimensions of the specimen were 92 mm in diameter and 175 mm in length.

The axial and transverse (circumferential) strains were measured, using three couples of strain gauges glued on the middle part of the specimen (Fig. 3.13a). Measuring points (identified as A, B and C) were located at 120° around the specimen, and their position with respect to the compaction direction is outlined in

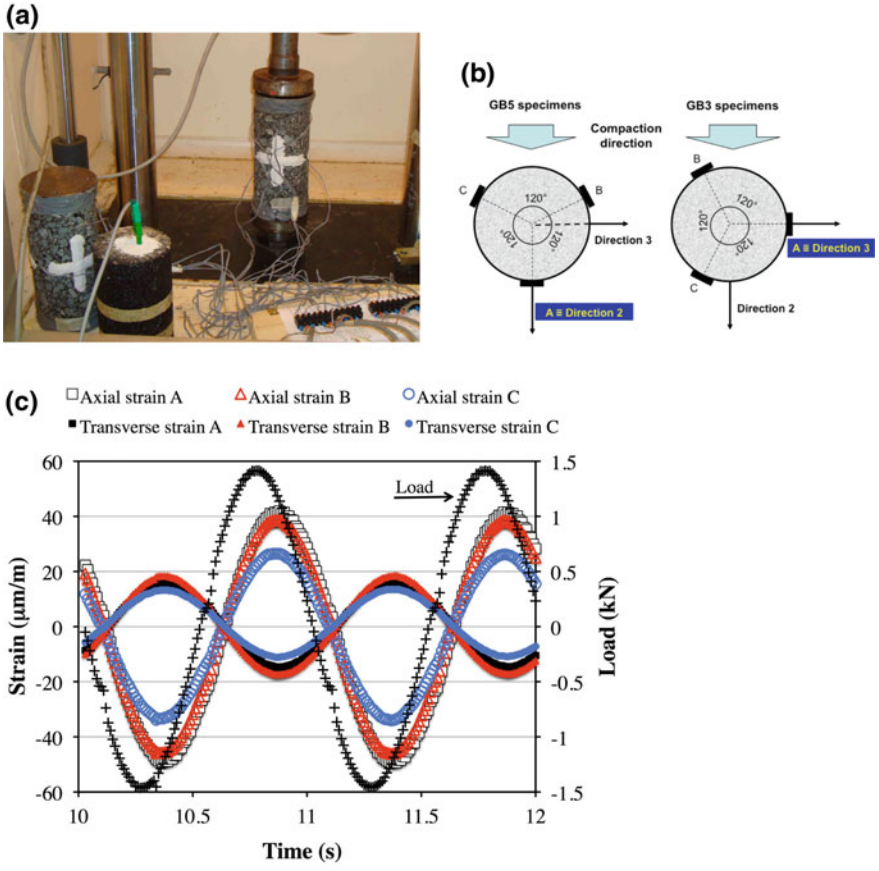

Fig. 3.13 Setup used by lab2: **a** test specimen and dummy specimens for temperature compensation and measurement; **b** configuration of measuring points; **c** example of force and strain measurements (2 cycles at f = 1 Hz and T = 20 °C)

Fig. 3.13b. Conventional bonded wire strain gauges with polyester resin backing (TML P60) were used. The gauge length was 60 mm and the nominal resistance was 120 Ω. A two-component room-temperature curing polyester adhesive (TML RP-2) was used to glue the strain gauges. Moisture and physical protection were achieved with a 3 mm covering agent (TML SB tape). For each sensor, a separate Wheatstone half-bridge circuit was employed to compensate for temperature effects. The second half of the bridge was positioned on a dummy specimen (Fig. 3.13a), identical to the active one located within the same thermal chamber. An example of the 7 measured signals in each test is reported in Fig. 3.13c.

Tests were carried out at 5 frequencies (0.1–12 Hz) and 5 temperatures (0 to 40 °C). The stress level was adjusted for each test condition in order to obtain steady-state strain amplitude in the range of 40–50 μm/m. For each test condition, 40 load cycles were applied.

Signal conditioning, bridge compensation and A/D conversion were carried out using a portable HBM Spider8 unit. The HBM Catman Express software was used for data acquisition. The sampling frequency (f_s) was adapted to the test frequency (f_t) to obtain 100 samples per cycle ($f_s = 100 f_t$).

The periodic component of each measured signal was extracted using a moving average filter and approximated using Fourier polynomials (Graziani 2014a). The harmonic regression was carried out using the statistical software package R-project, using the algorithm described by Cowpertwait and Metcalfe (2009). The amplitude and phase angles of the first harmonic component (fundamental harmonic) were used to calculate the complex Young's modulus and Poisson's ratio.

Lab3 (Canada)

Sinusoidal loading in tension-compression (strain controlled) was applied to the glued specimen using a hydraulic press having a maximum load capacity of 100 kN and a ± 50 mm axial stroke. A thermal chamber was used to control the temperature of the specimen. The temperature was measured with a thermal gauge (PT100 surface temperature probe) placed and held against the specimen surface with a rubber band. The dimensions of the specimen were 74 mm in diameter and 123 mm in length.

The axial strain was measured on the middle part of the specimen using three extensometers (Fig. 3.14) located 120° around the specimen, with an initial length of 50 mm. Circumferential strains were measured in dir2 and dir3 using 4 strain gauges glued on the lateral surface of the core sample. Strain gauges 50.8 mm in length and with a 120 Ω resistance were used. Figure 3.14 shows the configuration of the instrumentation placed around the sample. For each transverse direction (dir2 and dir3), two strain gauges were glued face to face on the cylinder wall and centered on the transversal axis, as shown in Fig. 3.14. As wire connections were at one end of each strain gauge, the total length of a strain gauge could not allow all strain gauges (4) to be placed at the same height around the sample core. As shown in the front view of Fig. 3.14b, one set of two strain gauges (ε_{3a} and ε_{3b}) was placed

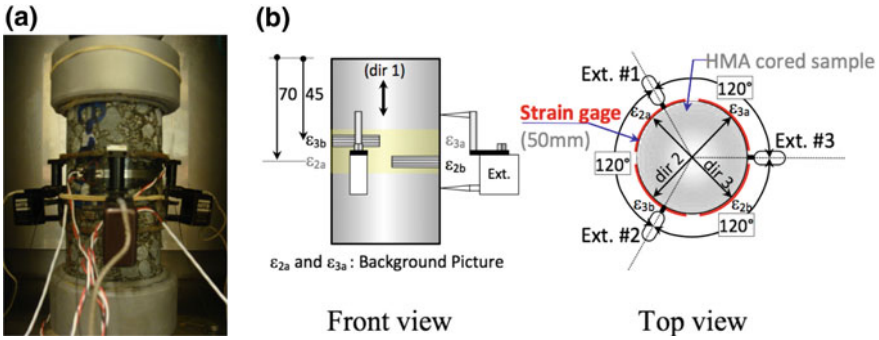

Fig. 3.14 Setup used by Lab3: **a** test specimen with axial extensometers; **b** strain gauge positioning

face to face 45 mm from the top surface of the sample, and the other set at 70 mm (ε_{2a} and ε_{2b}). A quarter-bridge strain-gauge configuration type X connection was used. To correct temperature effects, two other strain gauges were glued on a titanium silicate plate and subjected to the same test conditions as the tested sample. The titanium silicate is characterized by an exceptionally low thermal contraction-expansion linear coefficient of 0.03×10^{-6} μm/m/°K.

Tests were carried out at 6 frequencies (0.03–10 Hz) and 3 temperatures (0, 15 and 30 °C). Similar to Lab1, the sinusoidal axial strain (average of three extensometers) was controlled to assure it was 50 μm/m.

The data acquisition time interval was adapted to have 100 points per cycle and signal analysis was conducted step by step by considering two consecutive cycles at a time. Experimental data related to the force and strains measured by the load cell, extensometers and strain gauges were then fitted with sinusoidal functions. Amplitudes (σ_0 and ε_{0i}) and phase angles (φ_σ and $\varphi_{\varepsilon i}$) were determined at each step using the least squares method. By calculating a quality index (QI) at each step of the analysis process, the accuracy of the approximated sinusoidal function as regard to data signal was checked. Data too far from sinusoidal signal were rejected. The mean value of the three extensometers used for axial strain measurement was considered for ε_{01} and $\varphi_{\varepsilon 1}$. In addition, radial strain in directions 2 and 3 are given by the average values from the two pairs of opposite gauges

$$\varepsilon_{0i} = (\varepsilon_{0ia} + \varepsilon_{0ib})/2, \quad (i = 2, 3) \tag{3.13}$$

$$\varphi_{\varepsilon i} = (\varphi_{\varepsilon ia} + \varphi_{\varepsilon ib})/2, \quad (i = 2, 3) \tag{3.14}$$

Lab 4 (Austria)

Haversine loading in compression (force controlled) was applied to the specimen using a servo hydraulic testing machine having a maximum load capacity of 50 kN

and a ± 70 mm axial stroke. A thermal chamber was used to control the temperature of the specimen during the test (Fig. 3.15a). A second dummy specimen was placed in the chamber as well, with a thermal gauge (PT 100) placed within a drilled hole of the specimen to record its core temperature. The dimensions of the specimen were 100 mm in diameter and 200 mm in length.

The axial displacement was measured on the middle part of the specimen (±20 mm from half height) by two LVDTs located 180° around the specimen, with a nominal measuring range of ±2.5 mm. The circumferential strain was only measured in dir2 by using two strain gauges glued on the surface of the specimen around its circumference at mid height. The strain gauge lengths were 100 mm. Figure 3.15b shows a specimen placed in the testing machine, with one axial LVDT, and one circumferential strain gauge.

Tests were carried out at 6 frequencies (0.03–10 Hz) and 3 temperatures (0, 15 and 30 °C), with a total number of load cycles below 400. In a series of pre-tests on another specimen of the same mix design, axial stress amplitudes were determined, with the strain amplitude around 50 μm/m for each test temperature and test frequency.

Data from the axial load cell were used to calculate axial stresses, the mean value of data from the two axial LVDTs allowed calculating axial strain, whereas the mean value of data from the two radial strain gauges was used to calculate the radial strain in dir2. These data were fitted with sinusoidal functions. For optimization stability, data fitting was carried out for subsequent packages of 3 load cycles.

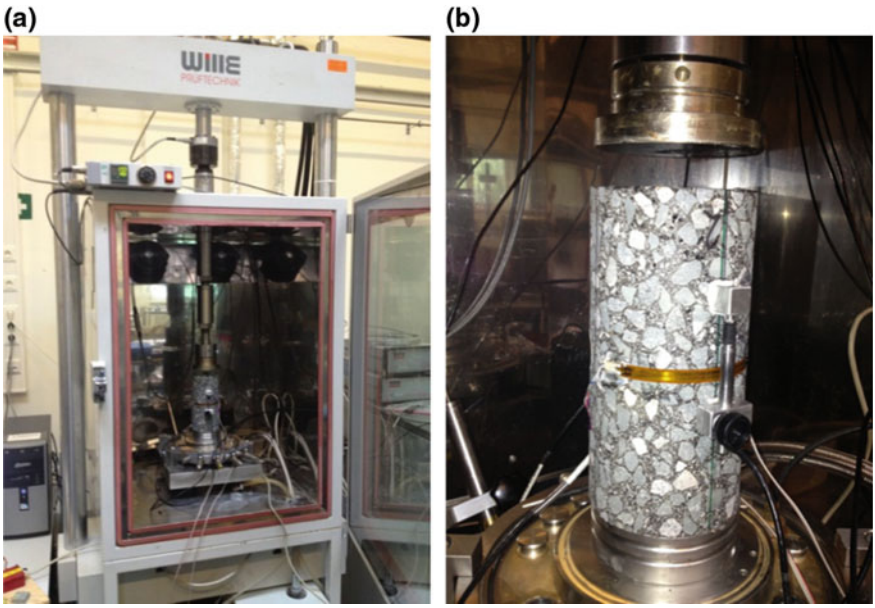

Fig. 3.15 Setup used by lab4: **a** test specimen mounted inside thermal chamber; **b** detail of axial LVDT and circumferential strain gauge

Lab 5 (Switzerland)

Haversine loading in compression (force controlled) was applied to the specimen using a servo hydraulic testing machine having a maximum load capacity of 25 kN and a ± 50 mm axial stroke. A thermal chamber was used to control the temperature of the specimen during the test. The temperature was measured on the surface of the specimen, inside the specimen at 1⁄4 height from bottom, and on a dummy specimen that was not tested, but located at the same level in the chamber as the tested specimen. Very little variation in temperature was noted, indicating that the temperature inside the specimen did not significantly change during the experiments, and that the temperature was homogeneous within the specimen (<0.3 °C difference). Before the experiments, the specimens were conditioned at the test temperature for at least four hours. The dimensions of the specimen were 100 mm in diameter and 200 mm in length.

The axial displacement was measured using two LVDTs located 180° around the specimen. The circumferential strain was measured in dir3 by using two strain gauges (DMS1 and DMS2) facing each other, as shown in Fig. 3.16.

Tests were carried out at 6 frequencies (0.03–10 Hz) and 3 temperatures (0, 15 and 30 °C). For each test condition, between 10 and 200 loading cycles were applied. The upper and lower stress amplitudes were defined using pre-calibration tests. The stress amplitudes were chosen so that the resulting strain amplitude remains below ±50 μm/m.

The axial stress was obtained from the load cell signal. Axial and radial strains were calculated from the two pairs of LVDT and strain gauges. The resulting values were the average of the two measurements both in the axial direction and radial direction.

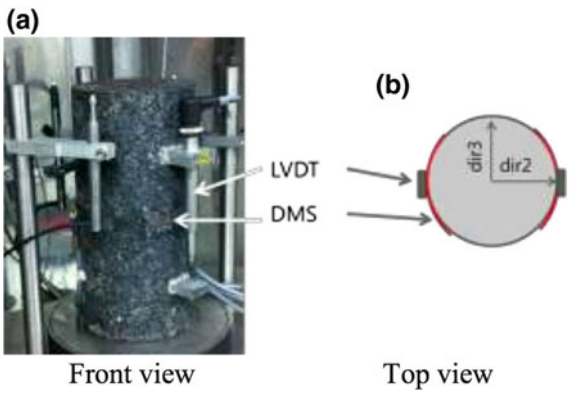

Fig. 3.16 Setup used by lab5: **a** test specimen mounted inside thermal chamber; **b** detail of axial LVDT and circumferential strain gauge

3.3.3 Results and Analysis

The presentation and analysis of RRT results are performed in two steps. First, in order to provide overall trends and variability of the measured complex Young's modulus and complex PRs, unprocessed results are compared. In a second step, an analysis based on simulations using the 2S2P1D model in 3 dimensions (Di Benedetto et al. 2007a) is proposed. As small differences in testing conditions do exist between the laboratories, any direct comparison may bring unrealistic conclusions. To overcome this drawback, the 2S2P1D model is used as a reference to quantify the differences between the laboratories.

3.3.3.1 Complex Young's Modulus

Experimental results for complex Young's modulus E^* are plotted in Figs. 3.17 and 3.18, for GB3 and GB5 mixes, respectively.

The Black diagrams (φ_E, E_0) and the Cole-Cole plots (E_1, E_2) allow direct comparison of the measured values because the trend described by the data is not affected by differences in test temperature. As can be observed, the E^* data measured by each laboratory, at different temperatures and frequencies, follow unique curves, which indicates that the TTSP can be applied.

Some scattering is present in both plots, in particular for GB3 specimens. Such variability can be explained by inherent differences among the tested specimens and by the different measurement techniques adopted by each laboratory. In particular it can be noticed that results obtained by Lab1 and Lab3, which employed the same testing setup, are very close.

In the following Sections, specimen Lab1_sp1 will be used as reference for quantitative comparisons based on the 2S2P1D model (Sect. 3.3.3.5) for the GB3 mixtures. The fitted 2S2P1D model (Table 3.3) is also reported in Figs. 3.17 and 3.18 (solid line).

3.3.3.2 Complex Poisson's Ratio

Experimental results for complex PRs in directions 2 and 3 (ν_2^*, ν_3^*) are plotted in Figs. 3.19 and 3.20 (GB3 mixture) and Figs. 3.21 and 3.22 (GB5 mixture). Similar to complex Young's modulus, data are reported in the Black diagram (φ_{vi}, ν_{0i}) and in the Cole-Cole plot (ν_{1i}, ν_{2i}). Contrary to the usual practice for complex moduli, in the Black diagram absolute values of the PRs are reported on a linear scale, not on a logarithmic scale. In Figs. 3.19 and 3.20, the behavior of the fitted 2S2P1D model for specimen Lab1_sp1 (Table 3.3) is also reported (solid line).

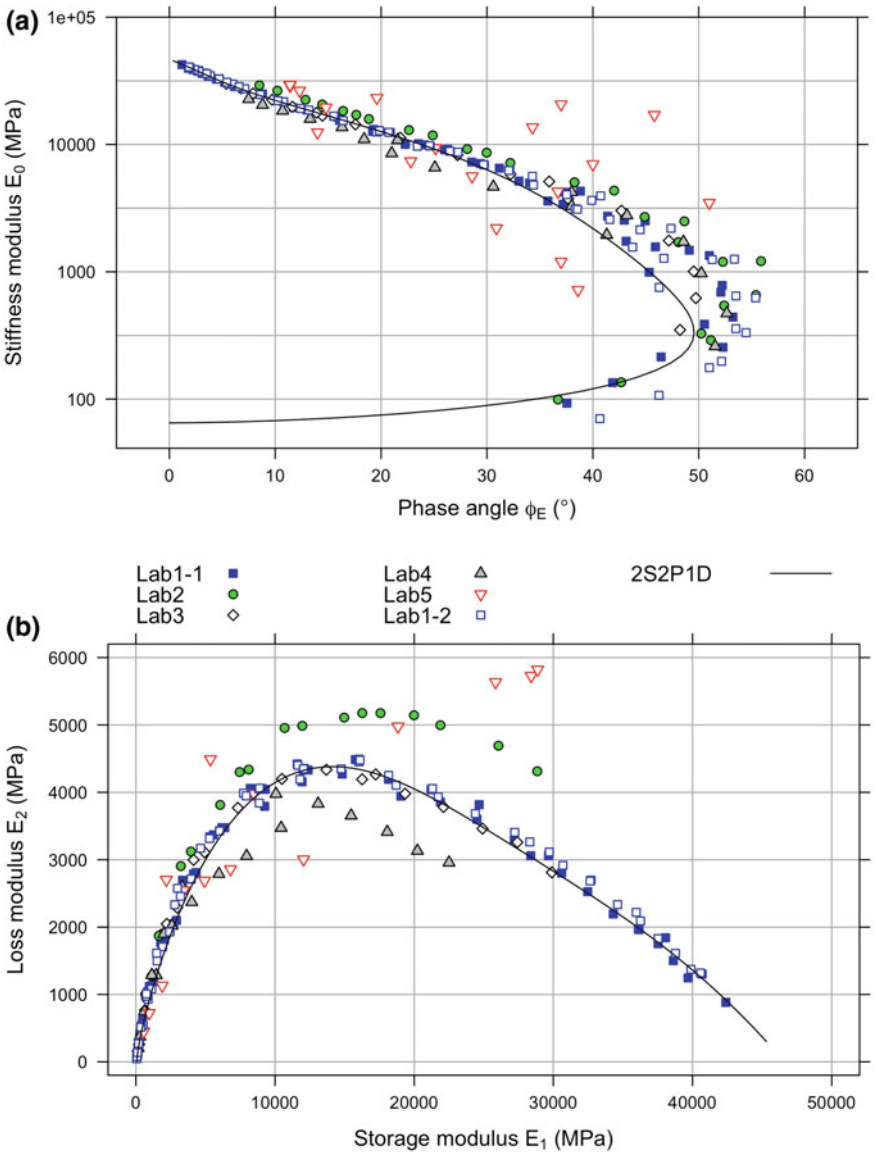

Fig. 3.17 Complex Young's modulus of GB3 specimens: **a** black diagram; **b** Cole-Cole plot

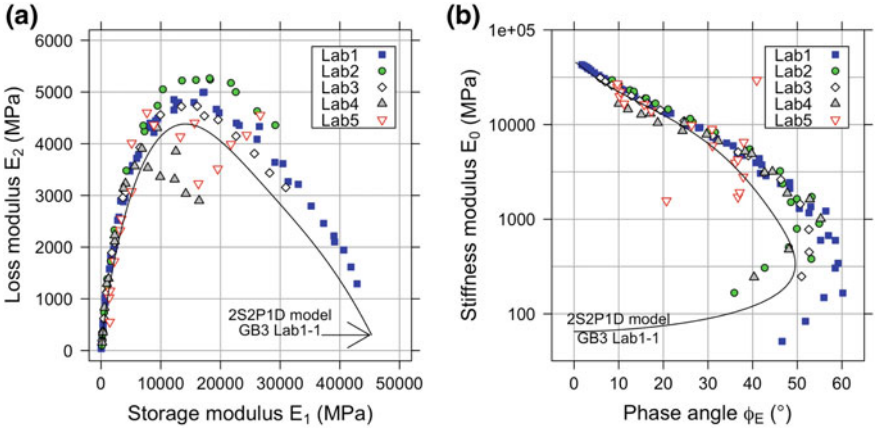

Fig. 3.18 Complex Young's modulus of GB5 specimens: **a** Cole-Cole plot; **b** Black diagram

Qualitative Description of Measured Data

Similar to the complex Young's modulus, the values of the complex PR measured by each laboratory, on each specimen, describe unique curves in both the Black diagram and the Cole-Cole plot (Figs. 3.19, 3.20, 3.21, 3.22). This confirms that the TTSP can be applied for the complex PR, as reported by the research studies summarized in Sect. 3.2.2.2.

The lowest norm values of PR were measured at low temperatures/high frequencies. For mixture GB3, the minimum was about 0.25 for both ν_{02} and ν_{03}, whereas, for GB5 values as low as 0.22 were measured for ν_{02}. In these conditions (low temperatures/high frequencies) the phase angle of PR was negative and very close to 0 (Fig. 3.19, Zone A). It is recalled that a negative sign indicates that transverse contraction/dilation lags behind the axial dilation/contraction (Fig. 3.7b), which is the expected behavior for a conventional material.

Increasing temperature (decreasing frequency), the magnitude of both the absolute value ν_{0i} and the phase angle $\varphi_{\nu i}$ increases. Following the path indicated by the arrows reported in the Black diagram (Fig. 3.19a) it is observed that:

- $\varphi_{\nu i}$ reaches a minimum (negative) value (about −5° for GB3 and −6° for GB5), then increases towards 0 and ultimately becomes positive at higher temperatures/lower frequencies (Fig. 3.19a, Zone B), generally above 30 °C;
- ν_{0i} increases to a maximum value (about 0.48 for GB3 and 0.60 for GB5) then slightly decreases at higher temperatures/lower frequencies;
- when ν_{01} reaches the maximum, $\varphi_{\nu i}$ changes its sign.

Similar considerations derive from the observation of the Cole-Cole plots. At low temperatures/high frequencies both the real and the imaginary components of the PR (ν_{i1}, ν_{i2}) are minima. In particular the imaginary component ν_{i2} is very close to 0. Increasing temperature (decreasing frequency) the magnitude of both ν_{i1} and

Table 3.3 2S2P1D parameters and WLF constants set at T_{ref} = 0 °C in accordance with data of lab1_sp1 tested sample

	2S2P1D parameters												WLF parameters	
Mix	E_s (MPa)	E_g (MPa)	k	h	δ	τ_{0E} (s)	β	v_{s2}	v_{g2}	v_{s3}	v_{g3}	τ_{0v} (s)	C_1	C_2
GB3	65	46,600	0.15	0.50	1.54	4.57	180	0.45	0.20	0.41	0.18	4.58	29.45	174.4

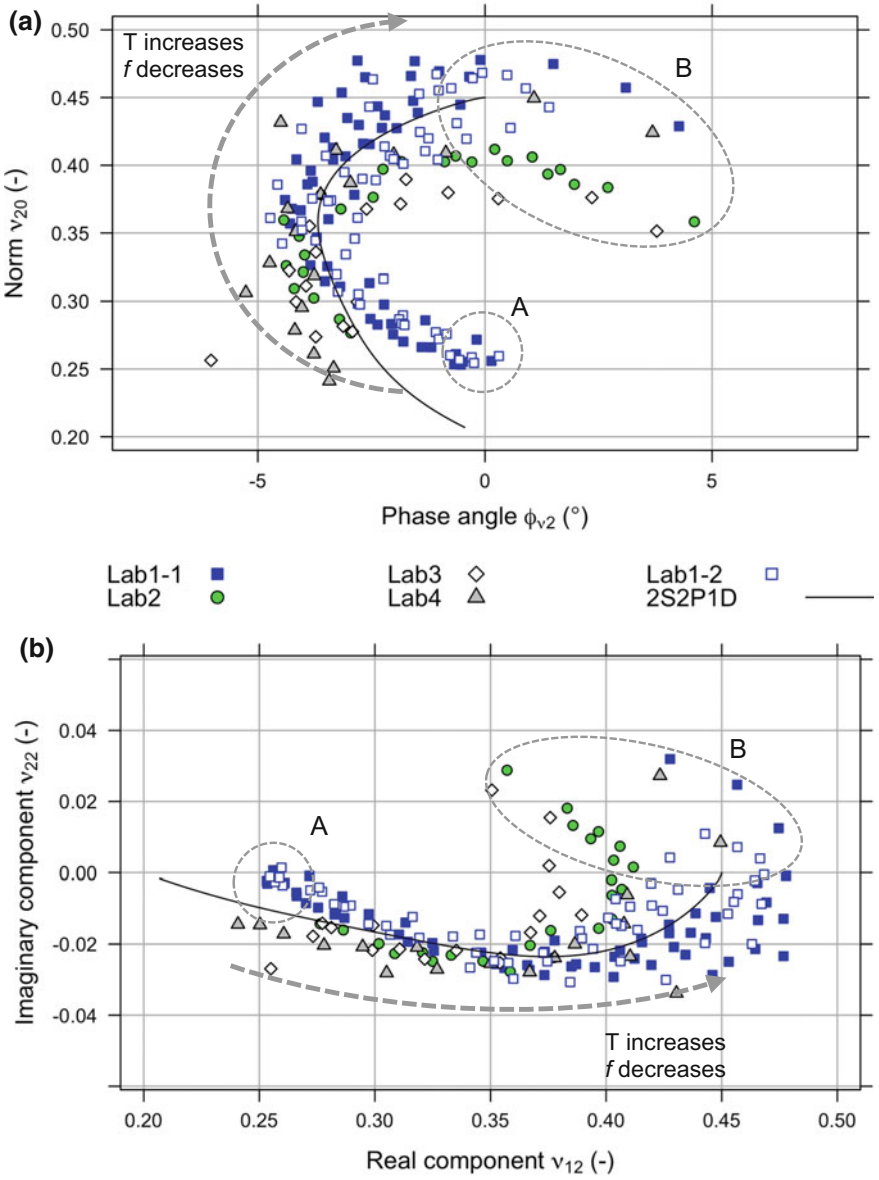

Fig. 3.19 Complex PR in direction 2 (ν_2^*) of GB3 specimens: **a** black diagram; **b** Cole-Cole plot

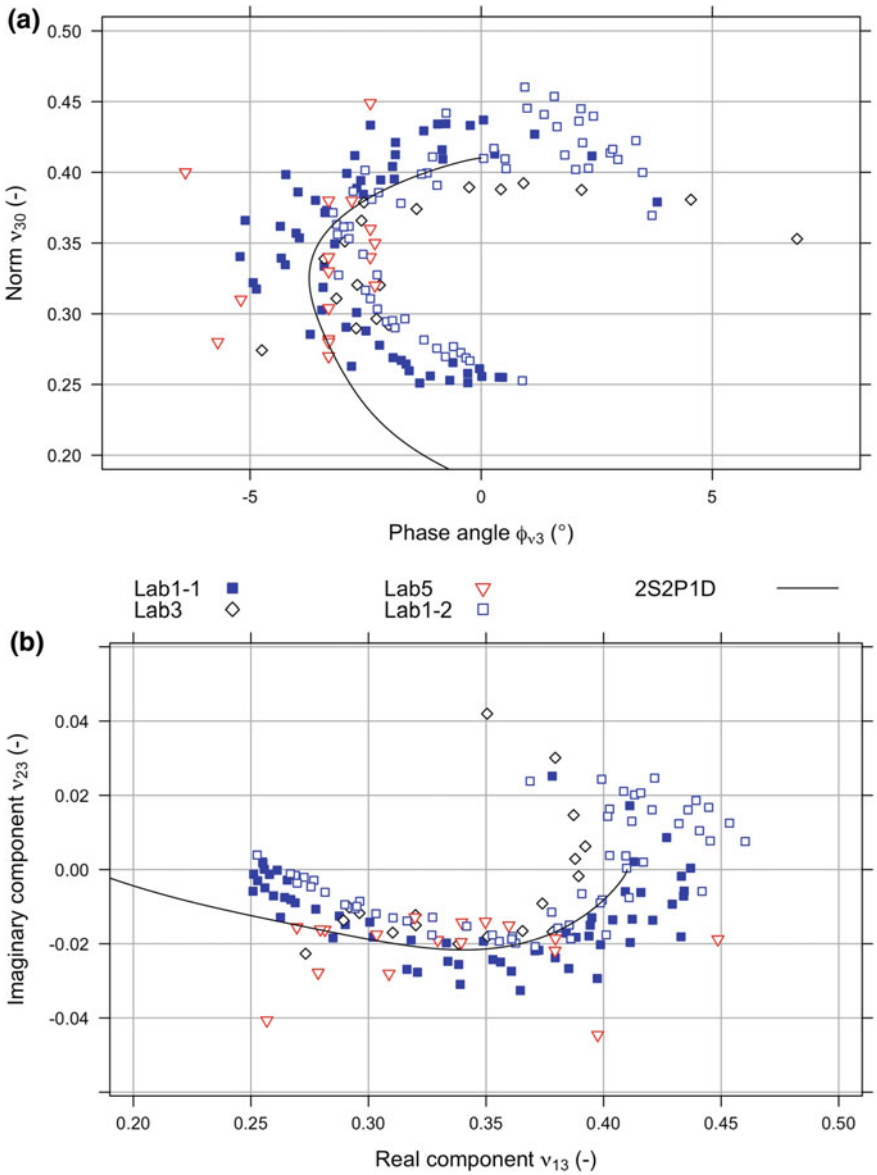

Fig. 3.20 Complex PR in direction 3 (ν_3^*) of GB3 specimens: **a** black diagram; **b** Cole-Cole plot

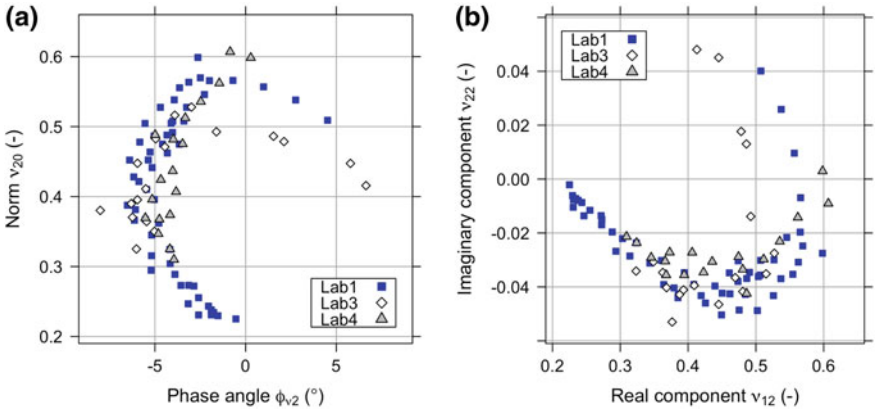

Fig. 3.21 Complex PR in direction 2 (ν_2^*) of GB5 specimens: **a** black diagram; **b** Cole-Cole plot

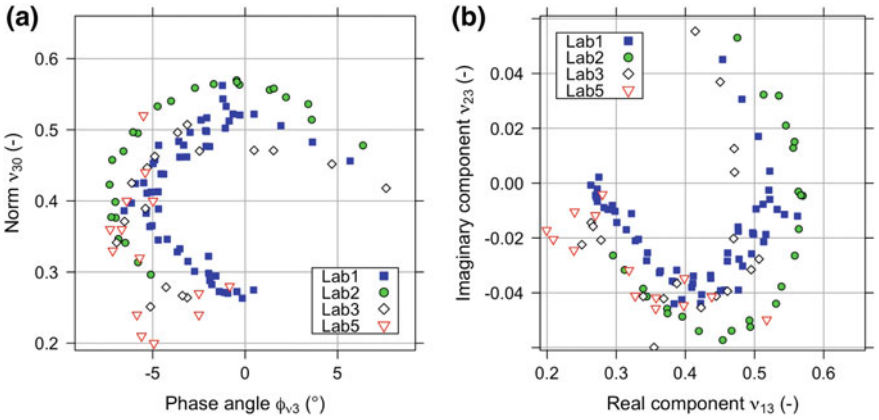

Fig. 3.22 Complex PR in direction 3 (ν_3^*) of GB5 specimens: **a** black diagram; **b** Cole-Cole plot

ν_{i2} increases. Following the path indicated by the arrows reported in the Cole-Cole plots (Figs. 3.19b) it is observed that:

- the Imaginary component ν_{i2} decreases to a minimum (negative) value, (about −0.03 for GB3 and −0.05 for GB5), then increases towards 0 and ultimately becomes positive at higher temperatures/lower frequencies (Fig. 3.19b, Zone B).
- the Real component ν_{i1} increases to a maximum (about 0.46 for GB3 and 0.58 for GB5) then slightly decreases at higher temperatures/lower frequencies;
- when the Real component ν_{i1} reaches the maximum, the Imaginary part ν_{i2} changes its sign.

In summary, the qualitative description of the measured PR, for both GB3 and GB5 specimens, shows that:

a. the phase angle was small but not null and therefore the PR should be treated (and modeled) as a complex function of temperature and frequency;
b. the TTSP can be applied to both the absolute value and the phase angle;
c. the absolute values measured for GB3 ranged from 0.25 to 0.48;
d. the absolute values measured for GB5 ranged from 0.22 to 0.60 (i.e. exceeding the maximum theoretical value for an isotropic material of 0.5);
e. for both GB3 and GB5 at high temperatures/low frequencies the sign of the phase angle changed.

These findings are generally in accordance with the literature review reported in Sect. 3.2.2.2. In particular, the material behavior described in items (d) and (e) is interesting since it is apparently in contrast with the LVE theory. The fact that such behavior was found by all laboratories suggests that it is not a consequence of the measurement technique or measurement errors. In addition, the fact that the same behavior was observed for other mixes (Pouget et al. 2012a; Nguyen et al. 2015) suggests that it could be a characteristic feature of bituminous mixtures.

A number of explanations can be put forward for such a peculiar behavior. For example non-homogeneous or anisotropic response, confinement effect due to the loading platens or other disturbances due to the test setup. On the other hand, these experimental findings may simply be a confirmation that the physical interpretation of complex PR is not straightforward (Lakes and Wineman 2006; Hilton 2009).

Dispersion of the Measured Data

In order to measure the complex PR in the LVE domain, small axial strain must be applied and consequently small transverse strains are obtained.

Consider for example the values of ν_{02} measured at low temperatures on specimen GB3 (Fig. 3.19a, Zone A); a variation of about 0.02 in the PR magnitude is observed at $\varphi_{\nu 2} = 0$. For the chosen axial strain level of 50 μm/m, such variation corresponds to a variation or 1.0 μm/m in the diametral or circumferential strain. For specimens with diameter of 100 mm, this corresponds to a change in diameter or approximately 0.10 μm or a change in circumference of about 0.31 μm. Clearly both the resolution and the precision of the measurement chain (strain gauges, amplifiers, data acquisition systems) is extremely important.

From both the Black diagrams and the Cole-Cole plots (Figs. 3.19, 3.20, 3.21, 3.22) it can be observed that the scattering of the complex PR increased at higher temperatures and/or lower frequencies. As previously observed, in Fig. 3.19a ν_{02} falls in the range 0.25–0.27 at low temperatures/high frequencies ($\varphi_{\nu 2} = 0$, Zone A) whereas, at high temperatures/low frequencies, when ν_{02} reaches its maximum ($\varphi_{\nu 2} = 0$ Zone B) its values fall in the range 0.35–0.48.

It is emphasized that, for the measurements of each laboratory, results are less dispersed when the norm values are lower, even though in such conditions the transverse strain is smaller and therefore a higher effect of measurement uncertainty (noise) on the results is expected. This suggests that the higher dispersion of the data at higher temperatures is not due to measurement uncertainties but instead may be due to the material response. The same behavior was highlighted by Graziani et al. (2014a). A possible physical explanation is the increasing influence of the aggregate skeleton on the transverse response as temperature increases and bitumen stiffness decreases.

Furthermore, the PR values for the GB3 mix in direction 2 reported by Lab2 and Lab3 are closer (Figs. 3.19, 3.20, 3.21, 3.22), and seem to be slightly lower than the one measured by Lab1. One contributing factor could be that the strain gauges glued around the sample may restrain transversal deformation. However, based on the testing program, this question could not be properly answered.

Comparison Between Transverse Directions (Anisotropy)

The difference in PRs in both directions, that allows to check whether the tested material is isotropic regarding transversal deformation, can only be obtained from Lab1 and Lab3 data. Figure 3.23 shows the relationship between the norm of the complex PR values in dir2 (ν_{02}) and the norm values in direction 3 (ν_{03}), from 3 tests on GB3. Results from Lab1 are mainly above the equality line, while those from Lab3 are somewhat below. The maximum absolute difference in the norms of

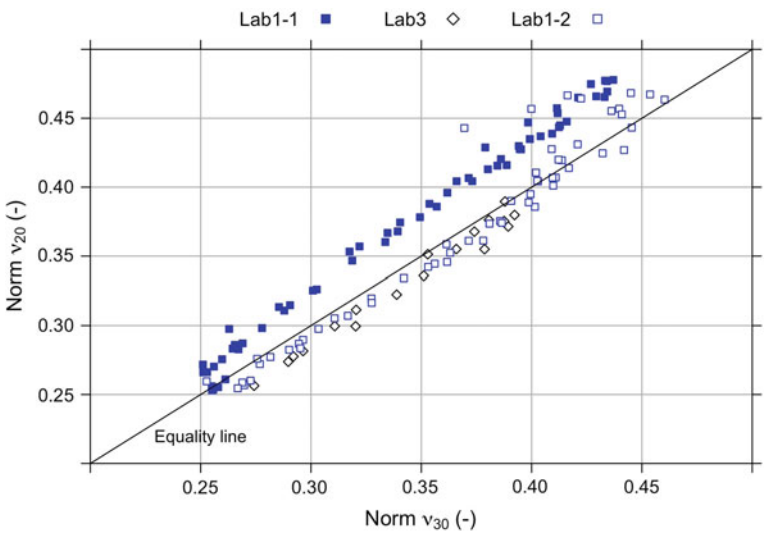

Fig. 3.23 Comparison between the norm of the complex PRs in direction 2 (ν_{02}) and in direction 3 (ν_{03})

the complex PRs to the equality line is less than 0.05. As the magnitude of the applied axial strain amplitude was close to 50 μm/m, 0.05 difference in PR values corresponds to a difference of about 0.19 μm in diameter amplitude variation for the tested sample. Consequently, it can be considered that the difference is quite small and situated within the accuracy range of the experimental procedure. Then, the authors believe that this small difference is related to measurement accuracy and not to the anisotropic behavior of the material.

3.3.3.3 Master Curves of Complex Young's Modulus

Master curves of complex Young's modulus can be used when the TTSP is respected. After choosing an arbitrary reference temperature (in the present report T_{ref} = 0 °C was selected) values of both absolute value E_0 and phase angle φ_E measured at each temperature were shifted parallel to the frequency axis until a unique curve was obtained. Then, only one variable, the equivalent frequency f_{eq} takes into account the effect of both temperature and frequency:

$$f_{eq} = a_{Tref}(T) * f \tag{3.15}$$

where f is the actual loading frequency and $a_{Tref}(T)$ is the shift factor which depends on the test temperature (T) and the chosen reference temperature (T_{ref}).

Figure 3.24 shows the values of experimental shift factors, used for both E_0 and phase angle φ_E, as a function of test temperatures adopted by each laboratory. As it can be observed, the results from each laboratory follow the same trend and are relatively close.

Figures 3.25 and 3.26 show the master curves of E_0 and φ_E, obtained by each participating laboratory for GB3 and GB5 mixtures. As expected, E_0 increases as a function of reduced frequency, while φ_E first increases up to a given maximum, and then decreases.

Differences were observed in the complex modulus master curves between the laboratories. In particular for the GB3 mixture, contrary to what was observed in the Black diagram and Cole-Cole plot (Fig. 3.17), the complex modulus master curves of Lab3 show a clear difference with those of Lab1. As Fig. 3.17 shows close results for Lab1 and Lab3, the observed differences in the master curves can be attributed to a temperature measurement error between the two laboratories. This point is confirmed because a shift along the equivalent frequency axis makes the curves from the 2 laboratories identical. The shift value is 0.31, which, from Fig. 3.24, gives a temperature error of 3 °C between the 2 laboratories. The techniques used to measure the testing temperature at the sample surface could mainly explain the gap. Lab1 used a PT100 rubber coated temperature probe put on the sample surface and held in place with a rubber band. In contrast, Lab3 used a PT100 uncoated temperature probe, also placed on the sample surface and held in place with a rubber band. The utmost importance of a correct temperature conditioning and measurement is then again to be stressed.

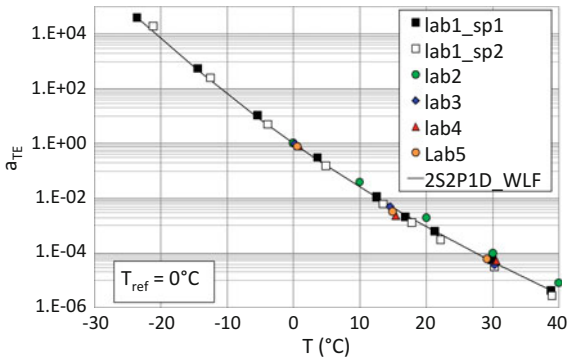

Fig. 3.24 Shift factors a_{TE}, obtained for complex Young's modulus on GB3 mixture

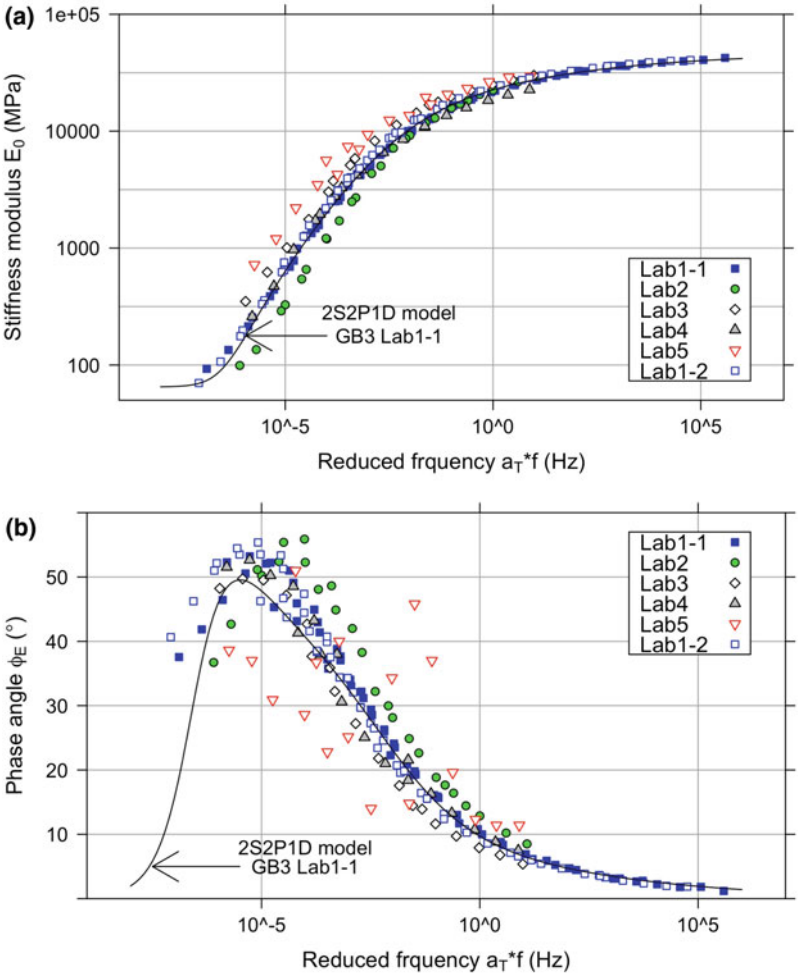

Fig. 3.25 Master curves of complex Young's modulus of GB3 specimens: **a** norm of E^*; **b** phase angle of E^*

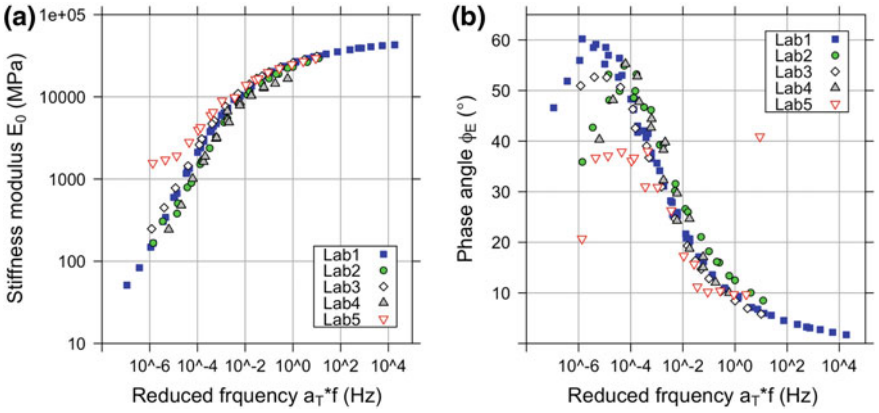

Fig. 3.26 Master curves of complex Young's modulus of GB5 specimens: **a** norm of E^*; **b** phase angle of E^*

3.3.3.4 Master Curves of Complex Poisson's Ratio

Master curves of complex PR on GB3 specimens, obtained using the same technique described for the complex Young's modulus, are reported in Fig. 3.27. The same shift factor values were used to build master curves for complex PRs (directions 2 and 3) and complex Young's modulus (Fig. 3.24). This is based on the results presented by Di Benedetto et al. (2007a, b), Clec'h et al. (2010), Nguyen et al. (2013), Nguyen et al. (2013) and Tapsoba et al. (2014), who already showed the validity of TTSP for PR measurements. They also showed that shift factors used to build the PR master curve are very close to those obtained for the complex modulus.

As shown by previous studies, the absolute values ν_{0i} increases as reduced frequency decreases. However, asymptotic values (glassy and static) are not so obvious. In particular, as reduced frequency decreases, the ν_{0i} master curves show a maximum value. For example, in Fig. 3.28, the point of maximum for ν_{02} and ν_{03} is located at reduced frequencies between 10^{-4} and 10^{-6} Hz. As already highlighted in the description of the Black diagrams and Cole-Cole plots (see, for example, Fig. 3.19), when ν_{0i} reaches the maximum value the corresponding phase angle φ_{ni} changes its sign.

This behavior can be qualitatively explained by the Kramers-Kronig (K-K) relations (Tschoegl 1989) which relate the real and imaginary parts of a complex function. It has been shown that the K-K relations can be applied to the complex Young's modulus of bituminous mixtures (Chailleux et al. 2006). In particular, for the complex PR, the local approximation proposed by Booij and Thoone (1982) can be used to relate absolute value and phase angle as follows:

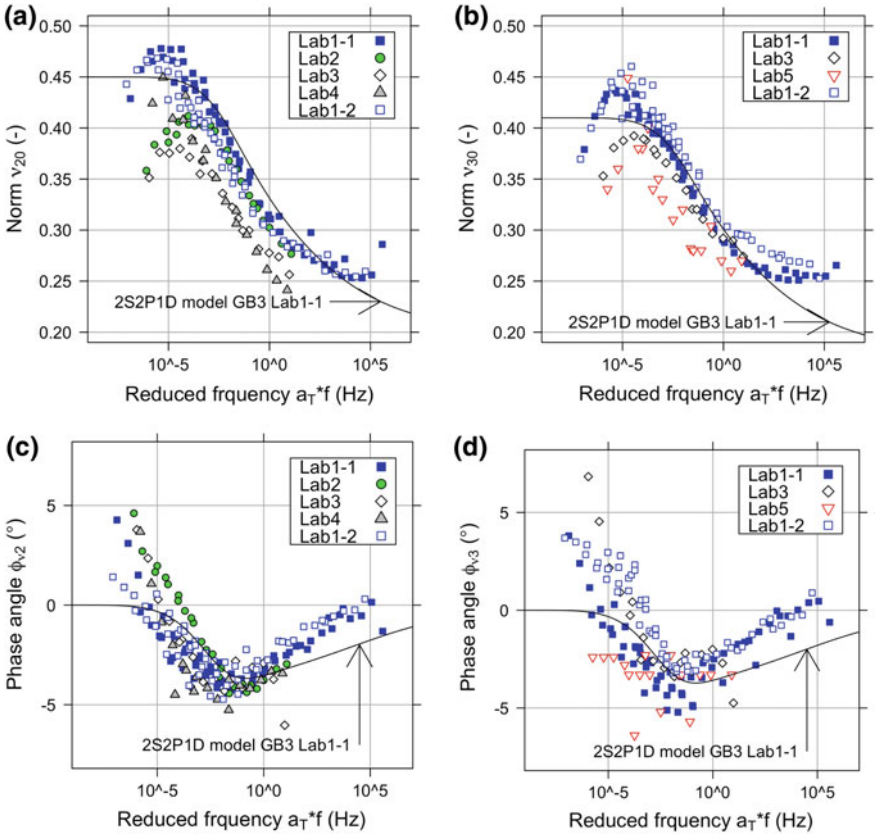

Fig. 3.27 Master curves of complex PR for GB3 (data points) and 2S2P1D simulation curves (solid lines): **a** norm of ν_2^*; **b** norm of ν_3^*; **c** phase angle of ν_2^*; **b** phase angle of ν_3^*

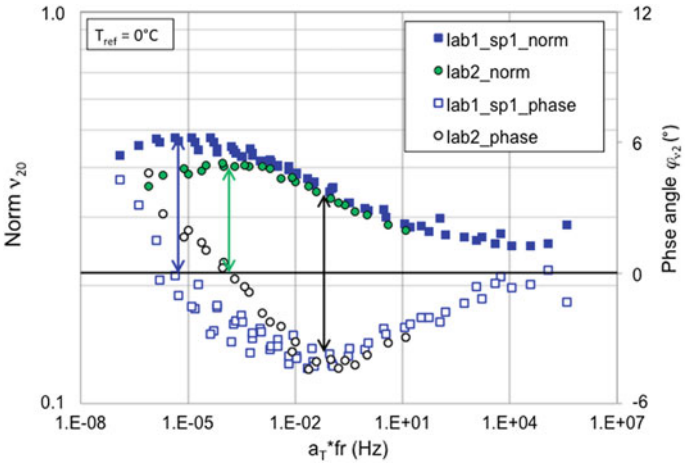

Fig. 3.28 Master curves of ν_2^* (norm and phase angle) for GB3 specimens (lab1_sp1 and lab2)

$$\varphi_{vi}(\omega) \approx \frac{\pi}{2}\frac{\mathrm{d}\log v_{0i}}{\mathrm{d}\log \omega} \tag{3.16}$$

$$\frac{\mathrm{d}\varphi_{vi}(\omega)}{\mathrm{d}\log \omega} \approx \frac{\pi}{2}\frac{\mathrm{d}^2\log v_{0i}}{\mathrm{d}\log \omega^2} \tag{3.17}$$

The first relation states that the slope of the absolute value curve is proportional to the phase angle, whereas the second states that the slope of the phase curve is proportional to the curvature of the absolute value diagram (Caracciolo and Giovagnoni 1996).

The application of Eqs. 3.16 and 3.17 to the measured PR values is shown in Fig. 3.28 where, for clarity, only the data from two GB3 specimens are reported: Lab1-1 and Lab2. It is highlighted that both Lab1 and Lab2 performed tension-compression tests, however different loading modes (control strain versus control stress), and different axial and transverse strain measurement techniques (Sect. 3.3.2.5) were adopted. It can be observed:

- when log ν_{02} reaches a maximum (i.e. d log ν_0/dlog $\omega = 0$), φ_{v2} crosses zero (sign change), according to Eq. 3.16
- when φ_{v2} shows a maximum (i.e. dφ_{v2}/dlog $\omega = 0$), a change of curvature (flex point) of log ν_{02} is observed, according to Eq. 3.17.

This behavior could also be anticipated observing the Cole-Cole diagrams (Figs. 3.19b, 3.20b, 3.21b, 3.22b) and confirms the thermo-rheological validity of the measured PR data for all the tested specimens.

3.3.3.5 Simulation and Comparison Using the 2S2P1D Model

As measurements from each laboratory are not performed at exactly the same temperatures and frequencies, it is not possible to compare the data directly. It was decided by the group to compare all data to a common reference given by the tri-dimensional formulation of 2S2P1D LVE model (Di Benedetto et al.2007a, b). The following procedure was followed:

- The tri-dimensional formulation of 2S2P1D model was fitted to the complex Young's modulus and PR data measured on specimen lab1_sp1;
- The fitted model was used to calculate reference values for E^* and ν^* at the experimental reduced frequencies of all other specimens;
- model data (used as reference) and experimental data (at the same reduced frequency) were directly compared.

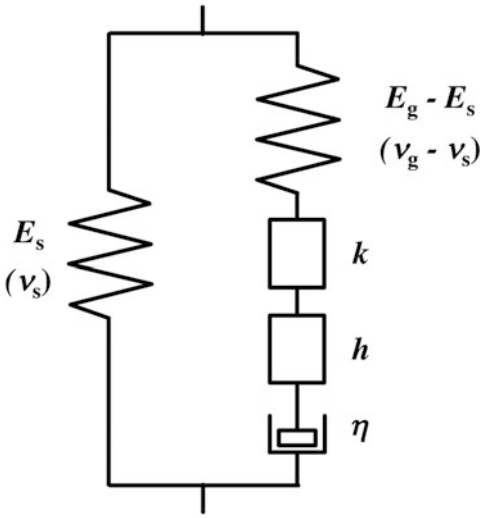

Fig. 3.29 Analogical representation of the 2S2P1D model

Presentation of 2S2P1D Model and Calibration

The 2S2P1D model, developed at the University of Lyon/ENTPE, is a generalization of the Huet-Sayegh model. The 2S2P1D model is based on a simple combination of physical elements: 2 springs, 2 parabolic elements, 1 dashpot (Fig. 3.29). It is widely used to model the LVE 1D or 3D behavior of bituminous materials (including binders, mastics and mixes) (Olard and Di Benedetto 2003; Delaporte et al. 2009; Tiouajni et al. 2011; Mangiafico et al. 2013, 2014).

The 2S2P1D analytical expression of complex Young's modulus and the Poisson's ratio, at a specific temperature, is given by:

$$E^*_{2S2P1D}(\omega) = E_s + \frac{E_g - E_s}{1 + \delta(j\omega\tau_E)^{-k} + (j\omega\tau_E)^{-h} + (j\omega\beta\tau_E)^{-1}} \tag{3.18}$$

$$\nu^*_{2S2P1D}(\omega) = \nu_s + \frac{\nu_g - \nu_s}{1 + \delta(j\omega\tau_\nu)^{-k} + (j\omega\tau_\nu)^{-h} + (j\omega\beta\tau_\nu)^{-1}} \tag{3.19}$$

where j is the imaginary unit, $\omega = 2\pi f$ is the angular frequency (f is the reduced frequency), k, h are constant exponents such that $0 < k < h < 1$, δ is a constant, E_s is the static modulus ($\omega \to 0$), E_g is the glassy modulus ($\omega \to \infty$), ν_s is the static Poisson's ratio ($\omega \to 0$); ν_g is the glassy Poisson's ratio ($\omega \to \infty$), β is a parameter linked with η, the Newtonian viscosity of the dashpot, $\eta = (E_g - E_s)\beta\tau_E$, and τ_E, τ_ν are characteristic time values depending only on temperature and have a similar evolution:

$$\tau_E(T) = a_{Tref}(T)\,\tau_{0E} \quad \text{and} \quad \tau_v(T) = a_{Tref}(T)\,\tau_{0v} \tag{3.20}$$

where $a_{\mathrm{Tref}}(T)$ is the shift factor (Eq. 3.15), $\tau_{0\mathrm{E}}$ and τ_{0v} are the values of τ_{E} and τ_v at the reference temperature T_{ref}. Ten constants (E_{s}, E_{g}, δ, k, h, β, v_{g}, v_{s}, $\tau_{0\mathrm{E}}$, τ_{0v}) are required to completely characterize the 3D LVE properties (with isotropy hypothesis) of the tested material at a given temperature. The evolutions of τ_{E} and τ_v were approximated by the WLF equation

$$\log a_{Tref}(T) = -\frac{C_1(T - T_{ref})}{C_2 + (T - T_{ref})} \tag{3.21}$$

where C_1 and C_2 are numeric constants. Therefore, when the temperature effects are considered twelve constants are required.

In this report the 2S2P1D and WLF constants were fitted using results from specimen lab1_sp1 and are reported in Table 3.3.

Difference Between Experimental Results and 2S2P1D Simulated Values

The relative differences between the calibrated WLF values, using constants of Table 3.3, and the corresponding experimental data for shift factor $a_{\mathrm{Tref}}(T)$ are presented in Fig. 3.30. What should be observed to characterize reproducibility of the test is the difference between the different data points and not the obtained relative difference values. These last values give information on quality of the simulation for each test condition.

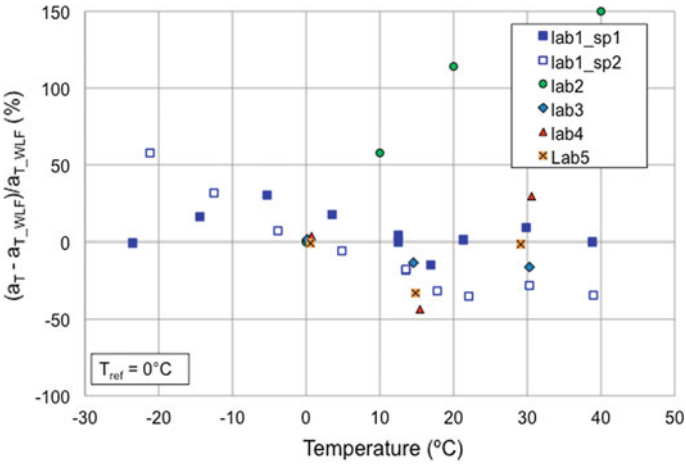

Fig. 3.30 Relative differences between experimental results and simulated values using the WLF equation calibrated with test lab1_sp1 (GB3 mixture)

If results from Lab2 are not considered, the differences between values for other specimens are within a range of ±25% on the whole frequency and temperature range. This value is quite small when comparing to the range of variation of the shift factor parameter, which covers more than 10 decades: from 3×10^{-6} to 4×10^{-4} (Fig. 3.24). Larger differences observed for the specimen from Lab2, up to 150%, are probably due to inaccuracy of the temperature measurement system.

The complex moduli and complex PR are calculated with the 2S2P1D model considering exact temperature and frequency values for each data condition. Obtained values are noted with subscript "2S2P1D lab1_sp1" indicating that the calibration was performed using specimen lab1_sp1.

Figure 3.31 shows the relative differences between simulated and experimental values for complex modulus norm (Fig. 3.31a) and differences between simulated and experimental values for the 5 other parameters (Fig. 3.31b–f).

At first glance Fig. 3.31 shows that, for all equivalent frequencies, points having the lowest difference values are from test lab1_sp1. This result was expected as the calibration of the model is made from the data of this test. The rather low difference values for this specimen indicate that 2S2P1D is able to simulate correctly the observed behavior over the whole range of temperatures and frequencies. For all 6 parameters, simulation results are better for low temperature and/or high frequencies. Comparison between results from the different tests should consider the thickness of the clouds of points (i.e. the range of variation) and not the position on the y axis.

Figure 3.31a shows that the scattering of the relative difference in the values of modulus increases for low values of reduced frequencies and reach an overall difference of 250% for GB3 (between +200 and −50%) at $a_T \cdot fr = 10^{-6}$. Complex Young's modulus values of Lab3 and Lab5 show the maximum deviation. For Lab3 this large difference can be explained by an error in sample temperature measurements, as explained further (see Fig. 3.32).

Figure 3.31c shows that differences in the norms of the complex PR for GB3 are smaller than about ±0.05. As already noted in Sect. 3.3.3.2, this value is in the range of the accuracy limit of measurement systems and should be considered as good reproducibility.

It was noted previously that Lab3 may have recorded incorrect temperature measurements. In Sect. 3.3.3.3, it is estimated that, for GB3, the temperature error is about 3 °C. 2S2P1D values for Lab3 were then recalculated considering a shift in temperature of −3 and −2 °C. Differences between experimental values of Lab3 and 2S2P1D values, calculated at −3 and −2 °C, are plotted in Fig. 3.32. Previous difference values for Lab1 (determined at 0 °C) are also plotted in Fig. 3.32. As compared with results of Fig. 3.31 scattering of results is considerably reduced, which confirms the probable error of 2–3 °C in temperature measurement between the two laboratories, confirming the importance of accurate temperature measurements.

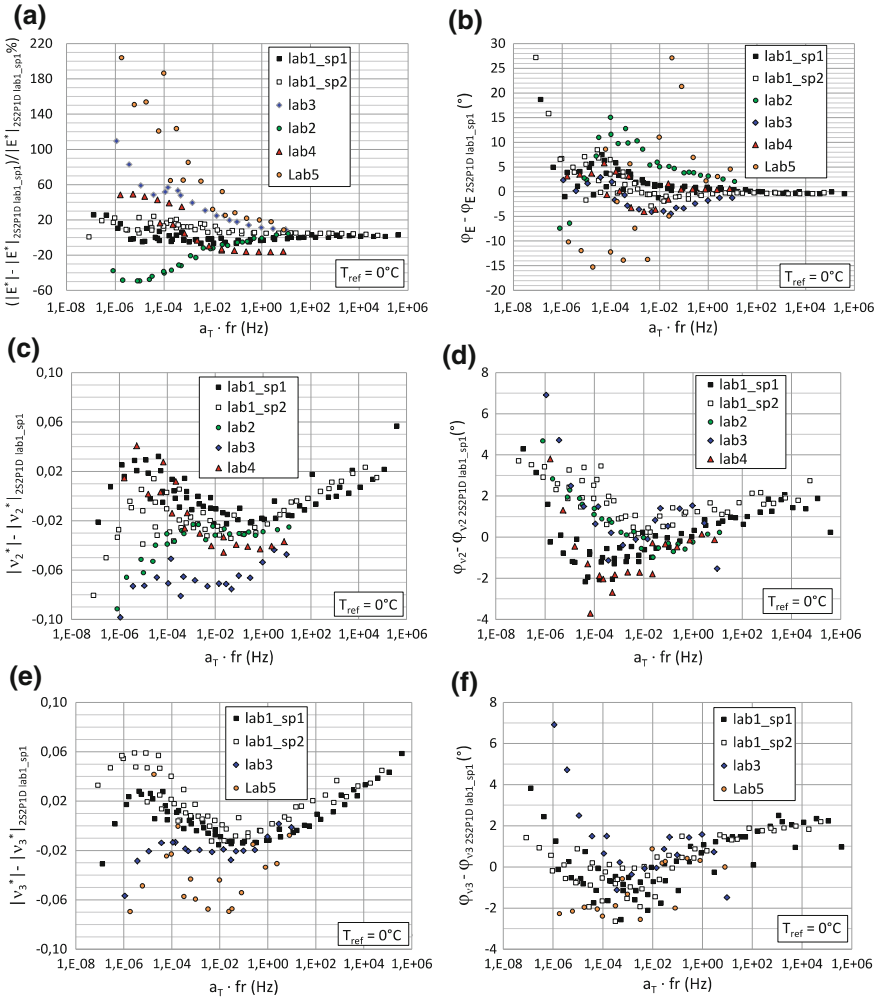

Fig. 3.31 Difference between experimental results and simulated values from 2S2P1D model calibrated with test lab1_sp1 (GB3 mix): **a** norms of the complex modulus; **b** phase angles of the complex modulus; **c** norms of the complex Poisson's ratio in dir2 (ν2); **d** phase angles of the complex Poisson's ratio in dir2 (ν2); **e** norms of the complex Poisson's ratio in dir3 (ν3); **f** phase angles of the complex Poisson's ratio in dir3 (ν3)

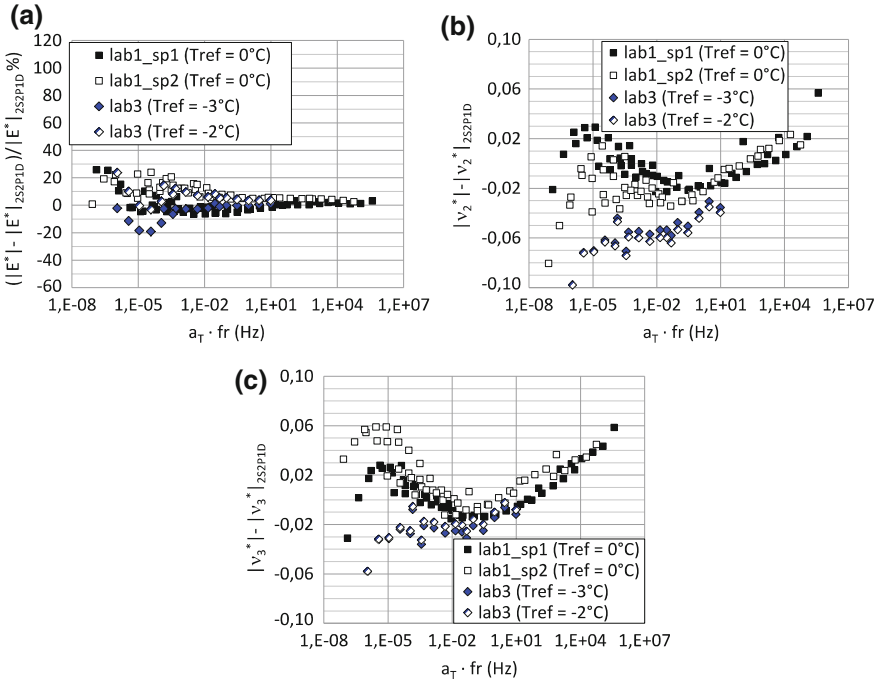

Fig. 3.32 Differences between experimental values of Lab3 and 2S2P1D lab1_sp1 values calculated at $T_{ref} = -3$ °C and $T_{ref} = -2$ °C against reduced frequencies (aT·fr): **a** norms of the complex modulus; **b** norms of the complex Poisson's ratio in dir2 ($\nu 2$); **c** norms of the complex Poisson's ratio in dir3 ($\nu 3$)

3.4 Conclusion

This report focuses on the three-dimensional 3D-LVE behavior of bituminous mixtures. In particular, the results of a round robin test organized in order to obtain the simultaneous measurement of the complex Young's modulus E^* and the complex Poisson's ratio (PR) ν^* are presented and discussed.

Uniaxial cyclic (sinusoidal or haversine compression) tests at different temperatures and loading frequencies were carried out on cylindrical specimens cored from laboratory-compacted slabs. Two types of bituminous mixtures, called GB3 (continuously graded) and GB5® (gap graded), were analyzed.

Each participating laboratory measured axial and transverse (or diametral) strains using different sensors (LVDT, strain gauges and non-contact sensors) and measurement configurations. In addition, different numerical algorithms were also employed to analyze the measured data and calculate the relevant rheological parameters. Transverse strains were measured along two orthogonal directions in order to evaluate the effect of compaction-induced anisotropy on PR.

The measured values of E^* ranged from 70 to 40,000 MPa and confirmed the validity of the time-temperature superposition principle (TTSP) for both mixtures.

Measured values of ν^* showed that its phase angle is small (less than 6°) but not null and therefore the PR should be treated (and modeled) as a complex function of temperature and frequency. In particular, results showed that the TTSP can be applied to both the absolute value and the phase angle (i.e. to the complex function ν^*).

The absolute value (norm) of PR measured for GB3 specimens ranged from 0.25 (low temperatures/high frequencies) to 0.48 (high temperatures/low frequencies), whereas for GB5 specimens $|\nu^*|$ ranged from 0.22 (low temperatures/high frequencies) to 0.60 (high temperatures/low frequencies), thus exceeding the maximum theoretical value for an isotropic material ($|\nu^*| = 0.5$). Therefore, this value is possible for anisotropic materials (Di Benedetto et al. 2016).

At high temperatures/low frequencies, for both GB3 and GB5 mixes, the PR phase angle showed a change of sign, whereas its absolute value showed a maximum. Such behavior is in accordance with the predictions of the Booij and Thoone relations and therefore confirms the thermo-rheological coherence of the measured data.

The comparison between the norm of the complex PR values in dir2 (ν_{02}) and dir3 (ν_{03}) on GB3 showed that the maximum absolute difference is less than 0.05. This difference is quite small and situated within the accuracy range of the experimental procedure. Then, the authors believe that this small difference is probably related to measurement accuracy and not to the anisotropic behavior of the material.

The tri-dimensional formulation of 2S2P1D rheological model was used to fit the 3D response (E^* and ν^*) of specimen lab_sp1 for GB3 mix. The fitted model was used as a reference to compare the measurements carried out by the participating laboratories. Results showed that the scattering of test results becomes higher at lower reduced frequencies. For the norm of the complex PR, the differences between the model and the measured data are always smaller than about ± 0.05, i.e. within the range of the accuracy limit of measurement systems.

It is finally remarked that the same conclusions can be drawn based on the results of all participating laboratories, regardless of employed strain sensors, measurement configurations and numerical analysis technique. Thus it is possible to conclude that cyclic uniaxial tests could be good candidates to become a standard test for evaluating the 3D LVE behavior of bituminous mixtures.

References

Airey GD, Rahimzadeh B, Collop AC (2003) Viscoelastic linearity limits for bituminous materials. Mater Struct 36(10):643–647

ARA (2004) Guide for mechanistic-empirical design of new and rehabilitated pavement structures, NCHRP Project 1-37A, Final Report, Washington DC

Booij HC, Thoone GPJM (1982) Generalization of Kramers-Kronig transforms and some approximations of relations between viscoelastic quantities. Rheol Acta 21(1):15–24

Bocci E, Graziani A, Canestrari F (2015) Mechanical 3D characterization of epoxy asphalt concrete for pavement layers of orthotropic steel decks. Constr Build Mater 79(2015):145–152

Caracciolo R, Giovagnoni M (1996) Frequency dependence of Poisson's ratio using the method of reduced variables. Mech Mater 24:75–85

Chabot A, Chupin O, Deloffre L, Duhamel D (2010) Viscoroute 2.0: tool for the simulation of moving load effects on asphalt pavement. Road Mater Pavement Des 11(2):227–250

Chailleux E, Ramond G, Such C, de La Roche C (2006) A mathematical-based master-curve construction method applied to complex modulus of bituminous materials. Road Mater Pavement Des 7(sup1):75–92

Charif K (1991) Contribution à l'étude du comportament mécanique du béton bitumineux en petites et grandes déformations. Thése de Doctorat, Ecole central Paris

Clec'h P, Sauzéat C, Di Benedetto H (2010) Linear viscoelastic behavior and anisotropy of bituminous mixture compacted with a French wheel compactor. In: 2nd international GeoShanghai conference

Cowpertwait PS, Metcalfe AV (2009) Introductory time series with R. Springer, Berlin

Delaporte B, Di Benedetto H, Chaverot P, Gauthier G (2007) Linear viscoelastic properties of bituminous materials: from binders to mastics. J Assoc Asphalt Paving Technol 76

Delaporte B, Di Benedetto H, Chaverot P, Gauthier G (2009) Linear viscoelastic properties of bituminous materials including new products made with ultrafine particles. Road Mater Pavement Des 10(1):7–38

Di Benedetto H, De la Roche C (1998) State of the art on stiffness modulus and fatigue of bituminous mixtures. In: Francken LE, Spon FN (eds) Bituminous binders and mixes: state of the art and interlaboratory test on mechanical behavior and mix design. Rilem Report 17, London, pp 137–180

Di Benedetto H, Partl MN, Francken L, Saint André CDLR (2001) Stiffness testing for bituminous mixtures. Mater Struct 34(2):66–70

Di Benedetto H, Delaporte B, Sauzeat C (2007a) Three dimensional linear behavior of bituminous materials: experiments and modeling. Int J Geomech. 7:149–157. doi:10.1061/(ASCE)1532-3641(2007)7:2(149)

Di Benedetto H, Mondher N, Sauzeat C, Olard F (2007b) Three-dimensional thermo-viscoplastic behaviour of bituminous materials—the DBN model. Road Mater Pavement Des 8(2):285–315. doi:10.3166/RMPD.8.285-315

Di Benedetto H, Sauzeat C, Sohm J (2009) Stiffness of bituminous mixtures using ultrasonic wave propagation. Road Mater Pavement Des 10(4):789–814. doi:10.3166/RMPD.10.789-814

Di Benedetto H, Nguyen QT, Sauzeat C (2011) Nonlinearity, heating, fatigue and thioxotropy during cyclic loading of asphalt mixtures. Road Mater Pavement Des 12(1):129–158

Di Benedetto H, Sauzéat C, Clec'h P (2016) Anisotropy of bituminous mixture in the linear viscoelastic domain. Mech Time Dependent Mater 19. doi:10.1007/s11043-016-9305-0 (April 2016)

Doubbaneh E (1995) Comportament mécanique des enrobées bitumineux des petites aux grandes déformations. Thése de Doctorat, Institut National des Sciences Appliquées de Lyon, ENTPE

Gayte P, Di Benedetto H, Sauzéat C, Nguyen QT (2015) Influence of transient effects for analysis of complex modulus tests on bituminous mixtures. Road Mater Pavement Des 19. doi:10.1080/14680629.2015.1067246 (July 2015)

Graziani A, Bocci M, Canestrari F (2014a) Complex Poisson's ratio of bituminous mixtures: measurement and modeling, Mater Struct 47(7):1131–1148

Graziani A, Bocci E, Canestrari F (2014b) Bulk and shear characterization of bituminous mixtures in the linear viscoelastic domain. Mech Time-Depend Mater 18(2014b):527–554. doi:10.1007/s11043-014-9240-x

Huang YH (2004) Pavement analysis and design, 2nd edn. Prentice Hall, Upper Saddle River, NJ

Huet C (1963) Etude par une methode d'impedance du comportement viscoélastique des materiaux hydrocarbons. Thèse de Docteur Ingénieur, Faculté des Sciences de l'Université de Paris

Hilton HH (2001) Implications and constraints of time-independent Poisson ratios in linear isotropic and anisotropic viscoelasticity. J Elast 63(3):221–251

Hilton HH (2009) The elusive and fickle viscoelastic Poisson's ratio and its relation to the elastic-viscoelastic correspondence principle. J Mech Mater Struct 4(7–8):1341–1364

Hilton HH (2011) Clarifications of certain ambiguities and failings of Poisson's ratios in Linear viscoelasticity. J Elast 104(1):303–318

Islam MR, Faisal HM, Tarefder RA (2015) Determining temperature and time dependent Poisson's ratio of asphalt concrete using indirect tension test. Fuel 146:119–124

Kassem E, Grasley ZC, Masad E (2011) Viscoelastic Poisson's ratio of asphalt mixtures. Int J Geomech 13(2):162–169

Kim YR (2008) Modeling of asphalt concrete, ASCE Press

Kim YR, Seo Y, King M, Momen M (2004) Dynamic modulus testing of asphalt concrete in indirect tension mode. Transp Res Rec 1891:1631173

Lakes RS (1987) Foam structures with a negative Poisson's ratio. Science 235(4792):1038–1040

Lakes RS, Wineman A (2006) On Poisson's ratio in linearly viscoelastic solids. J Elast 85(1):45–63

Lee HS, Kim J (2009) Determination of viscoelastic Poisson's ratio and creep compliance from the indirect tension test. J Mater Civ Eng 21(8):416–425

Lekhnitskii SG (1977) Theory of elasticity of an anisotropic elastic body. MIR Publishers, Moscow

Maher A, Bennert T (2008) Evaluation of Poissons's ratio for use in the mechanistic empirical pavament design guide (MEPDG). Report submitted to Federal Highway Administration U.S., Department of transportation, Washington, D.C., #FHWA-NJ-2008-004, 60p

Mangiafico S, Di Benedetto H, Sauzéat C, Olard F, Pouget S, Planque L (2013) Influence of RAP content on complex modulus of asphalt binder blends and corresponding mixes: experimental results and modelling. Road Mater Pavement Des 14(Suppl 1):132–148

Mangiafico S, Di Benedetto H, Sauzéat C, Olard F, Pouget S, Planque L (2014) New method to obtain viscoelastic properties of bitumen blends from pure and RAP binder constituents. Road Mat Pavement Des 15

Mounier D, Di Benedetto H, Sauzeat C (2012) Determination of bituminous mixtures linear properties using ultrasonic wave propagation. Constr Build Mater 36:638–647. doi:10.1016/j.conbuildmat.2012.04.136

NCHRP (2009) NCHRP 1-37A design guide software. American Association of State Highway and Transportation Officials, Washington, DC. Available from: http://www.trborg/mepdg/software.htm. Accessed Apr 2015

NF EN 12697-33+A1 (2007) Mélange bitumineux - Méthodes d'essai pour mélange hydrocarboné à chaud - Partie 33: confection d'éprouvettes au compacteur de plaque, European Standard—French Standard AFNOR

NF EN 12697-35+A1 (2007) Mélanges bitumineux - Méthodes d'essai pour mélange hydrocarboné à chaud - Partie 35: malaxage en laboratoire, European Standard—French Standard AFNOR

Nguyen HM, Pouget S, Di Benedetto H, Sauzeat C (2009) Time-temperature superposition principle for bituminous mixtures. Eur J Environ Civil Eng 13(9):1095–1107. doi:10.3166/EJECE.13

Nguyen QT, Di Benedetto H, Sauzéat C (2012) Determination of thermal properties of asphalt mixtures as another output from cyclic tension-compression test. Road Mater Pavement Des 13(1):85–103. doi:10.1080/14680629.2011.64408

Nguyen QT, Di Benedetto H, Sauzéat C (2013) Prediction of linear viscoelastic behaviour of asphalt mixes from binder properties and reversal. Multi-scale modeling and characterization of infrastructure materials. Springer, Netherlands, pp 237–248

Nguyen QT, Di Benedetto H, Sauzéat C (2015) Linear and nonlinear viscoelastic behaviour of bituminous mixtures. Mater Struct doi:10.1617/s11527-014-0316-5 (On Line First, May 2014)

Olard F (2012) GB5 mix design: high-performance and cost-effective asphalt concretes by use of gap-graded curves and SBS modified bitumens. Road Mater Pavement Des 13(Suppl 1):234–259

Olard F, Di Benedetto H (2003) General "2S2P1D" model and relation between the linear viscoelastic behaviors of bituminous binders and mixes. Road Mater Pavement Des 4(2):185–224

Papazian SH (1963) The response of linear viscoelastic materials in the frequency domain with emphasis on asphalt concrete. In: Proceedings of the 1st international conference on the structural design of asphalt pavements, pp 454–463, Ann Arbor, 20–24 Aug 1962

Perraton D, Di Benedetto H, Sauzéat C, Hofko B, Graziani A, Nguyen QT, Pouget S, Poulikakos LD, Tapsoba N, Grenfell J (2016) 3Dim experimental investigation of linear viscoelastic properties of bituminous mixtures. Mater Struct. doi:10.1617/s11527-016-0827-3 (On Line March)

Pham NH, Sauzéat C, Di Benedetto H, Gonzalez-Leon JA, Barreto G, Nocolai A, Jajubowski M (2015a) RAP and additive influence on 3D linear behaviour of warm bituminous mixtures. Road Mater Pavement. doi:10.1080/14680629.2015.1021108 (On Line First, March 2013)

Pham NH, Sauzéat C, Di Benedetto H, Gonzalez-Leon JA, Barreto G, Nocolai A, Jajubowski M (2015b) Analysis and modeling of 3D complex modulus tests on hot and warm bituminous mixtures, Mech Time Depend Mater. doi:10.1007/s11043-015-9258-8 (On Line First, March 2015)

Pouget S, Sauzeat C, Di Benedetto H, Olard F (2010) From the behavior of constituent materials to the calculation and design of orthotropic bridge structures [Special Issue: EATA 2010]. Road Mat Pavement Des 11:111–144. doi:10.3166/RMPD.11HS

Pouget S, Di Benedetto H, Sauzeat C, Olard F (2012a) Effect of vehicle speed on the millau viaduct response. J Test Eval 40:7

Pouget S, Sauzeat C, Di Benedetto H, Olard F (2012b) Modeling of viscous bituminous wearing course materials on orthotropic steel deck. Mater Struct 45(7):1115–1125. doi:10.1617/s11527-011-9820-z

Sayegh G (1965) Contribution à l'étude des propriétiés viscoélastique des bitumes purs et des béton bitumineux. Thèse de Docteur Ingénieur, Faculté des Sciences de l'Université de Paris

Sayegh G (1968) Viscoelastic properties of bituminous mixtures. In: Proceedings of the 2nd international conference on the structural design of asphalt pavements, pp 743–754, Ann Arbor, 7–11 Aug 1967

Schwartz CW, Li R, Ceylan H, Kim S, Gopalakrishnan K (2013) Global sensitivity analysis of mechanistic-empirical performance predictions for flexible pavements. In: Transportation research board (TRB) 92nd annual meeting, Washington, D.C., 13–17 Jan 2013

Stephenson RW, Manke PG (1972) Ultrasonic moduli of asphalt concrete. Highway Res Rec 404:8–21

Tapsoba N, Sauzéat C, Di Benedetto H, Baaj H, Ech M. (2014) Behaviour of asphalt mixtures containing reclaimed asphalt pavement and asphalt shingle. Road Materials and Pavement Design, 15(2), 330–347

Tiouajni S, Di Benedetto H, Sauzeat C, Pouget S (2011) Approximation of linear viscoelastic model in the 3 dimensional case with mechanical analogues of finite size. Road Mater Pavement Des 12(4):897–930. doi:10.3166/RMPD.12

Tschoegl NW (1989) The phenomenological theory of linear viscoelastic behavior: an introduction. Springer, Berlin

Tschoegl NW, Knauss WG, Emri I (2002) Poisson's ratio in linear viscoelasticity—a critical review. Mech Time-Depend Mater 6(1):3–51

Van Der Poel C (1954) A general system describing the visco-elastic properties of bitumens and its relation to routine test data. J Appl Chem 4:221–236

Witczak MW, Mirza MW (1999) Development of relationships to predict poisson's ratio for paving materials, interteam technical report for NCHRP 1-37A. University of Maryland, College Park, MD

Chapter 4
Advanced Interface Testing of Grids in Asphalt Pavements

Francesco Canestrari, Antonio D'Andrea, Gilda Ferrotti, Andrea Graziani, Manfred N. Partl, Christophe Petit, Christiane Raab and Cesare Sangiorgi

Abstract Nowadays, road pavements are subjected to steadily increasing traffic volumes generating accelerated functional and structural distresses that require frequent and expensive maintenance. On the basis of such needs, in recent years, practical applications and theoretical studies have proved that the service life of flexible pavements can be extended by installing geosynthetic reinforcements. In particular, grids can be placed at the interface of bituminous layers for both new constructions and rehabilitation of existing pavements, in order to improve repeated loading and rutting resistance and to prevent or delay reflective cracking. However, the presence of an interlayer reinforcement may also hinder the full transmission of horizontal shear stress between asphalt layers (debonding effect), penalizing the overall efficiency of the pavement system. For the above-mentioned reasons, both laboratory and in situ investigation are needed in order to better understand the real role played by the grid reinforcement. The achievement of such objective is the main goal of the RILEM TC 237-SIB/TG4 that carried out an interlaboratory experiment focused on the "Advanced Interface Testing of Geogrids in Asphalt Pavements". In this context, the participating laboratories were involved with a twofold objective: to compare the predictive effectiveness of different experimental approaches and to analyze the behavior of different grid types. For this purpose, two experimental reinforced pavement sections were realized with the same materials and construction techniques. The first pavement section was used to prepare

F. Canestrari · G. Ferrotti · A. Graziani (✉)
Università Politecnica delle Marche, Ancona 60131, Italy
e-mail: a.graziani@univpm.it

A. D'Andrea
Università di Roma "Sapienza", Rome 00184, Italy

C. Petit
University of Limoges, Egletons 19300, France

M. N. Partl · C. Raab
Empa. Swiss Federal Laboratories for Materials Science and Technology, Duebendorf 8600, Switzerland

C. Sangiorgi
Università di Bologna, Bologna 40136, Italy

M. N. Partl et al. (eds.), *Testing and Characterization of Sustainable Innovative Bituminous Materials and Systems*, RILEM State-of-the-Art Reports 24,
https://doi.org/10.1007/978-3-319-71023-5_4

samples for the interlaboratory experiment, the second one was specifically designed and instrumented to analyze the field performance of the grids under heavy traffic conditions. The objective is the characterization of the mechanical behavior of grid reinforced interfaces in asphalt concrete pavements using different test methodologies and the analysis of the relationship between laboratory test results and actual field performance. To this purpose, the laboratory research activities were based on the analysis and comparison of the results obtained following specific testing protocols proposed by the participating laboratories that combine performance-based tests (e.g. interlayer shear tests, static and dynamic bending tests, tensile-bending tests), in order to investigate the overall behavior of double-layered asphalt systems. The role of the instrumented pavement section was complementary and oriented towards an improvement in the existing design and testing approaches. Such goal was attained by analyzing the actual stress-strain response of grid-reinforced systems under vehicular loads, also monitoring the natural and induced field cracking evolution. Despite the variety of the testing equipment and protocols adopted by the participating laboratories, all test results were consistent. Moreover, such experimental results contributed, together with the data analysis collected on the instrumented pavement section, to the correct understanding of the grids performance that were characterized by specific peculiarities making them appropriate for different applications.

Keywords Asphalt pavement · Interface testing · Horizontal shear
Interlayer bond · Mechanical behavior · Performance · Reinforcement
Tack coat · Interlaboratory test · Real scale analysis

Glossary

List of Symbols

α	Slip parameter
c_0	Pure shear strength
D	Diameter
$\delta_{r,0}$	Periodic recovered beam deflection amplitude
δ_F	Maximum pre-cracking flexural deflection
$\|E^*\|$	Norm of complex young's modulus
E_{app}	Apparent stiffness modulus
$\varepsilon_{r,app}$	Apparent recovered strain
Φ_{peak}	Peak friction angle
H	Height
I5, I10, I20	ASTM toughness indices
N^i_{flex}	Number of cycles at the flex point of interface type i
P_0	Haversine load amplitude
P_F	Maximum pre-cracking flexural load
σ_{app}	Apparent stress
σ_n	Vertical stress

T	Temperature
τ	Interlayer shear stress
τ_{peak}	Interlayer shear strength
T_{ref}	Reference temperature

List of Abbreviations

3PB	Three-point bending
4PB	Four-point bending
AC	Asphalt concrete
ANOVA	Analysis of variance
ASG	Asphalt strain gage
ASTM	America society for testing and materials
ASTRA	Ancona shear testing research and analysis
CBR	California bearing ratio
CF	Carbon fiber/glass fiber
DCP	Dynamic cone penetrometer
GB	Granular base
Empa	Swiss Federal Laboratories for Materials Science and Technology
EN	European norm
EPC	Earth pressure cell
FP	Glass fiber reinforced polymer
FWD	Falling weight deflectometer
IBDiM	Road and Bridge Research Institute
IF	Improvement factor
IFSTTAR	Institut français des sciences et technologies des transports, de l'aménagement et des réseaux
ISS	Interlayer shear strength
ITSM	Indirect tensile stiffness modulus
LET	Layered elastic theory
LFWD	Light falling weight deflectometer
LPDS	Layer-parallel direct shear
LVDT	Linear variable differential transformer
MMLS	Model mobile load simulator
MMLS3	One-third scale model mobile load simulator
SBS	Styrene-butadiene-styrene
SDSTM	Sapienza direct shear test machine
SIB	Sustainable and innovative bituminous materials and systems
ST	Shear tester
PA	Porous asphalt
RILEM	International Union of Laboratories and Experts in Construction Materials, Systems and Structures
TC	Technical committee
TG	Task group

UN	Unreinforced
UNIBO	Università di Bologna
UNIVPM	Università Politecnica delle Marche
UNIRM	Università di Roma "Sapienza"
USCS	Unified soil classification system

4.1 Introduction

4.1.1 Reinforcement of Asphalt Layers

Service life of bituminous pavements can be extended by applying a tensile reinforcement element. In particular, geosynthetics or steel nets installed at different depths within a pavement structure are capable of improving pavement performance in different ways (Brown 2006).

The first applications of pavement reinforcement concerned unbound layers with the purpose to prevent permanent deformation (Perkins 1999; Yang and Al-Qadi 2007), improve bearing capacity and filter and/or separate layers. The use of reinforcement systems within bound layers is mainly addressed to prevent or delay reflective cracking (Austin and Gilchrist 1996; Brown et al. 2001; Caltabiano and Brunton 1991; Elseifi and Al-Qadi 2003; Gillespie and Roffe 2002; Khodaii et al. 2009; Montestruque et al. 2004; Sobhan et al. 2004) and rutting (Komatsu et al. 1998) and improve fatigue life (Brown et al. 1985; Nguyen et al. 2013).

Positioning of the reinforcement at different levels within bituminous layers provides different beneficial effects on performance (Abd El Halim et al. 1991; Al-Qadi et al. 2007; Brown et al. 1985, 2001; Khodaii et al. 2009). In particular, the position strongly influences the reduction of both cracking under repeated loading cycles (Brown et al. 2001; Bocci et al. 2007; Grabowski and Pozarycki 2008; Khodaii et al. 2009; Khodaii and Fallah 2009; Lee 2008; Powell 2008; Prieto et al. 2007) and rutting (Al-Qadi et al. 2007; Brown et al. 1985).

Besides reinforcement position, its correct installation is essential to ensure the desired performance and it is still an important subject of debate (Button and Lytton 2003; Asphalt Academy 2008; Pasquini et al. 2013). In fact, in case of improper installation, the reinforcement might not work as expected, making its use ineffective from a technical and economic point of view (Francken 2005; Shukla and Yin 2004; Uijting et al. 2002; Vanelstraete and De Visscher 2004).

In terms of reinforcement materials, nowadays geosynthetics are often preferred over steel mesh because of recyclability and installation issues. Three types of geosynthetics have been used in between bituminous layers: geotextiles, geogrids and geocomposites.

Geotextiles mainly act as stress absorbing interlayers, also preventing the ingress of water into the pavement structure (Button and Lytton 2003). Vanelstraete and de Bondt (1997) observed that a given product will act as a reinforcement material if its overall stiffness modulus is higher than that of the bituminous overlay. For this reason, geotextiles are usually not effective as reinforcement products.

For pavement applications, the most used geosynthetics are geogrids. Their performance mainly depends on: mesh size and shape (Canestrari et al. 2006; Komatsu et al. 1998), surface coating (Aldea and Darling 2004; Ferrotti et al. 2012), position within the bituminous layers (Bocci et al. 2007; Sobhan and Tandon 2008) and strength (Brown et al. 2001; Caltabiano and Brunton 1991). The influence of these parameters has been thoroughly studied by means of both laboratory and in situ investigations but is still an important challenge. Grids provide good performance under repeated loading, especially when placed at the bottom of bound layers, where tensile stresses-strains are the highest and can be absorbed by the grid (Brown et al. 2001; Bocci et al. 2007). Moreover, the inclusion of a grid between asphalt concrete layers is very effective for increasing the service life of the pavement structures as, in most cases, it can be considered an anti-reflective cracking system (Komatsu et al. 1998; Abd El Halim et al. 1982, 1991; Brown et al. 2001; Khodaii et al. 2009; Zamora-Barraza et al. 2011).

Geocomposites are obtained by combining two or more geosynthetic products (e.g. bituminous membrane and geogrid). For pavement applications, they represent a promising option in the wide range of reinforcing products available on the market as they combine improved tensile properties of reinforcements with stress absorbing and waterproofing effects. It has been shown that road structures including membrane interlayer systems reinforced with geotextiles (Ramberg Steen 2002; Shukla and Yin 2004; Vanelstraete and De Visscher 2004) or glass fibers (Gillespie and Roffe 2002; Pasquini et al. 2014) provide extended pavement service lives and/or more cost-effective maintenance processes.

Despite the above-mentioned enhanced performance of reinforced bituminous systems demonstrated by many experimental investigations, limited positive practical experiences are documented (James 2004; Zou et al. 2007). For this reason, RILEM TC 237-SIB/TG4 “Pavement Multilayer System Testing” decided to investigate the effectiveness deriving from the installation of reinforcements between asphalt layers through laboratory tests and real scale instrumented field sections.

4.1.2 Interlayer Bonding of Reinforced Asphalt Interfaces

The presence of geosynthetics at the interface can cause an interlayer debonding effect that could affect the overall pavement performance (Vanelstraete et al. 1997; Brown et al. 2001; Canestrari et al. 2012a, b, Ferrotti et al. 2011; Zamora-Barraza et al. 2010). Both quasi-static (Ferrotti et al. 2011) and dynamic (Brown et al. 2001) shear tests performed on double-layered specimens with or without the application of a constant normal stress showed that when a reinforcement is placed at the interface, a general shear strength decrease occurs. This parameter is influenced by the mesh dimension of the grid (Canestrari et al. 2006; Asphalt Academy 2008) whose choice depends on the aggregate gradation and on the depth at which the grid is placed. In fact, the higher the aggregate size and the deeper the position of the mesh in the pavement, the higher should be the mesh size.

In terms of comparison between different types of reinforcing materials, several researchers (Caltabiano and Brunton 1991; Brown et al. 2001; Zamora-Barraza et al. 2011) observed a higher reduction in interlayer shear resistance with geotextiles than with geogrids, confirming the poor contribution of these fabric materials as pavement reinforcement.

In order to increase the adhesion properties between the asphalt concrete layers and the grids, the effect of coating materials applied on the surface of geogrids was investigated (Aldea and Darling 2004; Ferrotti et al. 2012), showing that specially designed coating can significantly improve the overall pavement structure performance. Analogous results were also found by Komatsu et al. (1998), who compared the mechanical behavior of systems reinforced with non-modified geogrids and geogrids treated on the surface with special chemical solutions.

Although interface bonding conditions influence pavement response in terms of stress-strain distribution (Shukla and Yin 2004; Sobhan and Tandon 2008), debonding is not necessarily a negative aspect for pavement mechanical performance. In fact, when geosynthetics are employed to improve load spreading ability, rutting resistance and fatigue resistance, a stable reinforced paving system is required and reinforcements should permit interlocking between the lower layer and the upper layer (Brown et al. 1985; Lee 2008). On the other hand, this may result in a limited capability to prevent crack propagation from the underlying pavement layers. In fact, when shear strength at the interface excessively decreases due to the presence of the reinforcement, the structural contribution of the grid may be limited and the overall pavement strength would be sensibly affected, making the debonding effect potentially positive.

4.1.3 Mechanical Response of Reinforced Bituminous Pavements

Performance improvement due to the installation of a reinforcement within bituminous layers can be evaluated using laboratory tests, reduced-scale models or full-scale pavements.

In laboratory tests, double-layered asphalt specimens with a reinforcing element placed at the interface are usually considered. The generalization of such test results to real pavement applications may be restricted by scale effects (Canestrari et al. 2012a), especially considering the characteristic dimension of the grid mesh. In addition, when preparing lab-scale reinforced specimens, the use of field installation techniques is impossible. Consequently, the construction of reduced-scale or full-scale pavement sections is generally more appropriate for studying the effects of geosynthetic interlayers (Arraigada et al. 2016).

Back in the 1990s, Ishai et al. (1992) described one of the first technological efforts of using geotextile-reinforced asphaltic membranes for subgrade and pavement improvement. Geosynthetic interlayers were applied either as a sealing and reinforcement between the subgrade and the pavement or as a reinforcement for the

retardation of reflective cracking overlaying existing cracked pavement surfaces in specific trial sections. In this real-scale research, a close control and follow-up system was applied for monitoring pavement performance with time under actual service and climatic conditions, giving a first look into the reinforcements behavior.

More recently a reduced-scale pavement model was realized by Correia and Zornberg (2014) to verify the effectiveness of geosynthetic reinforcement in reducing rutting in geogrid-reinforced asphalt overlays. Vertical load was applied by a rolling wheel, simulating a truck wheel, and surface deflections were measured by displacement transducers. The permanent deformation response was clearly improved by the grid installation.

Chehab and Tang (2012) used a one-third scale model mobile load simulator (MMLS3) to verify the improvement in reflective cracking resistance obtained by incorporating a geosynthetic interlayer on a 30 m long pavement test section. Siriwardane et al. (2010) carried out a study on flexible pavement systems reinforced with fiberglass grids installed within asphalt layers. The experimental pavements were instrumented with pressure cells, displacement transducers and strain gauges. Static load test data, along with a computer analysis performed by using the finite element method, showed that grid reinforcement is able to spread the vertical loads over a larger area and slightly reduce vertical stresses. Full-scale tests on grid reinforced low-traffic pavement structures carried out on the accelerated testing facility of IFSTTAR were also described by Hornych et al. (2012) and by Nguyen et al. (2013). Results obtained from the instrumented pavement confirmed that fiberglass grids were able to significantly improve fatigue life, provided that a good bonding between the asphalt layers is ensured.

Grid reinforcement was also proven effective when Porous Asphalts (PA) are used. Kim et al. (2009) investigated the fatigue of reinforced PA composite systems, verifying that the reinforcement layer could increase the fatigue life by 23% in dry and by 27% in wet conditions, based on model mobile load simulator (MMLS) test results.

4.2 Project Description

4.2.1 Objectives

The project focuses on the mechanical characterization of grid-reinforced asphalt pavements. The main objectives are:

- to compare laboratory devices and procedures currently used to test the mechanical behavior of reinforced asphalt layers;
- to analyze the relationship between laboratory test results and actual field performance of the reinforced system;
- to compare different pavement grid types based on their effects on pavement performance.

The experimental program is divided in two parts, an interlaboratory testing phase and a real scale analysis, and is based on the construction of two full-scale pavement sections. A double-layered asphalt surfacing with three different interlayer systems characterizes both sections. In particular, each section is composed by:

- a reference subsection with a conventional tack-coat interface (without reinforcement);
- two subsections with different types of pavement grid installed at the interface.

The first section (Section A) was used to obtain double-layered samples for the interlaboratory test (Graziani et al. 2014; Canestrari et al. 2015). The second one (Section B) was built along an in-service road and was fully instrumented to analyze the behavior of the same double-layered asphalt systems under real-scale conditions.

4.2.2 Methodology

4.2.2.1 Interlaboratory Test

Laboratories invited to join the research project were asked to perform the mechanical characterization of double-layered asphalt samples obtained from Section A. No limitations were imposed on the selection of the test type/procedure; however, two test categories were preliminary identified:

- tests intended to measure the properties of reinforced interfaces (e.g. shear strength);
- tests intended to measure the properties of double-layered reinforced systems (e.g. stiffness/fatigue).

The main intention was to simulate typical shortcomings of real scale applications where the structural improvement provided by pavement grids can be compromised if a significant shear strength reduction (debonding effect) occurs at the interface between asphalt layers.

Double layered samples (slabs) were collected from Section A and shipped to the participants according to their experimental plan (e.g. number of replications, testing parameters, specimen shape and dimensions).

4.2.2.2 Real Scale Analysis

The real scale analysis was complementary to the interlaboratory test and oriented towards an improvement in the existing design and testing approaches. Such goal was attained in two ways:

- by analyzing the pavement performance under traffic (i.e. surface cracking evolution);

– by measuring actual stresses and strains due to vehicular loads at specific positions in both the reinforced and unreinforced pavements.

To perform stress and strain measurements Section B was instrumented with pressure cells, asphalt strain gauges and temperature sensors.

Falling weight deflectometer (FWD) tests were carried out to analyze pavement response in terms of surface deflections, strain and stress measurements. This allowed an overall assessment of the grid effects by comparing the behavior of reinforced and unreinforced sections. FWD results, along with laboratory test results, were also used to develop a simple layered elastic theory (LET) model for both reinforced and unreinforced pavements.

Real-scale load tests were carried out using fully loaded trucks. This allowed the measurement of stress and strains induced by single and tandem axles, single and dual tire configurations and horizontal forces transmitted by traction axles.

In addition, simulated constructions defects (i.e. interface contamination, cracks) were included in Section B in order to evaluate the reinforcement effect on the pavement performance under such critical conditions.

4.2.3 Participating Laboratories

Seven laboratories participating on a voluntary basis are listed as follows:

– Empa Dübendorf, Switzerland;
– Laboratoire GEMH, Centre Universitaire de Génie Civil, Université de Limoges, Egletons, France;
– Road and Bridge Research Institute, Jagiellonska, Poland;
– Università di Bologna, Bologna, Italy;
– Università di Roma “Sapienza”, Roma, Italy;
– Università Politecnica delle Marche, Ancona, Italy;
– University of Wuppertal, Wuppertal, Germany.

4.3 Experimental Pavement Sections

The two full-scale test sections were constructed in November 2009 near the city of Ancona (Italy), under the supervision of Università Politecnica delle Marche, using real scale paving equipment and grid installation techniques.

4.3.1 Materials and Preliminary Tests

Section B was realized along an in-service secondary road. The existing asphalt surfacing was milled, whereas the unbound granular base (200 mm) and the subgrade were maintained and characterized by means of physical and mechanical tests.

The subgrade is an inorganic clayey soil of medium plasticity (Liquid Limit = 42; Plasticity Index = 18) that can be classified as CL-ML according to the Unified Soil Classification System (USCS). In situ CBR values were estimated using Dynamic Cone Penetrometer (DCP) tests (Fig. 4.1), and found to vary from 5% (underneath the base) to 10% (at 900 mm depth).

The unbounded base course is composed by 100% crushed limestone aggregates, with a nominal maximum dimension of 25 mm. In situ CBR values for the base course, estimated with DCP tests, exceed 100.

A single Asphalt Concrete (AC) mixture was used to construct the double-layered surfacing of both sections A and B. The mix was characterized by 12 mm maximum aggregate dimension (AC 12) and a 70/100 pen bitumen dosed at 5.5% by aggregate weight. The mix was produced in a nearby asphalt plant, according to typical Italian dense graded mix specifications. A summary of the quality control tests performed for both sections during and after construction is reported in Table 4.1 and in Fig. 4.2.

The mechanical properties of the AC mix were investigated by measuring the indirect tensile stiffness modulus (ITSM) on eight field cores of Section B listed in Table 4.1b. The upper and lower layers were tested separately at three different temperatures (T = 0, 10 and 20 °C) and the average ITSM values for the two layers were found to be very close (Fig. 4.3a).

In addition, complex modulus tests were carried out on four cylindrical specimens (D = 98 mm, H = 120 mm) prepared in the laboratory using the AC mixture sampled during construction. Specimens were compacted with a shear gyratory

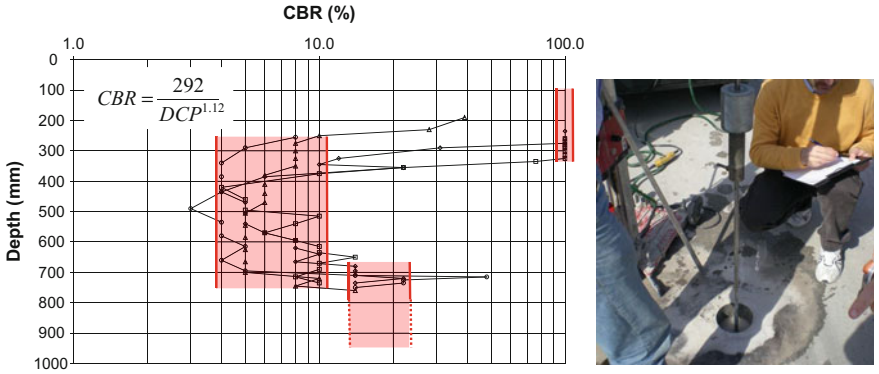

Fig. 4.1 Example of dynamic cone penetrometer (DCP) test results and measurement action

Table 4.1 (a) Quality control tests on Section A, (b) quality control tests on Section B

(a)					
		Lower layer		Upper layer	
Interface	Core	Thickness	Air voids	Thickness	Air voids
ID	N.	mm	%	mm	%
UN	1	51	10.4	50	10.3
UN	2	49	11.4	48	10.4
CF	1	48	9.0	44	11.2
CF	2	56	10.3	43	11.8
CF	3	56	9.0	44	10.6
CF	4	48	10.4	42	11.5
FP	1	65	8.8	53	9.6
FP	2	57	10.3	53	9.9
Average		54	10.1	47	10.7
(b)					
UN	1	45	10.4	50.0	10.0
UN	2	38	8.8	48.0	10.5
CF	1	41	11.8	45.0	11.6
CF	2	41	11.1	46.0	11.1
CF	3	42	9.7	45.0	9.3
CF	4	38	10.2	45.0	8.3
FP	1	44	8.2	59	9.4
FP	2	47	8.6	55	11.0
Average		42	9.9	49	10.2

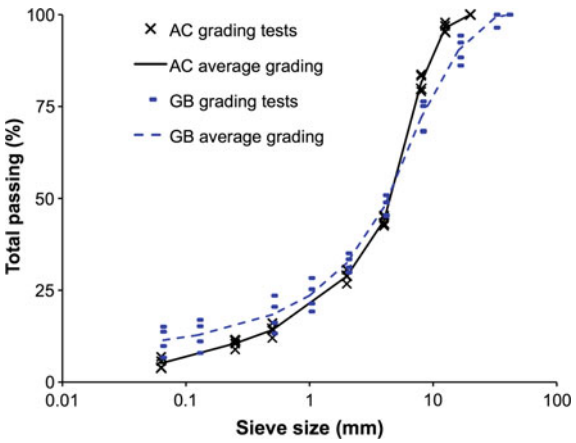

Fig. 4.2 Average grading of AC mixture and granular base (GB)

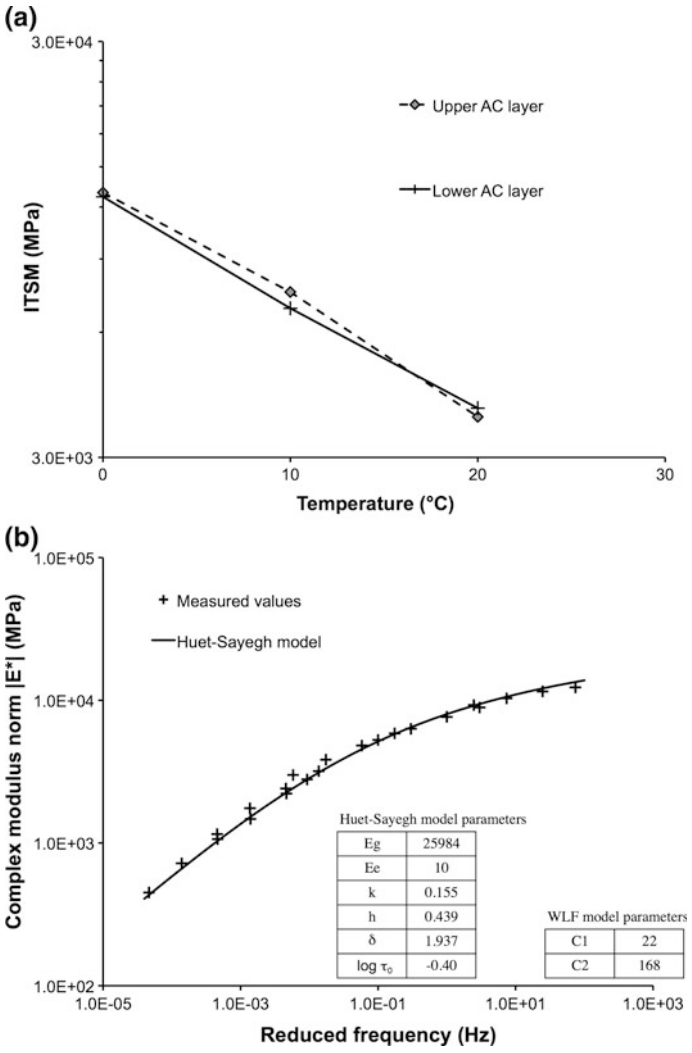

Fig. 4.3 Stiffness properties of the AC mixture: **a** average ITSM values measured on field cores; **b** master curve of |E*| at 10 °C

compactor at an average air void level of 10%. Frequency sweep tests were carried out at five temperatures (T = 0, 10, 20, 30 and 40 °C) and at a nominal strain level of 30 microstrain (30×10^{-6} m/m). The master curve of the complex modulus norm |E*| at reference temperature T_{ref} = 10 °C is plotted in Fig. 4.3b along with the calculated parameters of the Huet–Sayegh rheological model and the parameters of the Williams–Landel–Ferry model, which was used to fit the temperature shift factors.

Table 4.2 Properties of the residual binder of the modified emulsion used as tack-coat

Penetration @ 25 °C (dmm)	Viscosity @ 160 °C (Pa s^{-1})	Ring and ball temperature (°C)	Fraass breaking point (°C)
55–65	0.2–0.8	65–75	<−18

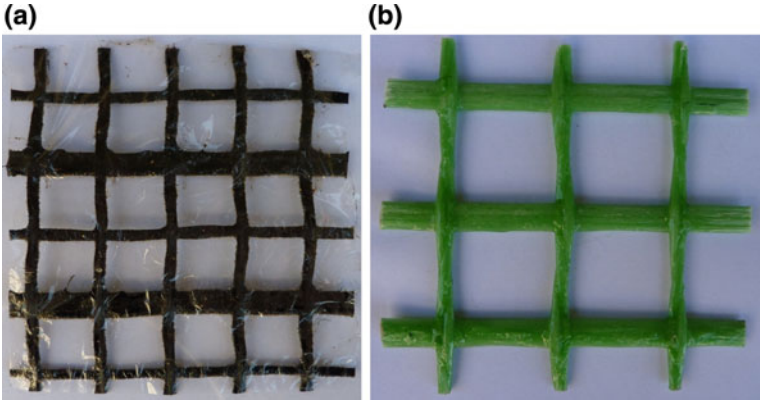

Fig. 4.4 Detail of the installed grids: **a** carbon fiber/glass fiber grid (CF); **b** glass fiber polymer grid (FP)

An SBS polymer-modified tack coat emulsion (Table 4.2), classified as C 69 BP 3 according to EN 13808, was applied on the surface of the lower asphalt layer with a rate of 0.25 kg/m^2 of residual binder in both reinforced and unreinforced interfaces.

Two different grids were installed (Fig. 4.4). The Carbon Fiber/Glass Fiber grid (CF) is pre-coated with bitumen and characterized by carbon fiber rovings in the transversal direction and glass fiber rovings in the longitudinal direction, with a 20 mm square mesh. The product is sanded on the upper side, whereas a burn off film is applied on the underside. The main characteristics of the CF grid are shown in Table 4.3. The Glass Fiber Reinforced Polymer grid (FP) is obtained by weaving continuous alkaline-resistant pre-tensioned glass fibers, covered with a thermosetting epoxy resin (vinylester). The grid has flat transversal strands woven into longitudinal twisted strands, with a 33 mm^2 mesh (Table 4.3).

Apart from the constituent material and mesh size, the main difference between the two grids is their torsional rigidity, also called aperture rigidity (Kinney and Yuan 1995). In fact, the FP grid is extremely stiff as twisting and distorting its square mesh is almost impossible, whereas the CF grid mesh is extremely flexible and deformable.

Table 4.3 Characteristics of CF and FP grids

Grid	Direction	Material	Aperture size (mm)	Tensile modulus (N/mm^2)	Elongation at rupture (%)	Tensile force mesh (kN/m)
CF	Longitudinal	Glass fiber	20	73,000	3–4.5	111
	Transversal	Carbon fiber	20	240,000	1.5	249
FP	Longitudinal	Glass fiber reinforced polymer	33	23,000	3	211
	Transversal	Glass fiber reinforced polymer	33	23,000	3	211

4.3.2 Inter laboratory Test Pavement (Section A)

Dimensions and position of the three sub-sections included in Section A are depicted in Fig. 4.5a. In each sub-section the asphalt surfacing was composed of two 50 mm thick layers, as shown in Fig. 4.5b. The same AC12 mix was used for both layers.

4.3.2.1 Construction of Section A

The working activities for the construction of Section A were scheduled and completed in three days.

– **First day**. An AC regulating course (Fig. 4.6a) was applied over the existing pavement to provide a regular and flat base surface for placing the two uppermost layers.

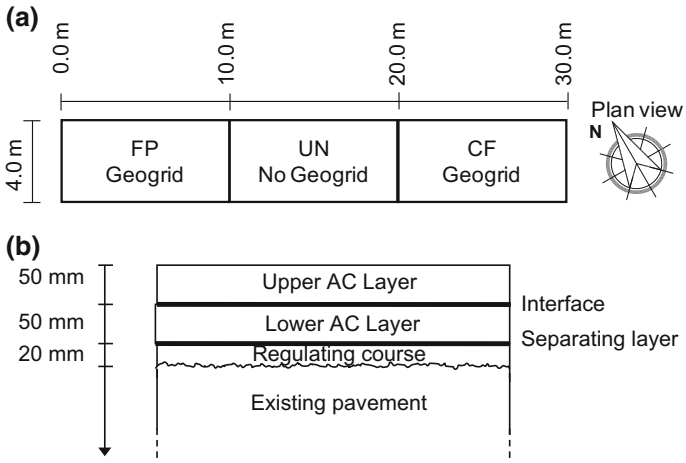

Fig. 4.5 Section A used for the preparation of slabs: **a** plan view; **b** cross section

Fig. 4.6 Working activities for the construction of Section A: **a** AC regulating course; **b** spreading of dry sand as separating layer; **c** laying of the AC12 upper layer for the "CF" sub-section; **d** laying of the AC12 upper layer for the "FP" sub-section

- **Second day**. (1) Dry sand was spread as separating layer (Fig. 4.6b) in order to facilitate the removal of the double-layered slabs after the saw cutting. (2) The lower AC12 layer was laid and compacted;
- **Third day**. (1) The tack coat was applied on the surface of the lower layer in all reinforced and unreinforced sub-sections; (2) the grids were installed in sub-sections "CF" and "FP" according to the product specifications; (3) the upper AC12 layer was laid and compacted (Fig. 4.6c, d).

From each sub-section of Section A, slab samples of different sizes (52 × 52 cm and 65 × 65 cm) were cut in order to fit the needs of the laboratories participating to the interlaboratory test (Fig. 4.7a). On the top of all slabs, a white line was marked parallel to the compaction direction (Fig. 4.7b) to allow a correct preparation of the test specimens in the laboratory.

4.3.3 Instrumented Pavement (Section B)

Dimensions and position of the three sub-sections included in Section B are shown in Fig. 4.8a. In each sub-section the asphalt surfacing was composed of a 40 mm thick lower layer, and a 50 mm thick upper layer as depicted in Fig. 4.8b. The same AC12 mix was used for both layers.

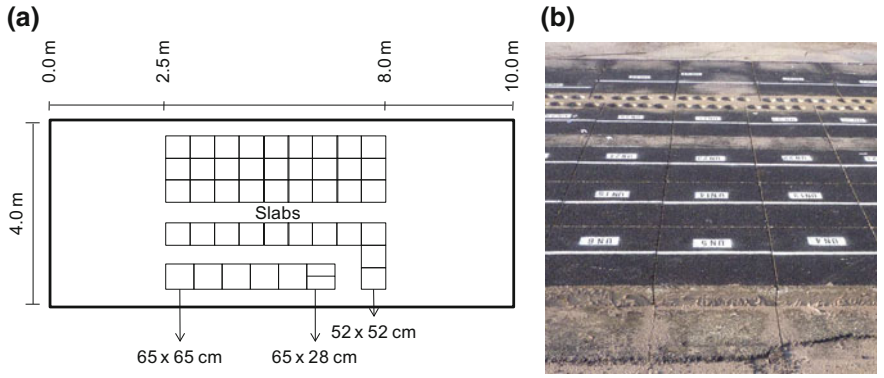

Fig. 4.7 Section A: **a** layout of each experimental sub-section; **b** detail of prepared slabs from sub-section UN

To simulate challenging situations frequently encountered in overlaying projects, areas with "simulated" cracks and critical bonding conditions (i.e. interface contamination) were prepared in the lower asphalt layer of each sub-section (Fig. 4.8c). The artificial cracks were produced with full-depth saw cuts in the lower asphalt layer, whereas a thin layer of fine sand was used to simulate interface contamination.

Each sub-section was instrumented with one earth pressure cell (EPC), four "H-shaped" ASGs and three temperature sensors (Fig. 4.9).

The EPCs were installed along the reference wheel-path (instrumentation axis), 50 mm below the interface between the asphalt surfacing and the granular base course (i.e., 140 mm below the pavement surface). This position was chosen in order to assess the load spreading ability of the reinforced asphalt surfacing, by measuring the vertical stress at the top of the unbound granular base.

The ASGs were installed along two longitudinal alignments, 300 mm apart on either side of the instrumentation axis, underneath the double-layered interface (approximately 60 mm below the pavement surface). This position was chosen in order to evaluate the horizontal strains, in both longitudinal (traffic) and transverse direction, as close as possible to the reinforcement location. In each subsection, two ASGs were also equipped with a resistance thermistor for temperature measurement.

4.3.3.1 Sensors Characteristics, Signal Conditioning and Data Acquisition System

EPC, Geokon® type 3500 (Fig. 4.10a), with a measuring range of 1.0 MPa were installed. The EPCs have a diameter of 230 mm and are equipped with a semiconductor strain gauge transducer. The sensors require an unregulated input of 7–35 VDC and produce a voltage output in the 0–5 V range. Moreover, each EPC is

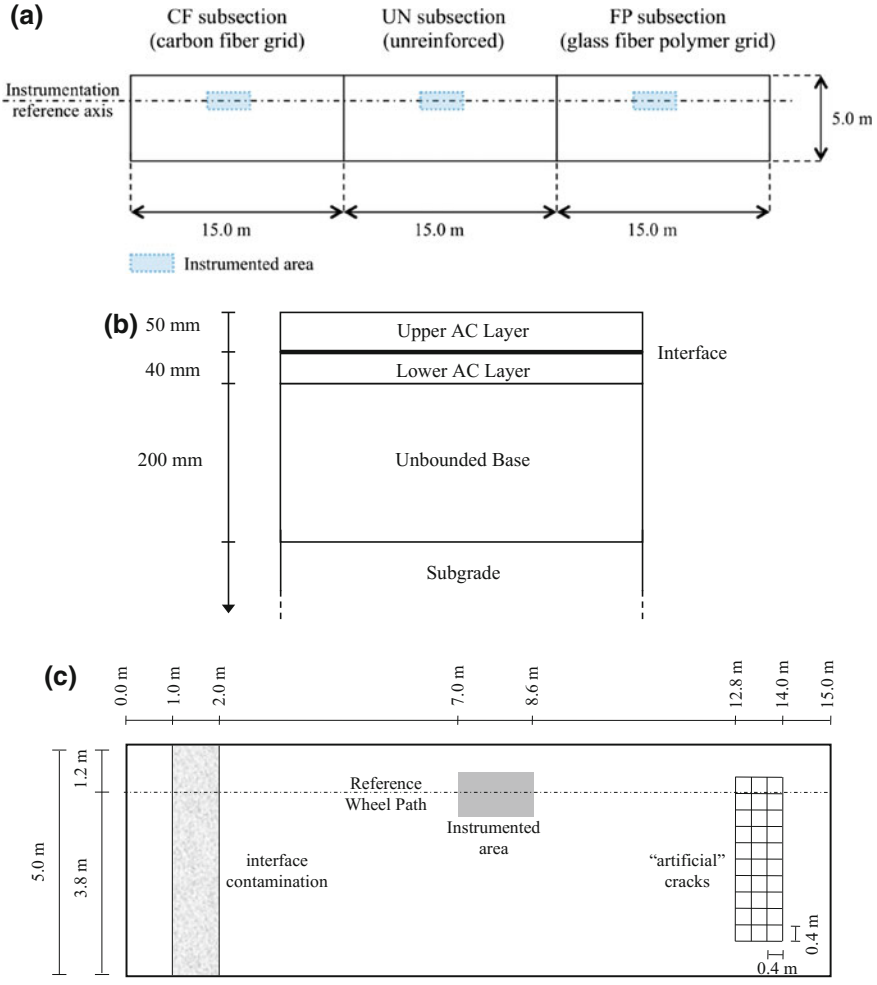

Fig. 4.8 Instrumented Section B: **a** plan view; **b** cross section; **c** interface contamination and "artificial" cracks on the lower asphalt layer

equipped with a resistance thermistor for temperature readings. The thermistor has a measuring range from −80 to 150 °C, with an accuracy of 0.5 °C. At normal operating temperatures, 0–35 °C, the thermistor output is in the 2–10 kΩ range.

ASG CTL ASG-152 (Fig. 4.10b), with a measuring base of 200 mm and a range of ±1500 με were installed. The ASGs have a full-bridge configuration that requires an excitation up to 10 VDC and produces a full scale output of 2 mV/V. In each subsection two ASGs were also equipped with a resistance thermistor for temperature readings. The thermistors have a measuring range from −80 to 150 °C, with an accuracy of 0.5 °C. At normal operating temperatures, 0–35 °C, the thermistors output is in the 16–33 kΩ range.

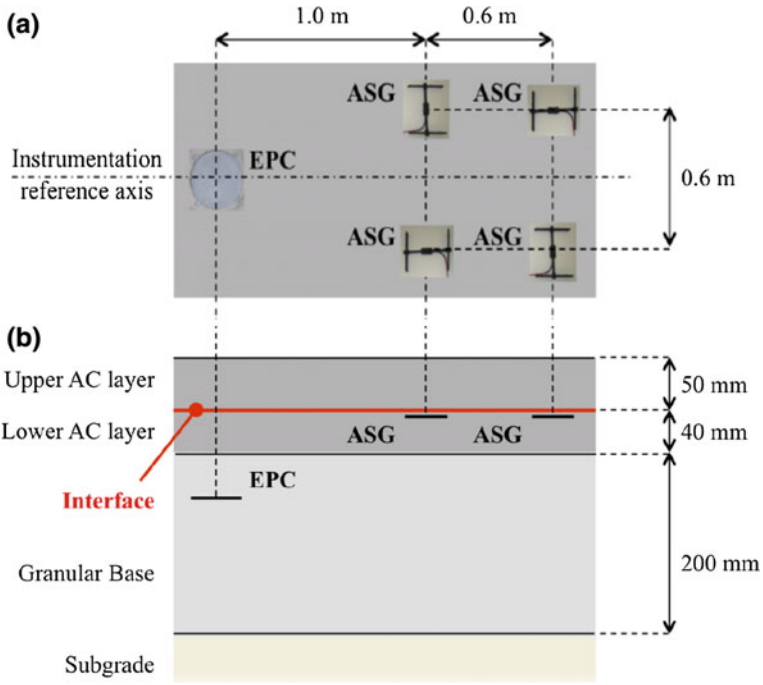

Fig. 4.9 Instrumented area: **a** plain view and **b** cross section

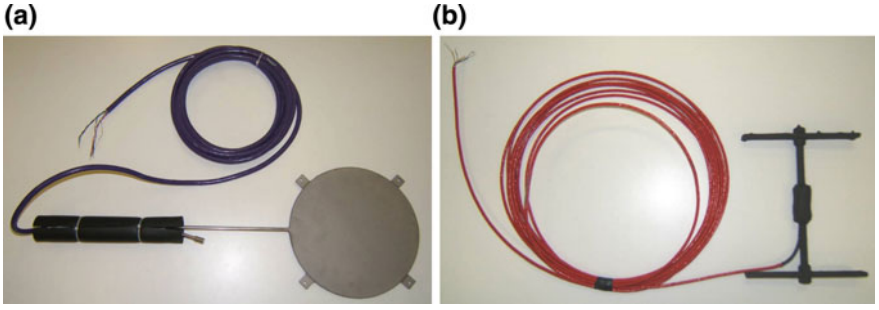

Fig. 4.10 Sensors installed in Section B: **a** Earth pressure cell and **b** "H-shaped" Asphalt strain gauges

For all instruments, signal conditioning, amplification and A/D conversion was carried out using two portable HBM Spider8 units, connected in series to a laptop computer. The HBM Catman Express software was used for data acquisition. Each Spider8 unit is equipped with four digital amplifiers modules (SR55) in 4.8 kHz carrier-frequency technology, suitable for passive transducers, like the ASG, and

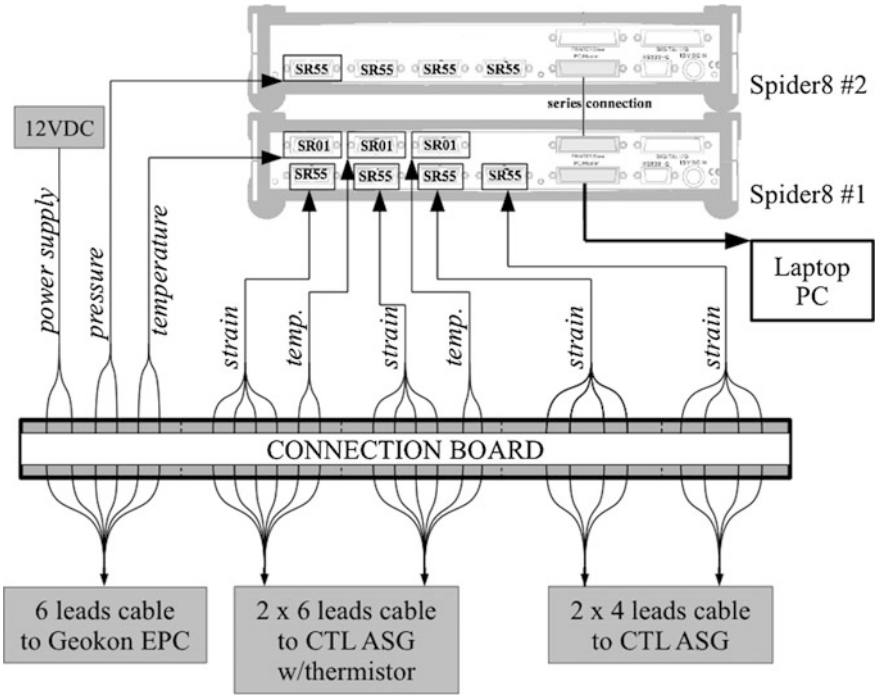

Fig. 4.11 Data acquisition system layout for each subsection

the DC voltage output of the EPC. The capability of one unit was extended with three DC modules (SR01) suitable for resistance measurements up to 4.0 kΩ.

The data acquisition system was designed to carry out independent, full-scale, field tests in each subsection. Therefore, the Spider8 units are connected to the sensors installed in each subsection in a flexible and efficient manner. For this task, a custom connection board was realized and installed at each subsection, along with custom connection cables. The main system structure in described in Fig. 4.11:

- the EPC vertical pressure readings were carried out with a SR55 amplifier module, while its excitation was provided by a separate 12 VDC power supply circuit (Spider8 units provide only 1 V excitation voltage);
- the four ASGs were connected to the SR55 modules (4-wires full-bridge circuits);
- the three thermistors (one from EPC, two from ASG) were connected to the three SR01 modules; a 4.8 kΩ shunt resistance circuit was necessary because the resistance of the thermistors at normal operating temperatures (1–50 kΩ) falls outside the measuring range of the SR01 amplifier module (0–4 kΩ).

4.3.3.2 Construction of Section B

The working activities for the construction of Section B were scheduled to be completed in six days:

- **First day**. (1) the existing asphalt layer (90 mm) was milled. (2) Plate load tests and Light Falling Weight Deflectometer (LFWD) tests were carried out on the surface of the unbounded base course (Fig. 4.12) in order to characterize the in situ existing bearing properties. (3) A shallow cavity was dug on the surface of the granular base to install the EPCs. The cavity, approximately 100 mm deep, was leveled using a 50 mm layer of clean sand (passing to the 2 mm sieve and retained to the 0.4 mm sieve) to prevent damage to EPCs from large, sharp aggregate particles. The cell and its stem were carefully placed and leveled (Fig. 4.13a) avoiding the formation of voids. The cavity was then filled with a second layer of sand (Fig. 4.13b).
- **Second day**. (1) To provide additional protection during paving operation a small amount of hot asphalt concrete was placed over the EPC and compacted using a portable Marshall hammer (Fig. 4.14). (2) The lower asphalt layer was laid and compacted. During paving operations, shallow cavities were created on the surface of the layer in order to obtain proper space for the installation of ASGs. Such cavities were obtained by means of wood plates placed at the installation points and pressed on the surface of the hot asphalt concrete lift, behind the paving machine (Fig. 4.15a). After compaction, the plates were easily removed from the warm layer and the cavities were ready to allow the sensors installation (Fig. 4.15b).
- **Third, fourth and fifth day**. (1) The ASGs were installed inside the prepared cavities using a thin layer of sand-asphalt mortar to tack the ASGs into the correct position and alignment (Fig. 4.16a). Wiring was also completed to connect the sensors to the data acquisition system. (2) Simulated cracks were

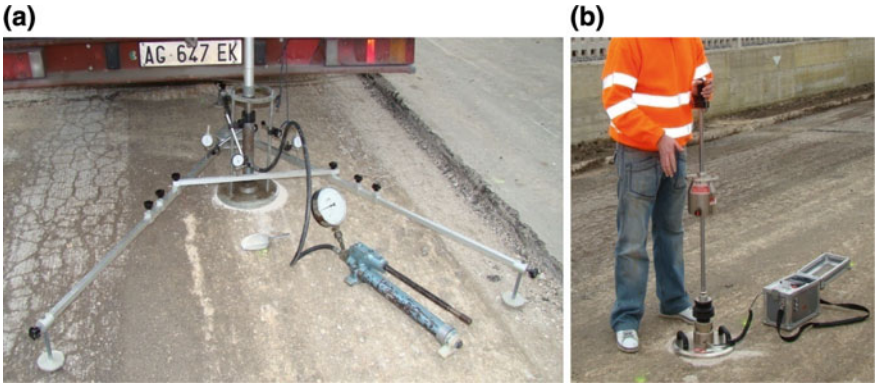

Fig. 4.12 Bearing characterization of the granular base course: **a** plate load test and **b** LFWD test

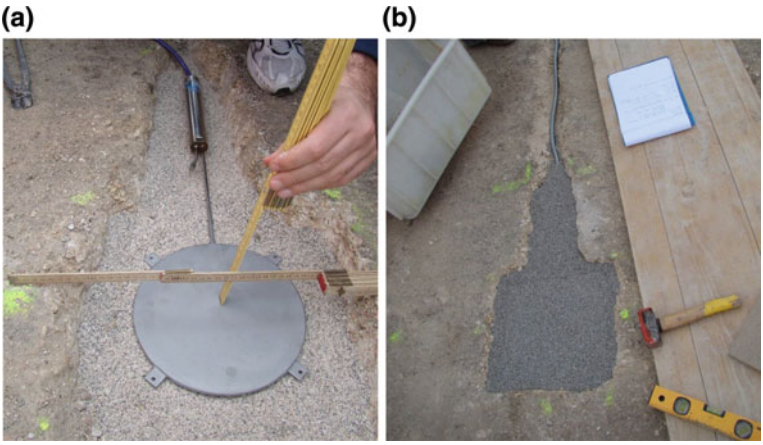

Fig. 4.13 EPC installation: **a** levelling and **b** final filling of the cavity with sand

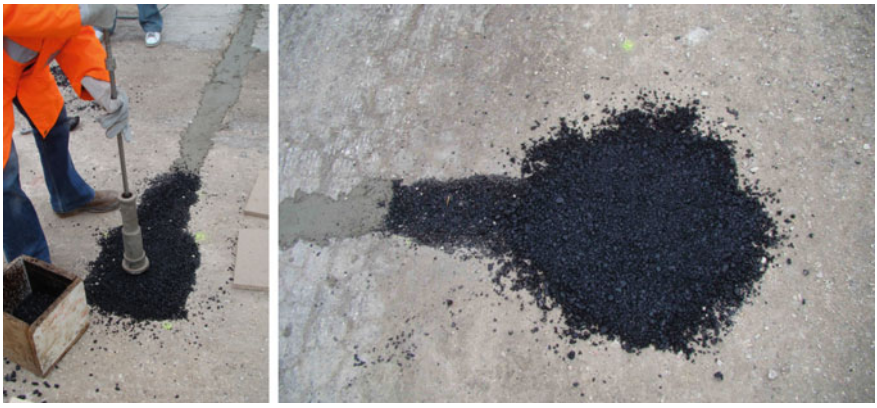

Fig. 4.14 EPC protection with hot asphalt concrete slightly compacted

prepared in the lower asphalt layer by full-depth saw cuts having a square pattern with an interaxis of 0.4 m (Fig. 4.17). The position of the simulated crack in each sub-section is shown in Fig. 4.8.

– **Sixth day**. (1) The installed ASGs were protected by filling and leveling the cavities with a small amount of asphalt concrete (Fig. 4.16b) which was obtained removing larger aggregate particles (retained on the 8 mm sieve) from the paving mix and compacted using a portable Marshall hammer. (2) The polymer-modified tack coat was applied in each sub-section with the fixed rate of the residual binder (0.25 kg/m^2), except in the area where fine sand was spread for the simulation of debonding conditions at the interface (Figs. 4.8c and 4.18). (3) Grids were installed in sections CF and FP with the same

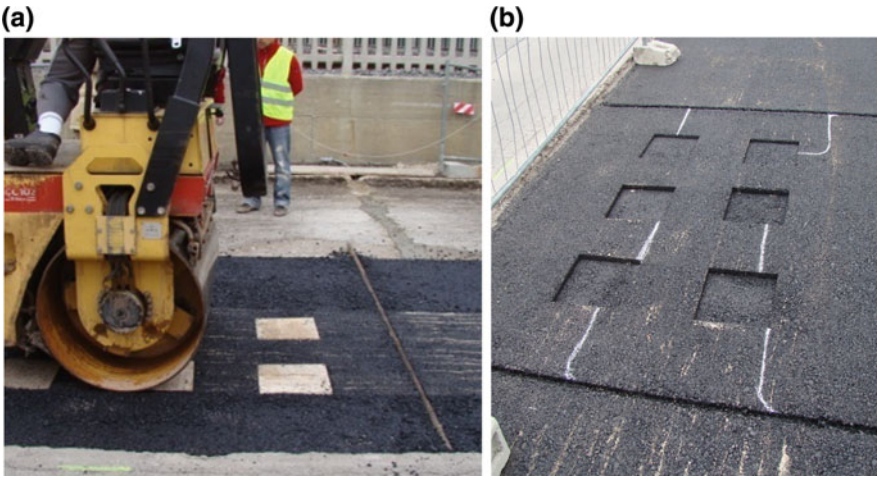

Fig. 4.15 Preparation of the shallow cavities for ASG installation: **a** placing and compaction of the wooden plates on the surface of hot asphalt concrete; **b** final aspect after plates removal

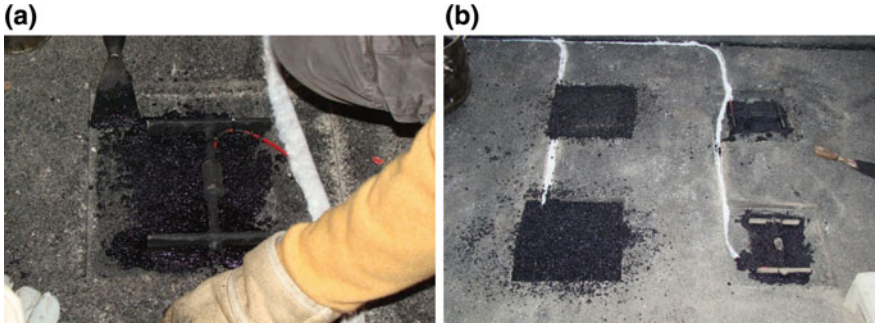

Fig. 4.16 ASG installation: **a** tacking and **b** protection

Fig. 4.17 Square pattern of artificial cracks

Fig. 4.18 Polymer modified tack coat and artificial debonding with fine sand

Fig. 4.19 Laying of the AC12 upper layer

procedure already described for the construction of section A (Sect. 4.3.2). (4) The upper AC12 layer was laid and compacted (Fig. 4.19).

A sensor survey carried out at the end of construction revealed that all pressure cells survived the working operations. Two strain gauges, both located in the FP subsection, were irreparably damaged.

4.4 Interlayer Bonding Characterization of Reinforced Asphalt Interfaces

4.4.1 Test Methods

4.4.1.1 Shear Test Devices and Procedures

Leutner test

The Leutner test (Leutner 1979; Collop et al. 2003) consists in applying a constant displacement rate across the interface of a double-layered specimen while recording the resulting shear force and the applied displacement. The testing frame (Fig. 4.20) is installed into an ordinary Marshall equipment and allows testing 100 mm or 150 mm-diameter specimens, either taken from a pavement structure or prepared in the laboratory. The standard shear displacement rate is 50.8 mm/min. The test output is a shear force-shear displacement curve, that allows the interlayer shear strength (ISS) to be obtained, corresponding to the failure conditions.

Layer-Parallel Direct Shear (LPDS) test

The Layer-Parallel Direct Shear (Raab and Partl 2009) is an Empa modified version of the Leutner equipment, being more accurate in the clamping mechanism. It allows pure direct shear testing of multi-layered cylindrical specimens with a nominal diameter of 150 mm. One part of the pavement core is laid on a circular u-bearing and held with a well-defined pressure of 0.5 MPa by a pneumatic clamping system. The other part, the specimen head, remains unsuspended. Shear

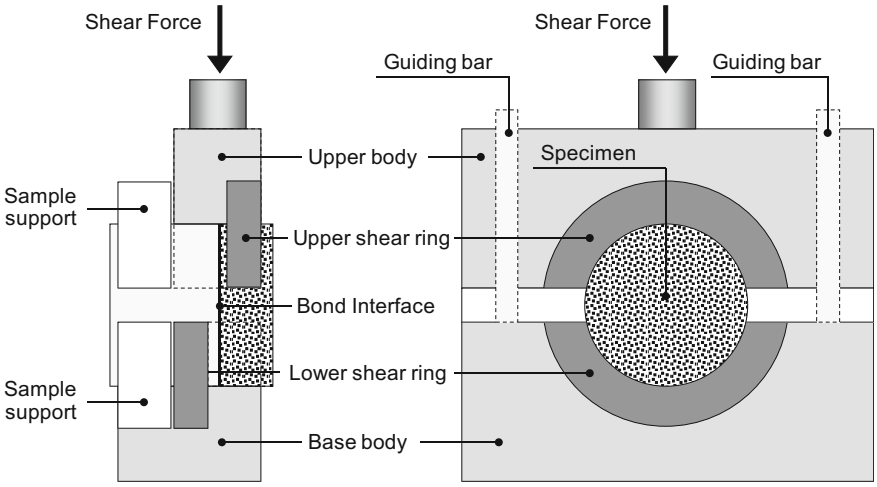

Fig. 4.20 Scheme of the Leutner device

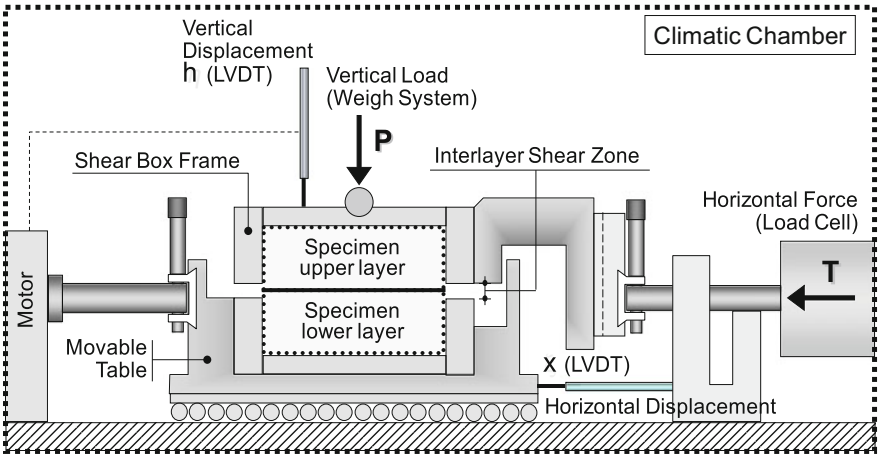

Fig. 4.21 Scheme of the ASTRA device

load is induced to the specimen head by a semicircular shear yoke with a displacement rate of 50.8 mm/min, thus producing fracture along the pre-defined shear plane. The gap width between the shearing rings is 2.5 mm.

Ancona Shear Testing Research and Analysis (ASTRA) test.

The Ancona Shear Testing Research and Analysis device is similar to the direct shear box used in soil testing (Fig. 4.21). A double-layered specimen, with a nominal diameter of 100 mm, is installed in two half-boxes separated by an unconfined interlayer shear zone (Canestrari et al. 2012b). During the test, a constant shear displacement rate of 2.5 mm/min (standard conditions) occurs while a constant vertical stress (σ_n), perpendicular to the interface plane, can be applied using a weight system. The test returns a data-set where the interlayer shear stress (τ), the horizontal and the vertical displacements are reported as a function of time, allowing the calculation of the interlayer shear strength ISS (τ_{peak}). The whole apparatus is located in a climatic chamber with temperature control.

Sapienza Direct Shear Test Machine (SDSTM)

The Sapienza Direct Shear Testing Machine is able to test double-layered cylindrical specimens with a nominal diameter of 100 mm (Tozzo et al. 2016). The specimen is held in two moulds with a gap between the two restraints of 10 mm (Fig. 4.22). The specimen interface is placed in the middle, leaving 5 mm from the edge of each mould. A loading machine applies a constant shear displacement rate of 2.5 mm/min (in standard conditions) on one half of the specimen while the other half is fixed, allowing the measurement of the shear load. A normal load can also be applied. The device is equipped with LVDT for the interface displacement measurement. A shear force-shear displacement curve is obtained in order to determine the ISS.

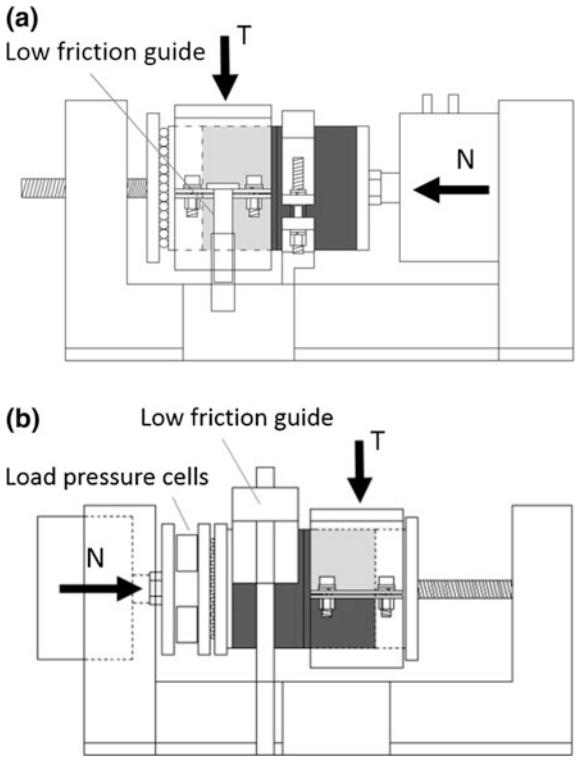

Fig. 4.22 Scheme of SDSTM device: **a** inhibited dilatancy; **b** allowed dilatancy

In this research project, the SDSTM device was assembled in two configurations: inhibited (Fig. 4.22a) and allowed (Fig. 4.22b) dilatancy.

Shear Tester (ST)

The Shear Tester (Fig. 4.23) is a device that allows testing double-layered specimens in shear configuration, through a MTS servo-hydraulic 100 kN loading frame (Gajewski and Mirski 2012). The apparatus allows fixing the specimen and applying the shear load in correspondence with the interface plane, parallel to the basis of the specimen. Additionally, a normal load, perpendicular to the specimen interface, can be applied through a pneumatic standalone controller. Tests were performed on 150-mm-diameter specimens, applying a constant displacement rate of 50.8 mm/min. The Shear Tester returns a shear force-shear displacement curve that can be used to determine the ISS. The apparatus is placed in a climatic chamber in order to perform controlled temperature tests.

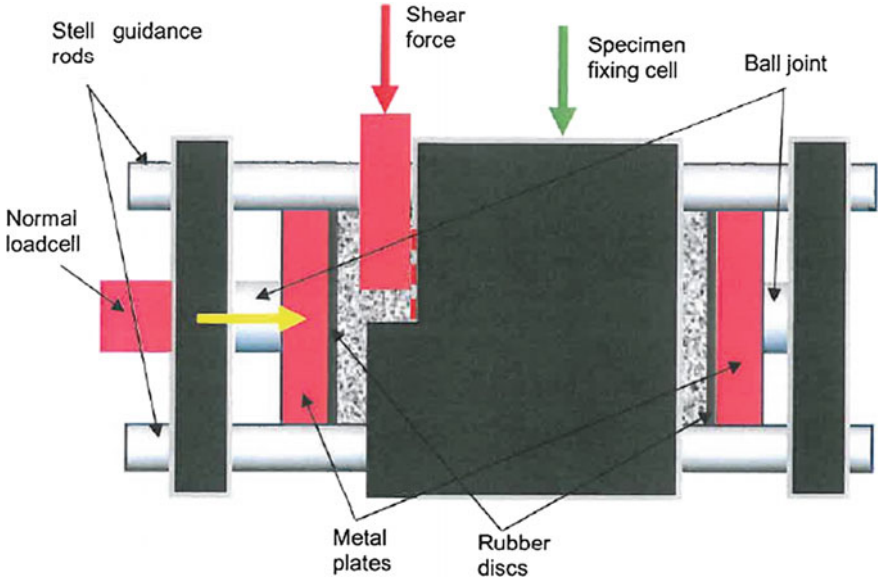

Fig. 4.23 Scheme of the Shear Tester

4.4.1.2 Pull-Off Test Device and Procedure

The pull off test was carried out according to the German testing specification ZTV-SIB 90 but a test disc diameter of 100 mm was used. The test was conducted with a pre-force of 100 N, a test speed of 300 N/s and a constant test temperature of 20 °C.

In this investigation, a modified laboratory method for core testing was used. In a first step the double-layered core was glued on a concrete plate and the steel test disc, with a diameter of 100 mm and a thickness of 60 mm, was fixed on top of the core (Fig. 4.24a). This system was placed inside a steel ring and an aluminum plate with a hole in the middle was located on the steel ring. The pull-off device is placed on top of the steel ring and connected to the test disc (Fig. 4.24b).

4.4.1.3 Experimental Program

This part of the RILEM research project focuses on the evaluation of interlayer bonding characteristics of reinforced and unreinforced double-layered bituminous systems. To achieve this goal, three different interlayer systems (UN, CF and FP) were investigated by performing shear tests and pull-off tests in accordance with the experimental program shown in Tables 4.4 and 4.5, respectively.

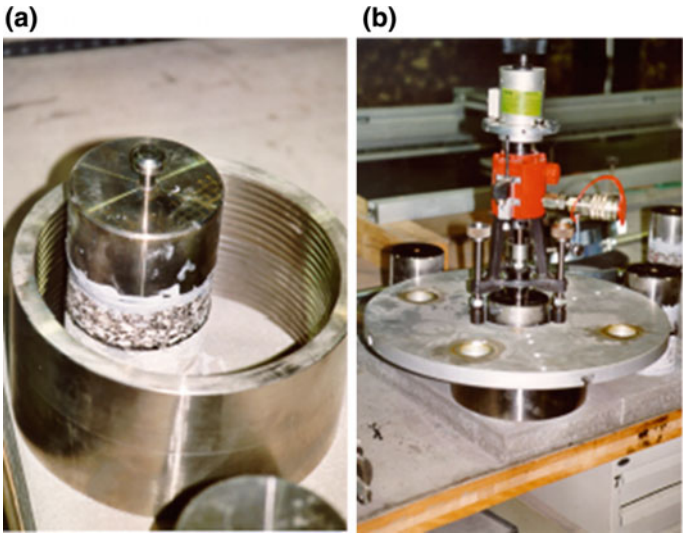

Fig. 4.24 Pull-off test: **a** core fixed on the concrete plate; **b** laboratory testing method

Table 4.4 Shear test program for each interlayer system (UN, CF, FP)

Lab	Test period	Specimen diameter, D (mm)	Test speed, v (mm/min)	Test temperature, T (°C)	Normal stress, σ_{nn} (MPa)	Number of replicatesfor each σ_n
Empa	Aug 2011	150	50.8	10	0.00	7
				20		7
				30		7
				40		6
IBDiM	Oct 2012	150	50.8	10	0.00; 0.15	1
				20		1
				30		1
UNIRM	March 2013	100	2.5	20	0.00; 0.20; 0.40	3
UNIBO	March 2013	150	50.8	20	0.00	9
UNIVPM	Jan 2010	100	2.5	10	0.00; 0.20; 0.40	4
				20		4
				30		4

Table 4.5 Pull-off test program for each interlayer system (UN, CF, FP)—August 2011

Laboratory	Specimen diameter, D (Mm)	Test speed, v (N/s)	Test temperature, T (°C)	Pre-force (N)	Number of replicates
Empa	100	300	20	100	7

Five laboratories participated in this part of the project:

- Swiss Federal Laboratories for Materials Science and Technology (Empa), Dübendorf, Switzerland
- Road and Bridge Research Institute (IBDiM), Warsaw, Poland
- Sapienza, Università di Roma (UNIRM), Italy
- Alma Mater Studiorum, Università di Bologna (UNIBO), Italy
- Università Politecnica delle Marche, Ancona (UNIVPM), Italy.

As far as the interlayer shear investigation is concerned (Table 4.4), depending on the test device and protocol adopted, each laboratory considered different test conditions in terms of specimen diameter, test speed, test temperature, normal stress applied to the interface and number of replicates. When several normal stress levels σ_n were applied, the assessment of the interface failure properties was obtained, according to the following equation:

$$\tau_{peak} = c_0 + \sigma_n \cdot \tan \Phi_p \tag{4.1}$$

where c_0 is the pure shear strength and Φ_p is the peak friction angle.

Pull-off tests allowed the localization of the failure plane (in correspondence of the interface or within the layers) and the determination of the pull-off strength. Shear tests described in Table 4.4 showed an inconsistency between UNIRM and UNIVPM laboratory results (Sect. 4.4.2.1). Therefore, tests were repeated according to the program shown in Table 4.6. In this case, UNIRM used a modified device (Fig. 4.22b).

Table 4.6 Shear test program for each interlayer system (UN, CF, FP)—December 2014

Laboratory	Specimen diameter, D (mm)	Test speed, v (mm/min)	Test temperature, T (°C)	Normal stress, σ_n (MPa)	Number of replicates for each σ_n
UNIRM[a]	100	2.5	20	0.00; 0.20; 0.40	3
UNIVPM	100	2.5	20	0.00; 0.20; 0.40	4

[a]Modified device (Fig. 4.22b)

4.4.2 Results and Analysis

4.4.2.1 Shear Tests

Laboratories performing tests at different temperatures allowed the investigation of the influence of temperature on ISS. Figure 4.25 shows that, for each normal stress, ISS decreased with increasing temperature for both reinforced and unreinforced interlayer systems, for all the investigated shear test devices.

Moreover, Fig. 4.25 shows that UN and CF systems provided very similar results, even if UN system guaranteed, in general, slightly higher interlayer bonding

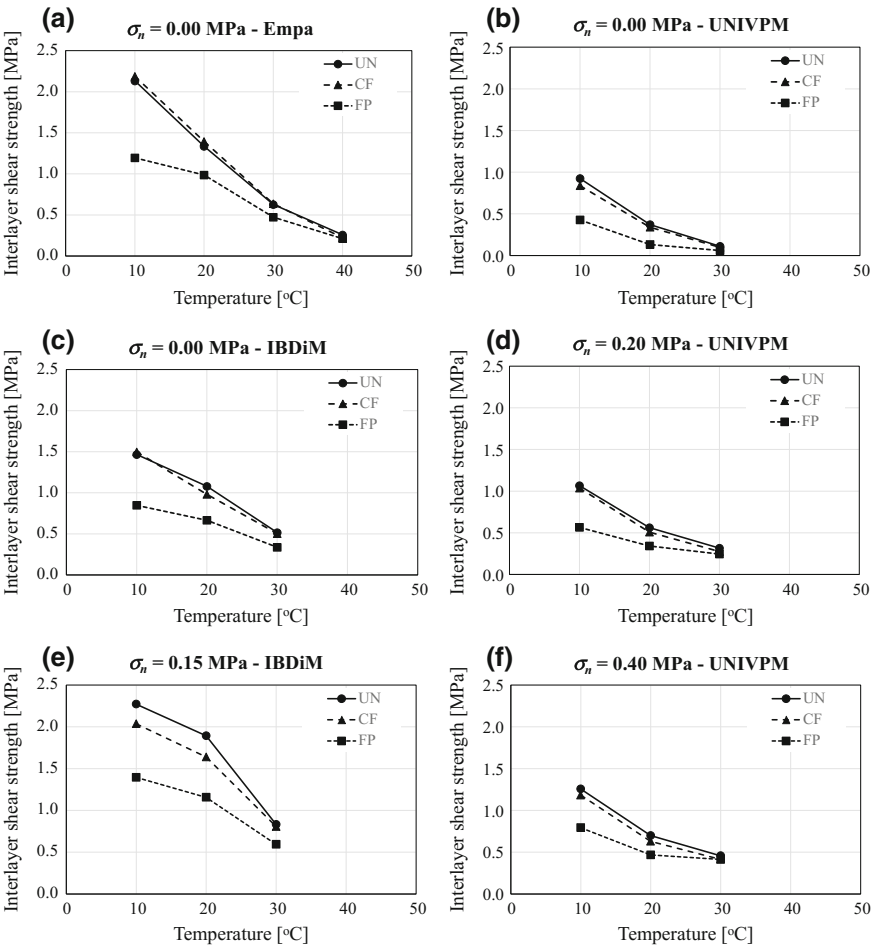

Fig. 4.25 Interlayer shear strength versus temperature for different laboratories and different test conditions

with respect to CF system. Differently, FP grid provided lower ISS with respect to the other two interlayer systems. This is probably due to the thickness and stiffness of FP grid that inhibit the achievement of an optimal compaction of the upper asphalt concrete layer in the interface zone, reducing aggregate interlock (Santagata et al. 2008).

In order to compare results obtained with different test devices, the influence of test speed on ISS should also be evaluated along with the influence of test temperature. To this end, for each interlayer system, Empa and UNIVPM results in the simple shear configuration (σ_n = 0.00 MPa) were represented in the same plot (Fig. 4.26). As it can be observed, higher test speeds resulted in higher values of ISS. The combined influence of speed and temperature on ISS was analyzed using the time-temperature superposition principle (TTSP), according to the approach of Canestrari et al. (2016). In this case, EMPA data obtained at v = 50.8 mm/min were superposed to UNIVPM data obtained at v = 2.5 mm/min (Fig. 4.27). The resulting shift factors ΔT were equal to −15.5, −16 and −22 °C for UN, CF and FP interlayer system, respectively. Following such a superposition, a unique curve of ISS versus temperature is obtained. In a semi-logarithmic plane such a curve was fitted using the following model (Canestrari et al. 2012b):

$$\log \tau_{peak} = a \times T + b \tag{4.2}$$

where a and b are regression parameters which represent the slope and the intercept of the linear regression, respectively (Fig. 4.28). The slopes obtained for UN, CF and FP interlayer systems were equal to −0.036, −0.037 and −0.032 respectively. This suggests that the dependence of ISS on temperature was related only to the thermal sensitivity of the asphalt concrete mixtures and was not influenced by the interlayer system. On the contrary, interlayer system strongly affected ISS, as shown by the intercept values (b = 1.77, 1.74 and 0.70 MPa, respectively).

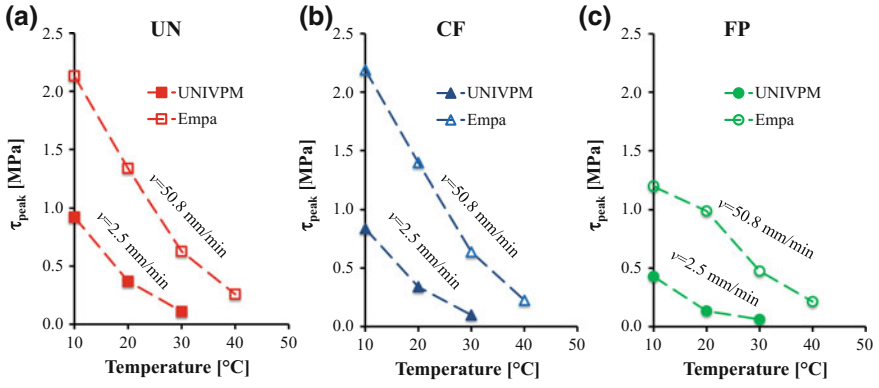

Fig. 4.26 Empa and UNIVPM test results for σ_n = 0.00 MPa: **a** UN interface; **b** CF interface; **c** FP interface

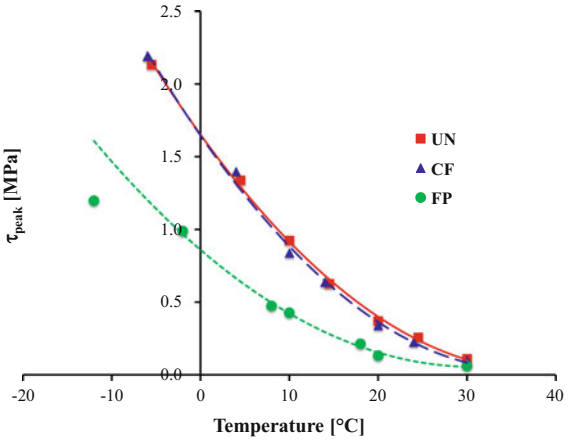

Fig. 4.27 Empa data shifted towards UNIVPM data for σ_n = 0.00 MPa

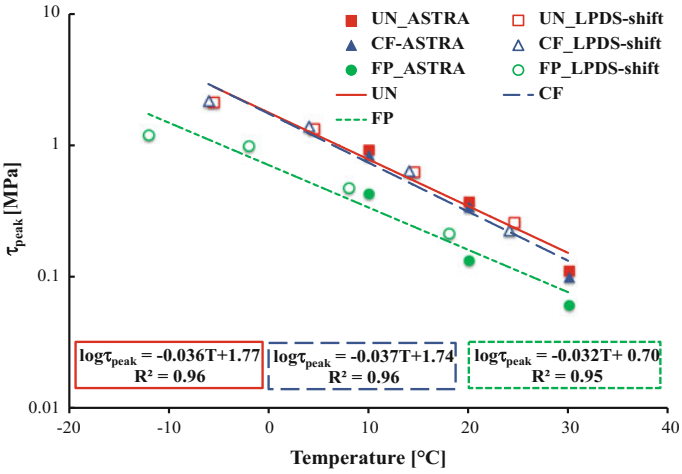

Fig. 4.28 Use of TTSP in interlayer shear strength measurements

Laboratories performing tests at different normal stress levels allowed obtaining the assessment of the interface failure properties for the three interlayer systems. Grid-reinforced systems provided lower ISS with respect to the unreinforced one (Fig. 4.29). Similarly to Fig. 4.25, differences between CF and UN systems were not marked, whereas FP system provided lower ISS with respect to CF, due to its higher thickness and stiffness.

The comparison between ISS envelopes obtained by different laboratories is shown in Fig. 4.29. As it can be observed, IBDiM tests provided higher ISS values with respect to UNIRM and UNIVPM laboratories, mainly because of its higher test speed (50.8 against 2.5 mm/min). Analogously, UNIRM and UNIVPM devices

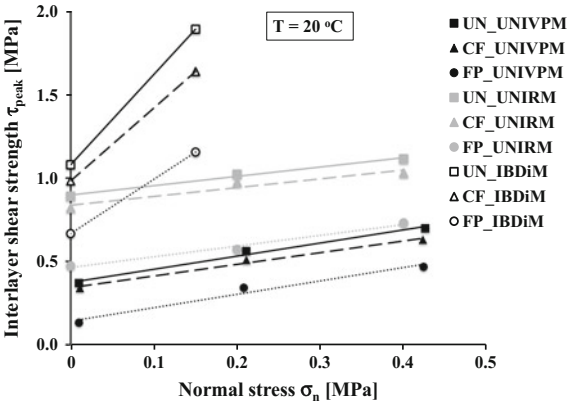

Fig. 4.29 Failure properties of different interlayer systems and for different laboratories

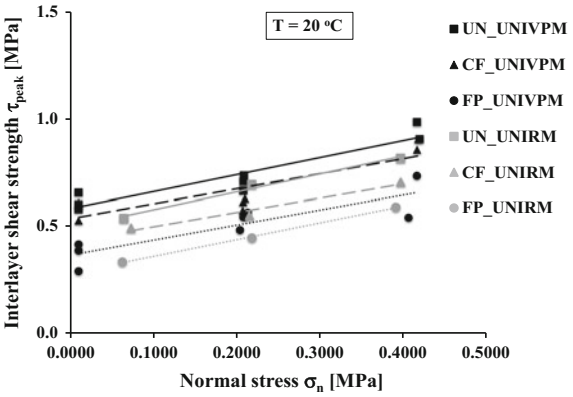

Fig. 4.30 Comparison between UNIRM and UNIVPM results

should provide similar results, because tests are performed at the same speed (v = 2.5 mm/min) on specimen with the same diameter (D = 100 mm). However, Fig. 4.29 shows that the two laboratories achieved very different interlayer shear strengths for each interlayer system. This can be attributed to UNIRM equipment (Fig. 4.22a) that inhibits dilatancy, causing an overestimation of ISS. For this reason, UNIRM equipment was modified allowing dilatancy (Fig. 4.22b) and shear tests at 20 °C were repeated in December 2014 (Table 4.6). Figure 4.30 shows that, in this case, the difference between results provided by the two devices can be considered negligible for each interlayer system, confirming the validity of UNIRM equipment modification and the necessity to allow specimen dilatancy. Moreover, Fig. 4.30 further confirms the ranking between the three interlayer systems: FP grid produced a significant debonding effect with respect to the unreinforced system, whereas CF grid and UN interface provided similar ISS values.

Finally, UNIVPM results allowed studying the effect of aging on ISS. Figure 4.31 shows that the peak friction angles for each interlayer system remained almost equal even after four years, indicating that aging produced the same effect at

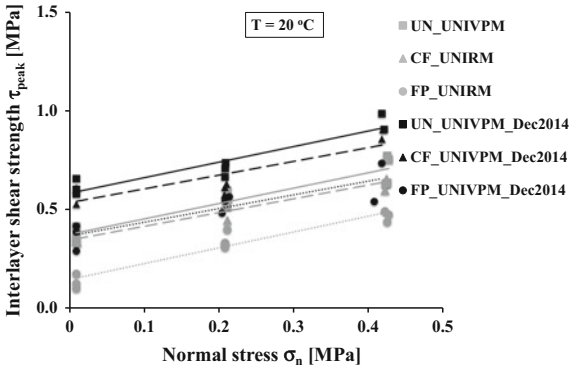

Fig. 4.31 Effect of specimen curing time on UNIVPM results

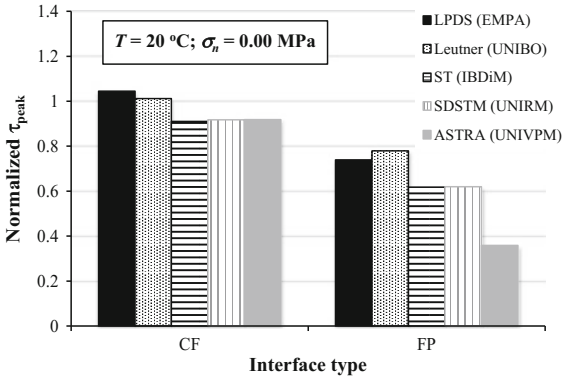

Fig. 4.32 Comparison between CF and FP interfaces

each normal stress. As expected, in absolute terms, aging of asphalt concrete resulted in an ISS increase.

The normalization of ISS of CF and FP interlayer systems with respect to ISS of UN system, is shown in Fig. 4.32, for all the investigated shear test devices, at T = 20 °C and σ_n = 0.0 MPa. As it can be observed, different devices provided similar normalized τ_{peak} values for the CF interlayer system whereas more scattered results were observed for the FP system. This is probably due to the mesh dimension (33 mm^2) of the FP grid, which results in a different number of strands in the single specimen, influencing the corresponding ISS.

For each device, shear test results were subjected to a one-way analysis of variance (one-way ANOVA) at 95% confidence level, in order to check the influence of the interlayer system (UN, CF and FP) on the ISS.

Results of ANOVA for all participating laboratories are summarized in Table 4.7, where the relevant p-value is shown for each test condition. In order to allow an easier interpretation of ANOVA results, the p-values that represent non-significant differences between two interlayer systems (>0.05) are reported in

Table 4.7 ANOVA: influence of interlayer system (UN, CF, FP) on interlayer shear strength

Lab	Test period	σ_n (MPa)	T (°C)	*p*-value	*p*-value	*p*-value
				UN versus CF	UN versus FP	CF versus FP
Empa	Aug 2011	0.00	10	**0.688**	2.6E−5	9.1E−6
			20	**0.256**	4.1E−3	1.2E−3
			30	**0.634**	1.4E−2	9.4E−3
			40	2.3E−2	**0.095**	**0.627**
UNIRM	March 2013	0.00	20	**0.284**	1.1E−3	4.8E−4
		0.20		**0.380**	1.2E−3	1.6E−3
		0.40		**0.175**	4.5E−3	5.9E−3
UNIBO	March 2013	0.00	20	**0.705**	3.0E−6	6.0E−6
UNIVPM	Jan 2010	0.00	10	**0.076**	2.8E−4	1.7E−4
			20	**0.258**	1.6E−3	7.3E−4
			30	**0.394**	2.9E−3	1.5E−2
		0.20	10	**0.641**	5.3E−5	1.2E−4
			20	**0.161**	6.4E−4	1.4E−3
			30	3.2E-2	2.3E−3	1.3E−2
		0.40	10	**0.216**	1.9E−4	3.3E−4
			20	**0.202**	4.6E−2	2.3E−3
			30	**0.088**	**0.120**	**0.986**
UNIRM[a]	Dec 2014	0.00	20	**0.284**	**0.058**	**0.107**
		0.20		**0.061**	3.8E−2	**0.051**
		0.40		**0.064**	2.5E−2	**0.212**
UNIVPM	Dec 2014	0.00	20	**0.409**	4.9E−3	9.5E−3
		0.20		2.1E−2	5.7E−3	**0.063**
		0.40		**0.304**	**0.098**	**0.135**

[a]Modified device (Fig. 4.22b)

bold in Table 4.7. ANOVA was not performed on IBDiM results because of the lack of replicates.

The analysis of variance shows that there is no statistical difference between UN and CF results in all laboratories and for almost all test conditions investigated. This suggests that CF grid does not significantly influence interlayer shear properties of double-layered systems. On the other hand, the ISS difference between FP system and UN or CF systems was found to be statistically significant.

As far as tests carried out in December 2014 are concerned, the ANOVA suggests that the difference between CF and FP systems is not statistically significant.

4.4.2.2 Pull-off Tests

Table 4.8 presents results in terms of pull-off strength and location of the failure plane for each specimen, whereas Fig. 4.33 depicts the mean values of pull-off strength (7 specimens) for each interlayer system.

For UN and FP interlayer systems, the failure always took place at the interface (Fig. 4.34a), whereas the CF system provided, in some cases, failure in the lower or in the upper asphalt concrete layer (Fig. 4.34b), demonstrating a good bonding at the interface.

The best adhesion properties (highest pull-off strength) can be found for UN and CF interlayer systems that also showed nearly identical standard deviations (about 0.02 N/mm^2). The mean value of the pull-off strength (=0.3 N/mm^2) for FP interlayer system is clearly lower with respect to the other two systems (standard deviations = 0.1 N/mm^2), analogously to shear test results.

Table 4.8 Pull-off results for each interlayer system (UN, CF, FP) and location of failure

Interlayer system	Pull-off force (kN)	Pull-off strength, σ_n (N/mm^2)	Location of failure
UN	5.382	0.68	Interface
	5.567	0.71	Interface
	5.852	0.75	Interface
	5.407	0.69	Interface
	5.600	0.70	Interface
	5.266	0.67	Interface
	5.729	0.73	Interface
CF	5.805	0.74	Interface
	5.415	0.69	Bottom layer
	6.048	0.77	Interface
	5.792	0.74	Interface
	5.488	0.70	Bottom layer
	5.845	0.74	Surface layer
	5.277	0.67	Interface
FP	2.556	0.32	Interface
	2.467	0.31	Interface
	1.964	0.25	Interface
	2.517	0.32	Interface
	2.137	0.27	Interface
	1.980	0.25	Interface
	2.360	0.30	Interface

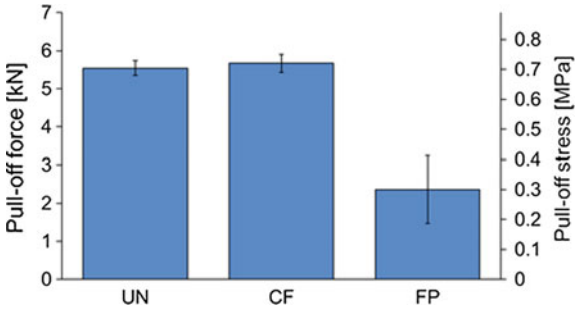

Fig. 4.33 Pull-off test results: mean values including standard deviation

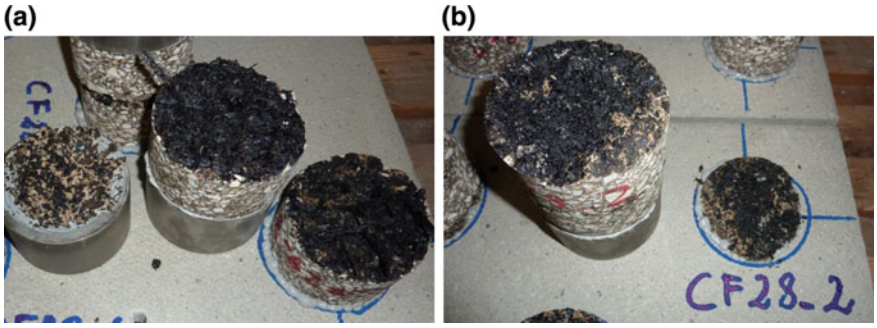

Fig. 4.34 Type of pull-off test failure: **a** at the interface; **b** in the surface layer

4.4.3 Summary

Shear tests and pull-off tests were carried out by six laboratories in order to characterize the interlayer bonding behavior of both reinforced and unreinforced asphalt interfaces.

Regardless of the shear testing device employed by the participating laboratories, the experimental results showed that:

- the installation of a grid reinforcement at the interface between asphalt layers resulted in a decrease of the ISS with respect to the unreinforced interface;
- an ISS reduction was observed for all the investigated parameters (temperature, speed and vertical stress), even if results suggested that at higher temperatures the ISS reduction tends to vanish;
- ISS reduction was statistically significant only for the FP grid, which is characterized by higher thickness and torsional stiffness with respect to the CF grid;
- temperature and test speed had a clear effect on the measured ISS values. Specifically ISS decreased with increasing temperature and decreasing test speed;

- as long as tests without the application of vertical stress are considered, ISS values obtained at higher test speed and lower temperature can be superposed to ISS values obtained at lower test speed and higher temperature;
- superposition of temperature and speed effects allowed a direct comparison between ISS values measured with different devices (ASTRA and LPDS);
- binder aging led to an increase of ISS, especially in terms of pure shear component, i.e. without vertical stress, for both reinforced and unreinforced interfaces.

The clear debonding effect produced by the installation of the FP grid was also observed in the pull-off tests.

The lower ISS values observed for FP double-layered specimens with respect to UN and CF systems can be explained by the higher thickness and stiffness of the FP grid, which probably hindered the achievement of an optimal compaction of the upper AC layer in the interface proximity, thus reducing the interlocking between the two layers in contact.

4.5 Mechanical Characterization of Reinforced Asphalt Systems

4.5.1 Test Methods

4.5.1.1 Bending Tests

Cyclic bending tests and monotonic bending tests were carried out by two laboratories, UNIVPM and UNIBO. The test configurations are depicted in Fig. 4.35, whereas specimen dimensions and test parameters are summarized in Table 4.9.

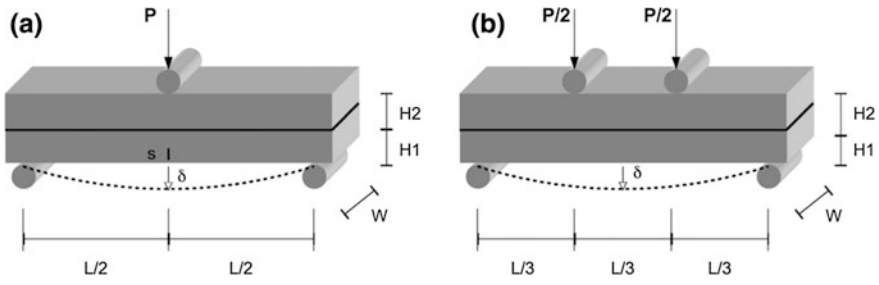

Fig. 4.35 Configuration of bending tests: **a** three point bending (3PB); **b** four point bending (4PB)

Table 4.9 Summary of 3PB test configuration

Laboratory	Specimen dimensions (mm)					Temperature (°C)	Type	Speed or frequency
	L	W	H1	H2	S[a]			
UNIVPM	240	90	30	45	–	20	4PB-cyclic	1 Hz
						20	3PB-monotonic	51 mm/min
UNIBO	400	100	50	50	20	10	3PB-cyclic	0.5 Hz
						10	3PB-monotonic	5 mm/min

[a]Notch depth

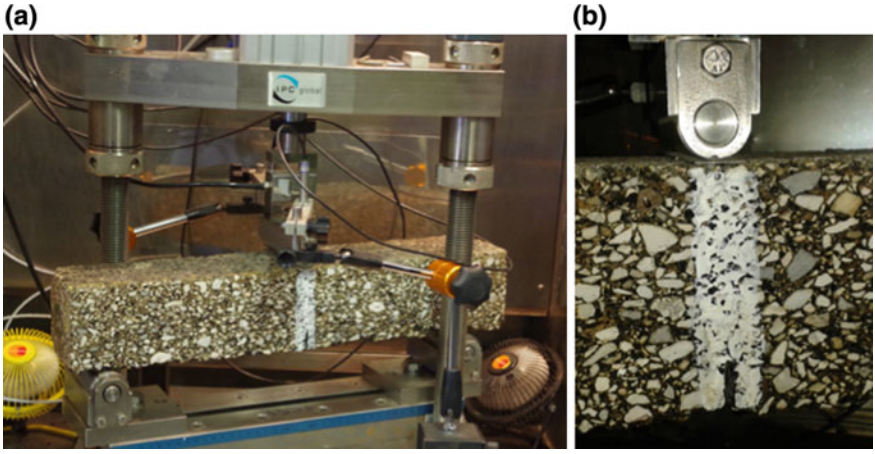

Fig. 4.36 Cyclic 3PB test carried out by UNIBO: **a** test configuration; **b** notched beam

Cyclic tests

Cyclic tests were carried out in both four-point bending (4PB—UNIVPM) and three-point bending (3PB—UNIBO) configuration. The 4PB devices were basically composed by a temperature controlled chamber, a loading frame and a hydraulic actuator able to apply haversine loading waves. The vertical displacement at the mid-span of the beam was measured through a strain gauge based extensometer (UNIVPM) and an LVDT displacement transducer (UNIBO) (Fig. 4.36).

In tests carried out at UNIVPM a haversine load with a frequency of 1 Hz and three amplitudes (P_0 = 1.0, 1.5 and 2.0 kN) was applied. The maximum duration of each test was 10 h, corresponding to a maximum of 36,000 load cycles. In tests carried out at UNIBO a haversine load with a frequency of 0.5 Hz and two amplitudes (P_0 = 0.85 and, 1.5 kN) was applied until failure. Two replicate

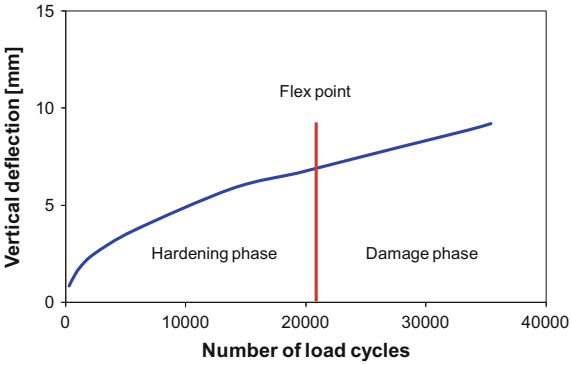

Fig. 4.37 Analysis of repeated loading 4PB test results

specimens were tested for each interface type and loading level by both UNIVPM and UNIBO.

The mechanical behavior of double-layered systems in the cyclic tests was analyzed in terms of permanent deformation and damage associated to crack propagation.

Permanent deformation was measured by means of the accumulated mid-span deflection at each load cycle. For the tests carried out at UNIVPM, since reinforced beams may not reach a complete collapse during the test, a failure criterion to compare different interface types (Virgili et al. 2009) was defined by the number of load cycles (or time) required to reach the flex point in the permanent deformation curve (Fig. 4.37).

Damage occurring to the tested specimen was evaluated considering the reduction of the apparent stiffness modulus E_{app} defined as:

$$E_{app} = \frac{\sigma_{app}}{\varepsilon_{r,app}} \tag{4.3}$$

where σ_{app} and $\varepsilon_{r,app}$ are the apparent values of stress and recovered strain, respectively. From the linear elastic beam theory the apparent stiffness modulus can be calculated as:

$$E_{app} = \frac{P_0}{\delta_{r,0}} \cdot \frac{L^3(3L^2 - 4a^2)}{12 \cdot W \cdot H^3} \tag{4.4}$$

where P_0 is the amplitude of the applied haversine load, $\delta_{r,0}$ is the amplitude of the periodic recovered beam deflection, $H = H_1 + H_2$ is the beam height, L is the beam span, W is the beam width and $a = L/3$ is the distance between the beam support and the point of load application (Fig. 4.35b). The calculated stiffness modulus is obviously an *apparent value* for two reasons: first, the span of the beams is about three times their height and therefore the application of the beam theory is not rigorous; second, Eq. (4.4) is applied also in the post-cracking phase of the tests.

Monotonic tests

Monotonic tests were carried out in three-point bending (3PB) configuration (Fig. 4.35a). At UNIVPM tests were carried out at 20 °C with a constant deflection rate of 50.8 mm/min, whereas at UNIBO tests were carried out at 10 °C with a constant deflection rate of 5.0 mm/min. In both laboratories, load and beam deflection at the mid-span of the specimen were measured through a load cell and a displacement transducer, respectively. Five replicate specimens were tested for each interface type by both UNIVPM and UNIBO.

The mechanical behavior of reinforced specimens in the monotonic tests was analyzed in terms of maximum pre-cracking flexural load P_F and deflection δ_F and flexural toughness, i.e. the area under the load-deflection curve up to a fixed value of the vertical displacement. Toughness provides an indication of the post-peak deformation behavior and can be used to evaluate the ability of the reinforced system to absorb energy in the crack propagation phase (Lee 2008; Pasquini et al. 2013). In order to compare the results obtained by the two laboratories, dimensionless toughness indices were also calculated. Such indices, originally developed to describe the fracture behavior of fiber reinforced concrete (FRC) (Gopalaratnam and Gettu 1995) are defined as the ratio of the area under the load deflection curve up to a specific deflection limit, to the area of the same curve up to the "first-crack" deflection (δ_F). In particular, the ASTM C 1018 standard defines the three toughness indices I5, I10 and I20, which are computed at deflection limits of $3\delta_F$, $5.5\delta_F$ and $10.5\delta_F$, respectively (Fig. 4.38). The rationale behind these indices is that they depend only on the energy absorption capability of the structural element regardless of other geometrical variables associated with the specimen and testing arrangement. In addition, for a linear elastic behavior up to the first crack, and perfectly plastic behavior thereafter, the values I5 = 5.0, I10 = 10.0 and I20 = 20.0 are obtained.

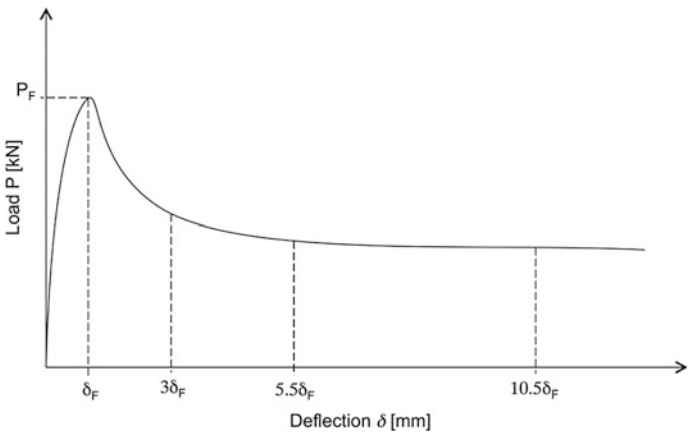

Fig. 4.38 Analysis of 3PB test results

4.5.1.2 Modified Wheel Tracking Test

The modified wheel tracking test, performed at the University of Wuppertal, is similar to the wheel tracking test described in EN 12697-22, where the configuration with small wheel is considered.

Differences with the standard test are listed below:

- double-layered samples were tested;
- specimens were sawn orthogonally to the driving direction in order to get a predetermined breaking zone for reflective cracking;
- specimens were bedded on a soft underlay.

The test allows the evaluation of the rut formed by repeated passes of a loaded wheel at constant temperature. In this research, three replicate specimens were tested at 40 °C for each interlayer system.

4.5.1.3 Tensile-Bending Test

The tensile-bending test (Vecoven 1989) allows the investigation of reflective cracking propagation rate of double-layered samples. Each sample (560 × 110 × 95 mm^3) undergoes tensile and bending loading at constant temperature (5 °C) simultaneously. The tensile horizontal loading simulates thermal effect and is applied through a displacement rate of 0.01 mm/min whereas the cyclic vertical bending simulates traffic loading and is applied by a pneumatic cylinder operating in control strain mode (amplitude 0.2 mm, frequency 1 Hz).

Both layers of the double-layered sample have a thickness of 40 mm; below the lower layer a sulfur bituminous material (thickness = 15 mm) is laid by applying a tack coat. The sulfur bituminous layer is sawed (notch amplitude = 3 mm) so that the top of the notch is just at the bottom of the AC lower layer (Fig. 4.39a).

Cracking detectors are installed in the front side of samples whereas five horizontal strain gauges (length = 20 mm) and four vertical strain gauges (length = 10 mm) are glued on the back side, as depicted in Fig. 4.39b.

The collected data are:

– the notch opening displacement and the vertical displacement due to bending effects on each side of the sample;
– the tensile horizontal load;
– the vertical crack propagation on the front side;
– the longitudinal and vertical deformations from sample back side;
– the sample temperature with PT100 thermal sensor.

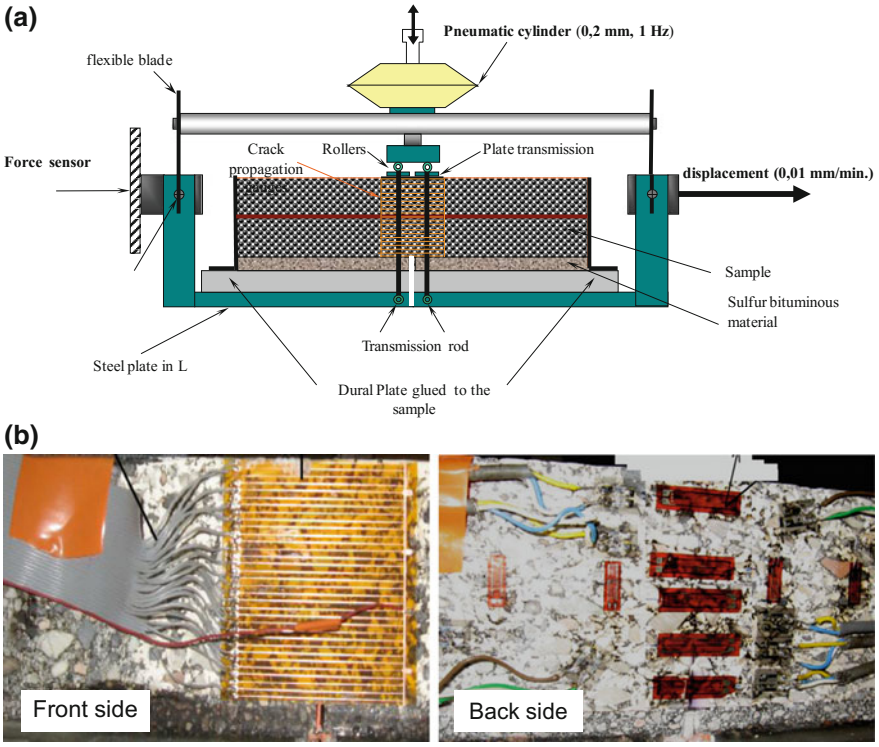

Fig. 4.39 Tensile-bending test: **a** configuration (Vecoven 1989); **b** Instrumentation on both sides of the sample

4.5.2 Results and Analysis

4.5.2.1 Cyclic Bending Tests

Permanent deformation response

The permanent deformation resistance of the double-layered systems measured by UNIVPM is depicted in Fig. 4.40, where the accumulated mid-span deflection of the beams is reported as a function of the number of loading cycles.

The grid installation improved the permanent deformation resistance of the double-layered systems with respect to the unreinforced specimens, which always reached collapse before the test conclusion (36000 cycles). In particular, at P_0 = 2.0 kN, collapse of UN systems was obtained within the first ten load cycles. On the contrary, CF and FP reinforced systems did not always reach complete collapse before test conclusion, therefore the flex point of the permanent deformation curves was used as failure criteria (Virgili et al. 2009). In these cases, in

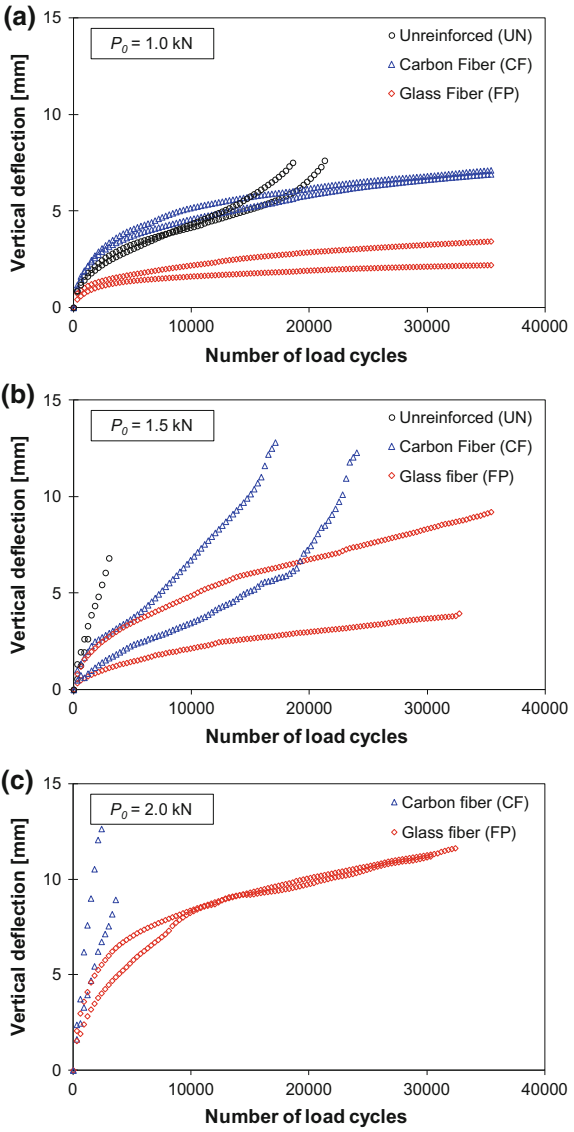

Fig. 4.40 Permanent deformation response in cyclic 4PB test results at different load levels: **a** 1.0 kN; **b** 1.5 kN; **c** 2.0 kN (Canestrari et al. 2015)

order to compare grid effectiveness, an Improvement Factor (IF) was calculated as follows:

$$IF = \frac{N_{flex}^{i}}{N_{flex}^{UN}} \tag{4.5}$$

where N_{flex}^{i} is the number of cycles at the flex point of interface type i (=CF, FP) and N_{flex}^{UN} is the number of cycles at the flex point of interface type UN.

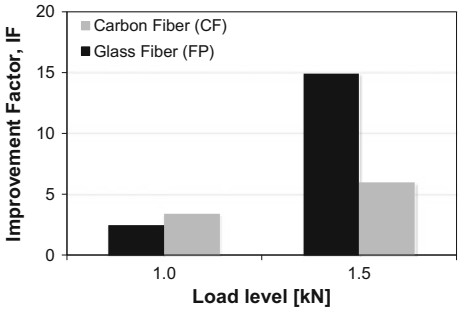

Fig. 4.41 Performance improvement due to grid reinforcement in terms of permanent deformation resistance (Canestrari et al. 2015)

As shown by the high IF values reported in Fig. 4.41, both FP and CF grids produced a remarkable increase of permanent deformation resistance, especially at higher load levels. These results confirmed the positive effect of CF grids observed in previous studies for porous asphalt surfacing (Kim et al. 2009). This performance improvement could be explained considering that, at each load cycle, the presence of the reinforcement reduces the load carried by the AC double-layer and therefore reduces damage accumulation of the AC mixture.

Damage and crack propagation

The evolution of the apparent stiffness modulus E_{app}, (Eq. 4.3) during the cyclic tests is reported in Fig. 4.42. Experimental data showed that grid reinforcement resulted in a stiffness increase of the double-layered systems, that is more evident with the FP grid, but is also observed for the CF grid. The higher flexural stiffness of the reinforced systems highlights the contribution given by the grid that works effectively as reinforcement. This implies that an appreciable level of shear stress is effectively transmitted across the reinforced interface. Such a behavior may appear in contrast with the direct shear tests results which highlighted a marked reduction of peak interlayer strength for grid-reinforced interfaces (see Sect. 4.4.2.1). However, considering the different stress level applied in the two tests, this may actually indicate that the debonding effect, particularly evident for the FP grid, is attained only when interface shear stress reaches failure conditions.

In Fig. 4.42 the flex point position of the permanent deformation curves (Fig. 4.40) is reported on the corresponding curves representing stiffness evolution. As shown by previous studies (Virgili et al. 2009; Ferrotti et al. 2011), the flex point indicates the phase of the test when macro cracks begin to propagate significantly. For UN and CF reinforced systems this behavior is confirmed by the E_{app} decrease that follows the flex point, whereas, for FP reinforced systems, the significant E_{app} decrease prior to the flex point suggests a different failure mechanism, that is confirmed by visual observations of double-layered specimens at the end of the test.

In fact, Fig. 4.43a shows that in CF systems the crack propagated vertically and across the grid, whereas in FP systems, when the crack reached the interface, it started to propagate horizontally (Fig. 4.43b). This change of crack propagation mode, that is also visible in 3PB tests (see Sect. 4.5.2.2), can be related to the

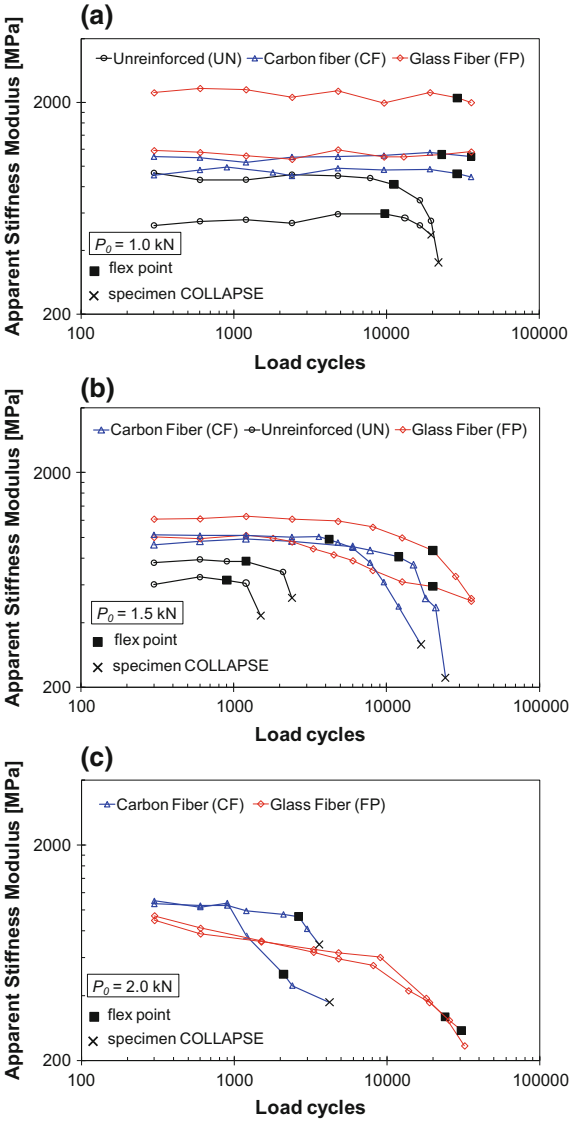

Fig. 4.42 Evolution of the apparent stiffness modulus at different load levels: **a** 1.0 kN; **b** 1.5 kN; **c** 2.0 kN (Canestrari et al. 2015)

marked reduction of peak interlayer shear strength measured by ASTRA tests for FP specimens. Indeed, this different type of separation mechanism allows for additional energy dissipation and brings to longer specimen life, in control stress loading mode. Despite this different crack propagation mode, it is worth noting that both CF and FP grids provided a considerable increase in terms of permanent deformation resistance and flexural stiffness of the double-layered system, working effectively as reinforcement.

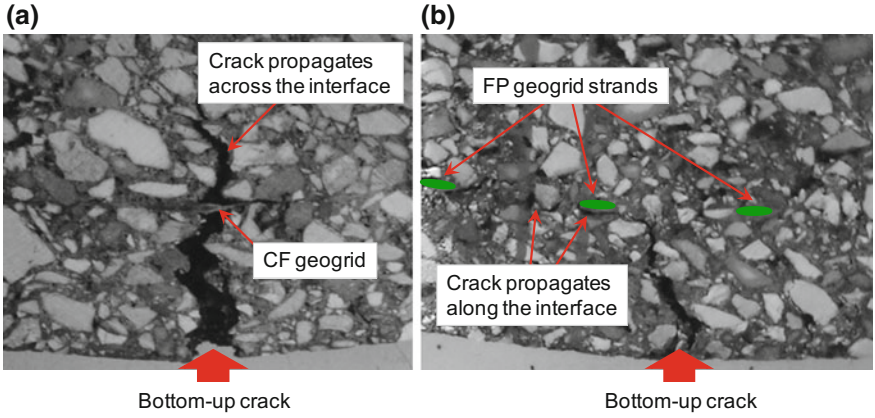

Fig. 4.43 Failure of reinforced beams in cyclic 4PB test: **a** CF grid; **b** FP grid (Canestrari et al. 2015)

4.5.2.2 Monotonic Bending Tests

Load-deflection curves and cracking behavior

The load-deflection curves obtained by UNIVPM and UNIBO in the monotonic 3PB tests are reported in Fig. 4.44 and the average values of the corresponding characteristic parameters are summarized in Table 4.10.

It can be observed that, in tests carried out by both UNIVPM and UNIBO, the shape of the P-δ curves is very similar. Within each set of tests, the values of P_F, and δ_F are rather close. Although the grids installation led to somewhat higher values of both P_F, and δ_F, results showed that these parameters largely depend on the characteristics of the un-damaged AC mixture.

This confirms that, in the pre-cracking phase, double-layered beams behaved like single-layered beams and that grid reinforcement had a minor impact on the crack initiation resistance.

Beyond the flexural strength point (P_F, δ_F), both reinforced and unreinforced systems initially showed a rapid decrease of load carrying capacity due to the crack propagation towards the interface. Afterwards, UN systems rapidly lost their resistance until complete failure, whereas CF and FP systems showed an important post-peak deformation phase, resulting in higher toughness values.

In the crack-propagation phase, CF systems showed a short delayed phase (Fig. 4.44b) and a rapid evolution toward collapse (strain-softening). On the other hand, FP systems, after the short delayed phase, showed a strain-hardening behavior (Fig. 4.44c) where the resistance of the double-layered system increased reaching values similar, or even above P_F.

The different behavior of the two reinforced systems can be related to the different failure mechanisms. Specifically, when the crack reached the interface, of CF systems, its bottom-up movement was shortly delayed before its propagation across

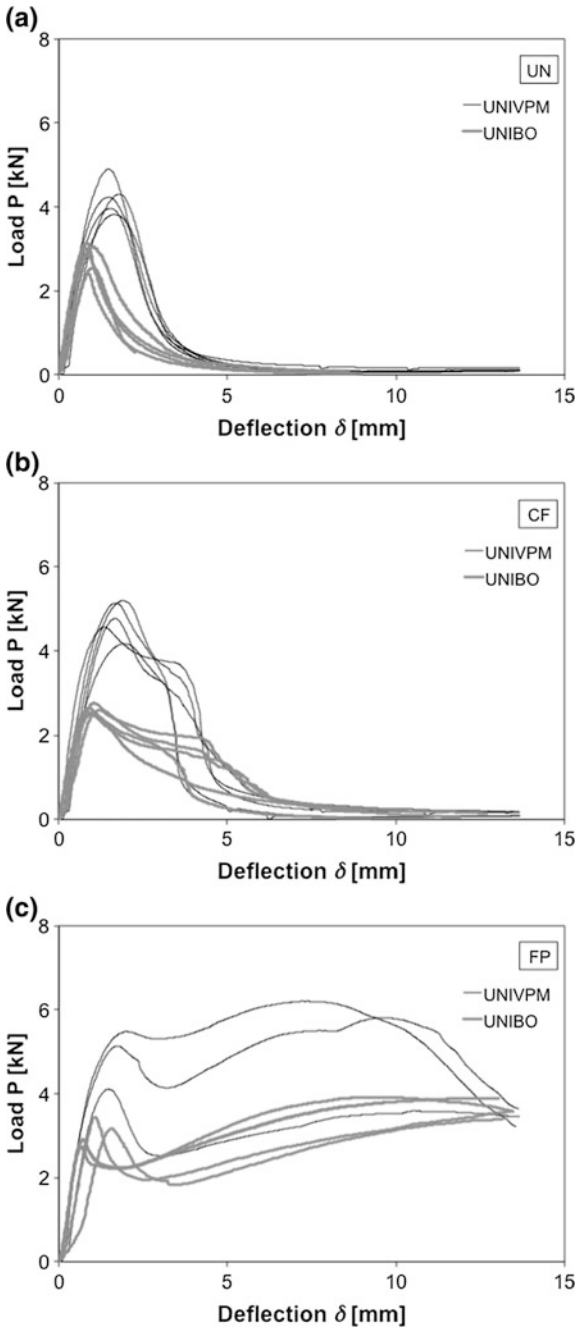

Fig. 4.44 Load-deflection curves of the monotonic 3PB tests

Table 4.10 Summary of 3PB test results (average, standard deviation and coefficient of variation)

Lab	System	Max load P_F (kN)			Deflection δ_F (mm)		
		Average	Std. Dev.	CoV (%)	Average	Std. Dev.	CoV (%)
UNIVPM	UN	4.24	0.42	9.82	1.59	0.13	8.05
	CF	4.77	0.42	8.91	1.73	0.25	14.28
	FP	4.91	0.71	14.54	1.75	0.25	14.51
UNIBO	UN	2.83	0.34	11.92	0.87	0.08	9.68
	CF	2.63	0.10	3.80	0.96	0.15	15.61
	FP	3.03	0.27	8.91	0.94	0.36	38.74

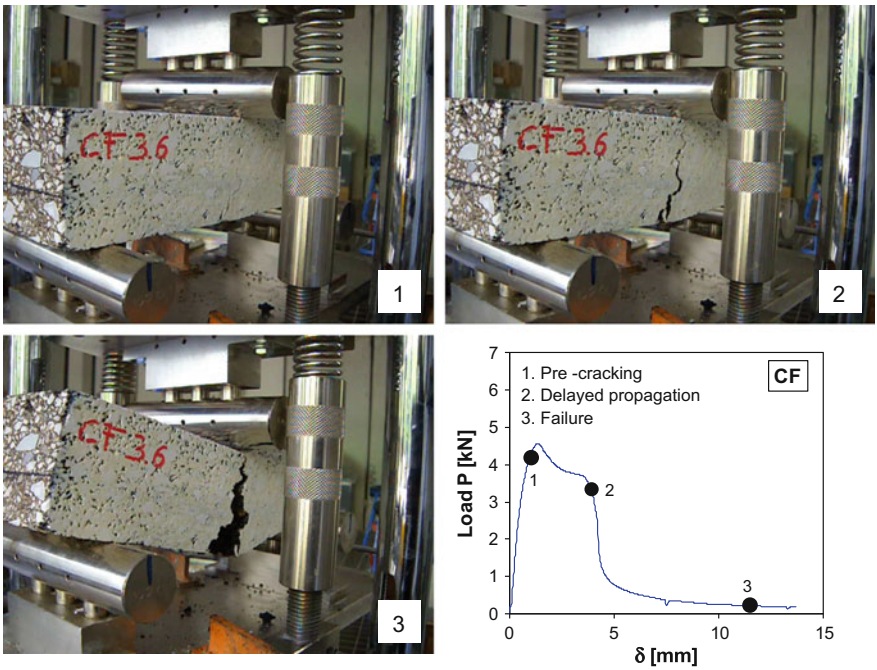

Fig. 4.45 Failure mechanisms of CF reinforced specimens in 3PB test (Canestrari et al. 2015)

the grid and the specimen collapse (Fig. 4.45). Conversely, in FP systems, when the crack reached the interface, its bottom-up propagation was diverted and it proceeded along the interface, allowing for additional energy dissipation (Fig. 4.46).

In the first case, a Mode 1 crack propagation (bottom-up opening) can be identified; in the second case the horizontal crack propagation is probably related to both the bending of the lower layer, due to the beam curvature (Mode 1), and the interlayer shear stress (Mode 2).

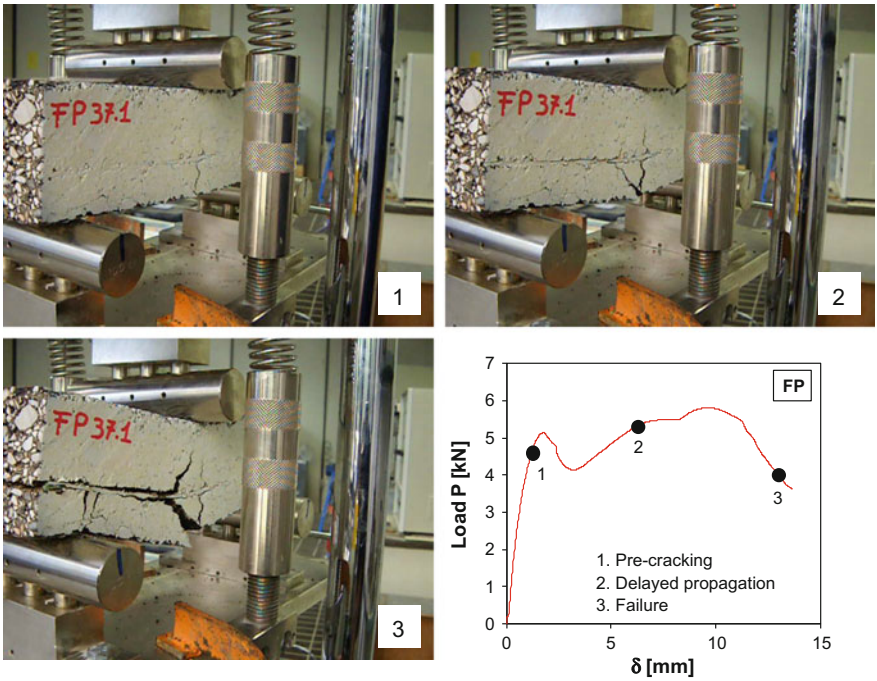

Fig. 4.46 Failure mechanisms of FP reinforced specimens in 3PB test (Canestrari et al. 2015)

In this sense, CF grid appears to be not effective in preventing crack propagation across the interface. On the contrary, FP grid significantly delayed the crack propagation, working effectively as anti-reflective cracking system.

Dimensionless toughness indices

As it can be observed in Fig. 4.44, results obtained by the UNIVPM and UNIBO were different in magnitude, due to the differences in beam geometry, test speed and test temperature. However, the effect of grid reinforcement on the load-deflection behavior was analogous. In particular, similar to Fiber Reinforced Concrete (FRC), the post-cracking behavior of CF and FP reinforced systems can be described as deflection-softening and deflection hardening, respectively (Di Prisco et al. 2009).

The values of dimensionless toughness indices I5, I10 and I20 computed from test results, are summarized in Fig. 4.47 and Table 4.11. It is highlighted that the first-crack deflection was defined on the basis of the maximum of the load deflection curve after the initial quasi-linear segment. The three indices are able to highlight the effect of grid reinforcement on the energy absorption capability of the double-layered systems. In particular, the ranking of the three systems (UN, CF and FP) is maintained, regardless of the test setup. The reinforcement effect is evident on I20, i.e. at higher limiting deflections. The hardening behavior of FP the systems

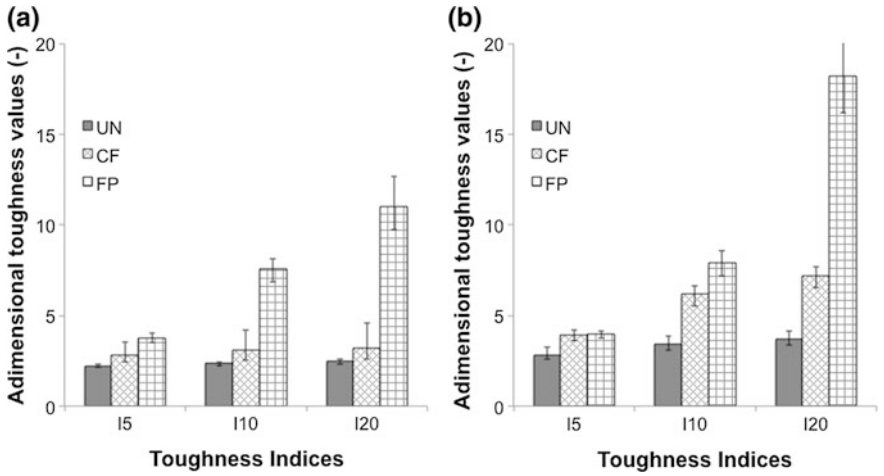

Fig. 4.47 Dimensionless toughness indices I5, I10 and I20 (average values and range of measured values): **a** UNIVPM; **b** UNIBO

Table 4.11 Summary of dimensionless toughness indices (average and standard deviation)

Lab	System	I5		I10		I20	
		Average	Std. Dev.	Average	Std. Dev.	Average	Std. Dev.
UNIVPM	UN	2.23	0.08	2.38	0.09	2.51	0.13
	CF	2.83	0.43	3.08	0.65	3.22	0.78
	FP	3.73	0.28	7.55	0.64	11.04	1.49
UNIBO	UN	2.84	0.26	3.40	0.33	3.71	0.38
	CF	3.92	0.23	6.17	0.48	7.18	0.45
	FP	3.96	0.16	7.89	0.54	18.19	1.69

is particularly evident in the tests carried out by UNIBO (notched beams) where an average I20 = 18.2 was obtained.

It is finally remarked that the use of dimensionless toughness indices allowed the practical characterization of reinforced systems, regardless of test arrangement, thus confirming that bending tests are suitable for evaluating the reinforcing effect of pavement grids.

4.5.2.3 Modified Wheel Tracking Test

Results of the modified wheel tracking test are shown in Fig. 4.48, where the rut depth is reported as a function of the number of loading cycles. The CF system provided a rut depth that is, on the average, slightly higher with respect to the UN

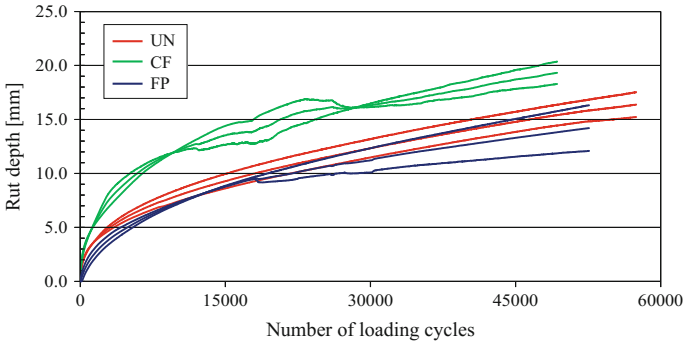

Fig. 4.48 Rut depth versus loading cycles during modified wheel tracking test

Fig. 4.49 Double-layered specimens at the end of the modified wheel tracking test

system. On the contrary, the FP system showed a behavior very similar to the UN interface. In Fig. 4.49, examples of test specimens at the end of the modified wheel tracking test are reported.

4.5.2.4 Tensile-Bending Test

The crack growth (measured from the bottom of lower layer) and the horizontal tensile force (mean and amplitude) against time are shown in Fig. 4.50a. On the basis of a study carried out through tensile-bending tests by Millien et al. (2012), after the initiation phase, two different macro-crack paths have been observed. In particular, a bottom-up reflective cracking starting from the artificial notch is followed by a top-down cracking in the upper layer that begins when the reflective crack tip is close to the interface (corresponding to a crack length of 400 mm). The observed crack path is vertical and quite symmetric on both sides. The evolution of the mean horizontal tensile force correlates well to the three cracking phases (initiation, reflective cracking and top-down cracking). The FP interlayer system response is clearly different from the others (UN, CF); in fact, the FP interlayer

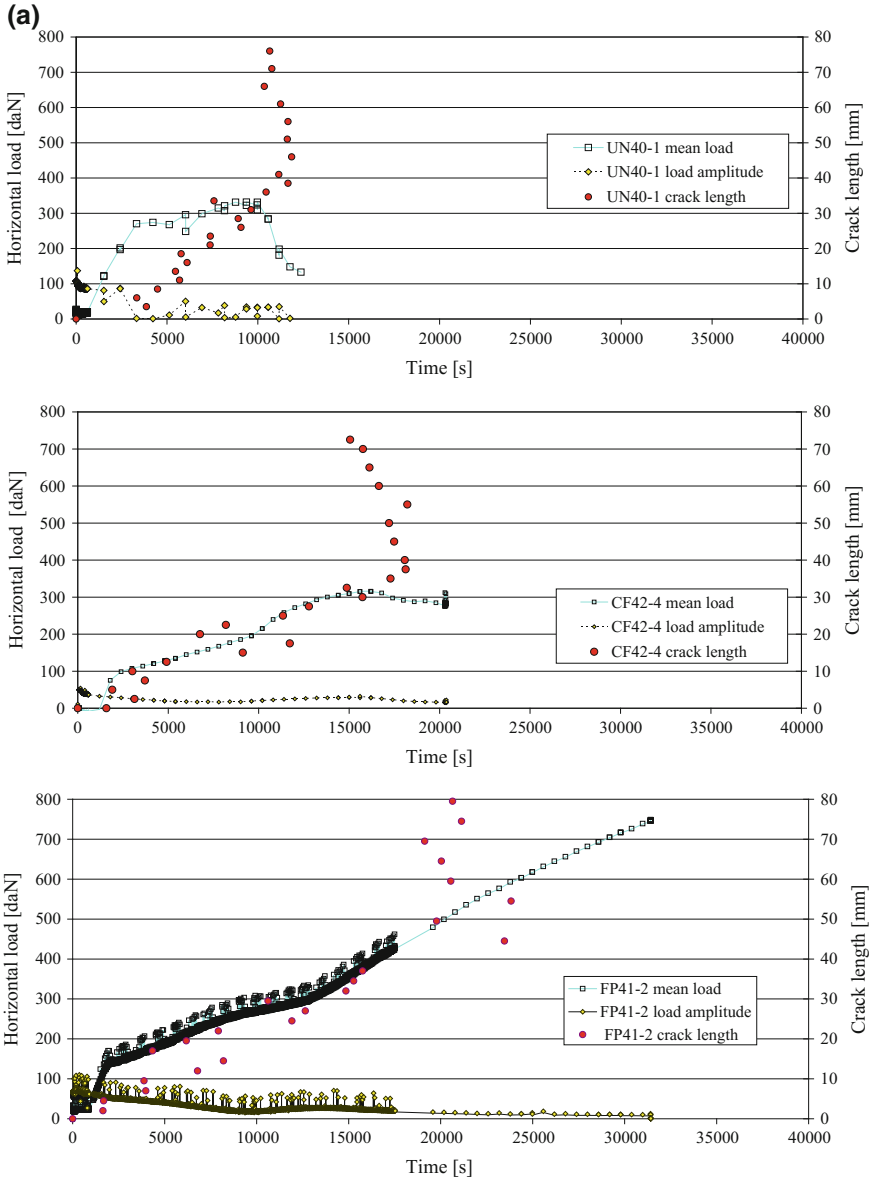

Fig. 4.50 **a** Crack growth and horizontal force evolution of UN, CF and FP samples (Millien et al. 2012). **b** Crack path of UN, CF and FP samples (Millien et al. 2012)

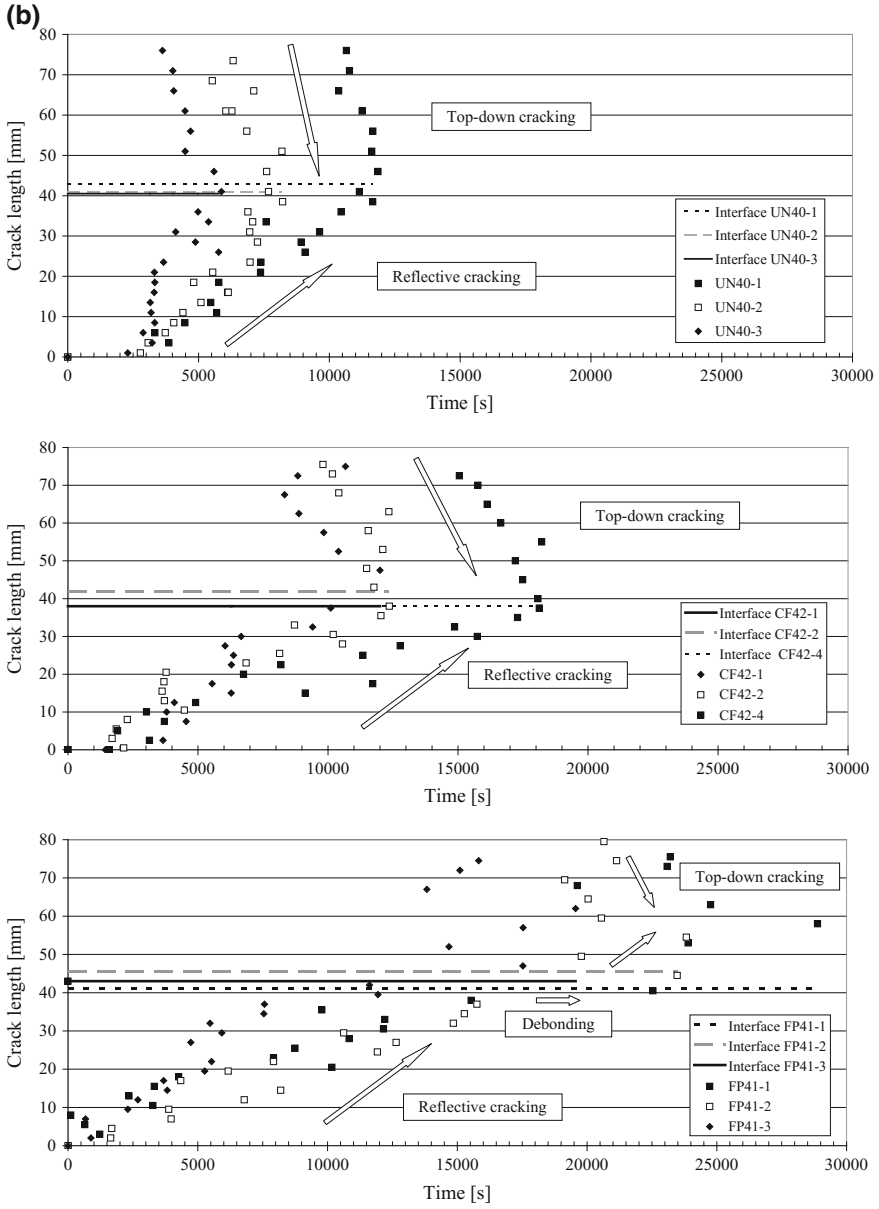

Fig. 4.50 (continued)

system is the only one that leads to debonding after the crack arrives at the interface as shown in Fig. 4.50b. Notwithstanding, the FP grid seems to improve the bearing capacity of the system, even if early debonded.

More in detail, Fig. 4.50b presents the crack propagation of the three samples tested for each system UN, CF and FP. Even though results dispersion is seen as usual for fatigue tests, these data show that the failure is obtained first for the UN, second for the CF, third for the FP system confirming that the high rigidity of the latter grid improves the performance against reflective cracking.

4.5.3 Summary

Bending tests and modified wheel tracking tests were carried out by three laboratories in order to characterize the structural behavior of both reinforced and unreinforced double-layered asphalt systems.

Results of cyclic 4PB tests showed that:

- the grid reinforcement led to a remarkable increase of permanent deformation resistance, especially at higher load levels, working effectively as reinforcement;
- both CF and FP grids produced an increase of the flexural stiffness of the undamaged systems (i.e. in the pre-cracking phase);
- the CF grid delayed the propagation of vertical cracks, whereas the FP grid induced a crack propagation along the interface, leading to longer specimens life.

Results of monotonic 3PB tests confirmed that, in the crack-propagation phase, CF and FP grids induced different failure mechanisms. Specifically:

- the CF grid delayed crack propagation across the interface, whereas FP grid stopped the upward crack propagation, which continued along the interface. This fracture behavior was observed regardless of specimen geometry, presence of notch, test temperature and loading speed;
- the influence of grid reinforcement was described using energy-based dimensionless indices (I5, I10 and I20) originally developed for the analysis of FRC;
- the reinforcement due to grid installation is more evident on I20, i.e. at higher limiting deflections.

4.6 Structural Response of Reinforced Pavements

4.6.1 Falling Weight Deflectometer Tests

The FWD survey was carried out one month after construction by applying a nominal load of 100 kN at each drop by means of a 300 mm footplate.

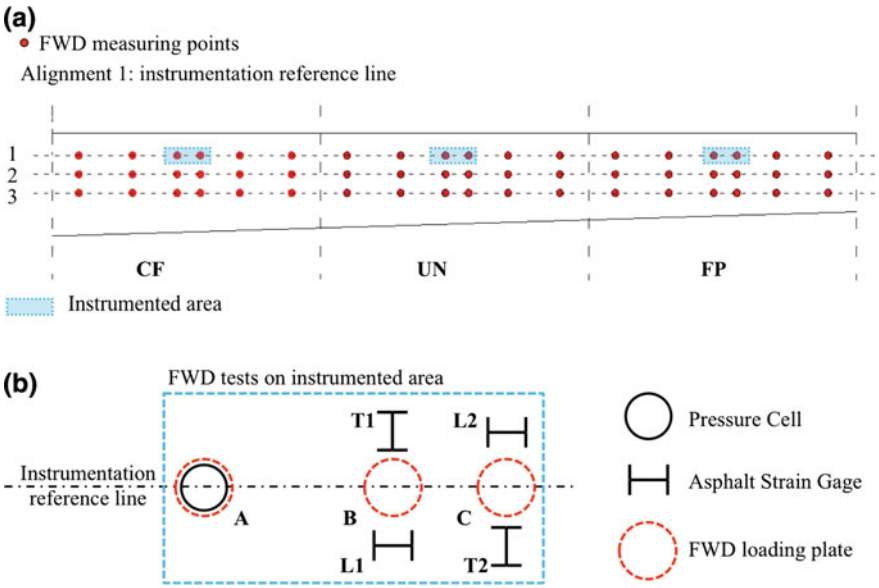

Fig. 4.51 Outline of the FWD survey: **a** measuring alignments on the entire test section; **b** measuring points on the instrumented area

Surface deflections were measured using a 9-sensor configuration with a constant spacing of 300 mm. The average pavement temperature recorded during the survey, as measured by the installed thermistors, was 7.0 °C.

In the first part of the FWD survey, 54 FWD drops were performed, distributed on three parallel alignments covering the entire pavement test section (Fig. 4.51a). Results allowed an overall assessment of the pavement response and were used to compare the reinforced and unreinforced double-layered surfacings.

In the second part of the FWD survey, in order to measure stress and strain values inside the pavement, additional tests were performed in each subsection at EPC and ASG positions (Fig. 4.51b). Tests were carried out at the position of the pressure cell (point A), at the intermediate position between strain gauges L1 and T1 (point B) and at the intermediate position between the strain gauges L2 and T2 (point C).

4.6.1.1 Deflection Measurements

Average deflection basins for each subsection, calculated on the basis of the data obtained from the first part of the FWD survey, are presented in Fig. 4.52a. As it can be observed, closer to the loading plate, subsection CF exhibited lower deflections with respect to UN and FP, highlighting a higher overall stiffness of the

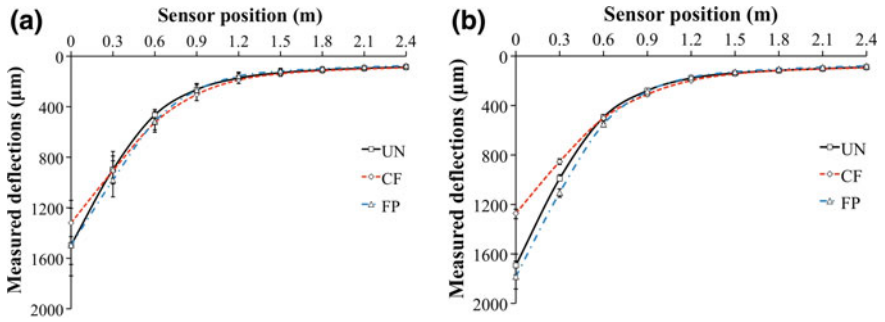

Fig. 4.52 Outline of the FWD survey: **a** measuring alignments on the entire test section; **b** measuring points on the instrumented area

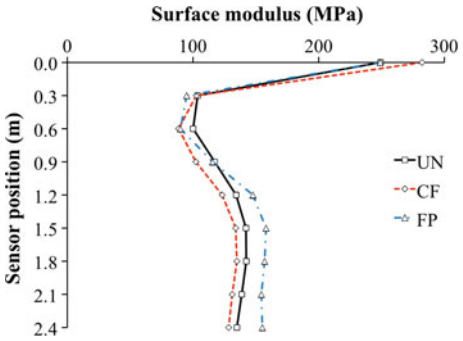

Fig. 4.53 Surface modulus calculated for the average deflection basins of the subsections

surface layers. Similar results were also obtained with the FWD measurements carried out in the instrumented area (Fig. 4.52b).

Surface deflections were also analyzed in terms of surface modulus, which can be calculated, for each deflection in the basin, assuming a homogeneous half space and using Boussinesq's equations (Ullidtz 1987). Surface modulus values (Fig. 4.53) calculated for the average deflection basins highlight that a low-stiffness layer is present in the road base, confirming the DCP results obtained before the construction of the test section (see Sect. 4.3.1). Based on these experimental findings in the modeling phase, the subgrade was divided into two sublayers.

4.6.1.2 Strain and Stress Measurements

Figure 4.54 shows an example of stress and strain measurements carried out in the second part of the FWD survey. Each plot reports the time-history of the vertical stress, measured by the EPCs, and the time-history of the horizontal strains (longitudinal and transverse) measured by the ASGs, for a single FWD drop according to the positions A and B indicated in Fig. 4.51b. Following the convention adopted

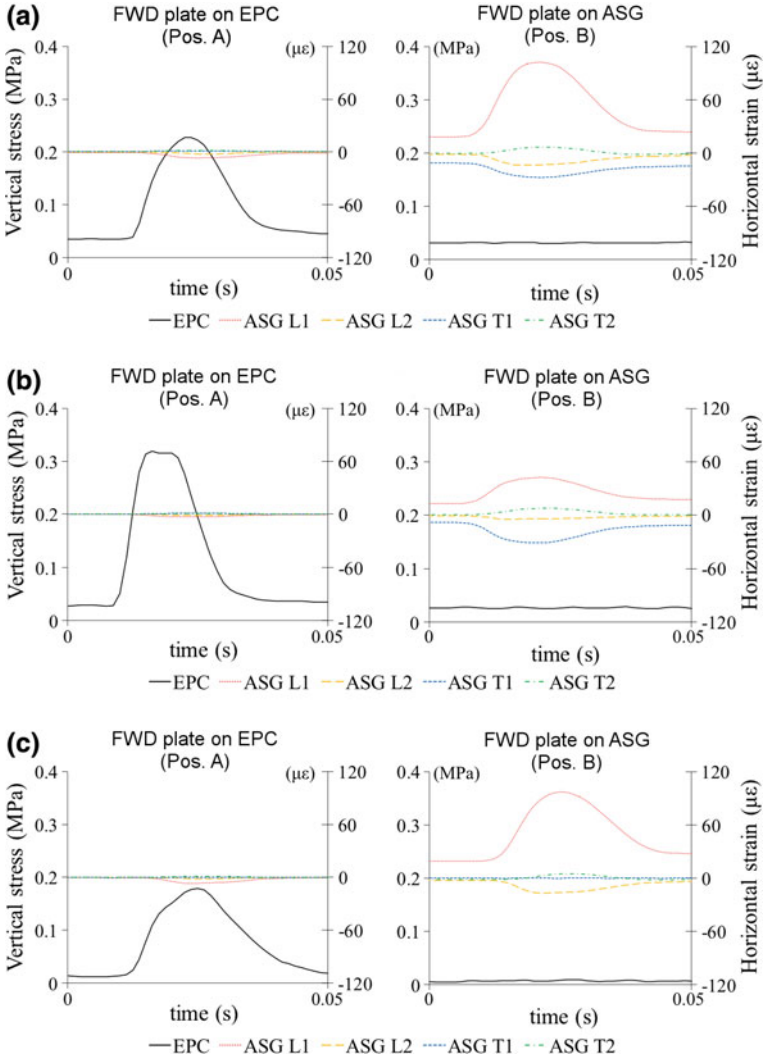

Fig. 4.54 Sample stress and strain measurements from FWD tests: **a** subsection UN; **b** subsection CF; **c** subsection FP

by the instrument manufacturers, compressive stress and tensile strain have a positive sign.

From Fig. 4.54 it can be noticed that, when the FWD test was carried out at the EPC position (see Fig. 4.51b, position A), the strain variations recorded by the ASG were less than 6 microstrain in all subsections. Similarly, when the FWD test was carried out at the ASG position (see Fig. 4.51b, position B), the stress variation recorded by the EPC was null. The duration of the load wave measured by the EPCs

Table 4.12 Normalized peak response under FWD loading (loading positions as specified in Fig. 4.51b)

Subsection	Loading position	Vertical stress (MPa)	Longitudinal strains		Transverse strains	
			LI (microstrain)	L2 (microstrain)	T1 (microstrain)	T2 (microstrain)
UN	A	0.20	−6	−2	1	I
UN	B	–	85	−12	−16	7
UN	C	–	−18	52	−2	−56
CF	A	0.29	−3	−1	1	1
CF	B	–	30	−4	−23	7
CF	C	–	−8	21	−1	−20
FP	A	0.16	−6	−2	Failed	Failed
FP	B	–	79	−15	Failed	Failed
FP	C	–	−25	84	Failed	Failed

and the duration of the strain response measured by the ASGs, generally ranged between 0.025 and 0.030 s, resulting in an equivalent loading frequency approximately between 30 and 40 Hz.

The normalized peak response values of each instrument for each drop were calculated. Normalization of the instrument response was achieved by subtracting the value before the initiation of the response from the peak load response (Al-Qadi et al. 2011). Average results for each loading position (three drops were performed at each position) are reported in Table 4.12.

Due to the symmetry of instrumentation and loading configurations (see Sect. 4.6.1; Fig. 4.51b), sensors L1/T1 and L2/T2 were expected to yield analogous readings when the load was applied in positions B and C, respectively. Actual readings (Table 4.12) highlight this symmetric pattern even if measured values showed some variability. For example, considering results for subsection UN, the strain measured by ASG L1, when load was applied in position B, was 85 microstrain, whereas the reading of ASG L2 was 52 microstrain, when load was applied in position C.

Analogously, for subsection CF, strain measured by ASG T1, when load was applied in position B was −23 microstrain, whereas reading of ASG T2, when load was applied in position C was −20 microstrain. Similar observations can be made considering all symmetrical ASGs in all subsections.

Differences between actual readings of symmetrical ASGs can be explained by considering uncertainties in sensor positioning during construction and in footplate positioning during FWD tests. Even with this variability, the average peak strains reported in Table 4.12 highlight an overall 65% reduction in the strain field inside the CF-reinforced double-layered surfacing with respect to the unreinforced surfacing. Conversely, strains measured inside the FP-reinforced double-layered surfacing do not show any reduction compared to the unreinforced case.

4.6.1.3 Homogeneous Layered Elastic Theory Model

A LET model was developed in order to analyze the FWD test results. The double-layered asphalt surfacing, both reinforced and unreinforced, was modeled as a single, homogeneous layer characterized by an "equivalent" modulus. The adopted four-layered pavement model comprised a 200 mm granular base and a subgrade, which was devided in two sublayers according to DCP tests and surface modulus values. Layer thicknesses were taken from the construction control data (Table 4.1b) and field tests; perfect bond between adjacent layers was assumed.

The back-calculated moduli, obtained with the BAKFAA software, are summarized in Table 4.13. Comparing the results obtained from the FWD test carried out on the entire section with those obtained on the instrumented area, a decrease in the double-layered surfacing modulus is observed. This reduction can be related to the inhomogeneities due to sensor installations.

In general, back-calculation results showed that the CF grid produced a higher equivalent modulus of the double-layered surfacing with respect to the unreinforced section (about two times). A less pronounced reinforcing effect was also measured for the FP subsection. These findings are in accordance with those reported by Kim et al. (2009), obtained on grid-reinforced porous asphalt surfacings, and by Henry et al. (2011), obtained on grid-reinforced granular base courses.

A LET model implemented using the BISAR software was also used for the forward-calculation of stresses and strains inside the pavement at the instrument positions. To this end, a FWD test was simulated by means of a static load applied on a circular area (D = 300 mm). The simulation results, along with the peak strain values actually measured during the FWD tests, are reported in Table 4.14. As it can be observed, compression (negative) strain values in the transverse direction were greatly overestimated whereas tension (positive) longitudinal strains were not even obtained. It was therefore clear that the homogeneous LET model with back-calculated moduli was unable to correctly predict the strain field inside the double-layered surfacing and thus a calibration process was needed.

4.6.1.4 Homogeneous LET Model Calibration

Calibration of the homogeneous LET model was carried out by adjusting the moduli of the double-layered surfacing and those of the granular base, using a trial-and-error procedure, in order to match simulated and measured strains.

The calibration procedure showed that for the considered structure and measurement positions, the transverse strain value was controlled by the stiffness of the double-layered surfacing, whereas the longitudinal strain value was mainly related to the stiffness of the granular base layer. Based on these observations, model calibration was not possible for the FP section due to the damage of both transverse ASGs.

Calibrated moduli for the LET model are reported in Table 4.15 (columns 3, 4), while the corresponding simulated strain profiles are represented in Fig. 4.55. In

Table 4.13 Back-calculated moduli from the FWD results on the entire section and on the instrumented area

Layer	Material	Poisson's ratio	FWD on entire section			FWD on instrumented area		
			UN modulus (MPa)	CF modulus (MPa)	FP modulus (MPa)	UN modulus (MPa)	CF modulus (MPa)	FP modulus (MPa)
1	AC surfacing	0.25	2,991	6,747	4,598	2,690	4,737	3,054
2	Granular base (200 mm)	0.35	248	268	173	202	391	154
3	Subgrade 1 (250 mm)	0.40	47	36	35	43	40	32
4	Subgrade 2 (halfspace)	0.40	144	139	160	136	136	144

Table 4.14 Measured peak horizontal strains (max/min values) and simulated strains (LET model with back-calculated moduli)

Subsection	Peak longitudinal strain		Peak transverse strain	
	Measured (max/min) (microstrain)	Simulated (LET) (microstrain)	Measured (max/min) (microstrain)	Simulated (LET) (microstrain)
UN	85/52	−16	−56/−16	−75
CF	30/21	−21	−23/−20	−47
FP	84/79	−5	−/−	−42

Table 4.15 Homogeneous LET model moduli calibrated on FWD tests and real-scale tests

Layer	Material	FWD tests calibration		Real-scale tests calibration		
		UN Modulus (MPa)	CF Modulus (MPa)	UN Modulus (MPa)	CF Modulus (MPa)	FP Modulus (MPa)
1	AC surfacing	4,500	8,000	700	2,000	500
2	Granular base (200 mm)	70	250	75	100	50
3	Subgrade 1 (250 mm)	40	40	40	40	40
4	Subgrade 2 (halfspace)	140	140	140	140	140

these plots, the LET-simulated strains are compared to the measured strains, which were also reported in Table 4.14. As it can be observed, a suitable representation of the strain field inside the pavement in the four selected measurement points was obtained, confirming that the CF grid produced a noticeable increase in the doublelayered surfacing equivalent modulus, with respect to both the unreinforced and the FP-reinforced sections.

Finally, in Fig. 4.56, the vertical stress measured by the installed EPC are compared with the stress profile simulated using the calibrated LET model. The plots clearly show that the homogeneous LET model calibrated to fit horizontal asphalt strains is able to predict the vertical stresses at the top of the granular base with reasonable accuracy.

4.6.2 Real-Scale Load Tests

Real-scale load tests were performed driving a fully-loaded two axle truck over the instrumented area of each subsection. The average pavement temperature during the tests, as measured by the installed thermistors, was 30 °C. An outline of the test procedure is shown in Fig. 4.57.

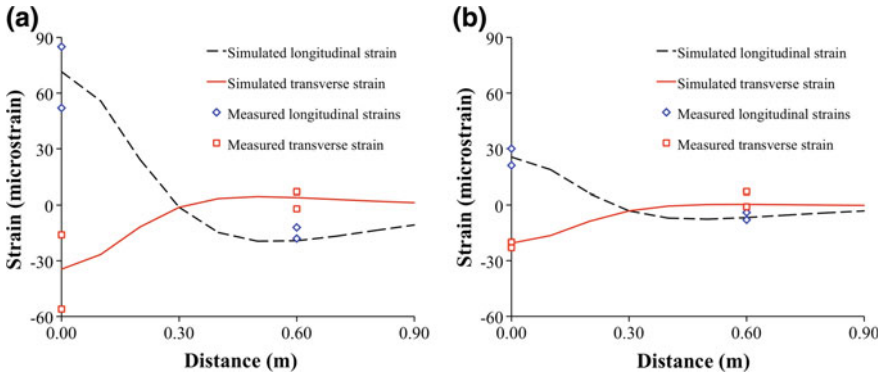

Fig. 4.55 LET-simulated horizontal strain profiles with calibrated moduli, compared to measured strain (see Table 4.12): **a** UN subsection; **b** CF subsection

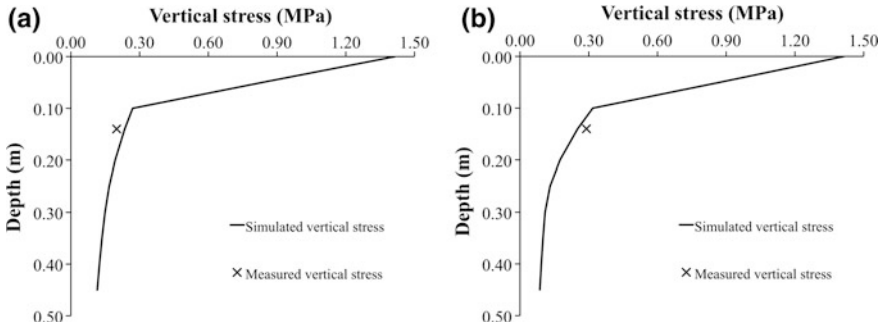

Fig. 4.56 LET-simulated vertical stress profiles with calibrated moduli, compared to measured stress (see Table 4.12): **a** UN subsection; **b** CF subsection

The fully-loaded truck was characterized by a 64 kN front axle with single tires and a 190 kN rear tandem axle with dual and single tires. Both axles were equipped with 315/80R22.5 tires, at a nominal inflation pressure of 0.6 MPa, resulting in a contact area of about 55,000 mm^2 for each tire.

Nine truck passes were recorded in each subsection (Fig. 4.58) trying to match the reference tire path and the instrumentation reference line. Truck speed was around 20 km/h and the average value for each pass was calculated forming the ratio of the axle spacing (4.58 m) to the measured time between the corresponding peak loads/strains.

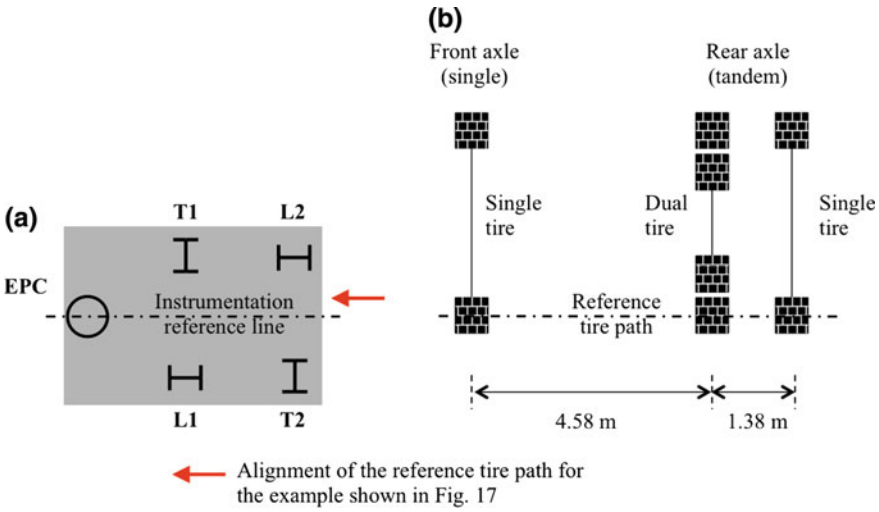

Fig. 4.57 Outline of real-scale tests: **a** instrumented area; **b** truck footprint and planned alignment

Fig. 4.58 Example of data acquisition during truck pass n. 5/9 in UN subsection

4.6.2.1 Strain and Stress Measurements

An example of the stress and strain signals recorded during a single truck passing over the instrumented area is shown in Fig. 4.59 (subsection CF).

The duration of the load waves produced by the tires and the corresponding duration of the strain responses, generally ranged between 0.1 and 0.12 s, resulting in an equivalent haversine frequency ranging between 8 and 10 Hz.

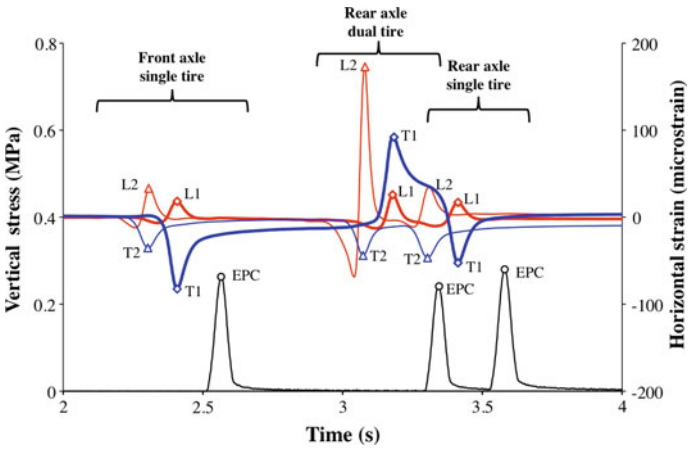

Fig. 4.59 Results of real-scale tests for a truck pass on CF subsection (alignment of reference tire path is shown in Fig. 4.57)

In Fig. 4.59, as the front axle crosses the instrumented area, longitudinal strains recorded at positions L2 and L1 show an initial contraction (negative strain) of reduced amplitude and then an extension (positive strain) when the tire footprint reaches the ASG position (positive peak). At the same time, the transverse strain recorded at positions T2 and T1 shows contraction (negative peak) only. The delayed recovery of the transverse strain, which does not undergo an inversion of sign, is particularly evident. In addition, the relative magnitudes of the extension/compression peaks recorded at positions L1/L2 and T1/T2, indicate that, in this case, the reference tire path is probably closer to sensors L2/T1 (Fig. 4.57).

When the dual tires of the rear axle pass over the instrumented area, the longitudinal strain measured at position L2 and the transverse strain measured at position T1 reach their maximum extension value. It was observed that the peak longitudinal strain value is more than four times the value produced by the front axis. This may be explained considering the alignment of the second tire, which passes directly above the sensor and the effects of the horizontal force transmitted by the dual tires, which are mounted on a traction axis.

Finally, when the single tire of the rear axle passes, the longitudinal and transverse strain evolution is similar to that recorded under the front axle. The delayed recovery of the negative transverse strain at position T2 is also evident.

4.6.2.2 Homogeneous LET Model Analysis

The analysis of the grid influence on the pavement response was first carried out using the homogeneous LET model previously developed to evaluate the FWD tests.

In order to perform such an analysis, only the front axle passes were considered. Initially, time–stress and time–strain signals recorded by the sensors (Fig. 4.59) were converted into distance–stress and distance–strain diagrams, multiplying the time abscissa by the load speed. Such diagrams, which may be considered as influence line graphs of the (live) tire load, were then superposed to the plots of simulated stress and strain obtained from the LET model with a (dead) load of 32 kN applied on a circular area equivalent to the area of the front tire footprint. Finally, in order to obtain the best possible match between measured and simulated responses, as indicated by the Betti reciprocity principle, the LET moduli were calibrated using a trial-and-error procedure similar to that described for the FWD tests.

The moduli obtained from the real-scale test calibration are reported in Table 4.15 (columns 5–7). As it can be observed, for the double-layered AC surfacing, these values are 4.0 and 4.5 times lower compared to the FWD-calibrated moduli of the UN and CF subsections, respectively. This ratio takes into account the reduction of asphalt stiffness due to temperature (from 7 to 30 °C) and loading frequency (approximately from 40 to 10 Hz).

The superposition of measured and simulated strain diagrams represented in Fig. 4.60 for the UN, CF and FP subsections (in the latter case only the longitudinal strain is reported). In these plots, the longitudinal (L1/L2) and transverse (T1/T2) strain profiles measured in a sample truck pass are represented with a simple space shift, in order to obtain exact correspondence of the peak values.

Since the exact position of the reference tire path with respect to the reference line of the instrumentation is not known, three simulated LET strain profiles are represented in each plot, corresponding to different loading positions: LET0 designates the simulated strain diagram obtained when the load is applied at the midpoint between the sensors; LET1 and LET2 designate the simulated strain diagrams obtained when the load is applied with an offset of ± 0.1 m with respect to the instrumentation reference line. These three simulated strain diagrams highlight the effect of the exact load position respect to the sensors.

As it can be observed, the simulated strain profiles are symmetric because of the axial-symmetry of the LET model, whereas the measured strain profiles do not exhibit such a trend. This is due to the delayed (viscoelastic/viscoplastic) asphalt response to the dynamic truck load which can not be simulated with an elastic response model. A good superposition between measured and simulated longitudinal strains was obtained in the first part of the diagrams, (i.e. when the load was moving towards the sensors). However, the corresponding simulated transverse strains were generally underestimated compared to the measured signals.

As it can be observed in Fig. 4.60, the strain field inside the double-layered surfacing was considerably reduced by the CF grid installation, and consequently, the calibrated value of its equivalent modulus was found to be about three times the value of the unreinforced surfacing (Table 4.15). Conversely, the presence of the FP grid caused an increase of the measured longitudinal strains and consequently a decrease in the calibrated equivalent modulus.

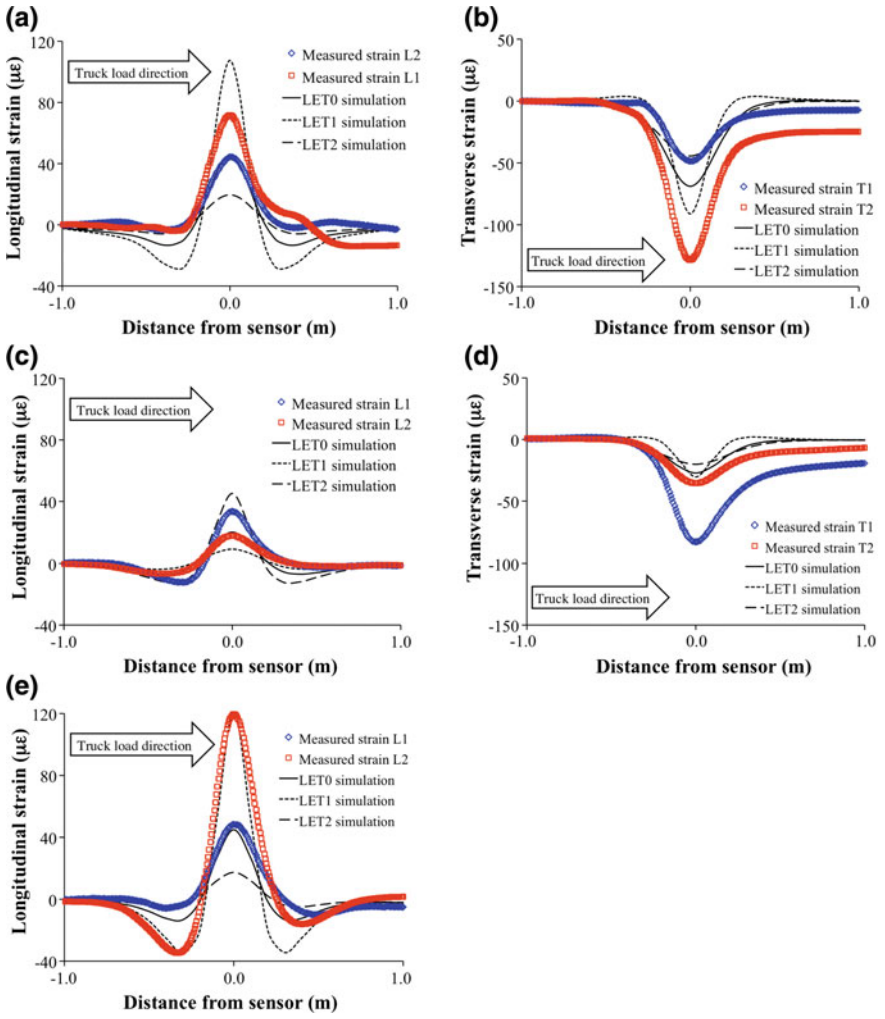

Fig. 4.60 Measured and simulated LET horizontal strains (homogeneous LET model): **a** longitudinal strain—UN subsection; **b** transverse strain—UN subsection; **c** longitudinal strain—CF subsection; **d** transverse strain—CF subsection; **e** longitudinal strain—FP subsection

4.6.2.3 Two-Layer LET Model Analysis

A further analysis of the strain field measured in the real-scale tests was carried out modeling the upper and the lower AC layers separately. This two-layer LET model allowed the potential reinforcing effect of the grid to be represented with an increase of the modulus of the upper AC layer with respect to the modulus of the lower AC layer. Moreover, the potential debonding effect of the grid was represented introducing partial slip between the two AC layers. In particular, in the BISAR software

Table 4.16 Two-layer LET model parameters calibrated on realscale tests

Subsection		CF	FP
Upper AC layer modulus	MPa	1,000	600
Interface slip parameter (α)	–	0.1	0.4
Lower AC layer modulus	MPa	800	400

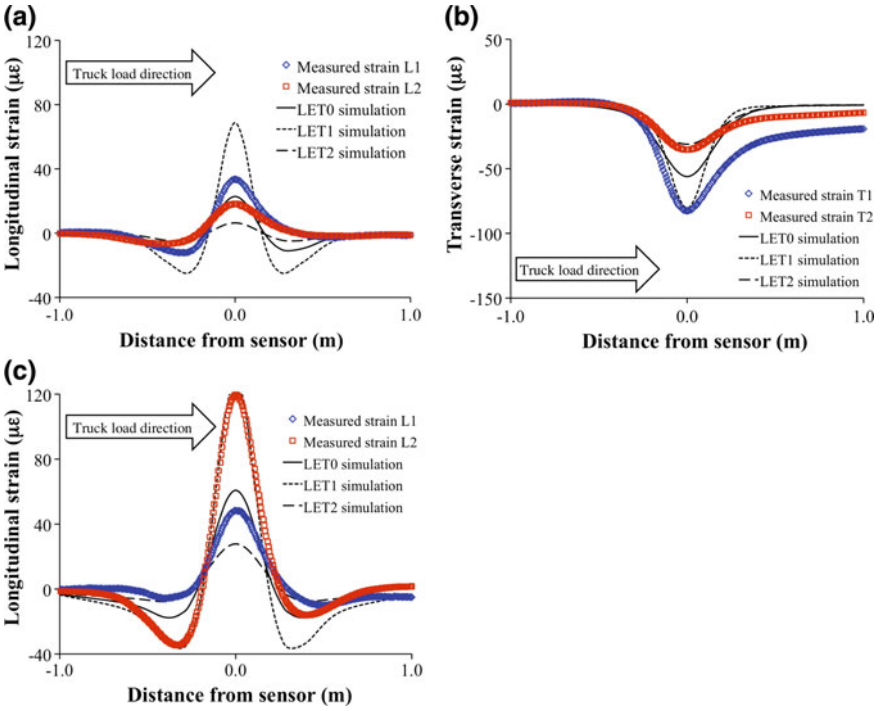

Fig. 4.61 Measured and simulated LET horizontal strains (two-layer LET model): **a** longitudinal strain—CF subsection; **b** transverse strain—CF subsection; **c** longitudinal strain—FP subsection

slip between layers is represented with a parameter α, where $\alpha = 0$ means full bonding, whereas $\alpha = 1$ means complete slip.

The moduli of the two AC layers and the parameter α were calibrated using a trial-and-error procedure in order to match the LET-simulated and the measured strains (Table 4.16). The superposition of measured and calibrated LET strain diagrams for the CF and FP subsections is represented in Fig. 4.61.

The calibrated two-layer model resulted in a better representation of the measured pavement strains in both the longitudinal and the transverse directions, with respect to the homogeneous model. The relative stiffness increase of the upper AC layer compared to the lower AC layer was 25 and 50% for the CF and the FP systems, respectively (Table 4.16). These values are probably due to the higher torsional rigidity of the FP grid compared to the CF grid. However, the FP grid also

resulted in a noticeable increase in the interface slip parameter ($\alpha = 0.4$) with respect to the CF grid ($\alpha = 0.1$). This debonding is probably the main cause of the overall increase of the measured strain field and may potentially create a risk for the long-term pavement performance.

The analysis of the real-scale tests confirmed the main findings of the FWD survey. In particular, a reinforcing effect was not observed with the FP grid, which may be due to a debonding effect also observed in a previous laboratory study on the same FP-reinforced double-layered system (Canestrari et al. 2012a). The debonding is probably related to the high torsional rigidity and thickness of the FP grid, which inhibited the achievement of an optimal compaction close to the interface and reduced the interlocking between the two bituminous layers in contact (Santagata et al. 2008). On the other hand, the more flexible CF grid showed better compatibility with the AC double-layered surfacing, reducing the overall strain field compared to the unreinforced surfacing and potentially increasing the long-term pavement performance.

4.6.3 Analysis of Pavement Distress Evolution

In this section an attempt is made to relate the results of laboratory tests on double-layered specimens obtained from section A to the field performance of the same double-layered systems on section B. The comparison is focused on the crack-propagation behaviour observed in the lab and on the reflective cracking performance observed in the field.

To this purpose, during the construction of section B, areas with "simulated" cracks were prepared in the lower asphalt layer (see Sect. 4.3.3, Fig. 4.8c) in order to evaluate the performance of the reinforcement grids in terms of reflective cracking inhibition. The simulated cracks were obtained by full-depth saw cuts with an inter-axis of 0.4 m (see Sect. 4.3.3.2, Fig. 4.17).

As shown in Fig. 4.62a, b, a similar reflective cracking pattern developed in UN and CF subsections. It started about 6 months after construction and rapidly grew in the following weeks. In both subsections, the typical double-asymmetric crack pattern due to traffic loading developed above transverse cuts, whereas single cracks developed above longitudinal cuts. One year later, these two zones had completely failed (Fig. 4.62c, d).

On the other side, after the same 22 months period, a double-asymmetric crack pattern was barely visible in the FP reinforced sub-section (Fig. 4.62e) subjected to the same traffic and environmental conditions, highlighting the ability of the FP grid to extend service life of asphalt surfacings when cracks are present in the underlying asphalt layers. This capability can be related to the post-cracking behavior previously observed in the bending tests where FP systems showed better performance. In addition, it can be observed that the debonding effect highlighted by ASTRA tests did not reduce the overall pavement performance in this area.

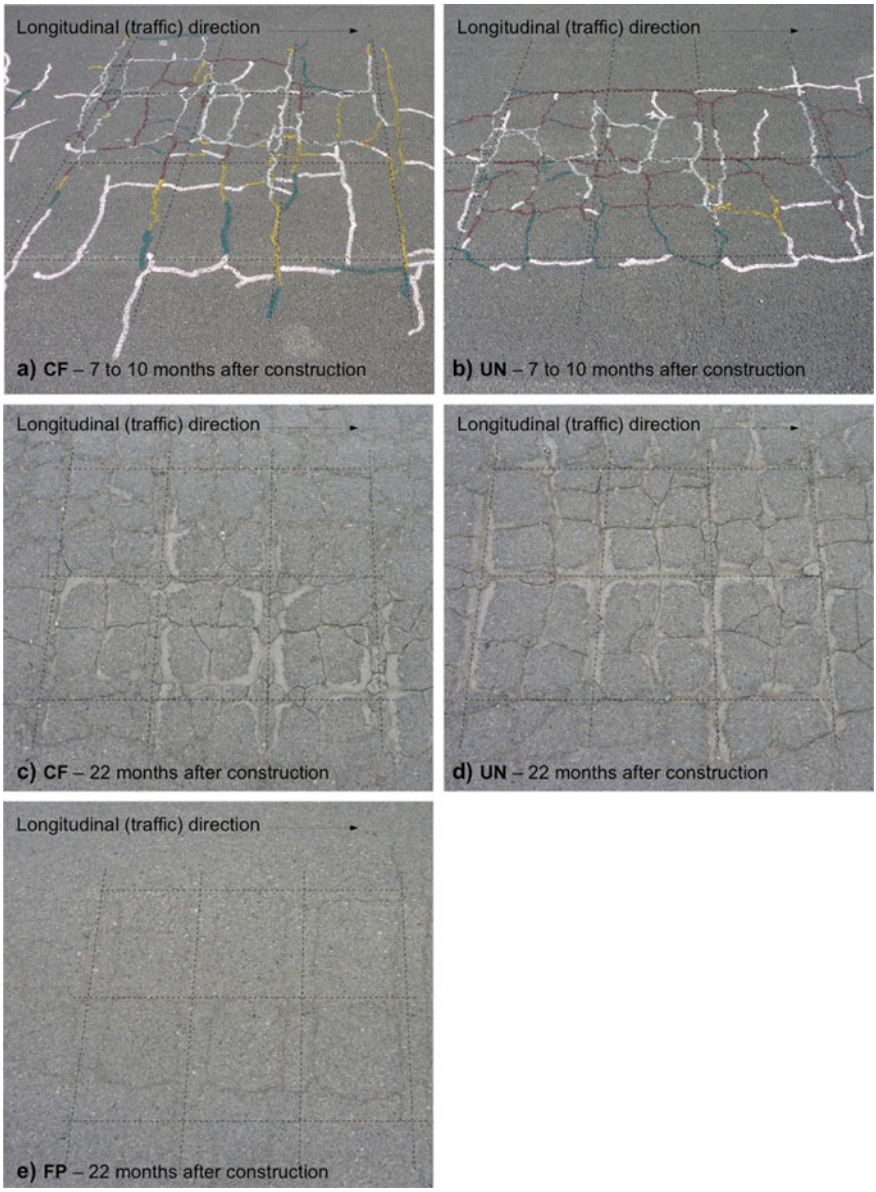

Fig. 4.62 Visual surveys of pavement condition above simulated cracks (section B)

It is worth noting that outside the area with artificial cracks, after 22 months, the observed overall performance was better for CF subsection than for FP subsection, as shown in Fig. 4.63 comparing the crack pattern of the two subsections.

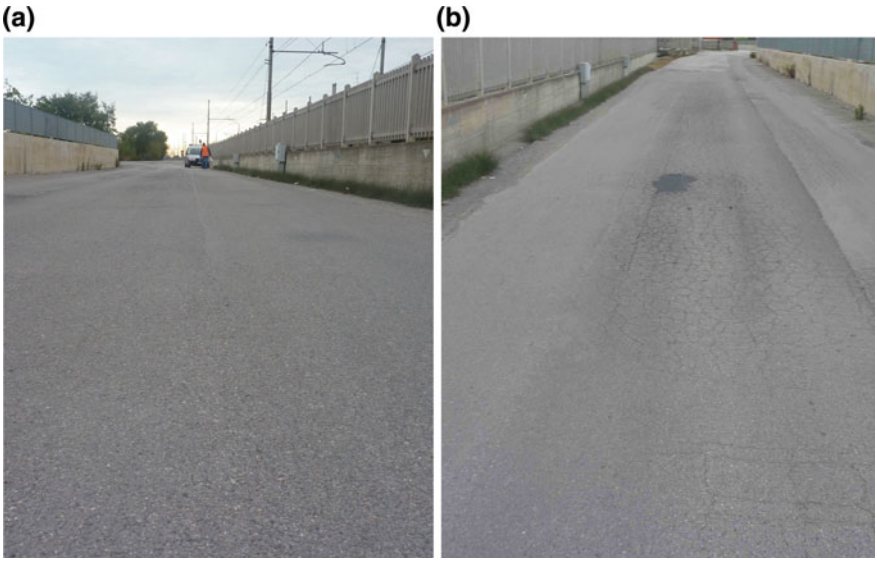

Fig. 4.63 Crack pattern outside the area with artificial cracks after 22 months: **a** no cracking in CF subsection; **b** severe cracking in FP subsection

These results allow concluding that the high rigidity of the FP grid induces a certain separation degree between the asphalt layers (experimentally confirmed by lower interface shear strength) leading to loading carrying compared to the CF grid. On the other hand, the same properties have to be considered beneficial to prevent reflective cracking propagation.

4.6.4 Summary

The structural behavior of reinforced and unreinforced systems was analyzed in the field by means of FWD and real scale load tests. Moreover their field performance was checked by visually monitoring the pavement distress evolution.

Results of FWD tests showed that:

- the CF grid produced an overall 65% reduction of the peak horizontal strains measured inside the asphalt double-layered system, compared to the unreinforced pavement;
- the FP grid did not produce any strain reduction;
- horizontal strains inside the asphalt double-layered system and vertical stresses at the top of the granular base were predicted using a calibrated LET model.

Results of the real scale tests showed that:

- the strain field inside the double-layered surfacing was considerably reduced by the installation of the CF grid, whereas the FP grid produced an increase in the measured longitudinal strains;
- the reinforcing effect of the grid was simulated using a LET model by increasing the modulus of the upper AC layer with respect to the modulus of the lower AC layer;
- the overall increase of the measured strain field obtained with the FP grid was simulated in the LET model by introducing a partial slip between the two AC layers.

The visual surveys of the pavement distress evolution revealed that the FP grid was effective in stopping the upward movement of the simulated cracks in the lower AC layer.

4.7 Synopsis of Main Outcomes

This report summarizes the results of a research project aimed at the mechanical characterization of grid-reinforced asphalt pavements. The experimental program was based on the analysis of two grid reinforcements: a carbon fiber/glass fiber grid (CF), characterized by a 20 mm mesh size and a glass fiber reinforced polymer grid (FP), characterized by a 33 mm mesh size.

A RILEM interlaboratory test was organized with the aim to compare devices and procedures currently adopted to investigate the properties of reinforced interfaces. The tested samples were obtained from an experimental test section where real scale grid installation techniques were used. The experimental results obtained by the six participating laboratories highlighted the importance of considering both the debonding and the reinforcing effect of the grids.

The debonding effects were evaluated by measuring the interlayer shear strength with five different devices, at different test temperatures and speeds. The results showed that the reduction of interlayer shear strength was statistically significant only for the FP grid, which is characterized by higher thickness and torsional stiffness with respect to the CF grid, whose mesh is extremely flexible and deformable.

The reinforcing effects were evaluated using both cyclic and monotonic bending tests on double-layered beams characterized by different dimensions, at different test temperatures and speeds. Results showed that the CF grid delayed the crack propagation across the interface, whereas the FP grid stopped the upward crack propagation. As a consequence, the permanent deformation resistance and the flexural toughness of the FP-reinforced system were significantly higher with respect to that of both unreinforced and CF-reinforced systems.

In parallel with the interlaboratory test, a second experimental test section was built along an in-service secondary road with the aim of analyzing the field performance of the grid-reinforced systems.

Asphalt strain gauges and pressure cells were used to measure the actual strains and stresses induced by FWD and truck loads. The measurements showed that the strain field inside the double-layered surfacing was considerably reduced by the installation of the CF grid, whereas the FP grid did not produce any strain reduction.

Moreover, visual surveys revealed that the CF-reinforced system improved structural performance and highlighted the ability of the FP grid to retard reflection cracking development.

In conclusion, the concurrent analysis of both laboratory tests and field behavior indicates that:

- when a pavement grid is able to increase the flexural toughness of double-layered asphalt specimens and is characterized by a limited reduction of interlayer shear strength, it will be effective as pavement reinforcement system but will have a limited impact on reflective cracking resistance;
- when a pavement grid is able to increase the flexural toughness but is also characterized by a significant reduction of interlayer shear strength it will not be effective as pavement reinforcement system but will retard the development of reflective cracking.

Finally, the results of the RILEM interlaboratory tests suggest that:

- shear tests currently employed to analyze unreinforced asphalt interfaces can be efficiently employed to test the debonding potential of pavement grids;
- measurements of interlayer shear strength obtained with different devices can be homogenized by superposing the effects of temperature and test speed;
- monotonic bending tests could be good candidates to be standardized for evaluating the reinforcing effect of pavement grids.

References

Abd El Halim AO, Haas R, Walls J, Bathurst R, Phang W (1982) A new method for effective reinforcement of asphalt pavements. Proc Road Transp Assoc Can 29–41

Abd El Halim AO, Haas R, Hozayen H, Gervais M (1991) Effective reinforcement of asphalt pavements. In: Proceedings of the Canadian technical asphalt association, pp 171–192

Aldea CM, Darling JR (2004) Effect of coating on fiberglass geogrids performance. In: Proceedings of 5th international RILEM conference on reflective cracking in pavements: Mitigation, Risk Assessment and Prevention, Limoges, pp 81–88

Al-Qadi IL, Tutumler E, Dessouky S, Kwon J (2007) Responses of geogrid reinforced flexible pavement to accelerated loading. In: Proceedings of the international conference on advanced characterisation of pavement and soil engineering materials, Athens, pp 1437–1445

Al-Qadi IL, Dessouky S, Tutumluer E, Kwon J (2011) Geogrid mechanism in low-volume flexible pavements: accelerated testing of full-scale heavily instrumented pavement sections. Int J Pavement Eng 12(2):121–135

Arraigada M, Perrotta F, Raab C, Tebaldi G, Part MN, (2016) Use of APT for validating the efficiency of reinforcement grids in asphalt pavements. In: Aquair-Moya et al (eds), The roles of accelerated pavement testing in pavement sustainability. Springer, Cham, pp 241–255

Asphalt Academy—CSIR Built Environment (2008) *Technical guideline: Asphalt reinforcement for road construction*. Asphalt Academy

Austin RA, Gilchrist AJT (1996) Enhanced performance of asphalt pavements using geocomposites. Geotext Geomembr 14:175–186

Bocci M, Grilli A, Santagata FA, Virgili A (2007) Influence of reinforcement geosynthetics on flexion behaviour of double-layer bituminous systems. In: Proceedings of the international conference on advanced characterisation of pavement and soil engineering materials, Athens, 20–22 June, Leiden, Taylor & Francis/Balkema, pp 1415–1424

Brown SF (2006) Reinforcement of pavements with steel meshes and geosynthetics: keynote presentation. In: COST action 348 Dissemination international symposium, London

Brown SF, Brunton JM, Hunghes DAB, Brodrick BV (1985) Polymer grid reinforcement of asphalt. In: Proceedings of Association of the Asphalt Paving Technologists, vol 54, pp 18–44

Brown SF, Thom NH, Sanders PJ (2001) A study of grid reinforced asphalt to combat reflection cracking. J Assoc Asphalt Paving Technol 70:543–569

Button J, Lytton R (2003) Guidelines for using geosynthetics with HMA overlays to reduce reflective cracking. Report 1777-P2 Texas Department of Transportation

Caltabiano MA, Brunton JM (1991) Reflection cracking in asphalt overlays. J Assoc Asphalt Paving Technol 60:310–330

Canestrari F, Grilli A, Santagata FA, Virgili A (2006) Interlayer shear effect of geosynthetic reinforcements. In: Proceedings of the 10th international conference on asphalt pavements, Quebec City, 12–17 Aug, pp 811–820

Canestrari F, Pasquini E, Belogi L (2012a) Optimization of geocomposites for double-layered bituminous systems. In: Proceedings of the 7th RILEM international conference on cracking in pavements, Delft, pp 1229–1239

Canestrari F, Ferrotti G, Lu X, Millien A, Partl MN, Petit C, Phelipot-Mardelé A, Piber H, Raab C (2012b) Mechanical testing of interlayer bonding in asphalt pavements. In: RILEM state-of-the-art-report: advances in interlaboratory testing and evaluation of bituminous materials, vol 9, pp 303–360. doi:https://doi.org/10.1007/978-94-007-5104-0

Canestrari F, Belogi L, Ferrotti G, Graziani A (2015) Shear and flexural characterization of grid-reinforced asphalt pavements and relation with field distress evolution. Mater Struct 48:959–975. https://doi.org/10.1617/s11527-013-0207-1

Canestrari F, Ferrotti G, Graziani A (2016) Shear failure characterization of time-temperature sensitive interfaces. Mech Time-Depend Mater

Chehab GR, Tang X (2012) The use of a multi-set-up, reduced-scale accelerated trafficking simulator for evaluating roadway systems and products. Int J Pavement Eng 13:535–552

Collop AC, Thom NH, Sangiorgi C (2003) Assessment of bond condition using the Leutner shear test. Proc Inst Civ Eng Transp 156(4):211–217. ISSN: 0965-092X. doi:https://doi.org/10.1680/tran.156.4.211.37816

Correia NS, Zornberg JG (2014) Quantification of rut depth in geogrid reinforced asphalt overlays using accelerated pavement testing. In: 10th international conference on geosynthetics

Di Prisco M, Plizzari G, Vandewalle L (2009) Fibre reinforced concrete: new design perspectives. Mater Struct 42(9):1261–1281. https://doi.org/10.1617/s11527-009-9529-4

Elseifi MM, Al-Qadi IL (2003) A simplified overlay design model against reflective cracking utilizing service life prediction. In: 82th transport research board annual meeting, Washington, D.C

Ferrotti G, Canestrari F, Virgili A, Grilli A (2011) A strategic laboratory approach for the performance investigation of geogrids in flexible pavements. Constr Build Mater 25(5):2343–2348

Ferrotti G, Canestrari F, Pasquini E, Virgili A (2012) Experimental evaluation of the influence of surface coating on fiberglass geogrid performance in asphalt pavements. Geotext Geomembr 34:11–18

Francken L (2005) Prevention of cracks in pavements. Road Mater Pavement Des 6(3):407–425

Gajewski M, Mirski K (2012) Shear tests of two-layer asphalt specimens made in a proposed apparatus allowing side pressure application. Logistyka J 3:593–602
Gillespie R, Roffe JC (2002) Fibre-DEC: a fibre-reinforced membrane to inhibit reflective cracking. In: 3rd international conference bituminous mixtures and pavements, Thessaloniki, Greece
Gopalaratnam VS, Gettu R (1995) On the characterization of flexural toughness in fiber reinforced concretes. Cement Concr Compos 17(3):239–254. https://doi.org/10.1016/0958-9465(95)99506-O
Grabowski W, Pozarycki A (2008) Energy absorption in large dimension asphalt pavement samples reinforced with geosynthetics. Found Civ Environ Eng 11:17–28
Graziani A, Pasquini E, Ferrotti G, Virgili A, Canestrari F (2014) Structural response of grid-reinforced bituminous pavements. Mater Struct 47:1391–1408
Henry KS, Clapp J, Davids WG, Barna L (2011) Backcalculated pavement layer modulus values of geogrid reinforced test sections. Geotech Spec Publ Dallas 211:4673–4682
Hornych P, Kerzreho JP, Sohm J, Chabot A, Trichet S, Joutang JL, Bastard N. (2012) Full scale tests on grid reinforced flexible pavements on the French fatigue carrousel. In: RILEM book-series, vol. 4. Springer, The Netherlands, pp. 1251–1260
Ishai I, Livnat N, Livneh M (1992) Pavement improvement with asphaltic membranes. Geotech Spec Publ 2(30):1067–1079
James GM (2004) Geosynthetic materials as asphalt reinforcement interlayers: the Southern African experience. In: Proceedings of the 8th Conference on asphalt pavements for Southern Africa, Sun City
Khodaii A, Fallah Sh (2009) Effects of geosynthetic reinforcement on the propagation of reflection cracking in asphalt overlays. Int J Civil Eng 7(2):131–140
Khodaii A, Fallah S, Nejad FM (2009) Effects of geosynthetics on reduction of reflection cracking in asphalt overlays. Geotextile Geomembr 27(1):1–8
Kim H, Sokolov K, Poulikakos LD, Partl MN (2009) Fatigue evaluation of carbon FRP-reinforced porous asphalt composite system using a model mobile load simulator. Transp Res Record 2116:108–117
Kinney TC, Yuan X (1995) Geogrid aperture rigidity by inplane rotation. In: Proceedings of geosynthetics'95, Nashville, pp 525–537
Komatsu T, Kikuta H, Tuji Y, Muramatsu E (1998) Durability assessment of geogrid-reinforced asphalt concrete. Geotextile Geomembr 16:257–271
Lee SJ (2008) Mechanical performance and crack retardation study of a fiberglass-grid-reinforced asphalt concrete system. Can J Civ Eng 35(10):1042–1049
Leutner R (1979) Untersuchung des Schichtverbundes beim bituminösen Oberbau. Bitumen 3:84–91
Millien A, Dragomir ML, Wendling L, Petit C, Iliescu M (2012) Geogrid interlayer performance in pavements: tensile-bending test for crack propagation. RILEM Bookseries 4:1209–1218
Montestruque G, Rodrigues R, Nods M, Elsing A (2004) Stop of reflective crack propagation with the use of pet geogrid as asphalt overlay reinforcement. Cracking in pavement–mitigation, risk assessment and prevention, RILEM meeting, Limoges, France
Nguyen ML, Blanca J, Kerzréhoa JP, Hornych P (2013) Review of glass fibre grid use for pavement reinforcement and APT experiments at IFSTTAR. Road Mater Pavement Des 14(1):287–308
Pasquini E, Bocci M, Ferrotti G, Canestrari F (2013) Laboratory characterisation and field validation of geogrid-reinforced asphalt pavements. Road Mater Pavement Des 14(1):17–35
Pasquini E, Bocci M, Canestrari F (2014) Laboratory characterization of optimized geocomposites for asphalt pavement reinforcement. Geosynth Int 21(1):24–36
Perkins SW (1999) Mechanical response of geosynthetic-reinforced flexible pavements. Geosynth Int 6(5):347–382
Powell RB (2008) Installation and performance of a fiberglass geogrid interlayer on the NCAT pavement test track. In: Proceedings of the 6th RILEM conference on pavement cracking: mechanisms, modeling, detection, testing and case histories, Chicago, pp 731–739
Prieto JN, Gallego J, Pérez I (2007) Application of the wheel reflective cracking test for assessing geosynthetics in anti-reflection pavement cracking systems. Geosynth Int 14(5):287–297

Raab C, Partl MN (2009) Interlayer bonding of binder, base and subbase layers of asphalt pavements: long-term performance. Constr Build Mater 23:2926–2931. https://doi.org/10.1016/j.conbuildmat.2009.02.025

Ramberg Steen E (2002) Road maintenance: causes to highlight when choosing in between geosynthetics. In: Nikolaides AF (Ed) Proceedings of the 3rd international conference on bituminous mixtures and pavements, vol 1, Thessaloniki, Greece, Nov 2002, pp 273–282

Santagata FA, Partl MN, Ferrotti G, Canestrari F, Flisch A (2008) Layer characteristics affecting interlayer shear resistance in flexible pavements. J Assoc Asphalt Paving 77:221–256

Shukla SK, Yin J-H (2004) Functions and installation of paving geosynthetics. In: Proceedings of the 3rd Asian regional conference on geosynthetics, Seoul, pp 314–321, 21–23 June 2004

Siriwardane H, Gondle R, Kutuk B (2010) Analysis of flexible pavements reinforced with geogrids. Geotech Geol Eng 28:287–297

Sobhan K, Tandon V (2008) Mitigating reflection cracking in asphalt overlay using geosynthetic reinforcements. Road Mater Pavement Des 9(3):367–387

Sobhan K, Crooks T, Tandon V, Mattingly S (2004) Laboratory simulation of the growth and propagation of reflection cracks in geogrid reinforced asphalt overlay. In: Cracking in pavement—mitigation, risk assessment and prevention. RILEM meeting, Limoges, France

Tozzo C, Fiore N, D'Andrea A (2016) Investigation of dilatancy effect on asphalt interface shear strength. In 8th RILEM International symposium on testing and characterization of sustainable and innovative bituminous materials. RILEM Bookseries vol 11, Springer, Berlin (2016). ISBN: 978–94-017-7341-6 (Print) 978-94-017-7342-3 (Online). doi:https://doi.org/10.1007/978-94-017-7342-3_72, pp 335–346

Uijting BGJ, Jenner CG, Gilchrist AJT (2002) Evaluation of 20 years experience with asphalt reinforcement using geogrids. In: Proceedings of the 3rd international conference on bituminous mixtures and pavements, Thessaloniki, pp 869–877, 21–22 Nov 2002

Ullidtz P (1987) Pavement analysis. Elsevier, New York

Vanelstraete A, de Bondt AH (1997) Crack prevention and use of overlay systems. In: Vanelstraete A, Franken L (eds) Prevention of reflective cracking in pavements. RILEM Report, vol 18, pp 43–60

Vanelstraete A, De Visscher J (2004) Long term performance on site of interface systems. In: Petit C, Al-Qadi IL, Millien A (eds) Proceedings of the 5th international RILEM conference, Limoges. RILEM, Bagneux, pp 699–706

Vanelstraete A, de Bondt AH, Courard L (1997) Characterization of overlay systems. In: Vanelstraete A, Franken L (eds) Prevention of reflective cracking in pavements. RILEM Report, vol 18, pp 61–83

Vecoven JH (1989) Méthode d'étude des systèmes limitant la remontée des fissures dans les chaussées. In: 1ere Conférence RILEM, Reflective Cracking in Pavements, 8–10 mars 1989, Liége, Belgique, pp 57-62

Virgili A, Canestrari F, Grilli A, Santagata FA (2009) Repeated load test on bituminous systems reinforced by geosynthetics. Geotext Geomembr 27(3):187–195

Yang S-H, Al-Qadi IL (2007) Cost-effectiveness of using geotextiles in flexible pavements. Geosynth Int 14(1):2–12

Zamora-Barraza D, Calzada-Peréz M, Castro-Fresno D, Vega-Zamanillo A (2010) New procedure for measuring adherence between a geosynthetic material and a bituminous mixture. Geotext Geomembr 28:483–489

Zamora-Barraza D, Calzada-Peréz M, Castro-Fresno D, Vega-Zamanillo A (2011) Evaluation of anti-reflective cracking systems using geosynthetics in the interlayer zone. Geotext Geomembr 29(2):130–136

Zou W, Wang Z, Zhang H (2007) Field Trial for asphalt pavements reinforced with geosynthetics and behavior of glass-fiber grids. J Perform Constr Facil 21(5):361–367

Chapter 5
Recycling

Paul Marsac, Wim Van den bergh, Nathalie Piérard, James Grenfell, Thomas Gabet, Virginie Mouillet, Laurent Porot, Miguel Perez Martinez and Fabienne Farcas

Abstract Recycling of old pavements is becoming a widespread technique; in order to preserve the natural resources of aggregates and binder, the materials reclaimed from the damaged layers of the pavements maintained are generally reincorporated in the material for new maintenance layers. However, recycling induces some technical challenges. In the case of the Hot mix asphalt (HMA), the most commonly used road construction material, one of the main concerns is ageing. Along with the heterogeneity of the RA properties in stockpiles, it is one of the main factors limiting the recycling rates in HMA. Therefore, the characterisation of ageing through reliable ageing indexes and of its impact on the bitumen physical properties is of paramount importance to improve the recycling techniques. The RILEM TC 237 SIB TG5 inherited a database from the previous work of the RILEM TC 206 ATB TG5 on a protocol for bituminous mixture ageing in laboratory. Taking advantage of these data, the work of the Task Group was first dedicated to a state of the art and an evaluation of the chemical ageing characterization through indexes based on Fourier Transform Infrared Spectroscopy (FTIR). In a second step, an attempt was made, in order to bring out the essential trends of

P. Marsac (✉) · T. Gabet · MiguelPerez Martinez · F. Farcas
LUNAM Université, IFSTTAR, CS4, 44341 Bouguenais, France
e-mail: paul.marsac@ifsttar.fr

W. Van den bergh
University of Antwerp, Antwerp, Belgium

N. Piérard
BRRC, 42, Boulevard de La Woluwe, 1200 Brussels, Belgium

J. Grenfell
University of Nottingham, Nottingham, UK

V. Mouillet
CEREMA/DTerMed, Aix-En-Provence, France

L. Porot
Arizona Chemical, Almere, Netherlands

M. N. Partl et al. (eds.), *Testing and Characterization of Sustainable Innovative Bituminous Materials and Systems*, RILEM State-of-the-Art Reports 24,
https://doi.org/10.1007/978-3-319-71023-5_5

the rheological data with ageing, by using a Huet modified rheological model. Then, exploring the potential of a recently developed method, an interpretation of these trends in terms of asphalt structure is suggested. Finally, possible empirical relationships between the chemical ageing indexes and the rheological parameters are investigated.

Keywords Bituminous binder · Recycling · Reclaimed asphalt
Ageing · Ageing index · Fourier transform infrared spectroscopy
Rheological model · Molecular weight distribution

5.1 Introduction

After a steady increase during the 20th century, the road networks of the main developed countries seem to have reached their maximum extension and therefore tend to require more maintenance than new developments. Meanwhile, a growing social sensitivity to environmental concerns has fostered sustainable development and resource preservation policies. In this context, the recycling of old pavements is becoming a widespread technique; in order to preserve the natural resources of aggregates and binder, the materials reclaimed from the damaged layers of the pavements needing maintenance are generally reincorporated in the material for new maintenance layers.

However, recycling induces some technical challenges. In the case of the Hot Mix Asphalt (HMA), the most commonly used road construction material, one of the main concerns is ageing. HMA is a blend of ca 5 wt% bitumen and ca 95% wt% aggregates. HMA milled from old pavements (RA: Reclaimed Asphalt) are easily re-mixed and re-compacted after heating, but the material obtained is generally too stiff and brittle to be suitable for road construction. This is assumed to be related to the alteration of the physical properties of the bitumen during in-service life. For this reason, RA is generally recycled with the addition of both a soft bitumen, to compensate for the hardening of the RA binder, and new aggregates, to maintain a suitable bitumen to aggregates ratio. Along with the heterogeneity of the RA properties in stockpiles, bitumen ageing is one of the two main factors limiting the recycling rates in HMA. Therefore, the characterisation of ageing through reliable ageing indexes and of its impact on the physical properties of bitumen is of paramount importance to improve the recycling techniques.

The RILEM TC 237 SIB TG5 inherited a database from the previous work of the RILEM TC 206 ATB TG5 (de la Roche et al. 2009, 2010) on a protocol for bituminous mixture ageing in the laboratory. Taking advantage of these data, the work of the Task Group was first dedicated to a state of the art and an evaluation of the chemical ageing characterisation through indexes based on Fourier Transform Infrared spectroscopy (FTIR) (Marsac et al. 2014). In a second step, an attempt was

made in order to bring out the essential trends of the rheological data with ageing by using a Huet modified rheological model. Then, exploring the potential of a recently developed method, an interpretation of these trends in terms of asphalt structure is suggested. Finally, possible empirical relationships between the chemical ageing indexes and the rheological parameters are investigated.

5.2 Chemical Ageing Characterisation

5.2.1 Mechanism of Bitumen Ageing

It has long been recognised that bituminous materials are significantly altered by time-related phenomena and tend to get stiffer and more brittle. This ageing effect is attributed to changes in the chemical structure of the bituminous binder (Petersen 2009). Bitumen is generally described as a complex colloidal mixture of different molecular weight hydrocarbon compounds (Corbett 1969); its macroscopic properties are linked to the relative proportions of these different molecular fractions and their interactions. Ageing development is thus considered to mainly reflect changes in the colloidal mixture associated with:

- the volatilisation of the lighter fractions,
- the oxidation of the other fractions as they are progressively exposed to the oxygen contained in air.

For a road construction material, two ageing steps are usually separated according to the range of the predominant factors governing oxidative ageing namely temperature and air exposure:

- the construction step, usually termed as Short-Term Ageing (STA), associated with high temperatures and high air exposure levels.
- the in-service step in the pavement structure, associated with moderate temperatures and moderate air exposure levels (compacted material), usually termed as Long-Term Ageing (LTA),

Carbonyl groups (esters, ketones etc.) and sulfoxides are the major functional groups formed during oxidative ageing (Petersen 2009). They are characterised respectively by C=O and S=O double bonds. It is generally observed that sulfoxides tend to form at a faster rate and at higher temperatures than carbonyl groups.

Although the global ageing mechanism is the same for all bitumens, its development and magnitude are known to vary significantly according to the origin and the distillation method of the crude oil the binder is derived from (Petersen 2009). Moreover, various studies show that the ageing process of bitumen in a bituminous mix also depends on the type of aggregate used (Bell 1989; Verhasselt and Puiatti 2004; Gubler and Partl 2005).

5.2.2 Fourier Transform Infrared Spectroscopy (FTIR)

5.2.2.1 FTIR Theory

In a material, the different types of molecular bonds are characterised by specific vibration and rotation modes. The energy associated to these modes is quanfied and a higher level can only be reached if a quantity of energy exactly equal to the difference between two energy levels is transmitted to the molecule. As the energy of a photon is equal to the product of the frequency of the radiation and the Planck's constant, a given type of bond can only reach a higher activation level by absorbing a quantum corresponding exactly to a specific infrared (IR) frequency. Thus each type of bond can be identified by characteristic bands in the absorption spectrum of the transmitted IR radiation and its concentration in the material can be deduced from the intensity of the absorption in these bands referring to the Beer-Lambert law (5.1):

$$A(v) = \mathrm{Log}\left(\frac{I_0}{I}\right) = \varepsilon_i(v)\ell C_i \tag{5.1}$$

with:

$A(v)$ absorbance for the wavenumber v
I_0 intensity of the incident light
I intensity of the transmitted light
$\varepsilon_i(v)$ molar absorption coefficient for the wavenumber$v$
ℓ optical path length
C_i studied species concentration

Hence, by providing a tool for tracking the formation of the sulfoxide and carbonyl bonds, FTIR is a powerful method for studying the ageing of bituminous mixes and the evolution of their properties for optimal recycling. However, although they are all based on the same theory, in practice, various measurement modes, sample preparation methods and index calculations are used in the different laboratories for research on bitumen.

5.2.2.2 FTIR Measurement Modes

Two FTIR measurement modes are commonly used for bitumen characterisation: transmission and reflection mode.

In transmission mode the IR beam passes through the sample. It requires a time-consuming preparation of very low thickness bitumen films or may need the use of a solvent. Thus, the sample preparation method can differ between laboratories. At least 3 sample preparation methods can be used:

- spreading of a hot binder droplet on an IR transparent plate with a spatula,
- spreading of a solution of bitumen on the plate followed by an evaporation of the solvent to obtain a film of bitumen,
- sample of bitumen solution.

Transmission mode was the first used to characterise bitumen and most of the data reported in the bibliography were obtained in this mode.

In reflection mode with the Attenuated Total Reflectance (ATR) technique, the beam enters a crystal with high refractive index held in contact with the sample. The beam reflects at the crystal/sample interface and penetrates for just a few μm into the sample. After one or more reflections, depending on the type of ATR-device and crystal, the radiation is attenuated for the specific wavelengths absorbed by the material. For bitumen, the material must be heated to cast a droplet at the surface of a base plate.

Moreover, for the same mode, FTIR spectrum measurements can also differ with regards to the number of individual scans averaged, the wavenumber range and the wavenumber resolution.

5.2.2.3 FTIR Index Calculation

Various methods are used to quantify the ageing related evolutions of the bitumen spectra at the sulfoxide (≈1030 cm^{-1}) and carbonyl (≈1700 cm^{-1}) wavenumbers specifically. In order to minimise the influence of sample thickness and IR radiation path length, the general principle is to normalise the absorption values V(1030) and V(1700) obtained for these specific wavenumbers by calculating a ratio of a value obtained at a reference wavenumber V(v_{ref}) which is supposed not to be significantly affected by oxidation. The mentioned absorption value can be the amplitude at wavenumber v or the area under the curve between two wavelengths. Thus, the generic semi-quantitative formulae for the sulfoxide index Iso (5.2) and the carbonyl index Ico (5.3) are given by:

$$Iso = \frac{V(1030)}{V(v_{ref})} \tag{5.2}$$

$$Ico = \frac{V(1700)}{V(v_{ref})} \tag{5.3}$$

with:

$V(v)$ value (amplitude or area) obtained for the wavenumber ν

The methyl (CH_3) and ethylene groups (CH_2) are generally considered not to be significantly affected by oxidation and their specific absorption bands (≈1375 and ≈1460 cm^{-1}) are usually taken as reference wavenumber v_{ref}.

From this generic form, two main types of methods are applied according to the type of values extracted from the spectrum for the index ratio calculation:

– amplitude methods: the values used for index calculation are the amplitudes of the spectrum at chosen wavenumbers. Peak determination procedures can significantly differ from one laboratory to another,

– area methods: the values used for index calculation are the areas obtained by integration of the spectrum on wave bands centred on given wavenumbers. Procedures can differ as regards to the bands limits and the baselines chosen for the integration.

5.2.2.4 Application of FTIR to Reclaimed Asphalt Characterisation

From this overview of the ageing mechanism and FTIR fundamentals some general comments can be made with regards to the potential application of the FTIR to Reclaimed asphalt (RA) characterisation and recycling.

– The ageing process of a binder in a mixture is dependent on the type of binder (crude oil origin, distillation process) and the type of aggregate used. Direct FTIR oxidation index comparisons are *a priori* limited to the same bitumen-aggregate combination.
– For the same bitumen-aggregate combination, the wide range of possible index calculation methods actually applied in the different laboratories hinders direct inter-laboratory index comparison.

5.3 RILEM TC ATB TG5 Round Robin Test (RRT)

In the framework of the RILEM TC ATB TG5 (Partl et al. 2013) aiming to devise an ageing method for the production of reproducible RA in laboratory, repeated FTIR, penetration, softening point and Dynamic Shear Rheometer (DSR) measurements were made on recovered binders from mixture samples in 9 different European laboratories (Table 5.1) after 6 controlled ageing steps:

– E0: mixing
– E1: STA (loose mix, 4 h at 135 °C in ventilated oven)

Table 5.1 List of the laboratories participating to the RILEM project. Names with (*) correspond to the 4 complete sets of FTIR data used in this study

Name (Acronym)	Country
Artesis University Antwerp (AHA)	Belgium
Delft University (DU)	Netherlands
*Danish Road Institute (DRI)**	*Denmark*
*ISBS**	*Germany*
*IFSTTAR**	*France*
LRPC-Aix	France
*NTEC**	*United Kingdom*
SINTEF	Norway
Total	France

– E2: LTA (loose mix, 2 days at 85 °C in ventilated oven)
– E5: LTA (loose mix, 5 days at 85 °C in ventilated oven)
– E7: LTA (loose mix, 7 days at 85 °C in ventilated oven)
– E9: LTA (loose mix, 9 days at 85 °C in ventilated oven)

The mix used was asphalt concrete with 0/10 mm aggregate gradation and 5.4% of 35/50 penetration grade bituminous binder. Two sets of mixture samples were distinguished according to their production mode: laboratory mix (batch B1) and plant mix (batch B3). For the two batches, two FTIR measurements were made for the 6 ageing steps in four laboratories (L1, L6, L7, and L9). These data were all obtained in transmission mode.

The raw data of the 96 FTIR spectra were compiled in a database, thus allowing post processing of the data. In order to evaluate the actual method dependence of the index results obtained, four carbonyl index calculation methods were applied to this database.

5.3.1 Different Index Calculation Methods Applied

5.3.1.1 RILEM Method (Ico)

The method initially used for area calculation of the carbonyl band in the RILEM RRT was an area method with fixed area limits and a baseline drawn between the values at these limits (Fig. 5.1). For the Ico method only the areas above the base line were taken into account (positive area).

– fixed carbonyl area (A_{Ico}) limits: 1660 and 1753 cm^{-1}
– fixed reference area (A_{ref}) limits: 1350 and 1525 cm^{-1}

This method is derived from a method adopted at IFSTTAR (Mouillet et al. 2009).

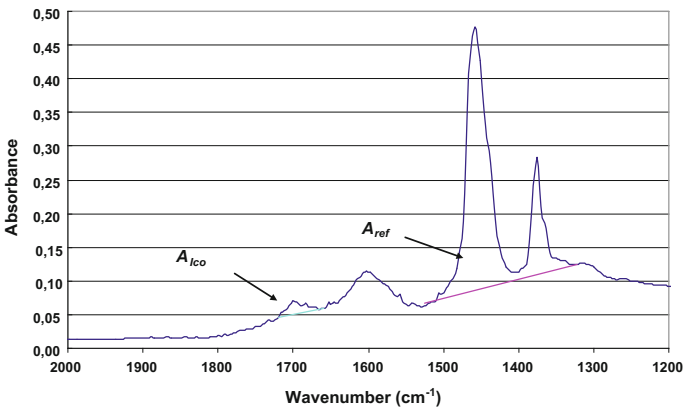

Fig. 5.1 Determination of the areas for the RILEM Ico index calculation

5.3.1.2 BRRC Methods (A1700 and H1700)

These procedures, previously developed to treat FTIR spectra taken in solution (Pierard 2013), consist of two steps: a deletion of the blind zone (specific to spectra taken in solution to delete the zone where the solvent is absorbing) and normalisation of the interesting part of the spectrum (400–2000 cm^{-1}).

As RILEM FTIR spectra were taken on bitumen in solid state, only the normalisation step was applied. This step is crucial to be able to compare the intensity or the area of different peaks and takes place as follows.

Firstly, the baseline is corrected to remove the slope in the zone of interest. This slope is due to the scattering of the infrared beam by the sample and to the FTIR method used. The baseline correction consists of two steps. In the first step, two points corresponding to the lowest absorbance in this zone are fixed in reproducibly flat parts of the absorption line (Stuart et al. 1996). These two points at 1886 and 706 cm^{-1} were defined by comparison of all the available RILEM spectra and by identification of wavenumbers where the intensity pattern is flat, showing a low absorption and do not change from one spectrum to another one. These points are not the same as the ones usually used for spectra taken in solution (1885 and 459 cm^{-1}). This is due to the fact that each laboratory carries out the characterisation of the aged recovered binder following its own FTIR protocol (different path lengths, zones of measurements, times of acquisition, etc.) and due to the lower resolution of RILEM spectra taken on solid samples. The next step consists of determining the linear equation between these two points and correcting the intensity of the spectrum between 2000 and 400 cm^{-1}. This means subtracting from each point of the spectrum the value calculated for that wavenumber by using the linear equation. In this way, the zone of interest of the spectrum is brought back to the zero line.

Secondly, the intensities of each peak on the FTIR spectrum are standardised by taking the absorbance of the peak with a maximum intensity in the normalisation zone at 1.2 and by recalculating the other values of the spectrum by applying the same correction factor. This peak, characteristic mainly of CH_2, is situated at 1458 cm^{-1} and is relatively insensitive to binder ageing.

Figure 5.2 shows the impact of the BRRC standardisation procedure on the bitumen spectrum.

The binder oxidation is determined from the carbonyl oxidation peaks at 1700 cm^{-1} (Pierard et al. 2010). In this publication, the area of interest was the carbonyl function by measurements of the height of the peak at 1700 cm^{-1} (H1700) and its area A1700. A1700 is the area between 1530 and 1770 cm^{-1} (new baseline between these two wavenumbers). Due to the overlapping peaks at 1700 cm^{-1} (carbonyl functions) and at 1600 cm^{-1} (aromatic functions); a preference has been given to consider the surface area between the two limits mentioned above (Verhasselt and Puiatti 2004).

Figure 5.3 shows the measurements of the peak height H1700 and peak area A1700 for the carbonyl content.

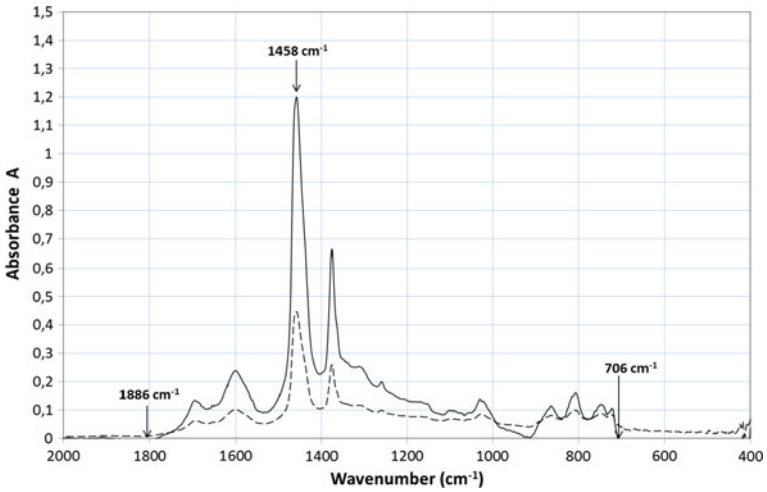

Fig. 5.2 FTIR spectrum before (dotted line) and after normalisation (solid line)

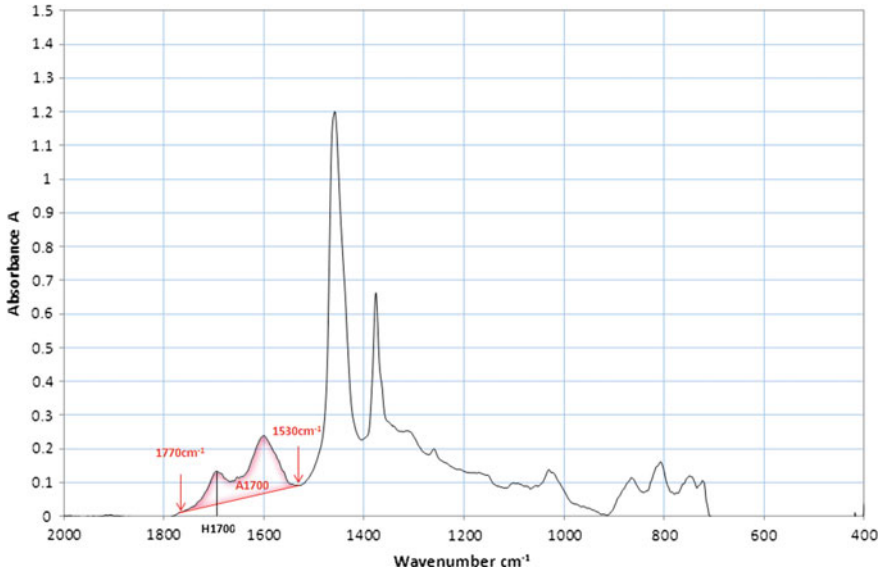

Fig. 5.3 Peak height and peak area characteristic of the oxidation state of the bitumen (carbonyl content)

5.3.1.3 Deconvolution Method (Decon)

In order to try to more precisely isolate the peak evolution for the very specific wavenumbers selected, an alternative method to the area and amplitude methods was also tested. This method consists of fitting the spectrum with a series of 5 Lorentzian functions (5.4) centred on wavenumbers 1700, 1460, 1375, 1600 and 1340 cm^{-1} and a parabolic function.

$$y = \frac{2A}{\pi}\left(\frac{w}{4(v - v_c)^2 + w^2}\right) \tag{5.4}$$

with:

A area of the function
w width at half the maximum height
v_c location of the peak (mode of the distribution)

The combination of the parabolic function and the Lorentzian function centred at 1340 cm^{-1} is intended to fit the base curve of the spectra while the other 4 Lorentzian functions are used to fit the specific peaks. The parameters A_i and w_i of the 5 Lorentzian functions and the parameters of the parabolic function are determined using a least squares adjustment method (Fig. 5.4).

The calculated carbonyl index obtained by deconvolution is the peak amplitude of the Lorentzian function centred at 1700 cm^{-1} divided by the sum of the peaks amplitudes of the Lorentzian functions centred at 1460 and 1375 cm^{-1}.

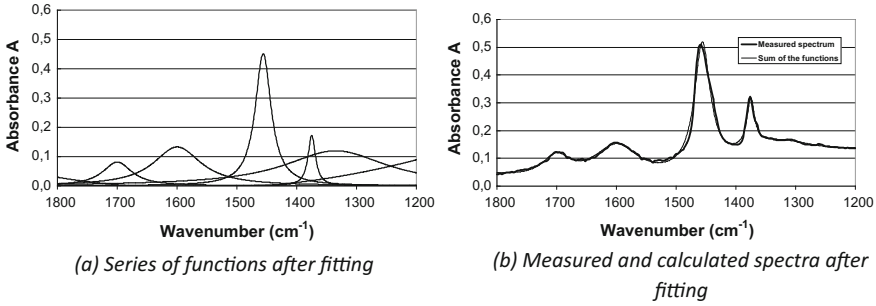

(a) Series of functions after fitting

(b) Measured and calculated spectra after fitting

Fig. 5.4 Example of spectrum fitting with 5 Lorentzian functions and a parabolic function

5.3.2 *Comparison of the Oxidation Indicators Obtained by 4 Different Methods of Calculation*

An appropriate ageing-oxidation indicator should be able to satisfy different criteria. In the framework of this study, it was assumed that this method must:

1. increase with the ageing level: the longer the ageing time, the higher the oxidation indicator;
2. display a limited spread of the results for a given ageing time;
3. present a sufficient sensitivity to the ageing state to be a suitable indicator of the ageing state;
4. exhibit good accuracy.

Figure 5.5 can be used to compare the evolution of the four ageing indicators (Ico, A1700, H1700 and Deconvolution) as a function of the steps of the RILEM ageing test, and to evaluate the most appropriate oxidation indicator to understand the ageing stages of a binder. This can be done because each oxidation indicator is determined from the same data set of FTIR spectra. These different values are the results of the standardisation and calculation method used for each indicator (RILEM method Ico, BRRC method A1700 and H1700 or Deconvolution).

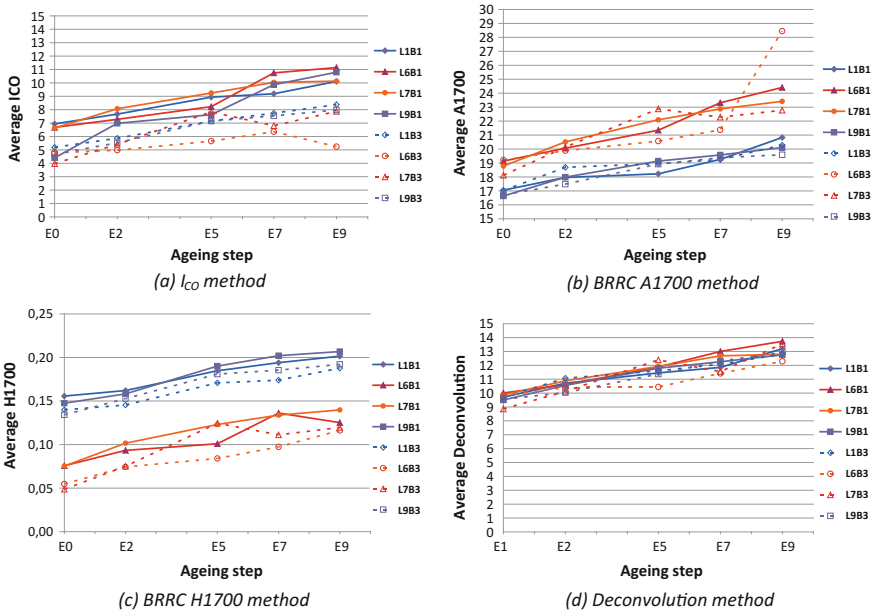

Fig. 5.5 Evolution of different ageing indicators (average of two repetitions) in function of the ageing steps separately for the laboratory (B1) and the plant (B3) mixes

From Fig. 5.5, it can be observed that globally each ageing indicator increases with ageing time. However, the Ico value sometimes does not really increase with the ageing time. A comparable decrease is generally not observed for the 3 other indicators.

For Ico (Fig. 5.5a) a batch effect can be observed. A shift of the evolution of the ageing indicator is observed between the batches produced in laboratory (B1) and in plant (B3).

For the A1700 (Fig. 5.5b) and H1700 (Fig. 5.5c) indicators, a shift is observed between two groups of laboratories (L1+L9, L6+L7). But this laboratory effect has a reverse influence on the two ageing indicators with L1+L9 showing higher H1700 and L6+L7 higher A1700.

For the Deconvolution method (Fig. 5.5d), neither a laboratory nor a batch effect is observed.

In the case of the Ico value, the data shift between batches produced in the laboratory (B1) and in the plant (B3) can be explained by the fact that after recording the FTIR spectrum of the binder, the content of the oxygenated species at 1700 cm^{-1} is determined by measuring the area of characteristic absorption bands in order to integrate several vibrations of the same type (for example, the C=O ester, acid, ketone and lactone vibrations between 1800 and 1635 cm^{-1}). As the two batches B1 and B3 are produced under different oxidation conditions (laboratory and in the plant), different C=O bonds could be created leading to a broadening of the area of the band around 1700 cm^{-1}. Conversely, the Deconvolution method could be considered as a selective frequency filter, which is blind to evolutions of the spectrum outside and even very near the selected vibration modes.

The data shift between laboratories observed by using the BRRC calculation method can be explained by the intensity of the original FTIR spectra. The comparison of the initial maximum absorbance measured for the peak at 1458 cm^{-1} on which the FTIR spectra are normalised can explain this separation between the laboratories. In fact for lab6 and lab7, the absorbance of this peak, after the baseline correction and before the normalisation of the spectra by bringing the intensity of this peak to 1.2, is three to four times lower than those of the two other laboratories (Table 5.2). The average intensity is around 0.1 for lab6 and lab7 and between 0.3 and 0.4 for lab1 and lab9. This low absorbance is reflected on each entire spectrum for lab6 and lab7. The consequence of this is a low definition spectrum and a loss of precision of the calculated ageing indicator (A1700 and H1700): the noise is

Table 5.2 Intensity of the peak used for the normalisation of the FTIR spectra following the BRRC method: average of these intensities, coefficient of variation (CV = standard deviation/average), minimum and maximum values for each laboratory

Laboratories	H1458			
	Average	CV (%)	Min	Max
Lab1	0.441±0.046	10	0.230	0.587
Lab9	0.324±0.061	19	0.226	0.470
Lab6	0.109±0.004	4	0.097	0.115
Lab7	0.110±0.003	3	0.104	0.116

amplified by the multiplication factor used for standardisation and decreases the precision of the indicator. This shows the need for a standard describing the acquisition of a FTIR spectrum of bitumen. For FTIR on solid samples the absorbance at 1458 cm^{-1} can be fixed to a minimum value of 0.4 (as obtained for lab1 and lab9). This minimal absorbance with a sufficient resolution of the spectrum can be reached by adapting the protocol for taking the spectra (method, number of runs, and time of acquisition).

The dispersion of an ageing indicator for a given ageing time varies in function of the calculation method used. The lowest dispersion is obtained with the Deconvolution method while the Ico method gives the highest dispersion. The BRRC method gives an intermediate dispersion which seems less pronounced for A1700 than for H1700.

To quantify the sensitivity and the precision of each indicator to ageing, Fig. 5.6 shows the relative average increase of each indicator after 9 days of the RILEM ageing.

It can be observed in Fig. 5.6 that the sensitivity to ageing of the Ico and H1700 indicators is the largest. These indicators can increase more with ageing but their standard deviation is also very high, leading to a loss of the sensitivity to the ageing state in certain cases. Despite the high sensitivity to the ageing, these two indicators (Ico and H1700) are less appropriate to evaluate ageing stage of bitumen. In the case of A1700 and the Deconvolution method, the sensitivity to ageing is lower but the variation of the results around the mean value is low. So, the use of these two indicators (A1700 and Deconvolution) seems to be preferable to estimate the evolution of the ageing state of bitumen. The Deconvolution indicator is more sensitive to ageing but the results are less precise. For the A1700 Indicator, the sensitivity to ageing is a bit less but the results are more precise.

The linear regression between the results obtained for A1700 and the Deconvolution indicator confirms a good correlation between these two indicators. It means that both indicators can be used and will show the same evolution of the ageing degree (Table 5.3).

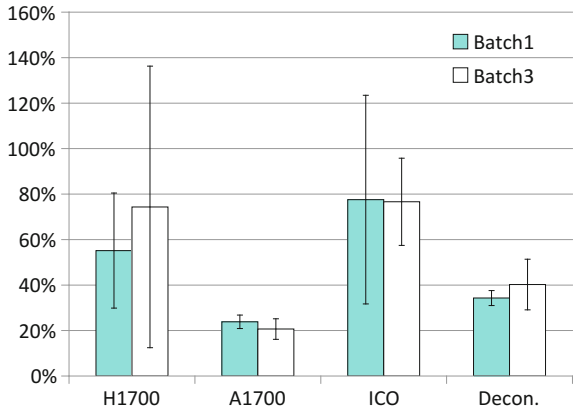

Fig. 5.6 Relative average increase of each indicator after 9 days of the RILEM ageing protocol compared to before ageing test

Table 5.3 Linear regression coefficients between A1700 and the Deconvolution indicators (A1700 = a·Decon +b) as calculated for the average values of each indicator at a given time while using the RILEM protocol (0 to 9 days)

Laboratory	Batch	a	b	R^2
1	1	1.082	6.344	0.96
6		1.397	5.102	0.99
7		1.512	3.947	0.99
9		1.045	6.799	1,00
1	3	0.993	7.465	0.98
6		1.351	6.037	0.91
7		1.058	9.296	0.89
9		0.848	8.883	0.95

5.3.3 Recommendations on the FTIR Ageing Indicators

From the study presented above, it is obvious that the conclusions of the analysis performed on the database of raw spectra can differ considerably according to the method adopted to calculate an FTIR oxidation index. For an FTIR oxidation index to be efficiently used for RA characterisation and to be an indicative parameter between laboratories, harmonisation of the methods is clearly needed. For improvement, the following suggestions can be made with regards to the data acquisition:

- harmonisation of the FTIR sample preparation procedure,
- harmonisation of the raw data format: number of individual scans averaged, wavenumber range, wavenumber resolution, intensity level range.

With regards to the ageing index calculation method, it is clear that this method should also be harmonised. However, the choice of a relevant method is not straightforward, as each method tends to reflect different aspects of the oxidation process. From the study above, the following general trends can be observed. Area methods mirror the evolution of a rather broad range of bonds. Therefore, they seem rather sensitive to temperature changes during the ageing process. On the other hand, methods with very specific frequency selections, such as the Deconvolution method, seem to be relatively insensitive to temperature changes. The (H1700) method could be considered as a compromise between these two cases.

However, for RA characterisation, an ageing indicator reflecting the physical property evolution of the binder is needed. The RILEM database offers an opportunity to evaluate this potential link between a given ageing index and the physical properties.

5.4 Effect of Ageing on Basic Physical Properties

While FTIR ageing indices are related to the chemical properties of materials, it was of interest to compare the degree of oxidation as assessed by the FTIR results with the basic physical properties. This should help to further strengthen a preferred method for harmonising the interpretation of FTIR results.

The carbonyl index, calculated by both the Ico and the Deconvolution methods were used and compared with basic physical properties. This analysis was conducted using the data generated during the RRT for the laboratory mixture ageing protocol (Partl et al. 2013). At the same time as FTIR measurements, physical properties were measured on both the laboratory mixed batch (B1) and the asphalt plant production batch (B3) with:

- Penetration at 25 °C in accordance with EN 1426 (EN 1426), which reflects the consistency of the bitumen at ambient temperature.
- Ring and ball softening point in accordance with EN 1427 (EN 1427), which reflects the consistency of the bitumen at higher temperatures.

5.4.1 Relationship Between Ageing Indicators and the Basic Physical Properties

In Fig. 5.7, the penetration and softening point values are plotted versus the carbonyl index calculated by both the Ico and the Deconvolution method.

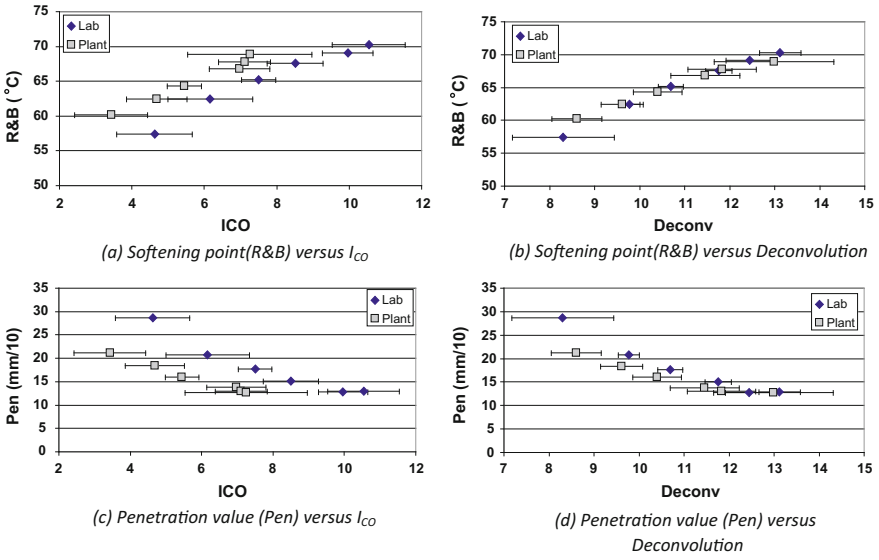

Fig. 5.7 Penetration and softening point values versus carbonyl index calculated by both the Ico (**a**, **c**) and Deconvolution (**b**, **d**) method (error bars represent ±1 standard deviation, n = 8)

For the Ico method, the laboratory (batch 1) and the plant (batch 3) mixture points are located on two clearly separate lines (Fig. 5.7a and c) while they are almost on the same line for the Deconvolution method (Fig. 5.7b and d). Therefore, the evolution of the penetration and softening point values of the binder during the ageing can be fairly well estimated from the FTIR Deconvolution index values using a unique relationship for both batches. This is not the case for the Ico index. For the limited set of data used, a method with a very specific frequency selection as the Deconvolution appears to allow a better prediction of the basic physical properties of the binder.

5.4.2 Conclusion on the Basic Physical Properties

This simple analysis shows that both FTIR index calculation methods, Ico or Deconvolution, follow the same trend as the softening point and the opposite trend to the penetration value. However, from these data it is not possible to make a more general conclusion on the correlation between these chemical indexes and the rheological properties of the binder.

5.5 Effect of Ageing on Rheological Properties

In the framework of the TC ATB TG5 round robin test, DSR measurements were made on the recovered binder to assess the changes on its rheological properties with ageing. For each ageing step, frequency sweeps were carried out at 11 equally logarithmic spaced frequencies from 0.1 to 10 Hz at 7 temperatures from −5 to 55 °C. This means at least 77 values of the complex shear modulus $|G^*|$ and its phase angle (delta) for each lab sample – and ageing combination. On account of this huge amount of data (about 3000 couples of values for $|G^*|$ and the phase angle), the analysis made by the TC ATB TG5 was in that first stage limited to one of these values (25 °C and 0.4 Hz), which is the condition allowing to calculate the penetration value by the Saal and Labout's equation.

In order to get a comprehensive overview of the trends for the complete DSR database and overcome the processing problems induced by the large amount of data, a new analysis is made with the raw values pre-processed through rheological model fitting. The basic idea is to concentrate the information of the frequency and temperature sweeps in a limited number of model parameters describing the properties of the binder in the time-temperature domain.

5.5.1 Choice of a Model

Several studies carried out in different countries demonstrate that the Huet modified model is one of the best suited rheological models for bitumen (Such 1983; Olard 2003; Yusoff 2012). For the purpose of our study, it also offers the additional benefit of requiring only 6 parameters for modelling both |G*| and the phase angle in the entire time-temperature domain. It is a combination of one spring, two parabolic creep elements and one dashpot, all placed in series with a coefficient regulating the balance between the two dashpots (Figs. 5.8 and 5.5).

The IFSTTAR software Visco-analyse (Chailleux et al. 2006) is used to fit the model on the experimental data. This software uses the approximation of Booj and Thoone of the Kramers-Kroning relations for the construction of the master curve at 10 °C and the model parameters are fitted using a trust region reflective algorithm.

After this pre-processing, the DSR database can be analysed as the evolution of 6 parameters with ageing for different lab/mixing process combinations. This analysis is conducted on all the combinations with complete DSR results:

- original binder for LAB1 and LAB8
- lab mix for 4 labs (LAB1, LAB4, LAB7, LAB8)
- plant mix for 2 labs (LAB1, LAB7)

5.5.2 Evolution of the Model Parameters with Ageing

The values of the 6 model parameters at the different ageing steps are plotted in Figs. 5.9, 5.10, 5.11, 5.12, 5.13 and 5.14. The physical meaning of each parameter and their trends with ageing are discussed separately.

G_∞ parameter

This parameter accounts for the spring stiffness. It represents the value of G* at infinite frequency also termed as glassy modulus. It remains almost constant for the

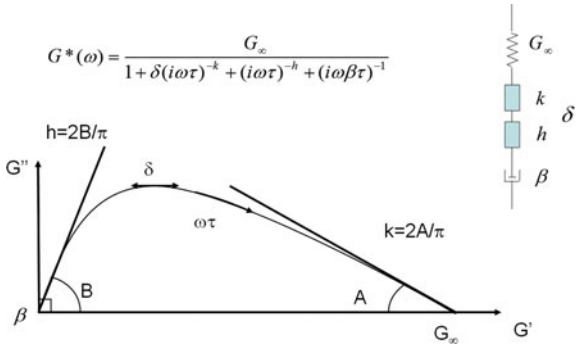

Fig. 5.8 Huet modified model, equation and representation in the Cole-Cole plot

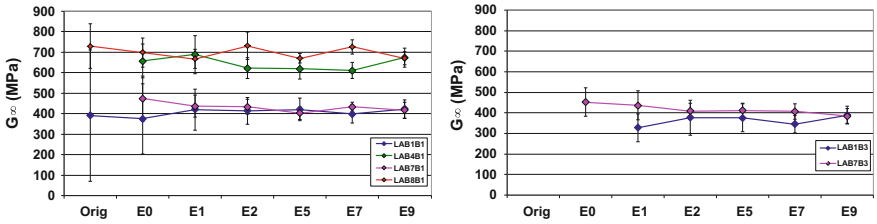

(a) batch 1 (lab mix) *(b) batch 3 (plant mix)*

Fig. 5.9 Evolution of G_∞ versus ageing steps

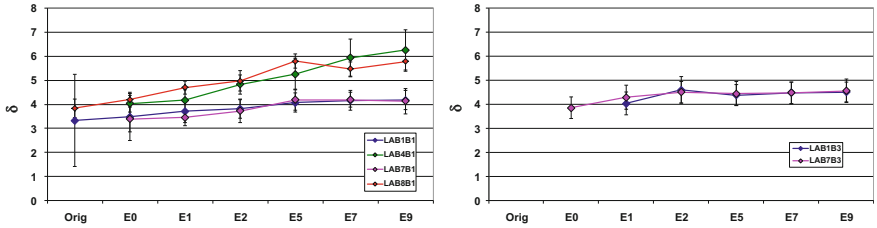

(a) batch 1 (lab mix) *(b) batch 3 (plant mix)*

Fig. 5.10 Evolution of δ versus ageing steps

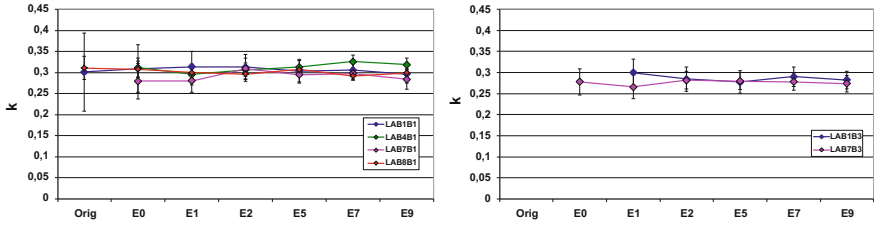

(a) batch 1 (labmix) *(b) batch 3 (plant mix)*

Fig. 5.11 Evolution of k versus ageing steps

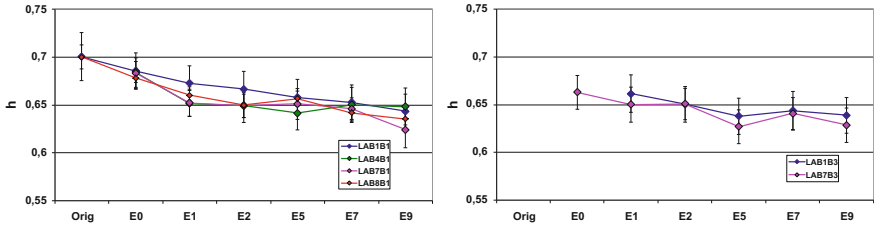

(a) batch 1 (lab mix) *(b) batch 3 (plant mix)*

Fig. 5.12 Evolution of h versus ageing steps

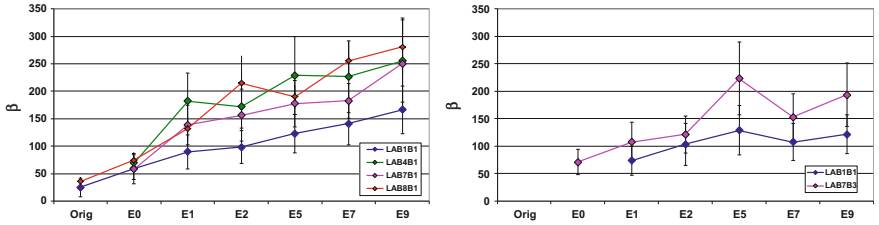

(a) batch 1 (lab mix) *(b) batch 3 (plant mix)*

Fig. 5.13 Evolution of β versus ageing steps

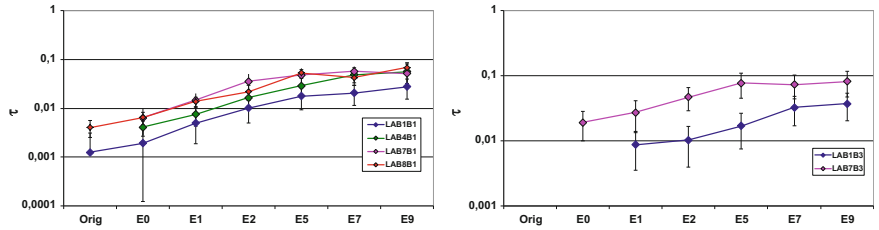

(a) batch 1 (lab mix) *(b) batch 3 (plant mix)*

Fig. 5.14 Evolution of τ versus ageing steps

4 laboratories regardless the ageing step and the mixing process (Fig. 5.9). However, a strong laboratory effect is detected with an average glassy modulus of ≈700 MPa obtained for Lab4 and Lab8 (which seems consistent with usual values for binders) while an average value of ≈400 MPa is obtained for the two other laboratories (Lab1 and Lab7). It should be noted that a variation of the value of G_∞ in the expression of G* (Fig. 5.8) represents a homothetic transformation of centre 0 in the Cole-Cole plot. In this way, the laboratory effect on G_∞ could be interpreted as a constant relative difference in all the |G*| measurements between the two groups of laboratories possibly related to difference in compliance, measurement conditions or calibration between the DSR devices. The other parameters, accounting for the shape of the model response in the Cole-Cole plot would not *a priori* be affected by this laboratory homothetic dependency.

δ parameter

The δ parameter represents the balance between the two parabolic elements k and h at medium temperatures or frequencies. The general trend is for δ to increase with ageing, reflecting a growing influence of the k parabolic element (Fig. 5.10). The amplitude of this variation seems to be affected by a laboratory effect, with the same two groups of laboratories noticed for the G_∞ parameter. This suggests a slight interdependence between the δ and the G_∞ parameters contrary to what was *a priori* assumed above. Thus, δ could be device dependent like G_∞.

k parameter

The k parameter, first parabolic element, is proportional to the slope of the model in the Cole-Cole plot at low temperature and/or high frequency (proportional to the ratio $\Delta G''/\Delta G'$). An almost constant average value of ≈ 0.3 is obtained for all laboratories, mixing procedures and ageing steps (Fig. 5.11). The ageing process shows no effect on this parameter.

h parameter

The h parameter, second parabolic element, is proportional to the slope of the model in the Cole-Cole plot at high temperature and/or low frequency (proportional to the ratio $\Delta G''/\Delta G'$). The trend for h value is consistent in all cases, with a decrease from 0.70 to 0.63 showing an effect of the aging process (Fig. 5.12).

β parameter

The dashpot parameter β represents the viscosity of the model at very high temperatures or very low frequencies. The tendency observed is a substantial increase with ageing, but there are laboratory differences within results, as well as possible plant/laboratory manufacturing effects (Fig. 5.13). One can notice a random increase/decrease experienced by the plant mixture of LAB7B3 on the ageing step E5, which may indicate a possible labelling error of the sample.

τ parameter

The frequency multiplier τ at 10 °C seems to grow with almost the same exponential rate for all laboratories when going through the ageing process but the curves show significant shifts between laboratories on the log(τ) axis (Fig. 5.14). The disposition of this parameter to change through the ageing phases is marked, being the main parameter affecting the value of $|G^*|$. From a mechanical point of view, the ageing process of the binder from the virgin step to E9 step is approximately equivalent to multiplying the angular frequency ω by a factor of 14.

5.5.3 *Discussion of the Trends Observed for the 6 Parameters*

The same trends are observed for the 6 parameters in all the laboratories but with different magnitude from one laboratory to another. These trends are summed up and classified according their ageing or laboratory dependence in Table 5.4.

The glassy modulus G_∞ is not affected by ageing. This is in accordance with the previous finding of Yusoff (2012) who suggested a constant value (G_∞ = 1000 MPa) for modelling unaged and aged unmodified bitumen. The laboratory dependence of G_∞ seems to confirm the findings of Mangiafico (2014) who detected a strong device effect between 2 different measurement devices, DSR and

Table 5.4 Ageing and laboratory dependence of the parameters

	Ageing dependent	Ageing independent
Lab dependent	δ, β, τ	G_∞
Lab independent	h	k

Metravib. Abnormal low G_∞ values for the DSR were attributed to experimental limitation of this device at low temperature.

The k parameter could be considered as a constant value independent of ageing and laboratory effect. This is again in accordance with the findings of Mangiafico (2014) and Yusoff (2012) Nevertheless, Yusoff suggests k = 0.22 while k ≈ 0.3 is obtained in this study.

The h parameter could be considered as laboratory independent and slightly dependent of ageing. The decrease observed from 0.70 to 0.63 is compared to the constant value h = 0.55 suggested by Yusoff (2012).

The 3 other parameters δ, β, τ are laboratory dependent but their evolutions follow the same increasing trends with ageing in all laboratories. This ageing dependence is in accordance with the results of Yusoff (2012) for β, τ but not for δ which he assumed to be a constant (δ = 2.30).

The general trends observed in all the laboratories are summed graphically in the Cole-Cole plot in Fig. 5.15.

5.5.4 *Conclusion on Rheological Properties*

This analysis confirms the laboratory or device dependence of the complex shear modulus measurements already observed by Mangiafico (2014). Hence, it is very likely that a substantial enhancement of the reliability of the data could be achieved through device or experimental protocol improvements. In the same way, the fitting of the model parameter could be significantly improved (notably for G_∞ and k) if the range of the data were extended to lower temperatures and higher frequencies.

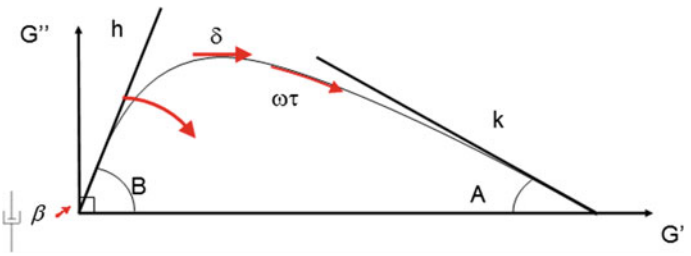

Fig. 5.15 General trends for the 4 ageing dependent model parameters

Nevertheless, the combination of complex shear modulus measurements and a Huet modified model could be a useful tool for recycling studies as the effect of ageing on the rheological properties of a binder over the complete time-temperature domain could be represented by the evolution laws of only 4 parameters.

5.6 Attempt Toward a Detection of Colloidal Structure Changes

5.6.1 Relationship Between Rheological Data and Colloidal Structure

A relationship between the rheological properties and the Molecular weight distribution (MWD) of bitumen is generally assumed in the literature. Hence, a relationship between the parameters of a Huet modified model and the colloidal structure of bitumen should be expected. Yusoff (2012) did indeed note that the presence of higher asphaltene contents plays a significant role to determine the β value (viscosity at very high temperatures or very low frequencies). Along the same lines, on the basis of a method proposed by Zanzotto et al. (1999), Themeli et al. (2015) developed a method (δ-method) for determining an apparent molecular weight distribution from the differentiation of the phase angle curve fitted with a Huet modified model. The database of the TC ATB TG5 with DSR measurements fitted with a Huet modified model gives a unique opportunity to assess the potential of this method through successive ageing steps.

5.6.2 Application of the δ-Method to the DSR Database

The basic assumption of the δ-method is that the phase angle for a given frequency is proportional to the fraction of relaxed molecules at that frequency. A relationship can be established between the frequency and the molecular weight. Thus, the master curve of the phase angle is assimilated to the cumulative distribution of the molecular weight. An Apparent Molecular Weight Distribution (AMWD) is then obtained from the differentiation of the phase angle master curve. This differentiation requires a continuous curve, so the data should be fitted with a continuous model, and the Huet modified model was chosen for this purpose as best suited. As the DSR measurements are already fitted by this model, the application of the δ-method to the database is straightforward and only requires the differentiation of the phase angle master curves calculated from the already available parameters and a transformation of the frequency axis into an apparent molecular weight axis using an experimental relationship established by Zanzotto et al. (1999) on regular bitumen. It should be noted that the δ-method only requires the phase angle as input

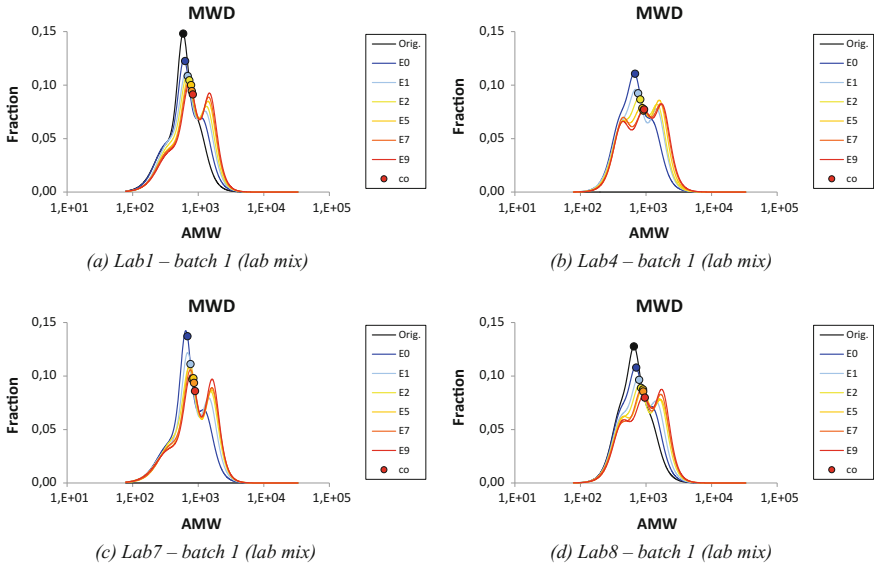

(a) Lab1 – batch 1 (lab mix) *(b) Lab4 – batch 1 (lab mix)*

(c) Lab7 – batch 1 (lab mix) *(d) Lab8 – batch 1 (lab mix)*

Fig. 5.16 Evolution of the apparent molecular weight distribution with ageing

data. As the angle measurements can be reasonably regarded as not affected by the compliance or the calibration of the DSR devices, the method also appears as a possible way to at least partly overcome this experimental bias.

The AMWD along with the cross-over point (CO: point where the phase angle is equal to $\pi/4$ i.e. $G'=G''$) for the laboratory mix (batch 1) are plotted for each laboratory at the successive ageing steps in Fig. 5.16.

5.6.3 *Discussion on the Trends Observed for the AMWD*

The general trend observed in all the laboratories is a gradual shift from a mono-modal to a bi or tri-modal distribution of the molecular weight according to the ageing steps. In particular, a growing peak appears in the high molecular weights. This peak is related to the value of β and the observed evolution tends to confirm the relationship between β and the asphaltene contents already mentioned by Yusoff (2012). The trend is also in accordance with the findings of Themeli et al. (2015) on a 50/70 bitumen at different ageing steps (original, RTFOT, RTFOT +PAV). According to Themeli et al. (2015), in terms of colloidal structure of the binder, the 3 modes could be interpreted as 3 different molecular populations, namely in increasing average molecular weight order: the intermicellar environment, the individual micelles of asphaltenes and the agglomerates of asphaltenes. In

this framework, the ageing effect could be interpreted as a shift from a continuum to separate intermicellar, micelles and agglomerates populations. This interpretation is summed up in Fig. 5.17.

The evolution of the cross-over frequency according to the ageing step is plotted is Fig. 5.18. The decrease of the cross over frequency with ageing is in accordance with the literature.

This is to compare to the shift of the cross-over point toward high molecular weights (i.e. low frequencies) observed in Fig. 5.16. The evolution of the cross-over frequency accounts for the evolution of only one point of the total AMW distribution. Thus, compared to the monitoring of the cross-over frequency, the δ-method could be seen as an extension to the complete time domain combined with a structural interpretation.

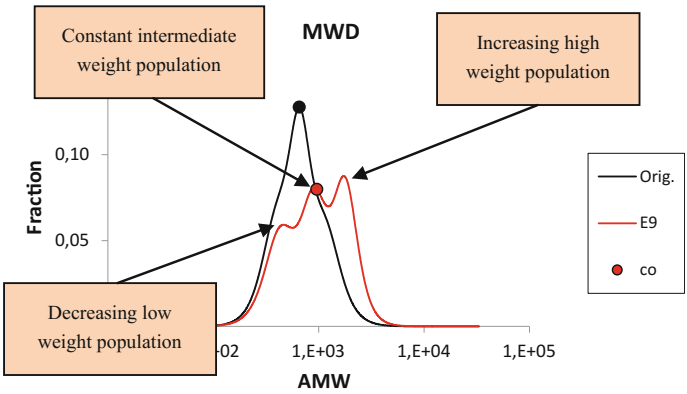

Fig. 5.17 Interpretation of the general trend of AMWD with ageing

Fig. 5.18 Evolution of the cross-over frequency with ageing

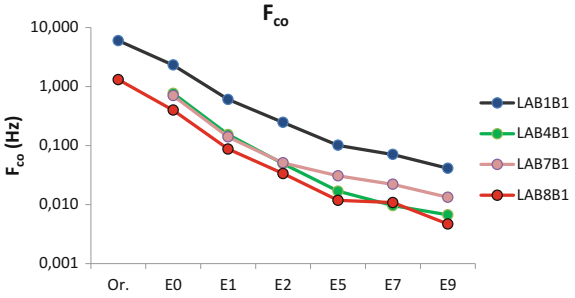

5.6.4 *Sensitivity of the δ-Method to the Laboratory Effect*

In order the assess the supposed independence of the δ-method results to the experimental inter-laboratories bias observed on the DSR measurements, the AMWD obtained in the 4 laboratories are plotted in the same graph for each aged step in Fig. 5.19.

The AMW distributions are rather similar except for a peak noticeably higher on the intermediate molecular weight for Lab1 and Lab7. This is due to the unexpected device dependence of the δ, β and τ parameters already mentioned in § 5.5.2. Thus, the δ-method is actually moderately device dependent.

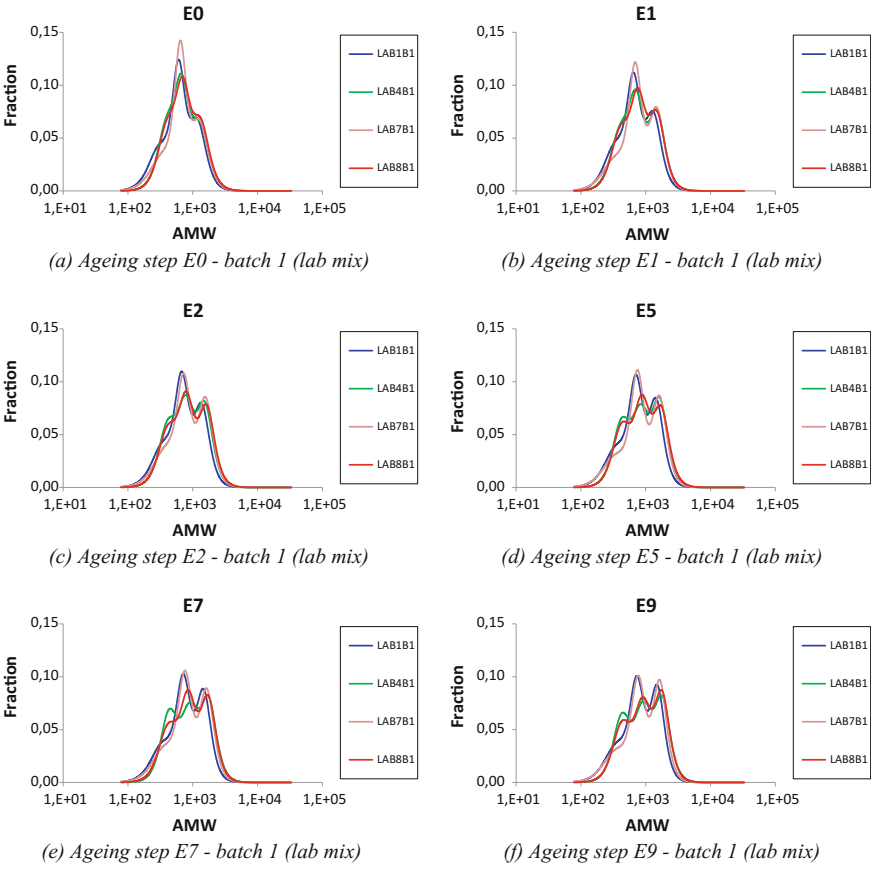

(a) Ageing step E0 - batch 1 (lab mix)

(b) Ageing step E1 - batch 1 (lab mix)

(c) Ageing step E2 - batch 1 (lab mix)

(d) Ageing step E5 - batch 1 (lab mix)

(e) Ageing step E7 - batch 1 (lab mix)

(f) Ageing step E9 - batch 1 (lab mix)

Fig. 5.19 Apparent molecular weight distribution for the 4 laboratories at each ageing step

5.6.5 *Confirmation of the δ-Method Results on Another Set of Data*

The application of the δ-method to the TC ATB TG5 DSR data seems to show that this method could be used to establish a link between the rheological properties and the colloidal structure of a binder. If this were confirmed, this would be a key instrument for recycling studies notably to exact the mixing laws and describe the rejuvenation processes. Although the results obtained above include 4 different laboratories, they are limited to a unique binder. In order to ascertain the conclusions and expand it to other binders it would be very valuable to apply the method to other independent sets of data.

5.6.5.1 Model Parameters from NTEC

In the framework of studies on the modelling of the linear viscoelastic rheological properties of bituminous binders, Yusoff (2012) fitted a whole set of measurements from the Nottingham Transportation Engineering Centre (NTEC) DSR database with a Huet modified model. This includes a group of 3 binders at 3 ageing steps and a group of 5 ageing steps for the same binder. The first group consists of a 80/100 penetration grade bitumen from a Middle East crude, a 80 penetration grade bitumen from a Russian crude and a 70/100 penetration grade bitumen from Venezuelan crude that underwent ageing processes via the rolling thin film oven test (RTFOT) and the pressure ageing vessel (PAV). The second group consists of a 160/220 bitumen unaged and aged at 1 h 15, 3 h, 5 h and 7 h with the RTFOT. Thus, the Huet modified model parameters published by Yusoff can be used as independent input data for a complementary δ-method analysis.

5.6.5.2 AMWD Results for NTEC Data

The results obtained with the NTEC data are plotted in Fig. 5.20.

The general trend for the 160/220 with ageing is strikingly similar to what was obtained with the TC ATB TG5 data (Fig. 5.20d). For the 3 other bitumen, a shift toward higher molecular weight is also observed but the transition from a mono-modal to a tri-modal distribution is much less obvious. This could be related to the fact that Yusoff chooses to set the h parameter to a constant value or to the type of crude oil. Nevertheless, these results obtained on different bitumen remain consistent with the results obtained on other binders by the TC ATB TG5 and by Themeli et al. (2015).

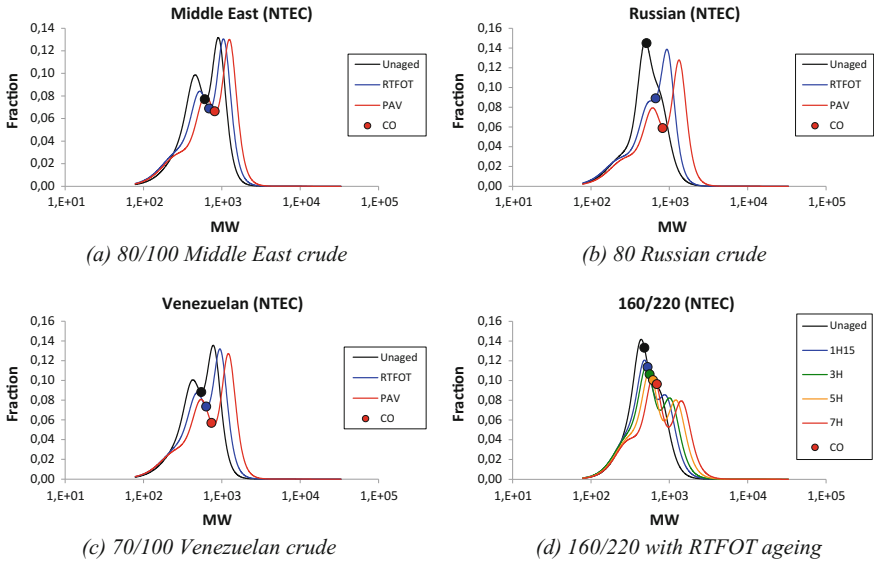

(a) 80/100 Middle East crude *(b) 80 Russian crude*

(c) 70/100 Venezuelan crude *(d) 160/220 with RTFOT ageing*

Fig. 5.20 AMWD results for NTEC data

5.6.5.3 Model Parameters from ENTPE

In the framework of another study on linear viscoelastic properties of bituminous mixtures with RAP, Mangiafico (2014) fitted a Huet modified model on a combination of DSR and Metravib data measured on binders extracted from bituminous mixtures with 20, 40 and 60% RAP content. Measurements were also made on the pure 35/50 added binder and on the binder extracted from the RAP. In addition to the analysis above on data from ageing processes, this new set of data offers an opportunity to assess the δ-method on data from a recycling process.

5.6.5.4 AMWD Results for ENTPE Data

The results obtained with the ENTPE data are plotted in Fig. 5.21.

The distribution is bi-modal for all the blends. Obvious trends are detected for the 2 peaks as the amount of RAP increases:

- the lower molecular weight peak decreases,
- the higher molecular weight peak increases,
- the 2 peaks are shifted toward the higher molecular weights.

This is to compare to the evolution of the SARA fractioning results obtained by Mangiafico (2014) on these binders plotted on Fig. 5.22.

As the amount of RAP increases:

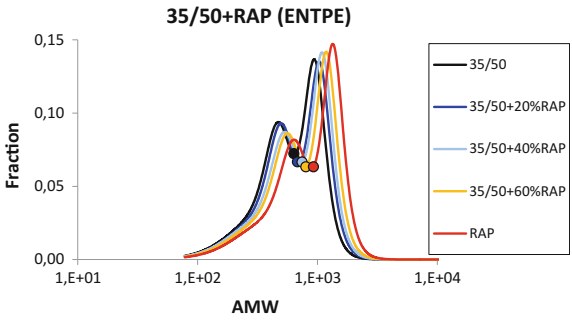

Fig. 5.21 AMWD results for ENTPE data (Mangiafico 2014)

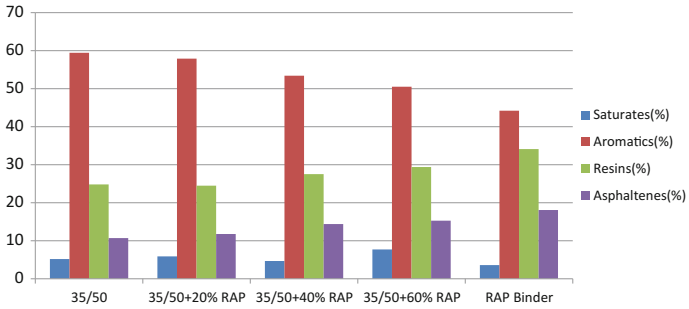

Fig. 5.22 SARA fractioning results for binder blends (Mangiafico 2014)

– the aromatics fraction decreases,
– the resins and the asphaltene fractions increase.

These results tend to confirm that a structural interpretation of ageing as well as recycling could be possible with the δ-method.

It should be noted that Mangiafico observed that the Huet modified model parameters of a blend of pure binders are the weighted averages of the parameters of the 2 blended binders (in log for τ). As the AMWD obtained with the δ-method is directly calculated from the Huet modified model parameters, this could indicate that no rejuvenating effect of the RAP binder is detected when pure bitumen is added (i.e. the AMWD of the RAP binder is not changed). The AMWD of the blend would be strictly the weighted average of the 2 AMWDs of the 2 blended binders.

5.6.6 Conclusion on the δ-Method

The application of the δ-method to the TC ATB TG5 DSR-data and to other sets of bitumen data tends to confirm its relevance for recycling studies and notably to exact

the mixing laws and to describe the rejuvenation processes. This method is probably moderately affected by the strong compliance or calibration effect affecting the DSR measurements. Nevertheless, the model parameters fitted on the data are not totally independent. These experimental biases are very likely to blur the picture obtained with the method. For a sound evaluation of the potential of the δ-method at an inter-laboratories level, it appears critical to improve the reliability of the input data.

5.7 Relationship Between Chemical Ageing Indexes and Rheological Parameters

5.7.1 General Hypothesis

As observed in § 5.3.2 and § 5.5.2, the chemical ageing indexes as well as the mechanical parameters h, δ, β and τ show significant evolution through the discrete ageing steps arbitrarily selected in the TC ATB TG5 ageing procedure. On this basis, it seems very likely that a relationship could be established between the evolution of a chemical ageing index and the evolution of the 4 mechanical parameters. Then it could be possible to estimate the mechanical properties of a binder at any ageing level as far as this ageing level can be quantified by an ageing index value.

5.7.2 Relationship Obtained in Each Laboratory

In order to verify this hypothesis, the values of the 4 mechanical parameters h, δ, β and τ are plotted versus the average values of the chemical ageing index for each laboratory and batch B1 in Figs. 5.23, 5.24, 5.25 and 5.26.

The general trend is the same for data of all laboratories with significant relationships between the chemical ageing index and the parameters: linear relationship for h, δ and β, and exponential relationship for τ; but the values of the slopes can be significantly different from one laboratory to another. The slopes obtained are summarised in the Table 5.5.

5.7.3 Possible Prediction of G from the Chemical Ageing Index Ico*

The significant relationships obtained tend to confirm the hypothesis and it seems possible to estimate the G* values of a given binder at any ageing level from an Ico

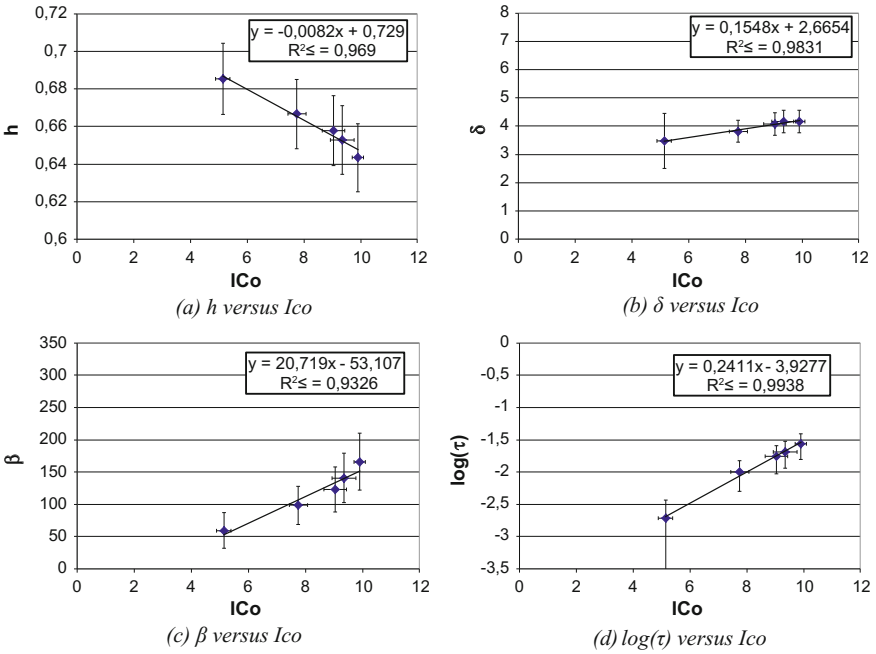

Fig. 5.23 Relationship between chemical ageing index and rheological parameters for Lab1

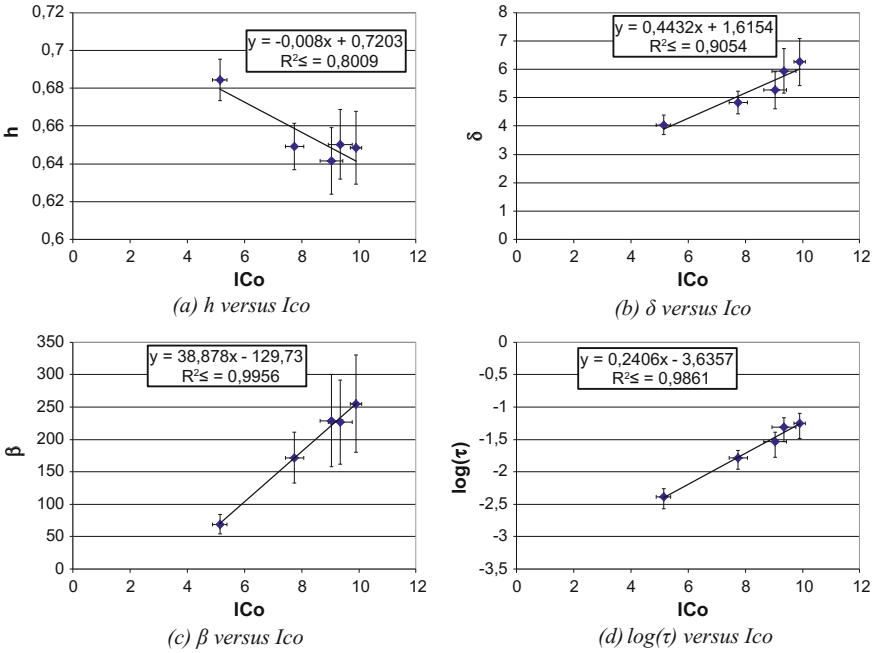

Fig. 5.24 Relationship between chemical ageing index and rheological parameters for Lab4

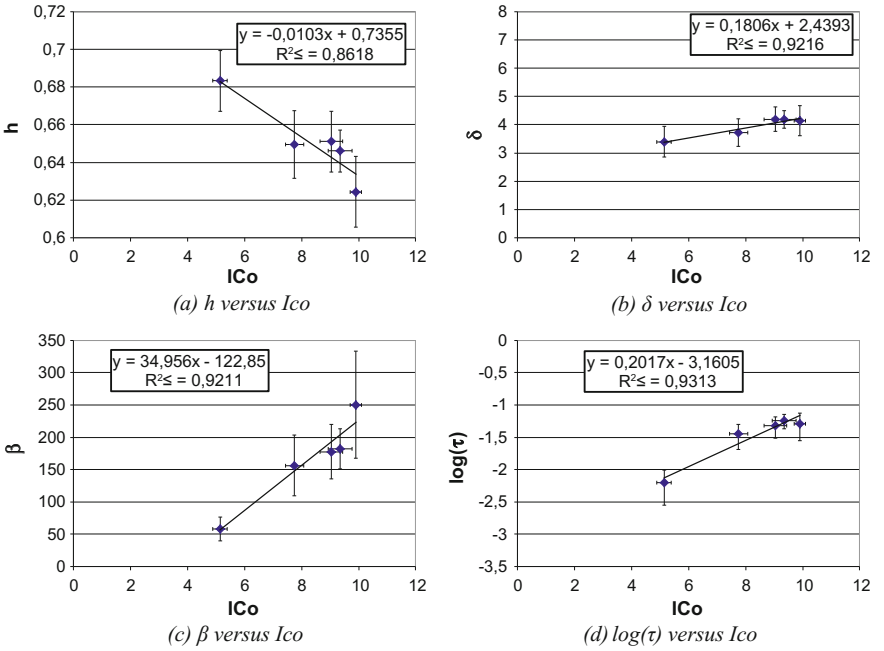

Fig. 5.25 Relationship between chemical ageing index and rheological parameters for Lab7

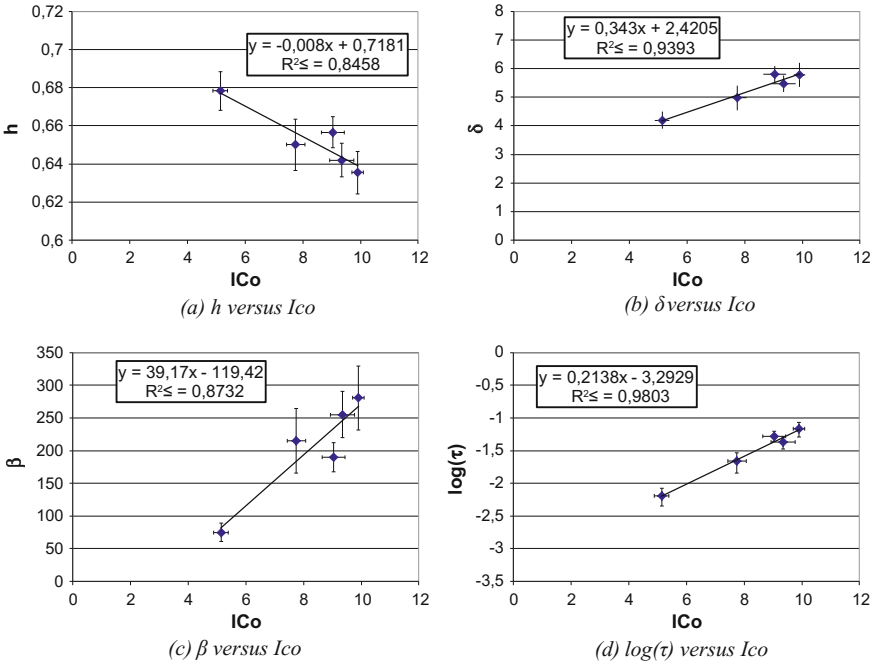

Fig. 5.26 Relationship between chemical ageing index and rheological parameters for Lab8

Table 5.5 Slopes obtained for each laboratory for the Ico versus parameter relationships

Parameter	a_h	a_δ	a_β	a_τ
LAB01	−0.0082	0.15	20.72	0.24
LAB04	−0.0080	0.44	38.88	0.24
LAB07	−0.0103	0.18	34.96	0.20
LAB08	−0.0080	0.34	39.17	0.21
Average	−0.0086	0.28	33.43	0.22

value at least within the same laboratory. This estimation could be obtained through 4 steps:

Step 1 determination of the Huet modified model parameters of the original binder. This step requires DSR measurements on the original binder and the fitting of these data with a Huet modified model. The complex shear modulus of the original binder G_{orig}* can then be expressed by (5.5)

$$G_{orig} * (\omega) = \frac{G_\infty}{1 + \delta(i\omega\tau)^{-k} + (i\omega\tau)^{-h} + (i\omega\beta\tau)^{-1}} \tag{5.5}$$

Step 2 determination of the effect of ageing on the Huet modified model parameters of the binder and the ageing index. This step requires applying an ageing protocol similar to the TC ATB TG5 ageing protocol to the original binder and the fitting of these data with a Huet modified model along with an ageing index calculation from FITR measurements at each ageing step. The slopes a_h, a_δ, a_β and a_τ for h, δ, β, and τ versus Ico can then be determined as in § 5.7.2.

Step 3 Estimation of the parameter h_{aged}, δ_{aged}, β_{aged}, and τ_{aged} at a given ageing level (for example of an on-site aged cored sample). This step requires a FTIR measurement on the aged sample binder and the calculation of the variation of the chemical index compared to the original binder: ΔIco. The parameter h_{aged}, δ_{aged}, β_{aged}, and τ_{aged} are then calculated from the slopes a_h, a_δ, a_β and a_τ:

$$\begin{aligned} h_{aged} &\approx h + a_h \cdot \Delta Ico \\ \delta_{aged} &\approx \delta + a_\delta \cdot \Delta Ico \\ \beta_{aged} &\approx \beta + a_\beta \cdot \Delta Ico \\ \tau_{aged} &\approx \tau \cdot 10^{a_\tau \cdot \Delta Ico} \end{aligned}$$

Step 4 Estimation of G_{aged}* at a the given ageing level using (5.6)

$$G_{aged} * (\omega) \approx \frac{G_\infty}{1 + \delta_{aged}(i\omega\tau_{aged})^{-k} + (i\omega\tau_{aged})^{-h_{aged}} + (i\omega\beta_{aged}\tau_{aged})^{-1}} \tag{5.6}$$

5.7.4 Comment on the Relationship Between Chemical Index and Rheological Properties

As observed in Table 5.5, the slopes a_h, a_δ, a_β and a_τ are laboratory dependent. This is obviously an experimental bias as the same binder aged in the same conditions should have the same chemical and rheological characteristics and hence the same relationships between them. As explained above, this reflects the heterogeneity of the measurement devices, measurement procedures and calculation methods already mentioned for the FTIR and the rheological measurements. As mentioned for the δ-method, this experimental bias is blurring the picture and it could hinder the studies on the question that really matters for recycling: how far the relationship between a simple chemical ageing index and the rheological properties is dependent of binder and ageing conditions?

5.8 General Conclusion

A precise quantitative index characterising the chemical ageing of bitumen would be of great help to improve recycling techniques. Applied on a database of spectra measured on a bituminous mixture aged at different levels in laboratory, the carbonyl index based on Fourier transform Infrared spectroscopy (FTIR) shows consistent empirical trends with ageing. However, the study was limited to a precise laboratory ageing procedure applied to a given bitumen and its conclusions are limited to these conditions. Furthermore, the FTIR measurement procedures and index calculation methods are very diverse between laboratories. This hinders direct comparison of the results. Independently from the relevance of the carbonyl index, harmonisation is clearly needed if this index is to be used for RA characterisation.

The analysis of the rheological data of the database through a Huet modified model confirms a laboratory or device dependence of the complex shear modulus measurements already mentioned in literature with an approximatively constant relative difference between the laboratories results. Nevertheless, the effect of ageing on the rheological properties of a binder over the complete time-temperature domain seems to be fairly well represented by the evolution laws of only 4 parameters of a Huet modified model.

Taking advantage of the modelling for the analysis of the rheological data, an attempt was made to explore the potential of a recently developed method that could allow the interpretation of rheological data in terms of apparent molecular weight. A gradual shift from a mono-modal to a bi or tri-modal distribution of the apparent molecular weight according to the ageing steps was observed. A similar trend was also observed on other independent sets of data. If this was confirmed, this method could be a valuable instrument for recycling studies notably to extract the mixing laws and to describe the rejuvenation processes.

Significant empirical relationships between chemical ageing indexes and the parameters of the rheological model are noticed for the set of data treated. But these relationships are significantly different from one laboratory to another and are probably dependent of binder and ageing conditions.

Glossary

$\boldsymbol{A}$	Absorbance
$\boldsymbol{I}$	Light intensity
ε	Molar absorption
ℓ	Optical path length
$\boldsymbol{C}$	Species concentration
$\boldsymbol{A}$	Area of a function
$\boldsymbol{w}$	Width at half the maximum peak height (distribution)
$\boldsymbol{v}$	Mode of a distribution
$\boldsymbol{CV}$	Coefficient of variation (standard deviation/average)
G^*	Complex shear modulus
$\lvert G^* \rvert$	Norm of the complex shear modulus
G_∞	Glassy shear modulus
G'	Real part of the complex shear modulus
G''	Imaginary part of the complex shear modulus
ω	Angular frequency
$\boldsymbol{k}$	First parabolic element for a Huet modified rheological model
$\boldsymbol{h}$	Second parabolic element for a Huet modified rheological model
δ	Balance parameter between the 2 parabolic elements for a Huet modified rheological model
β	Dashpot parameter for a Huet modified rheological model
τ	Frequency multiplier at a specific temperature for a Huet modified rheological model

References

Bell CA (1989) Summary report on aging of asphalt-aggregate systems, SHRP A-305

Chailleux E, Ramond G, Such Ch, de La Roche C (2006) A mathematical-based master-curve construction method applied to complex modulus of bituminous materials. Road Mater Pavement Des 7(sup1):75–92

Corbett LW (1969) Composition of asphalt based on generic fractionation, using solvent deasphaltening, elution-adsorption chromatography, and densimetric characterization. Anal Chem 41:576–579

de la Roche C, Van de Ven M, Van den bergh W, Gabet T, Dubois V, Grenfell J, Porot L (2009) Development of a laboratory bituminous mixtures ageing test. In: RILEM conference on advanced bituminous materials, Rhodes, Greece

de la Roche C, Van de Ven M, Van den bergh W, Gabet T, Dubois V, Grenfell J, Porot L (2010) Development of a laboratory bituminous mixtures ageing test ISAP Nagoya, Japan

EN 1426 (2007) Bitumen and bituminous binders—Determination of needle penetration

EN 1427 (2007) Bitumen and bituminous binders—Determination of softening point—Ring and ball method

Gubler R, Partl MN (2005) Einfluss schweizerischer Filler auf die Alterung von bituminösen Bindemitteln und die Rissbildung im Belag, Nr. 1138, EMPA Dübendorf, Bundesamt für Strassen, Switzerland

Mangiafico S (2014) Linear viscoelastic properties and fatigue of bituminous mixtures produced with reclaimed asphalt pavement and corresponding binder blends, PhD. Thesis, ENTPE

Marsac P, Piérard N, Porot L, Van den bergh W, Grenfell J, Mouillet V, Pouget S, Besamusca J, Farcas F, Gabet T, Hugener M (2014) Potential and limits of FTIR methods for reclaimed asphalt characterisation. Mater Struct 47(8):1273–1286

Mouillet V, Farcas F, Battaglia V, Besson S, Petiteau C, Lecunff F (2009) Identification and quantification of bituminous binder's oxygenated species. Analysis by fourier transform infrared spectroscopy, Méthode d'essai LPC n°69

Olard F (2003) Comportement thermomécanique des enrobés bitumineux à basse températures, PhD. Thesis, INSA Lyon

Partl, Bahia, Canestrari, De La Roche, Di Benedetto, Piber and Sybilski Editors (2013) Advances in Interlaboratory Testing and Evaluation of Bituminous Materials, State-of-the-Art Report of the RILEM Technical Committee 206-ATB, Springer–2012

Petersen JC (2009) A review of the fundamentals of asphalt oxidation—Chemical, Physicochemical, Physical Property, and Durability Relationships, Transportation Research Circular number E-C140

Pierard N (2013) Bitumen analysis with FTIR spectrometry: processing of FTIR spectra, BRRC Method of Measurement, ME85/13

Pierard N, Vansteenkiste S, Vanelstraete A (2010) Effect of extraction and recovery procedure on the determination of PmB content and on the properties of the recovered binder. Road Mater Pavement Des, EATA 2010:251–279

Stuart BH, George B, McIntyre P (1996) Modern infrared spectroscopy. In: Analytical chemistry by open learning, vol 40. Wiley

Such C (1983) Analyse du comportement visqueux des bitumes. Bulletin de liaison des laboratoires des ponts et chaussées 127

Themeli A, Chailleux E, Farcas F, Chazallon C, Migault B (2015) Molecular weight distribution of asphaltic paving binders from phase-angle measurements. Road Mater Pavement Des 16:228–244

Verhasselt A, Puiatti D. (2004) Effect of hydrated lime on ageing behaviour of bituminous mastics, 3rd Eurasphalt & Eurobitume Congress, Vienna

Yusoff NI (2012) Modelling the linear viscoelastic rheological properties of bituminous binders, PhD. Thesis, University of Nottingham

Zanzotto L, Stastna J, Ho S (1999) Molecular weight distribution of regular asphalts from dynamic material functions. Mater Struct 32:224–229

Chapter 6
Cold Recycling of Reclaimed Asphalt Pavements

Gabriele Tebaldi, Eshan Dave, Martin Hugener, Augusto Cannone Falchetto, Daniel Perraton, Andrea Grilli, Davide Lo Presti, Marco Pasetto, Andreas Loizos, Kim Jenkins, Alex Apeagyei, James Grenfell and Maurizio Bocci

Abstract Pavement engineers have in front of them multiple challenges linked to addressing issues related to social development and society's expanding needs. One of the most substantial of these issues is perhaps how to effectively rehabilitate and/or maintain the existing road network while preserving and sustaining limited natural resources. The re-usage of existing pavement materials to reconstruct/rehabilitate our future pavements is the solution that is now more and more selected

Contributors: Elie Hajj, Patrick Muraya, Giovanni Giacomello

G. Tebaldi (✉)
University of Parma, Parma, Italy
e-mail: gtebaldi@unipr.it

G. Tebaldi
University of Florida, Gainesville, USA

E. Dave
University of New Hampshire, Durham, USA

M. Hugener
Empa, Swiss Federal Laboratories for Materials Science and Technology, Dübendorf, Switzerland

A. C. Falchetto
Technische Universität Braunschweig, Braunschweig, Germany

D. Perraton
University of Québec, ETS, Montreal, Québec, Canada

A. Grilli
University of San Marino, San Marino, Italy

D. L. Presti · J. Grenfell
University of Nottingham, Nottingham, UK

M. Pasetto
University of Padova, Padova, Italy

A. Loizos
National Technical University of Athens, Athens, Greece

M. N. Partl et al. (eds.), *Testing and Characterization of Sustainable Innovative Bituminous Materials and Systems*, RILEM State-of-the-Art Reports 24,
https://doi.org/10.1007/978-3-319-71023-5_6

by the different road administrations around the world. However, upon closer inspection, one can find many areas and details, not negligible issues, that are simply extensions of HMA technology (i.e. mix design process in cold recycling) or empirical arrangements; in particular RAP still does not have an internationally recognized classification. So SIB – TG6 decided to develop a classification protocol of RAP, depending on its intended application. The objective has been followed by considering the procedures generally utilized to classify the natural aggregates: tests able to identify the main components (i.e. the geometrical and mechanical properties of aggregates and the characterization of recovered bitumen for RAP) and provide information on their behaviour under specific conditions, near to real life usage (e.g. the Los Angeles test for aggregates gives an idea of the potential behaviour of aggregates under the action of a roller compactor). The following sections illustrate and explain the actions of the TG in order to achieve the goals outlined above: the review of current standards, the protocol designed to classify RAP and the round robin tests carried out to validate the protocol.

Keywords Recycling · Reclaimed asphalt · Foam bitumen · Bituminous emulsion Cohesion test · Fragmentation test · BSM – bitumen stabilized materials

List of Symbols

Abs	Water absorption (%)
ANAS	Agenzia Nationale Autonoma delle Strade
ARRA	Asphalt Recycling and Reclaiming Association
b	Bitumen content (%)
BC	Bitumen content p. 22
BSM	Bitumen stabilized materials
BSM-Foam	Foamed bitumen stabilized materials
BSM-Emulsion	Bitumen emulsion stabilized materials
CBR	Californian bearing ratio
CBTM	Cement-bitumen treated materials
CIR	Cold in-place recycling
CMA	Cold mix asphalt
CMT	Cement treated materials
CPR	Cold plant recycling or Cold-central plant recycling

K. Jenkins
Stellenbosch University, Stellenbosch, South Africa

A. Apeagyei
Kingston University, Kingston upon Thames, UK

M. Bocci
Università Politecnica Delle Marche, Ancona, Italy

CRM	Cold recycled mixtures
CV	Coefficient of variation
DOT	Department of Transportation
ESAL	Equivalent Standard Axle
FI	Flakiness index
FDR	Full-depth reclamation
G_b	Specific gravity
HIR	Hot in-place recycling
HMA	Hot mix asphalt
ITRM	Indirect tensile modulus or resilient modulus
ITS	Indirect tensile strength
ITS_{dry}	Indirect tensile strength in dry condition
ITS_{wet}	Indirect tensile strength after soaking
kPa	KiloPascal
LA	Los Angeles
MDE	Micro Deval in water
MESA	Million equivalent standard axle
MMC	Mixing moisture content
M_{wet}	Soaked modulus
M_{dry}	Dry modulus
OD	Oven dried
OFC	Optimum fluid content
OMC	Optimum moisture content
PAH	Polycyclic aromatic hydrocarbon
PCS (%)	Percent passing through the control sieve
$PCS_{STD\ to\ 5\ °C}$	PCS result obtained at 5 °C
PLM	Polarised light microscopy
PG	Performance grade
RA	Reclaimed asphalt
RAP	Reclaimed asphalt pavement
RRT	Round robin test
SGC	Superpave gyratory compactor
SI	Shape index
TC	Technical committee
TEM	Transmission electron microscopy
TG	Task group
TMR	Transport and main roads
TR&B	Temperature from the ring and ball test
UCS	Unconfined compressive strength
USA	United States of America
VA	Virgin aggregate

6.1 General Introduction

Pavement engineers are presently faced with multiple challenges linked to addressing issues related to social development and with society's expanding needs. One of the most substantial of these issues is perhaps, how to effectively rehabilitate and/or maintain the existing road network while preserving and sustaining limited natural resources? Quarries from which currently the majority of material for roads procured are subjected to increasing environmental restrictions, while on the other hand the opening of new landfills for construction waste is becoming more expensive and less tolerated by society. These issues amongst others produce a scenario that points to one obvious solution: the repeated usage of existing pavement materials to reconstruct/rehabilitate our future pavements by substantially recycling materials in present pavements. This solution has become realistically possible due to well established research showing that existing asphalt pavement materials can be fully recycled and/or reused. To achieve and implement this solution is merely a matter of widespread and successful transfer to relevant stakeholders of both the knowledge and the utilization of the appropriate technology requirements.

Materials derived from the milling of older pavements are generally called *Reclaimed Asphalt* (RA) or *Reclaimed Asphalt Pavement* (RAP). Currently there are multiple methods to recycle these materials including for example: utilizing the material in unbound granular layers or mixed with various binders (hydraulic cement, bitumen, foam bitumen and bituminous emulsion) at varying temperatures to produce material for bound pavement layers. The techniques for recycling RAP are based on the utilization of bituminous binders that are classified as a function of temperature of the aggregates during the mixing process: if there is no aggregate heating, the technique is called cold recycling; if there is heating of aggregates, the technique is called either warm, half warm or hot recycling depending on the mixing temperature. These techniques are extensively utilized throughout the world and pavement engineers have developed experience regarding their implementation; as such, one could falsely derive the conclusion that there is limited requirement to further research the issue. However, upon closer inspection one can find many areas and details, not negligible issues, that are simply extensions of HMA technology (i.e. mix design process in cold recycling) or empirical arrangements (RAP still does not have an internationally recognized classification). Therefore, the characteristics and the classification of RAP is dependent on its intended application. With this in mind, the "TG6 – Cold Recycling" has focused its strategic plan.

The basic concept of TG6 activities was to start from the very basics, in order to identify all the currently available knowledge about RAP utilization and decipher among this data what has scientific value and can be transferred from empirical data to engineering data.

As previously mentioned, the current state of the art is proposing the investigation and/or implementing multiple techniques for the cold recycling of RAP; the decision was made for the TG6 to focus its main attention on further investigation cold recycling with bituminous emulsion or with foamed bitumen.

To avoid repetitions and/or duplication of research already performed, the first action of the group was an extensive review of the standards adopted by various governmental agencies and by responsible road administrations of a wide subset of countries located around the world. The results of this review confirmed the initial impression; in particular, they portrayed an absence of a specific characterization for RAP and a wide discrepancy amongst the methodologies utilized for specimen preparation as well as amongst the varying curing procedures implemented. With this in mind, TG made the decision to start to provide more clarity on the fundamental question, identifying and validating a procedure to classify RAP, leaving other topics for a following action in a future Rilem TC.

The objective has been followed by considering the procedures generally utilized to classify the natural aggregates as well as those for bound materials: tests able to identify the main components (i.e. the geometrical and mechanical properties of aggregates and the characterization of recovered bitumen for RAP) and provide information on their behaviour in specific conditions, near to real life usage (e.g. the Los Angeles test for aggregates gives an idea of the potential behaviour of aggregates under the action of a roller compactor).

The following sections illustrate and explain the actions of the TG in order to achieve the goals outlined above: the review of current standards, the protocol designed to classify RAP and the round robin tests carried out to validate the protocol.

6.2 Synthesis of Current Recycled Asphalt Classification, Specimen Preparation and Curing Processes for Cold Recycled Asphalt Mixes

6.2.1 RA Production Methods and Characterization

The production of recycled asphalt granulate is currently not defined by any standard but it is generally achieved in two ways, either the existing pavement is milled with a milling machine or the material is removed in sections with an excavator.

One of the most basic definitions of Reclaimed Asphalt (RA) can be found in the Washington Pavement Association literature. The Washington Pavement Association defines RA as a collection of old asphalt pavement in loose form. The RA can also be a collection of loose asphalt and aggregates from granular layers. In full depth reclamation processes, limited granular material from underlying layers is often removed from the base and blended with the old asphalt materials.

Homogeneity in terms of size, mineral type, binder type etc. is a crucial quality criterion for RA. However, homogeneity requirements are rarely demanded or investigated, except for example in the Netherlands, where standard deviations are defined for aggregate size distribution, binder content and penetration value of the recovered binder (RAW 2010). In the ideal case, RA is derived from only one source and one layer. However, this is often not possible and the RA material is

mixed together from different pavement layers and locations. Sampling of large stockpiles is difficult because the interior of the large stockpiles are difficult to access. The European standard EN 932-1 developed for the sampling of mineral aggregates, defines the number of minimum samples but offers only limited practical help for RA (EN 932-1 1996).

In order to increase the homogeneity or if different RA sizes are required, an additional screening operation is needed. In Norway, it is recommended for plant mixing to produce fractions like 0–4 mm and 4–11 mm, 0–6 mm and 6–11 mm, 6–16 mm or 0–8 mm and 8–16 mm. The use of sieves smaller than 4 mm can be difficult due to moisture in the RA (Cold Bitumen Stabilized Base Courses 1999). The maximum particle size of RA is generally defined and varies between 30 and 50 mm (Transportation Research Board 2011; Construction Specification for Cold In-Place Recycling 2010; Jahren et al. 1998). The European standard EN 13108-8 leaves it open to the countries to define a maximum particle size for RA (EN 13108-8 2005).

Once the proper RA is produced, care has to be taken to prevent RA to re-agglomerate or congeal in large piles. Recommendations for the size, cover and other criteria for stockpiles are by different states, countries and institutes (Cold Bitumen Stabilized Base Courses 1999; Transportation Research Board 2011; Reclaimed Asphalt Pavement: User Guideline).

In summation, the RA production process for cold recycling is not precisely outlined and requirements for important properties like homogeneity are regulated only in a limited number of countries.

6.2.2 RA Cleanliness and Foreign Matter

6.2.2.1 Typical Foreign Matter to be Detected and/or Removed Prior to Milling (De Bock et al.)

Some foreign matters can affect properties of future RA or contaminate it. They need to be detected or removed before pavement is milled.

Although RA is not heated in cold recycling, leaching is a major concern, especially if not enough binder is added to immobilize PAH (Polycyclic Aromatic Hydrocarbon). In Germany, leaching tests have to be carried out for tar-containing materials. Hence, a selective milling is highly desirable if one of the old asphalt layers contains tar. Two qualitative screening identification techniques are commonly used in the field: the tar test spray PAK-Marker® and the staining test with toluene. For a precise assessment, quantitative laboratory methods are used but they are more expensive and time-consuming (High Performance Liquid Chromatography, Thin Layer Chromatography and Gas Chromatography with Mass Spectrometric).

Asbestos: In the 1980s asbestos fibres were sometimes used in asphalt pavement to improve fatigue behaviour. As asbestos is harmful to health when inhaled, it is important that their presence in bituminous mixes is detected prior to milling. In case of doubts, Polarised Light Microscopy (PLM) and Transmission Electron

Microscopy (TEM) are the most commonly used method for the analysis of bulk samples of RA.

Road Markings: As they can affect the properties of the RA, thick thermoplastic road marking should be removed before milling the old pavement.

6.2.2.2 European Standardization

EN 12697-42 (FHWA-SA-98-042 1997) specifies a visual method for determining the amount and components of coarse foreign matter in RA. Coarse foreign matter is defined as "matter in reclaimed asphalt not derived from asphalt pavements or surplus production, and cold asphalt produced with cut-back bitumen". The following values are determined through a visual sorting of the particles greater than 8 mm diameter from the sample of RA:

- Content of material derived from asphalt;
- Content of cold asphalt produced with cut-back bitumen; and,
- Content of coarse foreign matter not derived from asphalt, divided into site materials and other materials.

Following note gives examples of site and other materials:

- Site materials: "cement concrete and cement concrete products; bricks; unbound pavement materials including fine natural aggregate, from secondary sources; cement mortar."
- Other materials: "metals; synthetic materials; plastic; wood."

For RA feedstock requirements EN 13108-8 (2005) defines two groups of foreign matter for RA:

- Group 1: Cement concrete including cement concrete products, bricks, sub base material (excluding natural aggregate), cement mortar and metals.
- Group 2: Synthetic materials, wood and plastics.

Then the RA shall be classified in 3 categories:

- F1: Content of group 1 material $\leq 1\%$ and content of group 2 material $\leq 0.1\%$
- F5: Content of group 1 material $\leq 5\%$ and content of group 2 material $\leq 0.1\%$
- Fdec: Content and nature of all foreign matter declared.

The discrepancy between the "site materials" and "other materials" definitions in EN 12697-42 and the "group 1" and "group 2" definitions in EN 13108-8 should be noted. In practice, EN 933-11 (Tests for geometrical properties of aggregates—Part 11: Classification test for the constituents of coarse recycled aggregate) is used instead of EN 12697-42 as it is applicable to all kind of mineral aggregates, which are treated in a recycling factory for construction products.

6.2.3 RA Size Distribution (Grading) Evaluation

According to EN 13108-8 (2005), the maximum size of the RA particles (noted as U) should be declared and the grading curve of the aggregate in the RA should be determined after extraction of the binder ("White curve" Sect. 6.3.3.1). For a given RA stockpile one sample should be tested for every 500 ton with a minimum of 5 samples. The grading homogeneity of the stockpile is one of the key parameters for further recycling processes.

6.2.4 RA Bitumen Content and Characteristics

In hot mix asphalt containing RA, the aged bitumen in the RA is often considered as part of the bitumen in the new asphalt mixture composed of the RA material. However, this is not always the case in cold asphalt mixtures containing RA. Some agencies consider the contribution of the aged bitumen in the mix design, while others do not take the aged bitumen in consideration. Table 6.1 shows a summary of some properties of the bitumen in the RA that are commonly considered in mix design.

Methods such as the Oregon method (FHWA-SA-98-042 1997) consider the penetration at 25 °C and absolute or dynamic viscosity at 60 °C of the extracted bitumen in the estimation of the required bitumen content. In other methods, such as

Table 6.1 Properties of bitumen in the RA

Design method	Comment on aged bitumen in the RA
California-foam bitumen (Jones et al. 2009)	Aged asphalt in the RA not considered in the bitumen content since cold recycling temperatures are lower than the minimum temperature required to soften the aged bitumen
Minnesota-emulsion (Standard Specifications for Highway and Bridge Construction 2011)	PG class of the extracted bitumen determined. Evaluation of a blend of extracted bitumen and emulsion in relation to the Minnesota DOT requirements recommended
Oregon (FHWA-SA-98-042 1997)	Penetration at 25 °C and dynamic viscosity of the bitumen extracted from the RA considered in the estimation of the required amount of bitumen
Wirtgen-emulsion/foam bitumen (Cold Recycling 2010)	RA is classified as active or inactive depending on the penetration value of extracted bitumen at 25 °C. Active RA has higher levels of cohesion than inactive RA or natural materials
New York State DOT, proposed specification (Cross et al. 2010)	The bitumen used to make the emulsion should meet the bending beam requirements of AASHTO M 320 and PG specifications. Aged bitumen in the RA not considered in the bending beam and PG requirements

California foam bitumen mixes (Jones et al. 2009), the aged bitumen is not factored into the binder content since the recycling temperatures are significantly below the minimum temperature required to soften the aged bitumen.

One of the questions that may need to be addressed is the effect of the properties of the aged bitumen in the RA on the properties of the added bitumen and additives. The other question is how this effect affects the required bitumen content. These two questions could be addressed by examining blends of emulsions or foam bitumen and bitumen extracted from the RA material.

6.2.5 *Aggregate Properties*

RA particles often consist not of a single aggregate particle but are conglomerates of smaller aggregates glued together by the mastic (Fig. 6.1). The Wirtgen Guide differentiates between inactive or "black rock" RA particles with a binder penetration value below 18 dmm and active RA with penetration values above 25 dmm (Cold Recycling 2010). However, this classification is valid only for cold recycling, at ambient temperature and not for recycling at elevated temperatures with foam bitumen as with lower viscosity the blending of the binders becomes better.

Inactive RA particles coated with aged binder act similar like pure aggregates, because only the surface film of the old binder up to a depth of 0.1–0.3 mm will mix with the new binder (TC 237-SIB 2010). Active RA particles are softer and have the tendency to break down further when subjected to mixing and compaction forces. Therefore, for cold recycling, requirements for aggregate properties themselves, associated with aged binders, are less important in comparison to hot recycling, where the angularity of mineral aggregates plays an important role. However, grading curves and sometimes shape and angularity are generally available from original construction data or cores, as pavements are analyzed prior to destruction (Maintenance Technical Advisory Guide (MTAG) 2008).

6.2.6 *RA Moisture Content*

Moisture content is not always recognized nor considered as one of the most important parameters to be evaluated on RA aggregate, even though it is clear that

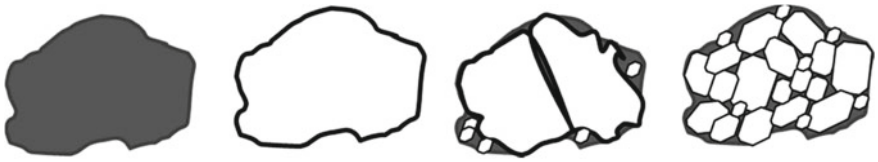

Fig. 6.1 From the outside of a RA particle it is difficult to suggest its composition, which can be very different (from left to right: RA particle from the outside, cross sections of possible compositions of a RA particle: single coated aggregate, two major aggregates with some mastic, conglomerate of small aggregate particles and mastic)

the water content and moisture resistance become the most important properties to be checked when such an aggregate is re-used in hot or cold recycled mixtures. The reason for this contradiction can perhaps be traced back to the erroneous belief that asphalt pavements are basically dry, and it only becomes important to take into account the role of water in the aggregate when they are milled and recycled.

An asphalt pavement is only subject to recycling when it is affected by extended distresses, wide and deep degradations which alter the surface integrity and permit the entry of water into the body of the structure. In these cases, the pavement to be reclaimed is potentially wet and the moisture content, depending on the surface damage, is crucial in order to choose the most suitable in situ or in-plant recycling process.

Where distresses are frequent and severe, Full-Depth Reclamation (FDR) or Cold In-place Recycling (CIR) are usually the most common solutions; in this case RA is frequently moist and can be used "as it is", provided that the moisture fits the purpose. In this circumstance, whatever the binder (emulsion or foam), bitumen is used with a reduced viscosity so it can be easily mixed with cold moist material, as RA can be.

When foamed bitumen is used, the RA moisture content can be relatively high (aggregate can be at ambient temperature with in situ moisture content (Austroads 2011)), but it needs to be accurately checked, since the consequence could be the underestimation of the role of moisture in the final mixture. In foamed Bitumen Stabilized Materials (BSM-Foam), the moisture in the mix, prior to the addition of the binder, plays an important role in dispersing the bitumen during mixing. It separates and suspends fines, making them available to bitumen during mixing, then acts as carrier for bitumen droplets.

When RA is a component of a Bitumen Emulsion Stabilized Materials (BSM-Emulsion), its moisture plays an important role in: reducing absorption of emulsion water into the aggregate; dispersing the emulsion and preventing a premature breaking during the mixing (likely at low temperatures, when the evaporation rate of the excess moisture in the material is slow); delaying curing. Moreover, in recycling projects, when the moisture content of the in situ material is relatively high (also due to a wet climate), the addition of emulsion can increase the total fluids content to beyond the zero-voids limit, when compaction energy is applied.

Finally, for in-plant applications of cold recycling technology, RA moisture content is not particularly important, since it can be changed there as required, depending on the construction technique subsequently adopted. Once processed, RA can be handled and stored as a conventional aggregate material. If the mixture is placed in a stockpile, its usability is also influenced by moisture content, which should be close to the Optimum Moisture Content (OMC), in order to avoid the bitumen droplets losing their adhesive capacity when the material dries out. It has been verified that in (horizontal as well conical) stockpiles, RA has the tendency to form a crust (due to heat from the sun) on the surface (200–250 mm circa), which tends to help shed water. RA also has a tendency to retain moisture without draining over time like an aggregate. Low, horizontal and flat stockpiles are subject to greater moisture accumulation than tall, conical ones. 7–8% RA moisture is

reported by some authors during the rainy season at facilities using low, horizontal stockpiling techniques (Decker and Young 1996). RA stockpiles are generally left uncovered, since covering with tarps can cause condensation and add moisture to the aggregate; RA is preferably stored in an open-sided building, but under a roof. Anyway, to ensure the RA quality in the course of time, the moisture content must be regularly checked.

Obviously, RA can be moist not only for intrinsic reasons but in a wet or rainy climate. In this case neither CIR nor Hot In-place Recycling (HIR) are recommended. In the first case, wet weather would compromise the use of emulsion binder and slow down curing; damp pavements also slow the hot recycling construction processes.

6.2.7 *Terminology, Process Classification and Definitions for Specimen Preparation and Curing of Cold-Recycled Asphalt Mixes*

Cold recycling of bituminous pavements involves reusing part of an existing pavement to produce, without (or with a limited amount of) heat, mixtures that will be included in new or rehabilitated pavement layers (TC 237-SIB 2010; RAW 2010; EN 932-1 1996).

Similar to Hot Mix Recycling, two methods of cold recycling can be distinguished: Cold Plant Recycling (CPR) and Cold In-place Recycling (CIR). In both cases RAP is mixed with a bituminous stabilizing agent and water. Virgin aggregates are often added to meet grading criteria, and active fillers, such as cement, lime, or fly ash, are normally used to accelerate the curing process and improve mixture properties (TC 237-SIB 2010; EN 932-1 1996).

CPR (also referred as Cold Central-Plant Recycling) is performed by hauling RAP material recovered the cold way, generally by milling machines, to a central plant where it is selected, pre-treated (crushed and screened) and tested before it is fed in the mixing process. Therefore, central plant recycling allows an optimal control over RAP variability and quality of the recycled mix (TC 237-SIB 2010; EN 932-1 1996).

In CIR all the operations, from milling to mixing, are performed directly on site using single-unit or multi-unit trains. Even if this results in a reduced control of material and mix properties, in-place recycling is generally preferred over plant recycling because the elimination of the haulage yields substantial economic and environmental advantages (TC 237-SIB 2010; EN 932-1 1996).

CIR can be accomplished as partial-depth or full-depth recycling. In the current practice, the term CIR is used to indicate partial-depth recycling, while the term Full-Depth Reclamation (FDR) is used in the second case (TC 237-SIB 2010; RAW 2010; EN 932-1 1996; Cold Bitumen Stabilized Base Courses 1999).

In CIR pavement milling is limited to the asphalt concrete layers; virgin aggregates may be added to RAP to meet grading requirements and bitumen emulsion is the most commonly used recycling agent. The recycled mix produced by CIR is a Cold Mix Asphalt (CMA) that is generally used for base or binder courses, depending on the traffic type and volume.

In FDR asphalt layers and portions of cement treated or unbound foundation layers are milled, mixed with binder, and placed as a new stabilized course. Modern recycling machines (recyclers) that combine milling and stabilization capabilities are used to complete the FDR process in a single or more passes. Bitumen emulsion and foamed bitumen[1] are the most commonly used recycling agents and virgin aggregates are usually added to the reclaimed materials to meet specific grading requirements. Active fillers are also employed, in particular Portland Cement (PC).

Because of the great variability in aggregate quality and composition, type and amount of recycling agents, recycled mixtures produced by FDR can exhibit a wide range of mechanical behaviors, for example: Cement Treated Materials (CTM) (Construction Specification for Cold In-Place Recycling 2010; Jahren et al. 1998), Bitumen Stabilized Materials (BSM) (EN 13108-8 2005) and Cement-Bitumen Treated Materials (CBTM) (Reclaimed Asphalt Pavement: User Guideline; De Bock et al.).

6.2.8 *French Procedure for Aggregate and Bitumen Emulsion Preparation for Making Lab Specimen*

A French laboratory procedure for aggregates and bitumen emulsion preparation has been developed and built on the basis of recommendations for the manufacture of the hot bituminous mix and the NF P98-250-1 Standard (Jones et al. 2009) for cold mixes.

6.2.8.1 Preparation of Aggregates (Virgin and RAP)

It is possible to stock aggregates after acceptance, under sealed conditions, in order to preserve their natural water content. One or a few days before cold mix manufacturing, water content must be measured again:

– If the aggregates are wet (water content <5% for sand and <2% for the fine gravels), they are packaged at the ambient temperature of the laboratory (18–25 °C) in sealed conditions. Additional water is then added during manufacturing.

[1]Actually the term "cold" is sometimes considered misleading when using foamed bitumen, because, although the pavement is not heated during the milling process, the asphalt binder used in the foaming process is very hot (i.e., 150 and 180 °C) (Transportation Research Board 2011).

- If the aggregates are too wet (water content >5% for sand and >2% for the fine gravels), they are conditioned in a low thickness layer in containers at least 12 h before manufacturing at ambient temperature; the second control of the water content of the aggregates can be useful right before manufacturing.
- The use of dry aggregates (water content <0.5% for sand) is proscribed. To be used, they will be humidified at least 24 h before manufacturing and will be preserved in sealed conditions. However, on site, aggregates stocked can present a dry state because of exceptional weather conditions (summer) and/or of storage conditions (shelter). In this case (rare), all the water will be added before or during mix manufacturing. Aggregates temperature must be around the lab ambient temperature (15–25 °C) and representative of that used on the power station.

6.2.8.2 Preparation of the Bitumen Emulsion

At the emulsion acceptance, it is recommended to preserve it in a temperature range from the ambient temperature of the laboratory (18–25 °C) up to 40 °C. Before using, the emulsion must be homogenized (mechanical or manual stirring). The emulsion is employed in a temperature range from the ambient temperature of the laboratory up to 60 °C. If the emulsion is fresh, a rest period of about 16 h will have to be observed. The bitumen emulsion must be stocked several weeks; a stirring action must be done every 15 days.

6.2.9 Laboratory Mixing and Mix Composition Methodologies for Cold Mixes

The aim of the laboratory mixing process is to distribute the different materials in the RAP mixture homogenously throughout the mixture. In addition, the laboratory mixing process should imitate the field mixing process, if possible. In order to ensure relatively constant moisture content, the RAP material is dried prior to mixing. The drying methods include air drying (EN 932-1 1996; FHWA-SA-98-042 1997) and oven drying. The oven drying temperatures vary from round 40 °C (Transportation Research Board 2011) to 60 °C (Maintenance Technical Advisory Guide (MTAG) 2008). It should be noted that temperatures as high as 60 °C are above the softening point of the binders and therefore are considered to change the nature of the mix.

Table 6.2 (a) Mixing conditions for cold RAP mixture without added bitumen (i.e. RAP, cement or lime and water) (b) Mixing conditions for cold RAP mixture (i.e. RAP, cement or lime and water)

Design method		California-foam bitumen (Transportation Research Board 2011)	
Temperature (°C)	Mixing order	Mixing method	Storage duration before compaction
25	RAP and cement mixed first. Then mixed with water	Customized mixer	0
Design method		Norway-emulsion/foam bitumen (FHWA-SA-98-042 1997)	
Temperature (°C)	Mixing order	Mixing method	Storage duration before compaction
Room temperature	RAP and water mixed together at once	Mixer	At least 12 h to allow moisture distribution
Design method		Wirtgen-emulsion/foam bitumen (EN 932-1 1996)	
Temperature (°C)	Mixing order	Mixing method	Storage duration before compaction
Room temperature	RAP and cement or lime mixed first. Then mixed with water	Mixer	1 h to simulate construction conditions. Mix after every 15 min
Design method		South Africa-Using vibratory compaction (EN 13108-8 2005; Jones et al. 2009)	
Temperature (°C)	Mixing order	Mixing method	Storage duration before compaction
25	RAP and cement or lime mixed first. Then mixed with water	–	15–30 min

Cold RAP mixtures are mixed in the laboratory at specific mixing conditions that may include temperature, mixing order and storage duration before compaction. In general, the mixing process can be divided into mixing conditions for RAP mixtures with and without added bitumen. Tables 6.2 and 6.3 show the laboratory mixing conditions for some of the cold mix design methods considered in this literature review. The tables show the mixing conditions for the RAP mixture with and without bitumen.

The composition of the RAP mixture depends on the intended characterization test. The characterization tests include OMC, Mixing Moisture Content (MMC[2]),

[2]MMC = moisture content at maximum dry density in specimens composed of RAP, water and emulsion or foam bitumen.

Table 6.3 (a) Mixing conditions for cold RAP (i.e. RAP, cement or lime and water) (b) Mixing conditions for cold RAP mixture (i.e. RAP, cement or lime and water)

(a)		
Design method		California-foam bitumen (Transportation Research Board 2011)
Temperature (°C)	Mixing order	Mixing method
25	RAP and cement mixed. Then mixed with water. Foam bitumen added	Customized mixer
Design method		Minnesota-emulsion (Standard Specifications for Highway and Bridge Construction 2011)
Temperature (°C)	Mixing order	Mixing method
60	RAP and water mixed. Then mixed with emulsion	Manual
Design method		Norway-emulsion/foam bitumen (FHWA-SA-98-042 1997)
Temperature (°C)	Mixing order	Mixing method
Room temperature	RAP, water and emulsion or foam bitumen mixed at once	Manual/mechanical
Design method		Wirtgen-emulsion/foam bitumen (EN 932-1 1996)
Temperature (°C)	Mixing order	Mixing method
25	RAP, cement and some water mixed first. Then with foam bitumen. Then rest of the water. RAP, cement, water and emulsion mixed at once. RAP, lime and water mixed at least 4 h prior to mixing with emulsion or foam bitumen	Mechanical mixer
(b)		
Design method		NYS DOT-proposed specification emulsion (Cold Recycling 2010)
Temperature (°C)	Mixing order	Mixing method
25	RAP mixed with water. Then with emulsion	Manual/mechanical, one specimen mixed at a time, mixing time ≤ 60 s
Design method		South Africa-emulsion using vibratory compaction (Jones et al. 2009)

(continued)

Table 6.3 (continued)

(a)		
Design method		California-foam bitumen (Transportation Research Board 2011)
Temperature (°C)	Mixing order	Mixing method
Temperature (°C)	Mixing order	Mixing method
Should match field temperature	RAP and cement or lime (if required) mixed. Then mixed with water and stored for 15–30 min. Mix with emulsion and store for 40–60 min before compaction	Pug-mill mixer recommended in order to simulate field mixing
Design method		South Africa-foam bitumen using vibratory compaction (Jones et al. 2009)
Temperature (°C)	Mixing order	Mixing method
Should match field temperature	RAP and cement or lime (if required) mixed. Then mixed with water. Mix with foam bitumen	Pug-mill mixer recommended in order to simulate field mixing

Table 6.4 Composition of cold RAP mixtures—Optimum moisture content (OMC)

Method	Composition
California-foam bitumen (Transportation Research Board 2011)	RAP + water (v) + cement (1%) or lime (2%)
Norway-emulsion/foam bitumen (FHWA-SA-98-042 1997)	RAP + water (v)
Wirtgen-emulsion/foam bitumen (EN 932-1 1996)	RAP + water (v) + cement or lime: cement or lime = (2–6%) by dry weight of RAP
South Africa (Jones et al. 2009)	RAP + water (v), cement or lime added if required

Optimum Fluid Content (OFC[3]) and evaluation tests for mixtures containing added bitumen. The tables[4] below give an overview of the composition of the cold mix designs considered in this review. Tables 6.4, 6.5 and 6.6 show the mix composition for determination of OMC, MMC and OFC respectively. Table 6.7 shows the mix composition and evaluation tests for mixtures containing added bitumen.

[3]OFC = total fluid content (i.e. water + emulsion/foam bitumen) at maximum dry density in specimens composed of RAP, water and emulsion or foam bitumen.

[4]In these tables, (co) refers to constant quantity while (v) refers to varying quantity.

Table 6.5 Composition of cold RAP mixtures—Mixing moisture content (MMC)

Method	Composition/comment
California-foam bitumen (Transportation Research Board 2011)	RAP + water (v) + cement or lime(co) + foam bitumen: foam bitumen = 3% by weight of dry material and MMC = 0.75–0.9 OMC
Norway-emulsion/foam bitumen (FHWA-SA-98-042 1997)	MMC between OMC and (OMC-0.5%)

Table 6.6 Composition of cold RAP mixtures—Optimum fluid content (OFC)

Method	Composition/comment
Wirtgen-emulsion (EN 932-1 1996)	RAP + water (v) + emulsion (co): bitumen content in emulsion = 2–3% by dry weight of RAP, specimens compacted using AASHTO T-180
Wirtgen-foam bitumen (EN 932-1 1996)	OFC = OMC for foam bitumen mixes
South Africa-emulsion (Jones et al. 2009)	RAP + water (v) + emulsion (v): cement or lime added if required

Table 6.7 Composition of cold RAP mixtures – Evaluation tests for mixtures containing added bitumen

Method	Composition {Intended test}
California-foam bitumen (Transportation Research Board 2011)	RAP + foam bitumen (v) + water (MMC) {Indirect tensile test CT 371}
Minnesota-emulsion (Standard Specifications for Highway and Bridge Construction 2011)	RAP + water (v) + emulsion (v): total water = 4% by total weight of mixture, emulsion <3%
Norway-emulsion/foam bitumen (FHWA-SA-98-042 1997)	RAP + water (MMC) + emulsion: emulsion = 2–3% {Indirect tensile test HB014 14.554}
Wirtgen-emulsion/foam bitumen (EN 932-1 1996)	RAP (co) + cement or lime (co) + water (v) + emulsion (v): water + emulsion = OFC RAP (co) + cement or lime (co) + water (co) + foam bitumen (v): water = 0.9 OMC for 100 mm diameter specimens or water = OMC for 150 mm diameter specimens {Indirect tensile test, unconfined compression strength}
Modified Marshall-emulsion ((Cross et al. 2010), AASHTO T-283)	RAP + water(v) + emulsion(v): total water = 3% {Maximum specific gravity} RAP + water (v) + emulsion(optimum) {air voids content}

(continued)

Table 6.7 (continued)

Method	Composition {Intended test}
NYS DOT-proposed specification emulsion (Cold Recycling 2010)	RAP + water (co) + emulsion (v): emulsion = 0.5–4% by dry weight of RAP, water = 1.5–4.5% {Marshall stability at 400 °C}
South Africa-emulsion (EN 13108-8 2005)	RAP + water (v) + emulsion (v) + cement/lime (if necessary): total water = OFC, {Indirect tensile test for level 1 and 2, triaxial tests for level 3}
South Africa-foam bitumen (EN 13108-8 2005)	RAP + water (co) + foam bitumen (v) + cement/lime (if necessary): water = 65 to 85% OMC, {Indirect tensile test for level 1 and 2, triaxial tests for level 3}

6.2.10 *Pre-compaction Curing and Specimen Compaction Methodologies*

CPR and CIR of asphalt pavements are characterized by specific equipment and practices. The mixing phase of CPR is followed by transportation, laying and compaction, whereas mixtures produced by CIR are mixed and immediately compacted in situ. The same rollers are generally employed for compaction in both technologies and pre-compaction procedures differ mainly in working time.

Cold Recycled Mixtures (CRM) produced by plant recycling CPR and CIR are physically and mechanically similar, and their laboratory pre-compaction and compaction processes share the same equipment and follow the same operating steps. However, time and temperature effects, along with production-related aspects, should be taken into account.

Currently a universally accepted compaction procedure for CRM is not available. At the state of the practice, two main categories of laboratory procedures can be distinguished. The first one uses impact compaction (Marshall and Proctor method), the second one applies kneading or vibratory stress on the material (shear gyratory compactor and vibratory compactor) simulating the effect of rollers and facilitating aggregates reorientation.

The compaction energy to be applied and the selection among these methods depend mainly on the specific role of CRM in the pavement structure and technical experiences. When CRM is used as an improved granular material, impulsive compaction could be more reliable, whereas when it is used as surrogate of a bound mixture the kneading or vibratory compaction could be more effective.

Cold recycled asphalt mixtures without added bitumen are mainly compacted using the Proctor or AASHTO T-180 method while mixtures with added bitumen are mainly compacted using the Marshall or gyratory compaction. Table 6.8 shows a summary of some of the compaction methods used for cold RAP mixtures with and without bitumen.

Table 6.8 (a), (b) Compaction methods used for cold RAP mixtures with and without bitumen

(a)		
Method	California-foam bitumen (Transportation Research Board 2011)	
Mixture without bitumen	Mixture with bitumen	Mould type and sizes-bituminous mixture
AASHTO T-180 (method D)	Marshall 75 × 2 blows	4 inch × 2.5 inch (diameter × height)
Method	California-emulsion (Maintenance Technical Advisory Guide (MTAG) 2008)	
Mixture without bitumen	Mixture with bitumen	Mould type and sizes-bituminous mixture
–	Marshall 75 × 2 blows 30 gyrations	–
Method	Minnesota–emulsion (Standard Specifications for Highway and Bridge Construction 2011)	
Mixture without bitumen	Mixture with bitumen	Mould type and sizes-bituminous mixture
–	Gyratory 600 kPa, 1.250°	101.6 mm diameter
Method	Norway-emulsion/foam bitumen (FHWA-SA-98-042 1997)	
Mixture without bitumen	Mixture with bitumen	Mould type and sizes-bituminous mixture
Modified proctor	Gyratory 600 kPa, 10, 30 rpm, indirect tensile test specimens compacted to 96% of density at 200 gyrations	100 mm diameter
Method	South Africa foam bitumen level 1 (EN 13108-8 2005; Austroads 2011)	
Mixture without bitumen	Mixture with bitumen	Mould type and sizes-bituminous mixture
Vibratory hammer	Vibratory hammer	150 mm diameter
Method	South Africa-foam bitumen level 2 (Austroads 2011)	
Mixture without bitumen	Mixture with bitumen	Mould type and sizes-bituminous mixture
Vibratory hammer	Vibratory hammer	150 mm diameter
(b)		
Method	Wirtgen-emulsion/foam bitumen (EN 932-1 1996)	
Mixture without bitumen	Mixture with bitumen	Mould type and sizes-bituminous mixture
AASHTO T-180	Marshall 75 × 2 blows or vibratory compaction	–
Method	Modified Marshall-emulsion ((Cross et al. 2010), AASHTO T-283)	
Mixture without bitumen	Mixture with bitumen	Mould type and sizes-bituminous mixture
	Marshall 50 × 2 blows	4 inch diameter
Method	NYS DOT-proposed specification emulsion (Cold Recycling 2010)	
Mixture without bitumen	Mixture with bitumen	Mould type and sizes-bituminous mixture
–	Marshall 75 × 2 blows or 30 gyrations at 25 °C	4 inch diameter

One of the aims of laboratory compaction is to compact specimens in a similar manner to field compaction. However, the extent to which any of these mix design methods simulate field compaction is not clear. As way forward, the mix design method or methods in TG-6 investigations should be chosen through consensus.

The following is a general discussion of various steps involved in both CPR and CIR pre-compaction and compaction procedures.

The ARRA guidelines (Decker and Young 1996) do not consider any specific pre-compaction phase but suggest three methods of compaction for CIR design. Two of these methods use specimens compacted with 50 blows (per face) of the Marshall hammer. In the third method, developed by Oregon State University, CRMs are placed and rodded in a split mold (diameter of 101.6 mm, height of 292.1 mm) in two lifts. Samples are gradually compressed in a hydraulic device for 1 min. The whole process of mixing and compaction is standardized at ambient temperature.

The South African guidelines (EN 13108-8 2005) do not discriminate between CIR and CPR. For BSM, the determination of the optimum fluid content and maximum dry density is carried out in accordance with the modified Proctor test. After mixing, the bitumen treated material is transferred into a container and immediately sealed to retain moisture. To minimize moisture loss from the prepared sample, specimens are compacted as soon as possible, following the relevant procedure AASHTO T-180 for 150 mm diameter specimens.

For BSM, three mix design levels are provided in relation to the traffic intensity and each mix design level allows two different laboratory compaction methods to be used.

The Level 1 mix design requires the Marshall or vibratory compaction (mould diameter of 150 mm). The Marshall equipment must not be heated but kept at ambient temperature. A sufficient material to achieve a compacted height of 63.5 mm $\pm$ 1.5 mm has to be weighted, poured into the mould and poked with a spatula (15 times around the perimeter and 10 times on the surface) leaving the surface slightly rounded. The sample is compacted by applying 75 blows per face with the Marshall hammer.

The vibratory compaction method for 100-mm diameter mould follows a similar preparation procedure. However in this case a loading weight of 25 kg (total mass of assembly: hammer + foot + surcharge) is used. When the vibratory hammer is moved into the mould, 15 s of vibratory compaction has to be applied for each face.

The Level 2 mix design provides the modified AASHTO T-180 or vibratory compaction (mould diameter of 150 mm). Using modified AASHTO T-180 method the material is placed in an airtight container immediately after mixing. Samples are compacted using a 150 mm diameter split-mould, applying modified AASHTO T-180 compaction effort (5 layers approximately 25 mm thick, 55 blows per layer using a 4.536 kg hammer with a 457 mm drop).

The vibratory compaction method for 150-mm diameter mould uses a loading weight of 30 kg (total mass of assembly: hammer + foot + surcharge). A sufficient material to achieve a compacted height of 47.5 mm ± 1.5 mm has to be poured into the mould (first layer). A 25 s of vibration for bitumen emulsion stabilized materials and a 35 s of vibration for foamed bitumen stabilized materials is applied. Using a chisel, the entire surface area of the top of the compacted layer has to be scarified to a maximum depth of 10 mm. For the second layer, sufficient material to achieve a compacted height of 95 mm has to be added into the mould (second layer). Once again a 25 s of vibration for bitumen emulsion stabilized materials and a 35 s of vibration for foamed bitumen stabilized materials is applied.

The Level 3 mix design establishes additional compaction procedures for triaxial testing. By using modified AASHTO T180 compaction effort, 12 layers, each approximately 25 mm thick, are compacted with 55 blows using a 4.536 kg hammer with a 457 mm drop. By using vibratory compaction, specimens are manufactured in 5 layers, each approximately 60 mm thick, using a hammer assembly of 30 kg total mass. Each layer is compacted for 25 s for BSM-emulsion, or 35 s for BSM-foam.

Californian guidelines (Transportation Research Board 2011) for full-depth pavement reclamation with foamed asphalt require to seal the mix in a suitable container and to prepare specimens with a diameter of 100 mm and a height of 63.5 mm, complying with the Marshall method of mix design. Seventy-five compaction hammer blows are applied on each face of a specimen. All compaction must be completed within 8 h of the mixes being prepared. However, the reference dry density is determined according to method D in AASHTO T-180.

Austroads (2011) for foamed bitumen stabilization recommends compaction of test cylinders using gyratory compaction (80 gyrations) or Marshall (50 blows per face) compaction. The mould shall not be heated.

For CIR design, the Kansas department of transportation (Santucci 2007) proposes specimens compacted immediately after mixing at ambient temperature with a Superpave® Gyratory Compactor (SGC) in a 100-mm mould for 30 gyrations. The mould shall not be heated.

Italian highway specifications for CRM require to compact 4.5 kg samples by means of SGC at 180 gyrations. The SGC protocol requires a 150 mm diameter mould, a constant pressure of 600 kPa, a speed of 30 rpm and an angle of gyration of 1.25°. For in situ control the CIR mixture has to be sampled after mixing (behind the recycler) and immediately compacted by means of a mobile SGC. Another study (Bocci et al. 2011) suggested some modifications to obtain a suitable specimen height (about 70 mm) for mechanical tests, such as indirect tensile stiffness modulus. In this case 2.7 kg specimens shall be compacted at 100 gyrations.

It should be noted that the mix design philosophy influences the applicable compaction technique. The SGC is more applicable for asphaltic type mixes (higher

BCs) such as cold mix asphalt. The BSM stabilized mixes (lower binder contents) do not respond well to SGC and need vibratory or drop weight compaction.

For cold mixtures produced by full depth reclamation, Tario et al. (2010) proposed a modified SGC mould, characterized by several holes to allow water flow during compaction. An absorbing cloth should be put around the mould to catch the water during compaction. The slots should be cleaned before each compaction. The emulsion treated samples have to be cured for 45 min at 40 °C and then compacted with the SGC at 75 gyrations.

For CRM with bituminous emulsion, Thompson et al. (2009) suggests the use of a SGC operated according to Superpave specifications (1.25° gyration angle, 30 rpm gyration speed, 600 kPa normal pressure) with a 100 mm mould. The bottom plate of the mould has a square grid of 2 mm holes distributed on a 0.85 cm × 0.85 cm grid. A cylinder placed in the mould under the plate allows the water, which is expelled during compaction, to be gathered. Specimens are prepared with 100 gyrations. Approximately 1100 g of dry material are employed for each sample. The time elapsed between mixing and compaction should be defined trying to meet the actual conditions in field applications.

6.2.11 Post Compaction Curing Processes for CRM

Curing is the process whereby the mixed and compacted material discharge water through evaporation, particle charge repulsion or pore pressure induced flow paths (Dave 2011). The reduction in moisture content leads to an increase in strength and rut resistance of the mix.

In the field, curing may take many months. The laboratory process needs to simulate field conditions of curing, but, as it is impractical to cure for months, an accelerated method is required to emulate field condition.

According to Charmot (2006), oven curing for three days at temperature of 60 °C appears appropriate. From United Kingdom study (Transportek 1998); both the resilient modulus and creep properties of laboratory specimens cured in this manner were similar to those of field cores taken after 12 months after construction. However, as discussed below, more recently the accelerated curing temperature has been lowered to 40 °C.

6.2.11.1 Austroads (2011)

Austroads recommends the following approach to specimens curing:

– Immediately after compaction the cylindrical specimens are tested for modulus without curing. The uncured modulus needs to exceed 700 MPa to ensure that the pavement can be opened to traffic;

- The specimens are then oven cured at 60 °C for three days and then tested for indirect tensile modulus;
- The specimens are then soaked in water prior to testing for their soaked modulus (M_{wet}). Two methods may be used for soaking the specimens: submerged under water for 24 h, or in a vacuum chamber for 10 min;
- The wet and dry modulus (M_{dry}) results are then plotted versus bitumen content to define the optimum modulus.
- Note: samples should be prepared with moisture contents such that M_{wet}/M_{dry} is 0.5 or more, because bituminous binders will not cure at excessive moisture contents.

Please note that the 60 °C curing temperature is typically higher than the softening point of the binder. On large projects, additional testing may be undertaken including unconfined compressive strength, flexural fatigue and creep.

6.2.11.2 Queensland Department of Transport and Main Roads (Kleyn 1984)

In the TMR (Transport and Main Roads) method, the prepared specimens are tested for modulus in three states as follows:

- Initial modulus after 3 h curing at 25 ± 5 °C is determined to provide an indication of susceptibility to permanent deformation early in pavement life. Where the initial daily traffic on opening is 1000 ESA (Equivalent Standard Axle) or more, TMR recommends this three hour curing time to confirm by wheel tracker testing;
- Cured modulus where the sample is oven cured at 40 °C for three days to provide an indication of medium term stiffness 3–6 months after construction;
- Soaked modulus where the sample is submerged under water for 10 min under a 95 kPa vacuum to provide an indication of the moisture sensitivity of the material.

Based on TMR experience, laboratory cured samples compacted to 50 blow Marshall compaction achieve resilient modulus values similar to the upper half of field cores after 12–24 months field curing.

TMR practice is not to seal the samples during curing.

6.2.11.3 Asphalt Academy (TG 2) (EN 13108-8 2005)

In the current South African method, the shortcomings of several curing methods in use were discussed as follows:

- Curing at 60 °C in an oven results in lower moisture contents than field equilibrium;

- Characterising materials with secondary binders, where curing for 7 days or 28 days results in time delays;
- Sealing specimens in plastic bags and curing for 72 h in an oven at 40 °C retains excessive moisture and gives conservative results;
- Curing for 24 h at 25 °C (unsealed) followed by 48 h sealed in a bag and cured in an oven at 40 °C more closely reflects equilibrium moisture content but does not provide evidence that the laboratory stiffness truly reflects field stiffness;
- Interpretation of stiffness from tangent modulus derived from modified Californian Bearing Ratio (CBR) compression tests and determination of curing time at ambient temperature yields modulus values comparable to that used in the mechanistic design—but results in time delays and requires more research;
- "Steady state" moisture content at 40 °C.

Whilst research is currently underway in southern Africa, the current recommended method is to cure for 48 h at 40 °C until steady state moisture content is reached; then seal, condition to test temperature of 25 °C overnight, and test.

In particular, considering the number of variables that need to be addressed in the mix design and the amount of material required to investigate these variables, the mix design procedure involves several steps and one or more series of tests (levels), depending on the magnitude of design traffic. The mix design procedure always starts by testing the material to be treated (preliminary tests) to determine whether it is suitable for treating with bitumen and, if not, the type of pre-treatment or blending required to make it suitable. Following this, the actual Asphalt Academy mix design procedure commences with an initial series of tests (Level 1 Mix Design) that provides an indication of the application rate of bitumen and active filler (if necessary) required to achieve an indicated class of BSM. Thereafter, depending on the design traffic, additional tests are undertaken to refine the application rate of bitumen and gain confidence in the performance potential of the treated material (material classification). These are the Level 2 and Level 3 Mix Designs. In summary, the mix design procedure consists of:

- Preliminary tests: These include standard laboratory tests to determine the grading curve, moisture, density relationships and Atterberg limits. Where the results indicate that some form of pre-treatment is required, additional tests must be undertaken after such pre-treatment to ensure that the desired result was achieved;
- Level 1 Mix Design: Level 1 starts with the preparation of samples that will be used to manufacture the specimens required for all levels of mix design testing. 100 mm diameter specimens (Marshall moulds) are compacted and cured for Indirect Tensile Strength (ITS) testing. Test results are used to:
  - Identify the preferred bitumen stabilising agent;
  - Determine the optimum bitumen content;
  - Identify the need for filler, and, where required, the type and content of filler.

Level 1 mix design is sufficient for lightly trafficked pavements, which will carry less than 3 MESA (Million Equivalent Standard Axle).

- Level 2 Mix Design: This level uses 150 mm diameter by 127 mm high specimens (Proctor specimens) manufactured using vibratory compaction, cured at the equilibrium moisture content and tested for ITS to:
  - Optimise the required bitumen content.

  This level is recommended for roads carrying 3 to 6 MESA.
- Level 3 Mix Design: This level uses triaxial testing on 150 mm diameter by 300 mm high specimens for a higher level of confidence. This step is recommended for design traffic exceeding 6 MESA.

Curing of BSMs is the process where the mixed and compacted layer discharges water through evaporation, particle charge repulsion and pore-pressure induced flow paths. Curing process depends on stabilising binder to be used:

- For emulsion bitumen stabilised materials, chemistry plays a significant role in the curing process. Water is an intrinsic component of bitumen emulsions. Breaking of the bitumen emulsion needs to take place before curing via migration and evaporation. BSM-emulsion usually requires longer curing times than BSM-foam because of the higher moisture contents.
- For BSM-foam, curing takes place as a result of migration of water during compaction and continues with evaporation of the water.

The reduction in moisture content leads to an increase in the tensile and compressive strength, as well as stiffness of the mix. It is imperative that this process is realistically simulated in the laboratory for mixes to be assessed for their expected field performance.

The rate of moisture loss from newly constructed BSM layers plays a significant role in determining the performance of the layer. It is in the early period of repeated loading that the majority of the permanent deformation takes place in BSM layers. Where a new BSM layer is to be trafficked immediately after finishing, it is important to minimise the moisture content during construction.

The lower the degree of saturation of the BSM, the greater the resistance to permanent deformation. The temperature of the layer in the field and the loss of moisture with time are the two factors to consider with curing, and hence, stiffness and strength gain. Although a BSM should have sufficient stiffness and strength to withstand moderate levels of early traffic, the layer will continue to gain strength over several years in the field.

The recommended curing procedure differs for the specimen size and bitumen types, BSM-emulsion and BSM-foam. Although the use of active filler has an impact on curing, its inclusion in a BSM does not justify extensions in the curing time as cementation is not one of the desired properties of these materials (cement content should remain under 1%).

For Level 1 mix designs, the 150 mm diameter specimens are cured until they reach a constant (dry) mass, typically with moisture contents of less than 0.5%.

Testing follows 72 h of curing at 40 °C without sealing the specimens to determine the ITS_{dry} value. Half the specimens are then soaked for 24 h before testing to determine the ITS_{wet} value. This procedure is aimed at evaluating the moisture susceptibility of the BSM.

The curing procedure for 150 mm diameter specimens used in Level 2 and Level 3 mix designs typically produces moisture contents of 43–50% of OMC (Optimum Moisture Content), which represents the long-term equilibrium moisture content of the material in the field. To achieve this, different curing periods are required for BSM-emulsion and BSM-foam. Unsealed specimens are initially placed in a draft oven at 30 °C to allow the moisture content to reduce. Thereafter, they are individually sealed in loose-fitting plastic bags (at least twice the volume of the specimen) and cured for a further 48 h at 40 °C. The wet plastic bags must be replaced with dry bags every twenty four hours.

Before the specimens are tested, they should be allowed to cool down to the required test temperature whilst sealed in a new dry plastic bag to prevent any further moisture loss.

6.2.11.4 Wirtgen Cold Recycling Manual (EN 932-1 1996)

The curing procedure recommended by the Cold Recycling Manual is the following: place the specimens in an oven at 40 °C for 20–24 h or until the moisture content has reduced to at least 50% of OMC. Thereafter place each specimen in a sealed plastic bag (at least twice the volume of the specimen) and in an oven at 40 °C for a further 48 h. Remove specimens from the oven after 48 h and take out of their respective plastic bags, ensuring that any moisture in the bags does not come into contact with the specimen. Allow to cool to ambient temperature.

6.2.11.5 University of California, Pavement Research Centre (Transportation Research Board 2011)

According the procedure suggested by the University of California, the mix preparation should follow following items:

- Prepare eight samples (25 lbs [10 kg] each) of pulverized material, sufficient for testing an untreated control and three asphalt binder contents, each with a replicate. Do not add active filler:
- Place the prepared material into the mixer and begin agitation;
- Add sufficient water to achieve the MMC. Keep the mixer running for approximately five minutes to allow the moisture content to equilibrate.
- Spray the specified foamed asphalt content onto the pulverized material (skip this step for the untreated control);
- Seal the prepared mix in a suitable container;

- From each batch, prepare six specimens with a diameter of 4 in. (100 mm) and a height of 2.5 in. (63.5 mm), complying with the specimen preparation procedure described in the Asphalt Institute's Mix Design Methods for Asphalt Concrete (MS-2) (Marshall Method of Mix Design). Seventy-five compaction hammer blows are applied on each face of a specimen. All compaction must be completed within eight hours of the mixes being prepared;
- Extrude the specimens from the mould immediately after compaction and cure in a forced draft oven at 105 °F (40 °C) for 72 h;
- After curing, remove the specimens from the oven and place in a water bath for 24 h. Water temperature should be between 68 and 77 °F (20 and 25 °C). Water depth should be 4.0 in. (100 mm) above the specimen surface. Specimens must not be stacked.
- After soaking, remove the specimens from the water and allow them to drain for 60 min and equilibrate to the room temperature. Ambient temperature should be 77 °F ± 4 °F (25 °C ± 2 °C). Specimens should be covered with a damp cloth to prevent excess evaporation. Care should be taken at all times to prevent damage to the specimens.

6.2.11.6 ANAS (Agenzia Nazionale Autonoma Delle Strade) Italian Road Authority (Hefer and Scullion 2002)

Subbase specimens made with foam stabilised materials must be compacted in 150 mm mould with 180 rotation of gyratory compactor (600 kPa vertical pressure, rotation angle 1.25° and speed 30 gyrations/min). Sample should then be cured for 72 h at 40 °C and cooled to 25 °C for four hours before testing. Same procedure should be followed when rehabilitation is made with bitumen emulsion.

6.2.12 Test Procedures to Evaluate Curing

6.2.12.1 Background on Curing Evaluation of Cold-Recycled Mixtures

The amount of curing in actual field conditions depends on several factors including climatic conditions, amount of moisture in the mix, level of compaction and drainage and moisture conditions of the underlying layers. As described in the previous section, a significant amount of curing procedures in the literature are prescriptive in nature, whereby a definite amount of time and temperature is required. In order to standardize protocols for specimen preparation to conduct mechanical and physical property tests, it is necessary to have a test procedure to evaluate the curing.

There have been numerous studies that reported physical and mechanical properties of cold recycled mixtures in cured conditions using laboratory curing process. While significant amount of literature is available, very little has been reported on quantitative and qualitative comparisons between material properties and curing of mixes. This literature review is limited to studies where evaluation of curing is presented by series of laboratory tests and not necessarily studies where single set of results are presented for so called cured samples.

The procedures commonly used to evaluate the curing can be divided into three main categories: (1) use of moisture content; (2) use of laboratory measured mechanical tests; and (3) field measurements. Since this paper focuses on laboratory specimen preparation the field measurement techniques are not included in the discussions.

6.2.12.2 Use of Moisture Content

The moisture content based evaluation can further be broken down to following categories:

- Absolute moisture content (Gray 1962; Saleh and Herrington 2003);
- Percent of optimum moisture content from moisture-density relationships (EN 932-1 1996; Transportation Research Board 2011; EN 13108-8 2005; Saleh 2004), and;
- Use of stable weight conditions (Santucci 2007).

The use of moisture content as means to indicate the amount of curing has been mostly based on empirical observations between lab and field moisture conditions. As pointed out by Asphalt Academy (2009), it is very important to determine the mechanical properties of cold recycled mixtures containing emulsion to evaluate curing. The stability and strength of cold recycled asphalt concrete layer in field has most significant effect on pavement performance thus, use of mechanical properties for evaluation of curing seems more reasonable.

6.2.12.3 Use of Laboratory Measured Mechanical Properties

A number of laboratory measured mechanical properties have been employed by researchers for evaluation of curing, including: indirect ITS, Indirect Tensile modulus or Resilient Modulus (ITRM), Unconfined Compressive Strength (UCS), Marshall and Hveem stability, and ravelling test. The following subsections provide a review on the use of mechanical tests for evaluation of curing in cold recycled asphalt mixtures.

Indirect Tensile Strength (ITS) Test

Historically the Indirect Tensile Strength (ITS) test has been prescribed by numerous cold recycled asphalt mix design procedures to evaluate the potential for moisture induced damage, such as Asphalt Academy Mix Design Procedures (EN 13108-8 2005) and Norwegian Public Roads Administration's Guidelines for Cold Bitumen Stabilized Base Course (FHWA-SA-98-042 1997). As per Asphalt Academy (EN 13108-8 2005), the ITS test is used as an indirect measure of the tensile strength and flexibility of the cold-mixes to reflect the flexural characteristics of the material. The widespread availability of ITS test equipment and its low cost has made it a popular choice for curing evaluation of cold recycled mixes. The ITS test protocols show minor variations between various agencies and researchers. The majority of test procedure follows the standard indirect tensile strength evaluation as per the AASHTO T-283 protocol used for determining moisture induced damage in asphalt mixtures.

Asphalt Academy (2009) provided an in-depth evaluation of curing criteria for cold in-pace recycling, their study focused on use of ITS as a parameter to evaluate effect of curing. The findings from their study further reinforce the superiority of using mechanical properties for curing evaluation as compared to use of moisture prescribed conditions. The study by Asphalt Academy (2009) involved testing of three cold recycled mixes at seven curing levels and three curing temperatures. The same study also showed a gradual increase in ITS values with reduction in moisture content from 3.5 to 1% as well as continued increase in ITS values of lab samples for as long as 28 days. A related study by New York State DoT (2010) concluded that duration of curing and moisture content showed most significant effects on the measured ITS values, furthermore even at a constant moisture content the ITS value increases with prolonged curing period.

Maccarrone et al. (1994) showed the applicability of ITS in designing cold recycled mixes. Their study pointed out that cold mixtures show approximately 15% improvement in ITS values for field samples between the duration of six months and three years. Ramanujam and Jones (2000) reported series of ITS results for cold in-place recycled asphalt mixes at various density levels. The test results were reported for ITS tests conducted in dry and wet conditions; the results showed significant improvement in ITS values with increasing density. Linearly increasing ITS values for cold recycled asphalt mixes have been reported by Mohammad et al. (2003) with increasing cement amount and curing times. A study by Salomon and Newcomb (Standard Specifications for Highway and Bridge Construction 2011) conducted series of ITS tests on mixes utilizing recycled materials from three field projects. The study showed that ITS values did not change significantly between one and seven days of curing, however remarkable differences were observed in the failure modes. Specimens that were cured longer showed minimal signs of failure at the point of ultimate strength, whereas significant disintegration is observed for short term cured specimens.

Indirect Tensile Modulus or Resilient Modulus (ITRM) Test

The Indirect Tensile Modulus or Resilient Modulus (ITRM) is typically measured using similar test configuration as the ITS. The main difference is the measurement of resilient (recovery) modulus under repeated (pulse) loading conditions at a given stress amplitude and loading frequency. The ITRM properties have been measured and reported with varying degree of sophistication: from simple measurements, such as instantaneous modulus at a given time and stress amplitude, to creep compliance master-curves, developed using measurements at multiple test temperatures and time increments.

The Queensland Department of Transport and Main Roads (Epps 1990) design method for cold mixes requires measurement of ITRM on uncured and cured samples. Early works by National Center for Asphalt Technology (1998), and Charmot (2006) showed potential of ITRM in correlating to the amount of curing. A model to predict ITRM values as function of curing time and temperature has also been proposed (Reclaimed Asphalt Pavement: User Guideline). A study conducted by Scholz et al. (1990) showed that ITRM values for loose mix curing showed reduction over period of time ranging from 0 to 50 h. However, in compacted samples the ITRM values improved significantly over the duration of 24 h as the specimens were left outdoors for curing.

Unconfined Compressive Strength (UCS) and Marshall/Hveem Stability

Apart from ITS and ITRM, the unconfined compressive strength (UCS) Marshall/Hveem stability have been most widely reported as properties for evaluation of curing in cold recycled mixes. While several studies have shown that UCS and stability values highlight good distinction between uncured and cured samples (Murphy and Emery 1996; AASHTO AGC–ARTBA Joint Committee 1997), no reported studies presented an in-depth investigation that shows quantitative relationship between curing at various times against these properties.

Ravelling Test

The ravelling test has been specified as ASTM D7196 test procedure for determining the potential for ravelling distress in asphaltic paving layers. The test procedure is recommended as optional test for New York State Department of Transportation (NYSDOT) (Cold Recycling 2010) to indicate the level of curing. The incorporation of ravelling test by NYSDOT as indicator of curing level is based on unpublished data from labs at private companies. The only other report showing correlation between level of curing and ravelling test results is due to Queensland Department of Main Roads (2009), Engineering Service Center (2005). This study showed that for two cold recycled mixes (one with emulsion and other with foamed asphalt) the amount of ravelling loss reduced significantly as the curing time increased from 4 to 8 h.

Triaxial Test

The triaxial testing has also been recommended by few cold recycling methods to determine the strength gain and extent of curing (EN 13108-8 2005). The triaxial testing of cold mixes at early age is natural, as the material behaviour is more "granular-like" rather than that of asphalt concrete. The triaxial testing is used to obtain shear properties of the cold recycled materials and their behaviour in confined conditions. The Asphalt Academy (South Africa) design manual for cold mixes (EN 13108-8 2005) recommend triaxial testing for roadways with traffic levels above 6 MESA. Duval (2008) has proposed a simplified triaxial test for cold recycling mixes that involves monotonic loading and specialized cell. The test procedure has shown very promising results and accommodates specimens prepared using the SGC. The work by Rogge et al. (1992) further confirms the utility of triaxial test in determining the extent of curing. Their study determined resilient modulus and shear strength of cold recycling mixes at three temperatures and three curing levels.

6.2.12.4 Summary of Post-compaction Curing Evaluation Methods

Based on the literature review on the topic of test procedures for evaluating curing in cold recycled asphalt mixes it can be found that the ITS is the most widely accepted test for curing evaluation with most supporting data available in literature. The indirect tensile strength is followed by indirect resilient modulus as an indicator test for evaluation of curing. Triaxial tests have also shown good potential in determining the extent of curing through use of shear strength. Other test procedures have been used and reported in literature. However, the extent of their usage and availability of published data is not comparable to indirect tensile strength and resilient modulus.

6.3 Description and Explanation of Test Protocol for RAP Classification Used During the Inter-laboratory Study

6.3.1 Introduction

The inter-laboratory study on the characterization of RAP was based on the evaluation of RAP material having different origins (i.e. different HMA, milling operation, pavement conditions, aging and distresses, and storage time/conditions) and consisted in a specifically designed testing protocol. Each participant institution and laboratory selected two different types of RAP, carefully ensuring that the two recycled materials were as different as possible. In addition, and for the purpose of calibrating the selected testing procedures, a conventional reference hot mix asphalt was distributed to all the participants for testing and characterization. The reference mixture was produced in a mixing plant and preliminary tested to ensure its homogeneity before being delivered to the participant laboratories.

6.3.2 Selection and Sampling

RAP was selected based on the simple criteria for which material sources need to be significantly different: different HMA, such as asphalt binder, aggregate type, particles size, particle size distribution; different milling operation; different pavement conditions, especially different pavement distresses; and different storage time and conditions. Figure 6.2 shows two stockpiles of RAP from two different geographic areas.

The sample amount obtained from each agency was large enough to be representative for the RAP origin and sufficient to complete the round robin testing (RRT) program. Figure 6.3 presents an example of two types of RAP analysed in the present inter-laboratory study.

For the pre-treatment of the RAP samples no specific protocol was applied. Some laboratories air dried the samples at room temperature for 24 h and then placed them in a thermostatically controlled oven at a temperature of 40 °C for 24 h. Homogenization of the main samples before reducing them to test samples was a standard practice.

Fig. 6.2 Two different storage conditions for RAP stockpiles

Fig. 6.3 Example of two different RAP types

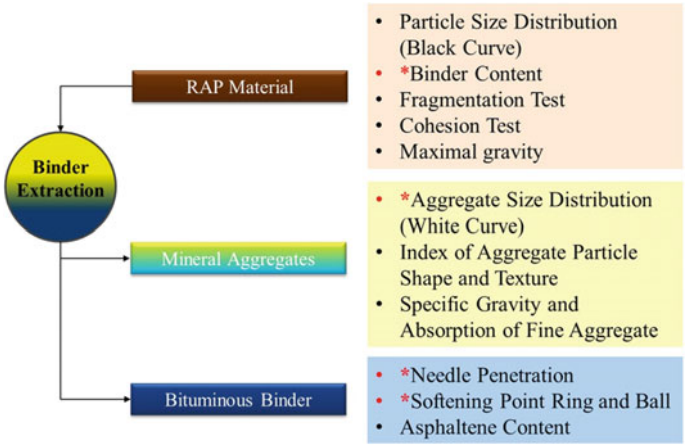

Fig. 6.4 Overview of important RAP characteristics. *These tests are carried out on several samples to determine the homogeneity of RAP

6.3.3 Testing

Because test methods are not internationally harmonized, American (ASTM, AASHTO) and European (EN) standards were applied to test the same characteristics. However, often the test methods are very similar and variation due to the different standards is acceptable. Furthermore, every laboratory tested the RAP material available in their country.

The properties depicted in Fig. 6.4 have been identified to be important for the characterization of RAP material and were applied in this inter-laboratory study. However, not all tests methods were carried out by every participating laboratory, either because the method is not used in that country, or the devices were not available or for other reasons.

6.3.3.1 Particle Size Distribution

Particle size analysis seems to be straight forward, but a set of variations are found across the world. The selection of sieve sizes is not only different between Europe and America, where the metric system is still not implemented in USA, but even in Europe two different sieve sets are used. Furthermore, there is a distinction between dry and wet sieving. In the wet sieving process either the sieving itself is carried out under running water or minerals are washed and then followed by dry sieving without water. This ensures that the small particles, essentially filler, are washed away and not sticking to larger aggregates.

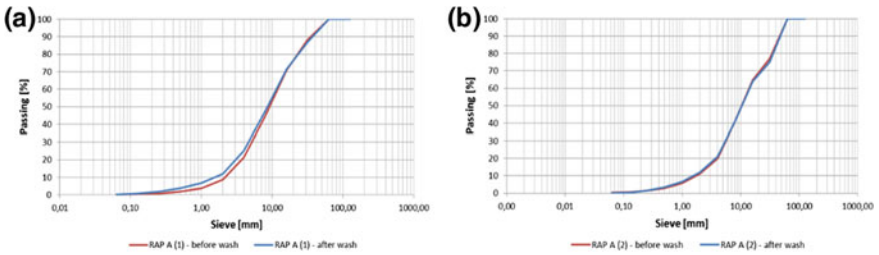

Fig. 6.5 Example of black curves before and after washing: **a** method A and **b** method B

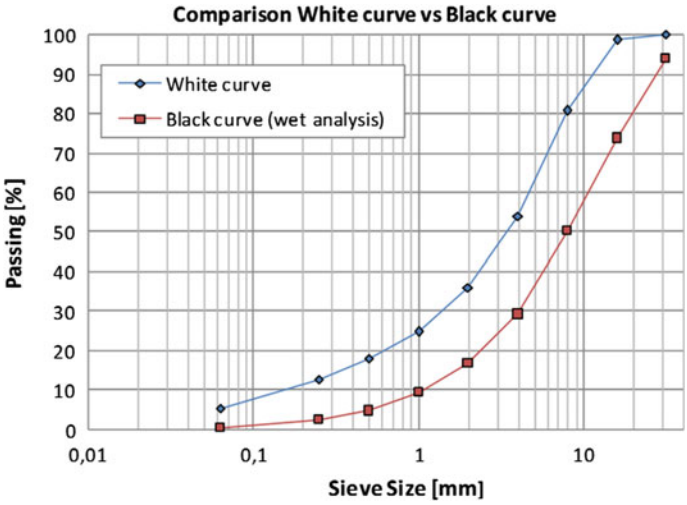

Fig. 6.6 Comparison between "black curve" and "white curve" for RAP A

Analysis of RAP Particle Size Distribution—Black Curve

In order to obtain what is conventionally known as "black curve", aggregate size analysis was performed on RAP after washing the material. There are two ways we could proceed to determine the "black curve" after washing: method A and method B. In the method A, the RAP material is washed with water over a 0.063 mm or 0.075 mm sieve to remove the finest particles in the range of filler (ASTM C136, EN 933-1). After washing, the retained RAP material on the chosen wash sieve is dried at 30 °C, and sieving and gradation are performed. Figure 6.5a shows the comparison between the sieve size analysis performed on RAP A before washing and after washing in reference to the method A. With the second approach (method B), the wet sieving of the RAP is carried out under a continuous flow of water during all the sieving processes. Figure 6.5b clearly shows that the method B could affect the grading curve on each sieve of the RAP aggregate when compared to the method A.

In contrast to mineral aggregates, RAP is partly composed of agglomerates sticking together. Depending on the sieving parameters (frequency, amplitude, time), as well as the type of sieving apparatus and the temperature, the agglomerates are broken down to different extents. For this reason, the black curve is difficult to reproduce unless the sieving parameters are defined, which was not the case in the present inter-laboratory study.

Particle Size Analysis of RAP Aggregates—White Curve

In addition to the particle size analysis of RAP, the size distribution of the mineral particles contained in the recycled material was investigated. Asphalt binder was recovered from RAP samples and the binder content (by percent of the weight of RAP) was determined (ASTM D2172, EN 12697-1). Alternatively, the binder content can be analysed by the ignition method (EN 12697-39, ASTM D6307). However, using this procedure, the bitumen properties cannot be tested. The aggregates obtained after binder recovering were used for aggregate size analysis (after washing) in order to determine the "white curve" of RAP (ASTM C136, EN 933-1). In Fig. 6.6 "black curve" and "white curve" are compared for RAP A, which allows the estimation of the amount of agglomerated particles in the recycled material (Fig. 6.6). For example, in Fig. 6.6 approximately 25% of the particles is passing the sieve 16 mm.

6.3.3.2 Fragmentation Test

The "dynamic" fragmentation test measures the particle resistance to fragmentation under a series of shocks induced by dropping a steel mass, called a rammer, on a confined sample placed in a cylindrical steel mould. In this specific case, the modified Proctor test procedure (EN 13286-2; ASTM D1557) was adopted to perform a series of impact tests on different sources of RAP.

The Fragmentation test consisted of an evaluation of the amount of a material passing through a control sieve after a fixed series of strokes carried out with a normalized falling mass. The material crushed to sizes finer than a control sieve is separated and expressed as a percentage of the original weight taken in the mould. The percent passing through the control sieve PCS(%) is noted.

A total of 5 laboratories (*LAB A to LAB E*) located in 4 different countries were involved in the testing program. Table 6.9 presents all details regarding the testing

Table 6.9 Summary of testing procedure used by each laboratory involved in the RRT

	LAB A	LAB B	LAB C	LAB D	LAB E
Inside mould diam. (mm)	101.6	150.0	100.0	151.2	152.3
Rammer weight (g)	4535	4535	4500	4535	4800
Height of fall (cm)	45.7	45.7	45.7	45.7	45.0
Blows per layer	56	56	56	56	50
Number of layers	5	5	5	5	5
Control sieve (mm)	1.6	1.6	1.6	1.7	1.6

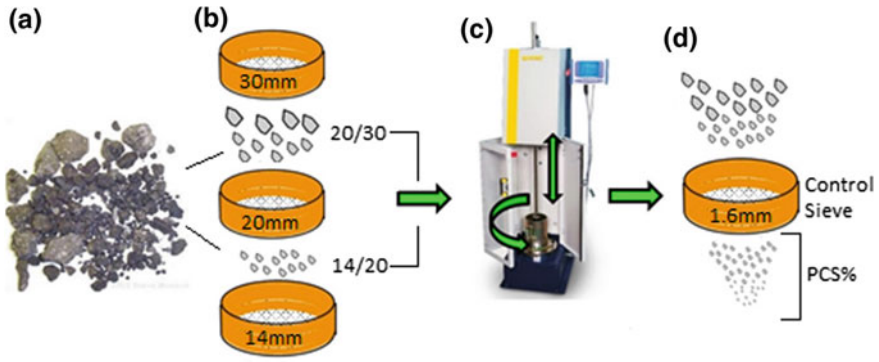

Fig. 6.7 Procedure and apparatus used in the fragmentation tests (ASTM D 1557)

procedure followed by each laboratory participating in the RRT. The test is performed on different aggregate fractions 20/30, 14/20, 10/14, and 5/10 mm. The first number of the fraction represents the size of the sieve for which 100% of material is retained, while the second number refers to the size of the sieve where 100% of material is passing.

Figure 6.7 shows a schematic of the fragmentation test procedure: the material is first sieved (Fig. 6.7a, b) and then compacted in five layers (Fig. 6.7c) with a fixed number of blows per layer (Table 6.9) using a standardized falling mass. At the end, the fine material produced by the impact of the hammer is sieved with the control sieve (Fig. 6.7d). An example of fragmentation test results is presented in Table 6.10.

6.3.3.3 Cohesion Test

RAP material can be classified as "active" or "inactive", depending on the capacity of the residual binder to glue the particles together after compaction. The resulting cohesion is directly linked to the penetration of the aged binder and the compaction temperature, for which three different temperatures 20, 70 and 140 °C have been chosen for the RRT. Even though in cold recycling the RAP is not heated, higher test temperature have been added in order to extend the RAP testing protocol to hot recycling.

The cohesion test was performed on the original RAP material (no additional asphalt binder was used) with a maximum aggregate size of 20 mm. Before testing the RAP was dried at 30 °C until the weight loss within 24 h was less than 1%. Compaction (Fig. 6.8b) was performed with a SGC, with using a 150 mm diameter mould, at 30 gyrations in agreement with ASTM D6925 or EN12697-31. During compaction the air void content was calculated continuously. Alternatively, Marshall compaction (ASTM D6926, EN 12697-30) with 50 blows on each side at the same three temperatures have been used. The compacted specimens were

Table 6.10 Example of fragmentation test results

RAP	A				
Temperature test: 5 °C					
Size classes	100% passing	30 mm	20 mm	14 mm	10 mm
	100% retained	20 mm	14 mm	10 mm	5 mm
Weight before hammering (g)		192	235	213	242
Material passing the control sieve after hammering (g)		24	19	17	21
Coefficient of fragmentation (PCS%)		12.5	8.1	8.0	8.7
RAP	A				
Temperature test: 20 °C					
Size classes	100% passing	30 mm	20 mm	14 mm	10 mm
	100% retained	20 mm	14 mm	10 mm	5 mm
Weight before hammering (g)		304	215	169	146
Material passing the control sieve after hammering (g)		14	15	12	13
Coefficient of fragmentation (PCS%)		4.6	7.0	7.1	8.9
RAP	A				
Temperature test: 40 °C					
Size classes	100% passing	30 mm	20 mm	14 mm	10 mm
	100% retained	20 mm	14 mm	10 mm	5 mm
Weight before hammering (g)		287	276	242	220
Material passing the control sieve after hammering (g)		8	8	9	9
Coefficient of fragmentation (PCS%)		35.9	34.5	26.9	24.4

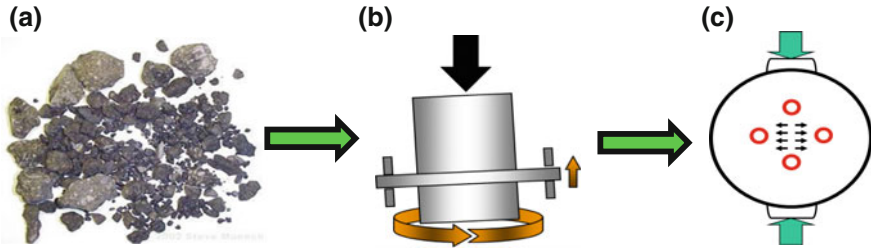

Fig. 6.8 Procedure and apparatus used in the cohesion test (ASTM D 6925)

conditioned in water at 25 °C for 24 h. The ITS test at 25 °C (ASTM D6931; EN 12697-23) (Fig. 6.8c) was selected to evaluate the degree of cohesion. Table 6.11 shows a typical cohesion test results obtained from the RRT.

6.3.3.4 Analysis on Extracted RAP Particles

The degree of agglomeration of RAP is dependent on the storage conditions and climatic conditions. Therefore, it is often preferred to perform determination of density and particle shape on the extracted mineral aggregates. The density of the RAP-particles can be back-calculated using binder and aggregate density. The extracted mineral particles or RAP-particles after extraction are analyzed with the following test methods:

- Aggregate Particle Shape and Texture (ASTM D 3398, EN 933-3 and 4)
- Specific Gravity and Absorption of Coarse Aggregate (ASTM C127, EN 1097-6)
- Specific Gravity and Water Absorption of Fine Aggregate (ASTM C128, EN 1097-7)

6.3.3.5 Specific Gravity, Water Absorption and Aggregate Particle Shape

In Europe, particle density is determined with EN 1097-6, whereas in USA the ASTM C127 and C128 specific gravity is preferred, which is the density relative to water (called relative density). Still, the methods are similar: coarse aggregates are measured in air and in water applying the Archimedes' principle of buoyancy. For fine aggregates this method is not applicable and specific gravity is measured indirectly through its volume in a calibrated solvent filled pycnometer. This method is applicable also for coarse aggregates. At the same time the water absorption and water content of RAP or aggregate particles can be determined.

Specific gravity itself is not a performance property, but is essential for the design of the aggregate composition. To obtain reasonable data it is necessary to determine the specific gravity on different fractions, at least on a fine (sand) and a coarse fraction.

Water content of RAP is an important parameter both for hot and cold recycling. In cold recycling, the amount of water has to be taken into account for the calculation of the optimum water content for compaction. In hot recycling, water will be evaporated in the drying and mixing process and therefore has to be minimized to reduce unnecessary energy consumption.

The aggregate particle shape and texture provides a quantitative measure of the aggregate shape and texture characteristics that may affect the performance of road and paving mixtures. These characteristics are measured with different methods according with EN and ASTM standards only on aggregates. In Europe the Flakiness Index (FI) is determined using bar sieves of half the maximum size of definite aggregate size fractions (EN 933-3). The FI is the relative amount passing the bar sieves and is a measure for the percentage of oblong particles. The Shape Index (SI) determines the percentage of non-cubicle particles which are defined as the dimensional ratio of length and thickness ≤ 3 (EN933-4). As the SI is measured

Table 6.11 Example of cohesion test results

Source of RAP	A
Temperature 20 °C	
ITS at 25 °C (dry) (kPa)	N/A
ITS at 25 °C (wet) (kPa)	N/A
Air voids level	N/A
Source of RAP	A
Temperature 70 °C	
ITS at 25 °C (dry) (kPa)	389
ITS at 25 °C (wet) (kPa)	61
Air voids level	23.0
Source of RAP	A
Temperature 140 °C	
ITS at 25 °C (dry) (kPa)	811
ITS at 25 °C (wet) (kPa)	765
Air voids level	18.2

N/A: It was not possible to test the compacted specimens, as they fell apart during the demoulding process

on each particle visually and with the help of a particle slide gauge, only coarse aggregates >4 mm can be measured. In ASTM C1252-06, the particle index is calculated using the voids of differently compacted dry aggregate particles.

6.3.3.6 Analysis on Recovered Binder

After recovery of the extracted RAP-binder the following binder tests were carried out:

- Needle penetration (ASTM D5, EN 1426)
- Softening point (ring and ball method, ASTM D36, EN 1427)

These binder properties deliver a rough indication on the aging degree. However, for a proper assessment of the aging degree, the binder characteristics of the virgin binder are needed. This is in general not possible, as the RAP is a mixture of various asphalt types, each produced with different binder grades. Nevertheless, it is an important property in hot recycling to determine the grade of the binder to be added and/or the amount of rejuvenating agent needed to decrease the viscosity of the hardened binder.

6.3.3.7 Homogeneity of RAP

Verifying the homogeneity of RAP properties is an important step in quality control when designing asphalt mixtures containing recycled material; the higher the RAP

content in a mix, the higher the demands on the homogeneity of the RAP. Using non-homogeneous RAP will result in non-reproducible asphalt mix properties. A minimum of three different samples taken from the same RAP stockpile was used to assess the homogeneity of a RAP source.

6.4 Analysis and Comment of Round Robin's Test Results

6.4.1 Introduction

This chapter focuses on the presentation of the test results obtained from the RRT program performed on different sources of RAP. In the RRT, the following tests were carried out on each selected RAP collected from laboratories:

- RAP particle size on the material before bitumen extraction (black curve) and after extraction (white curve);
- RAP particles characterization (shape, texture, absorption and specific gravity);
- analysis of recovered binder (binder content, penetration and ring-and-ball test);
- fragmentation test;
- cohesion test.

6.4.2 RAP Particle Size on the Material Before (Black Curve) and Following (White Curve) Bitumen Extraction

Figure 6.9 shows the grading curves of all RAP tested in the RRT. As expected, after extraction, all percentage passing values of the white curves are moving upward, thereby indicating that a part of particles in the recycled material were "debulked". Except in the case of the RAP C, where the nominal maximum size of the particles is bigger (31.5 mm), the main impact on the grading curves became far more marked starting from the 2.5 and 5 mm sieves. Overall, after extraction, the percentage of RAP particles that completely passed right through the eighty-micron sieve was more than 10%.

6.4.3 RAP Particles Characterization

Four characteristics were evaluated on RAP particles: (1) shape-index, (2) flakiness index, (3) relative density and (4) absorption. The last two properties were evaluated separately for fine and coarse parts of the RAP aggregates.

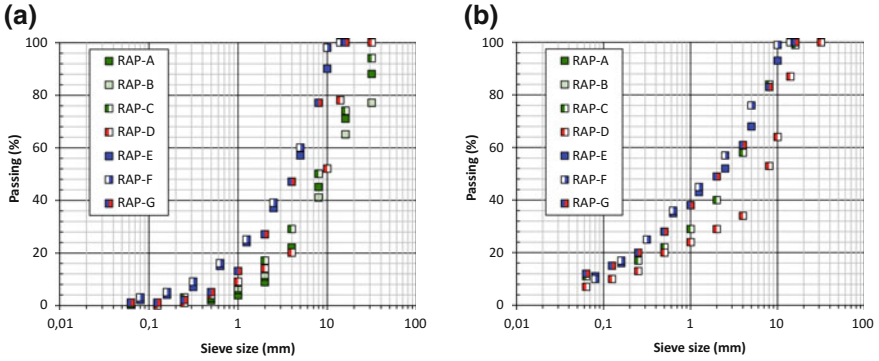

Fig. 6.9 **a** Black curve after washing and drying at 30 °C and, **b** white curve after washing and drying at 105 °C

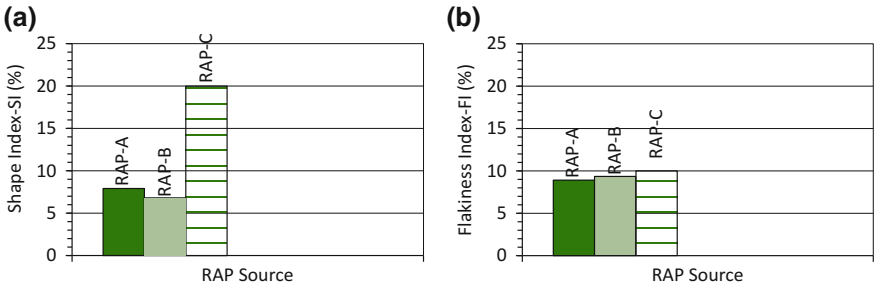

Fig. 6.10 **a** Shape index (SI) of RAP-A, RAP-B and RAP-C and **b** Flakiness Index (FI) of RAP-A, RAP-B and RAP-C

There have been few laboratories who have evaluated the shape index and flakiness index. Figure 6.10 shows the shape and the flakiness indexes of RAP-A, RAP-B and RAP-C. Furthermore, the values for the reference HMA supplied at each laboratory were 16 and 8% for the shape and the flakiness indexes respectively. Those values are typical for highway HMA mixes using 100% crushed aggregates. The milling process appears to have no significant effect.

Figure 6.11 shows the relative density (Oven Dried: OD) and the water absorption of tested RAP materials measured separately on the finer and the coarse fractions of the aggregates. The results are quite usual for aggregates used in HMA mixes.

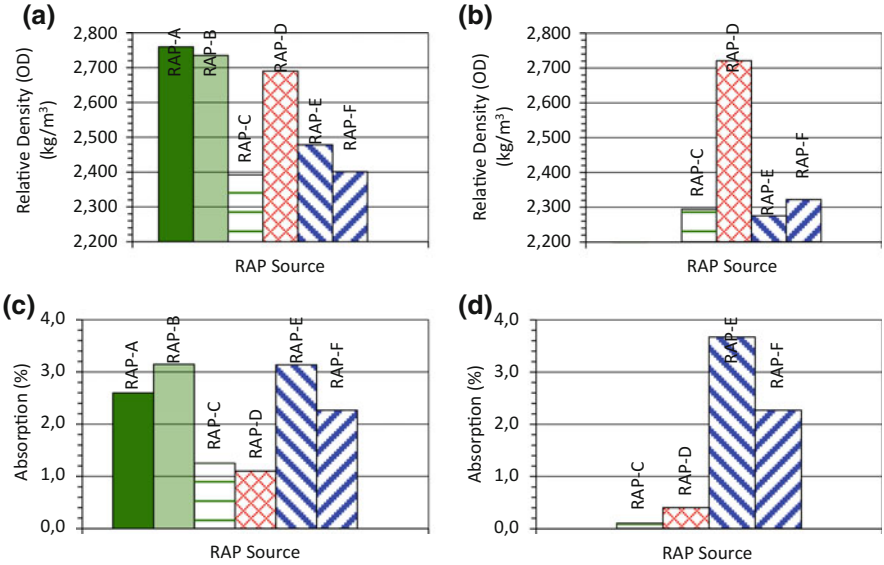

Fig. 6.11 **a** Relative density (OD) of coarse RAP aggregates, **b** relative density (OD) of fine RAP aggregates, **c** water absorption of the coarse RAP **d** water absorption of the fine RAP aggregates

6.4.4 Analysis of Recovered Binder

Properties of the recovered binder of the tested RAP samples are summarized in Table 6.12. The penetration index values of all tested RAP are quite low due to the aging effect. Although the tested RAP was randomly selected in different countries, we are surprised to note that the ranges of the Penetration (Pen) and the Temperature Ring and Ball (TR&B) values were quite narrow. Of course, it is fine if in the case where performances of recycled asphalt mixes with these RAP materials are equivalents. Nevertheless, if not, this suggests that the accuracy of such tests is precarious to be used to group RAP materials in the perspective to get recycled asphalt mixes with equivalent performances.

6.4.5 Fragmentation Test

As is well known, RAP can include aggregates covered by old bitumen and conglomerates of small aggregates glued together by mastic. These conglomerates can be broken during transportation and compaction phases. Since the grading curve influences the mixture performance, it is extremely important to keep under control the aggregate sizes and their distribution. The traditional methods used to classify RAP do not consider a quick, easy and effective test to provide reference values for the determination of the fragmentation resistance.

Table 6.12 Summary table of the main characteristics of the recovered binder of RAP materials

Lab.	A	
RAP	A	B
b (%)[a]	5.2	4.4
Pen (0.1 mm)	7	7
TR&B (°C)[b]	77	70
Lab.	B	
RAP	C	–
b (%)[a]	4.1	–
Pen (0.1 mm)	13	–
TR&B (°C)[b]	76	–
Lab.	C	
RAP	D	–
b (%)[a]	4.5	–
Pen (0.1 mm)	18	–
TR&B (°C)[b]	66	–
Lab.	D	
RAP	E	F
b (%)[a]	4.8	3.8
Pen (0.1 mm)	11	13
TR&B (°C)[b]	70	77

[a]b% = bitumen content—% parts by weight of the mixture
[b]TBA = temperature from the ring-and-ball test

In order to evaluate the capacity of the fragmentation test to characterize RAP from different sources, the RRT was performed by 5 laboratories located in 4 different countries.

The aim of the fragmentation test is to predict the reliability of the gradation of a granular mix taking in consideration the accidental changes caused by the breaking of RAP conglomerates. The test method is intended to fill a gap in the international standards for RAP characterization (Perraton et al. 2015; Tebaldi et al. 2014).

Four fraction classes were considered in this RRT: 20/30, 14/20, 10/14 and 5/10 mm. For each fraction, all RAP particles were completely retained on the smaller size sieve and passing through the larger size one. For each fraction, the mean particle size between two consecutive sieves was defined by the following relationship:

$$\text{mean particle size} = \sqrt{\text{size of the sieve}''\text{i}'' \times \text{size of the sieve}''\text{i}+1''} \qquad (6.1)$$

Figure 6.12 shows that the passing material through the control sieve (PCS) produced under fragmentation evolves differently according to the testing temperature: the PCS value decreases as the testing temperature increases, for all tested RAP sources. Moreover, with respect to the tested fraction classes, the PCS changes with the testing temperature according to the mean size of particles

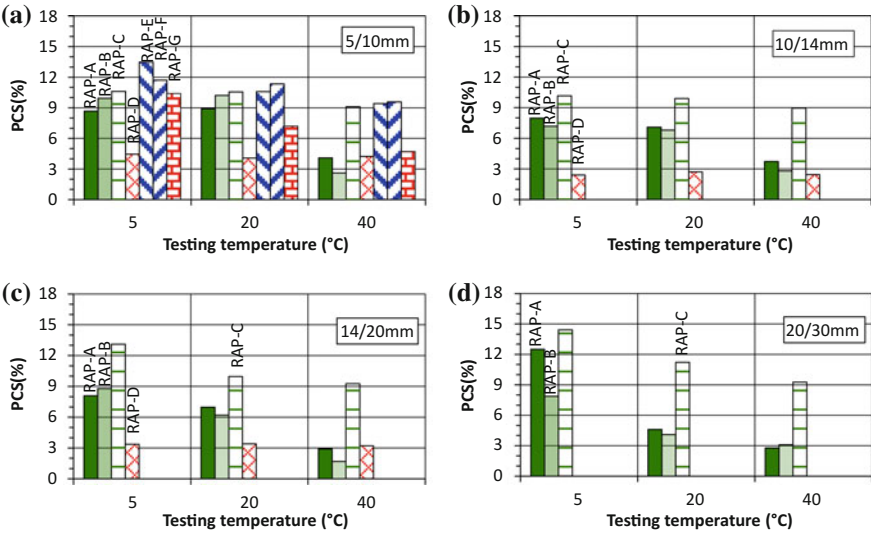

Fig. 6.12 Relationship between the percent passing through the control sieve (PCS (%)) and the fragmentation testing temperature on different RAP sources: **a** class 5/10 mm, **b** class 10/14 mm, **c** class 14/20 mm and, **d** class 20/30 mm

(Eq. 6.1). For a coarser fraction, the variation of the PCS with the temperature is more pronounced.

RAP particles containing a softer bitumen could agglomerate more easily under processing, and could significantly change the workability and the dynamic of the laying of the cold recycled material. This aspect could be more critical for recycling at elevated temperatures with foam bitumen. Moreover, agglomerate processes could also affect the coating quality of the binder system in cold recycling.

To get an overview of the overall trend of fragmentation results, the results presented in Fig. 6.12 could be plotted in the same graph by considering the mean particle size of tested fraction groups (Eq. 6.1). Figure 6.13 shows that the PCS values generally decrease as the mean particle size of RAP particles tested increases. Results show that the PCS values decrease as the mean particle size of RAP particles tested increases for groups smaller than the 20/30 mm.

The results could be used to figure out dispersion levels by calculating the Coefficient of Variation: CV% = (standard deviation/mean value) * 100%. Figure 6.14 shows the relationship between the CV values and the mean particle size of the fraction groups tested at different temperatures. CV is less than 21% although it changes with the tested particles size, and the higher the mean particle size, the greater the dispersion of the results. For the 5/10 mm, Fig. 6.14 shows that the CV is at a highly acceptable level (less than 11%). Furthermore, the results presented in Fig. 6.14 clearly show that the dispersion of the results is much lower for low temperature (5 °C) measurements compared to those obtained for high

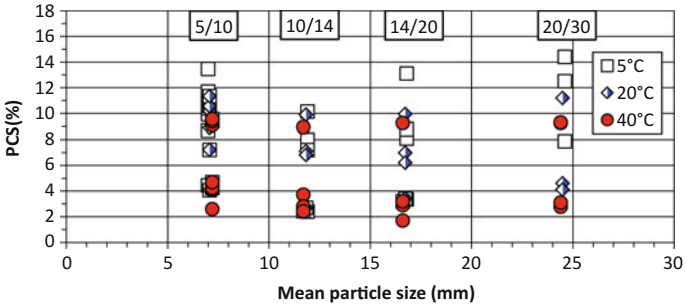

Fig. 6.13 Relationship between the percent passing through the control sieve (PCS (%)) and the mean particle size of fraction groups tested at different testing temperatures

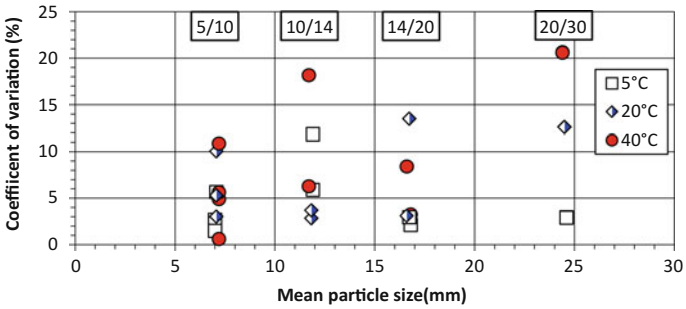

Fig. 6.14 Relationship between the coefficient of variation values (CV (%)) and the mean particle size of fraction group tested at different temperatures

temperature (40 °C) measurements. As previously, the fragmentation of RAP is more evident at low temperatures and could partly explain this observation.

6.4.5.1 Fragmentation Test Performed on Virgin Aggregates (VA)

Fragmentation tests were also performed, at different temperatures (5, 20 and 40 °C), on two typical Virgin Aggregates (VA) currently used as aggregate material in road construction. In this investigation, only the fraction group 5/10 mm was considered. The main characteristics of the tested aggregates are presented in Table 6.13. According to the NF 18-545 French standard, the VA-A and the VA-B are classified under categories B and D, respectively, for asphalt road applications.

The fragmentation test results on virgin aggregates are presented in Fig. 6.15. Results show that the PCS value does not change with respect to the temperature of the test. The behaviour is different between the two tested VAs. The PCS values are more significant for the VA-B than for the VA-A, and follow exactly the same trend as the one associated with the Los Angeles (LA) values of the aggregates.

Table 6.13 Main characteristics of tested aggregates

Properties					
Name	Type	G_b^1	Abs (%)[2]	LA (%)[3]	MDE[4]
VA-A	Basalt	2.812	0.5	12.3	11.6
VA-B	Limestone	2.681	1.3	30.0	15.5

NF 18-545 standard		
Name	Foundation and base layer (Art. 7)	Surface layer (Art. 8)
VA-A	B	A/B
VA-B	D	Not classified

[1]Specific gravity
[2]Water Absorption
[3]Los Angeles
[4]MicroDeval in water

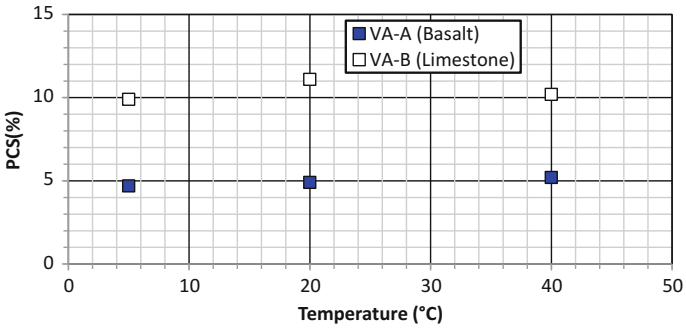

Fig. 6.15 Relationship between the percentage passing through the control sieve (PCS (%)) of fragmentation tests done on the 5/10 mm fraction group of two different sources of virgin aggregates (VA) and the testing temperature measurements

6.4.5.2 Classification Attempt from Fragmentation Test Results

One main goal of the RRT campaign was to explore the feasibility of classifying RAP materials based on different performance tests. To define a classification for any material, three different related aspects have to be considered: (1) the property to highlight; (2) the appropriate test method that must be referred to, and (3) how to set limits on categories. All these aspects depend on the intended use, and on how the material could change under production and implementation processes, as well as in its lifetime.

Based on the preceding statements, two issues were examined: (1) how the size of RAP particles could change under impacts, and (2) how RAP particles could agglomerate in its use.

6.4.5.3 Categorization of RAPs Based on Their Fragmentation Potential

To classify RAPs with respect to their susceptibility to undergo size changes while in use, the results are focused on fragmentation tests performed at 5 °C.

PCS values for virgin aggregates are not affected by the temperature at which the test was performed. Based on our fragmentation results, RAP sources can be classified by referring to the categories as defined in the NF EN 12620 European standard (B–E). Based on virgin aggregates fragmentation test results (VA-A and VA-B), PCS values of the 5/10 mm fraction are linked to the LA limit values of categories B to E, while assuming a linear relationship. As we can note in Fig. 6.16, we simply fixed the limit values of $PCS_{5\ °C\_5/10\ mm}$ (%) in phase with the upper LA limit values (B, C, D and E) as defined in the NF EN 12620 standard. Table 6.14 shows the different categories, limits, and the classification of the RAPs tested.

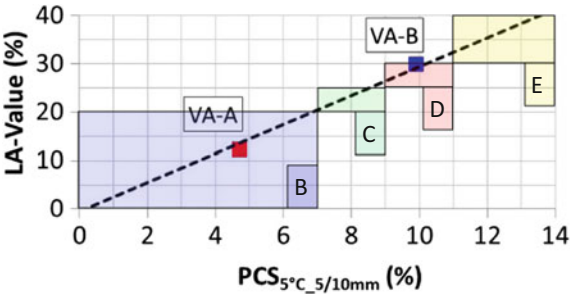

Fig. 6.16 Relationship between the LA-values of virgin aggregates and the percent passing through the control sieve (PCS (%)) of the 5/10 mm fraction group tested at 5 °C

Table 6.14 RAP categories and limits with respect to the vulnerability of RAP particles to change size while in use and the corresponding classification of RAPs tested

Categories	B	C	D	E
Limits on $PCS_{5\ °C\_5/10\ mm}$ (%)	≤ 7	≤ 9	≤ 11	≤ 14
Classification	RAP-D VA-A	RAP-A	RAP-B RAP-C RAP-G VA-B	RAP-E RAP-F

6.4.5.4 Categorization of RAPs Based on Their Agglomerate Potential

In the context of RAP recycling in cold mix applications, the interaction between RAP particles under processing could be affected by the bitumen phase of the RAP. RAP particles containing softer bitumen could agglomerate more easily under processing; they could significantly change the workability and the dynamic of the laying of the cold recycled material. This aspect could be more critical for recycling at elevated temperatures with foam bitumen. Moreover, agglomerate processes could also affect the coating quality of the binder system in cold recycling. To get a quick idea about the agglomeration potential of a RAP material, the feasibility of referring to the results of fragmentation tests performed at different temperatures was checked.

As pointed out previously, PCS values of RAPs change with the testing temperature. In first approximation, we can accept that this change will depend on the bitumen characteristic. Moreover, we noted that the PCS-T° relationship is almost nonexistent for VA tested. We thought to link the impact of RAP-source on the agglomeration potential of a RAP by referring to the slope of the PCS-T° relationship as expressed in Fig. 6.17.

To compare the slopes of the PCS-T° relationship from all data, RAP source results for each specific fraction group, were first normalized with respect to the PCS result obtained at 5 °C ($PCS_{STD\ to\ 5\ °C}$) as defined in Eq. (6.2). It should be noted that the PCS_5 °C value is typically the highest one in the testing temperature range. A standardized value of 1 means that the temperature does not affect the fragmentation results.

$$PCS_{STD\,to\,5\,°C} = \frac{PCS_{T°C}(\%)}{PCS_{T=5\,°C}(\%)} \tag{6.2}$$

As shown in Fig. 6.18a, for a given fraction group, a reduction of the standardized PCS values is observable when the temperature rises. This trend is typically observed for all normalized results of the tested RAP sources. In such cases, the reduction reveals a high thermal susceptibility of the material. By assuming a linear relationship, the thermal susceptibility can be associated with the slope value (s) of the $PCS_{STD\ to\ 5\ °C} - T°$ relationship. We did that with all results of the tested

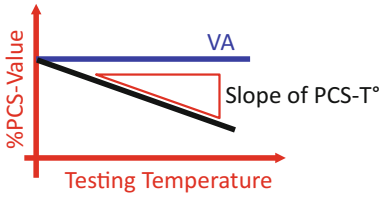

Fig. 6.17 Schematic representation of the relationship between the percent passing through the control sieve (PCS (%)) and the testing temperature

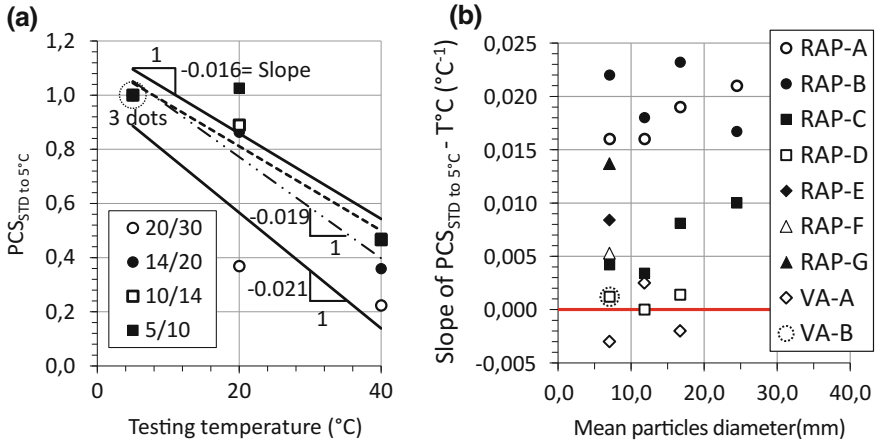

Fig. 6.18 Representation of the effect of the testing temperature on the potential RAP material fragmentation: **a** Example of relationships between the $PCS_{STD\ to\ 5\ °C}$ values and the testing temperature and, **b** relationship between the rate of change of $PCS_{STD\ to\ 5\ °C}$ with temperature and the mean size of tested RAP particles

Table 6.15 RAP categories and limits on with respect to the vulnerability of RAP particles to change size in its use and the corresponding classification of RAP tested

Categories	1	2	3	4
Absolute value of the rate of change of $PCS_{STD\ to\ 5\ °C}$ with temperature ($\times 10^3$) ($°C^{-1}$)	≤ 5	≤ 10	≤ 18	≤ 25
Classification	RAP-C RAP-D VA-A VA-B	RAP-E RAP-F	RAP-A RAP-G	RAP-B

RAP, and the overall results are presented in Fig. 6.18b with respect to the mean particle size of the tested fraction groups.

The categories and limits to classify the RAP source can be based on the slope value (s) of the $PCS_{STD\ to\ 5°} - T$ relationship, as presented in Table 6.15. The corresponding classification of the RAP material tested in this RRT is also reported in Table 6.15, considering results of the 5/10 mm fraction group.

The RAP categorization can also be referred to the RAP-bitumen content of the tested RAP (Fig. 6.19a) and with the penetration values (pen) of the recovery RAP-bitumen (Fig. 6.19b). As shown in Fig. 6.19a, a certain trend is observed, but the correlation is not highly significant. Nevertheless, if the RAP-G value is not considered, the correlation in that case becomes quite good, as shown in Fig. 6.19b (solid line).

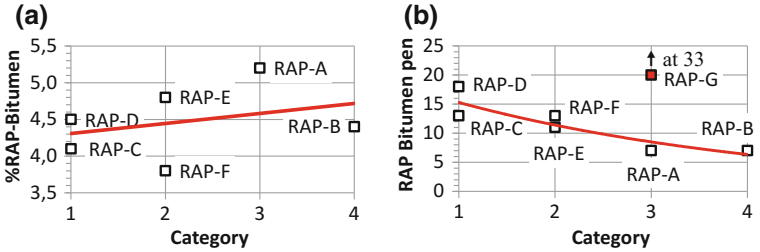

Fig. 6.19 Relationship between the RAP categorization and the asphaltic part of the RAP: **a** effect of the dosage of the bitumen on the RAP and, **b** effect of the penetration (Pen) measured on the recovery bitumen of the RAP

6.4.5.5 Conclusions

Results show that fragmentation is reduced when the testing temperature increases. Fragmentation tests performed on natural aggregates (VAs) indicate that they do not vary with the testing temperature. Regarding the testing temperature, fragmentation test results depend on the amount of foreign matter in the RAP. The results also from fragmentation test show that the test is suitable to differentiate RAP from different sources.

Based on results of the RRT program, we can conclude on the capability of the fragmentation test to characterize RAP material and to possibly classify RAP according to the source. RRT results clearly show that the fragmentation potential of RAP materials can successfully differentiate by referring to the fragmentation test.

6.4.6 Cohesion Test

The focus of this section is to present the use of ITS test method and results of the RRT performed on different sources of RAP. The purpose of the study was to develop a new, "simple" method of charactering RAP without having to recover binder and undertake rheological tests.

6.4.6.1 Evaluation of Indirect Tensile Strength Test to Characterize RAP

The ITS "cohesion test" protocol proposed by the researchers of the TG6 of RILEM TC 237-SIB, was designed with the idea of identifying a quick-to-obtain parameter of the RAP that could be measured directly in the field and within the time frame of the construction work plan. The goal was an easy-to perform test able

to provide a rapid classification of the RAP used by the contractor, to ensure that the RAP in the field has, within a certain level of tolerance, the same properties than the one used during laboratory mix design. With this RRT the TG6's researchers wanted to demonstrate that cohesion testing is able to identify whether RAP, coming from different sources but providing similar results when subjected to the "cohesion test", can be used indistinctively to manufacture asphalt mixtures with comparable properties.

To ascertain if the RAP could be classified as "active" or "inactive", a indicative test, was performed on 100% RAP samples by all the laboratories. This procedure has been expressed in Sect. 6.4.3. Six samples were manufactured for each of the three selected testing temperatures (20, 70 and 140 °C). Each group of 6 samples was separated into two sub-groups where one was tested in dry condition and the other one in wet condition. All the samples were subjected to ITS test at 25 °C, in accordance with EN 12697-23. If the tested specimen did not hold together at the testing time, or if the ITS value in the wet condition was less than 100 kPa at 70 °C, the RAP was considered to be inactive. As reported in Sect. 6.4.3, a series of samples was manufactured with RAP conditioned at 140 °C, assuming and proving, that the significant change in properties of the RAP, due to the melting of the bituminous binder layers, would make the RAP always active. Results are shown in Figs. 6.20, 6.21 and 6.22. They report the average ITS values and ratios obtained from three replicates at each laboratory. Being this type of tests greatly affected by the air voids content, the average value of each group of tested samples is reported in brackets in the graphs.

In most of the cases, RAP samples compacted at 20 °C did not hold. However, in all the other cases (Fig. 6.20), even in the dry conditions (Fig. 6.21), the values exceeded 100 kPa, indicating that the all RAP used in the studies can be classified as active.

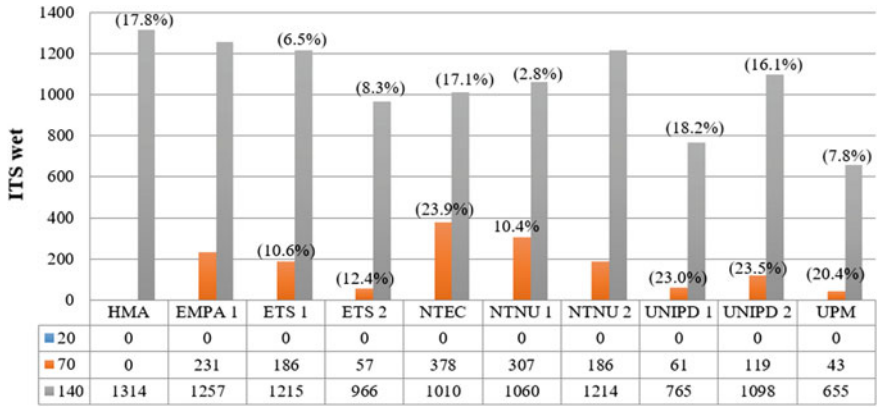

Fig. 6.20 Cohesion test results—WET condition (values in brackets express the average air voids content of a tested samples group)

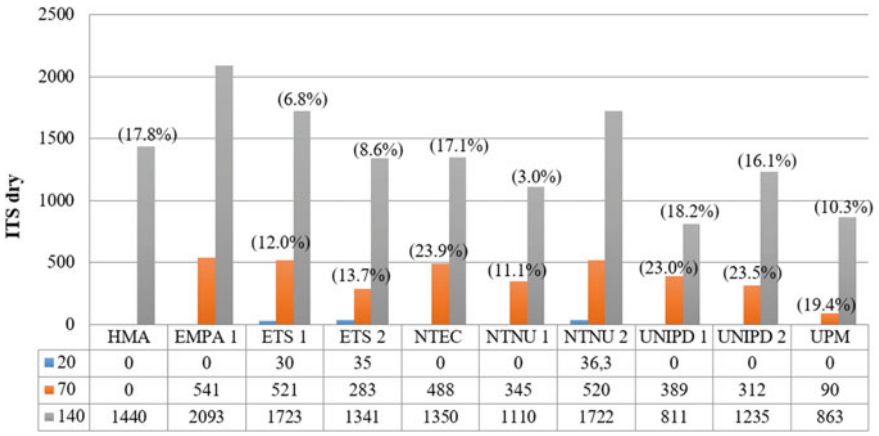

	HMA	EMPA 1	ETS 1	ETS 2	NTEC	NTNU 1	NTNU 2	UNIPD 1	UNIPD 2	UPM
20	0	0	30	35	0	0	36,3	0	0	0
70	0	541	521	283	488	345	520	389	312	90
140	1440	2093	1723	1341	1350	1110	1722	811	1235	863

Fig. 6.21 Cohesion test results—DRY condition (values in brackets express the average air voids content of a tested samples group)

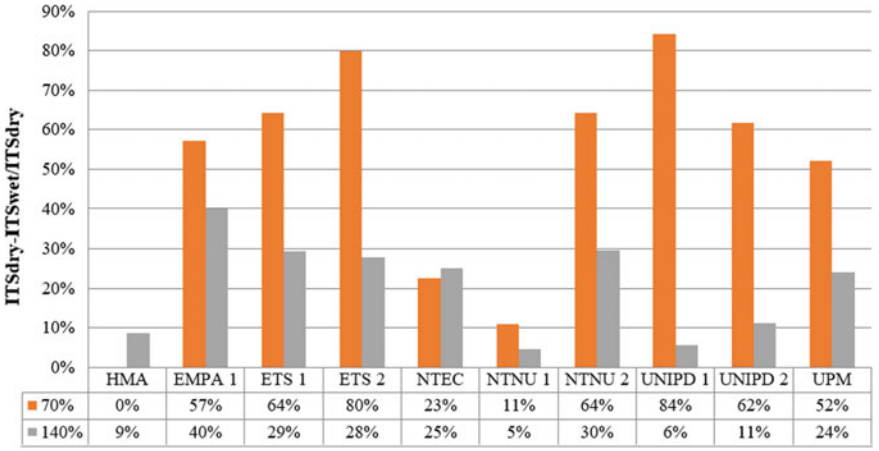

	HMA	EMPA 1	ETS 1	ETS 2	NTEC	NTNU 1	NTNU 2	UNIPD 1	UNIPD 2	UPM
70%	0%	57%	64%	80%	23%	11%	64%	84%	62%	52%
140%	9%	40%	29%	28%	25%	5%	30%	6%	11%	24%

Fig. 6.22 Reduction of ITS due to 24 h water soaking

It is also important to highlight that the reference HMA has an ITS_{wet} at 140 °C which is always higher than for several RAP materials (Fig. 6.20). However, this is not always true in dry condition (Fig. 6.21).

Results of cohesion test on 100% RAP samples vary a great deal after a water bath conditioning. The reduction in ITS due to the water bath conditioning is very pronounced at 70 °C, while in most cases differences tend to reduce drastically when specimens are compacted at 140 °C. Differences are less pronounced for hot mixes, but using a classification in wet condition might be important for half-warm mix applications.

6.4.6.2 Remarks

Results of this investigation demonstrate that the ITS cohesion test is quick, easy to perform and uses equipment that is widely used in laboratories and at asphalt plants.

Cohesion tests provide information on the latent adhesive properties of the RAP. This allows stating that this type of classification is particularly useful for RAP to be used at least in warm and hot mix application.

Comparative analysis between conventional properties of the recovered binder and results of the cohesion test shows that these properties are apparently not correlated. It is forecasted that a characterisation based on rheological and adhesive properties of the binders could provide more useful data.

6.4.6.3 Conclusions

Based on results of the RRT program, it can be affirmed that the ITS cohesion test is able to characterize and classify RAP material according to the source. RAP from different sources showed different results. This demonstrates the cohesion test is able to provide an easy-to-obtain parameter, that the differences between the different RAP.

Based on this experience it is possible to conclude that this test has the potential of being used to verify consistency between the RAP used for mix design in laboratories and for final mixing operations in the plants. However, further development and research is needed to interpret results and to identify absolute limits of ITS values, which will allow classifying the RAP and identify its most suitable final application.

6.5 Conclusion

All information presented in this chapter spanning across detailed literature and practice reviews, experimental procedures and round robin testing efforts are focused on identifying a characterization protocol for reclaimed asphalt on the basis of the most relevant standards and research work collected by TG6 around the world. The validation and verification of the protocol persued two fundamental goals:

(i) to have a tool simple enough to be efficiently used in the field;
(ii) to have a protocol able to identify if the reclaimed asphalt used in practice can be considered similar to the one used in the mix design.

At this point of the research work, it is still not possible to conclude on the effects of the properties measured in RAP characterization protocol regarding the properties and performance of mixtures made by such RAP. The most applicable outcome of the work presented herein is a practical method to practitioners for

determining if the RAP material is similar in nature to one used in design phase or not. Hence, the protocol can be used as a "warning tool" for the supervisor of work operations in context of material changes. To evaluate how the results provided by this characterization protocol (in particular the results provided by fragmentation test and cohesion test) are able to provide information on the performances of final mixtures, more research work is necessary. Ongoing and future Rilem TC work will address this issue by determining the suitability of properties measured in the RAP characterization protocol for use in asphalt mixture design processes. Further research is also needed to use the RAP protocol results for gaining insight into ability of RAP to contribute to mechanical and field performance properties of recycled asphalt mixtures.

Standard Test Procedures

Particle size distribution and binder content

- ASTM C136/C136M-14, Standard Test Method for Sieve Analysis of Fine and Coarse Aggregates, 2014.
- EN 933-1:2012 Tests for geometrical properties of aggregates—Part 1: Determination of particle size distribution—Sieving method
- EN 12697-1:2012 Bituminous mixtures—Test methods for hot mix asphalt—Part 1: Soluble binder content
- ASTM D6307-10 Standard Test Method for Asphalt Content of Hot-Mix Asphalt by Ignition Method, 2010.
- EN 12697-39:2012 Bituminous mixtures—Test methods for hot mix asphalt—Part 39: Binder content by ignition
- ASTM D2172/D2172M-11 Standard Test Methods for Quantitative Extraction of Bitumen From Bituminous Paving Mixtures, 2011.

Compaction methods

- ASTM D1557-12, Standard Test Methods for Laboratory Compaction Characteristics of Soil Using Modified Effort (56,000 ft-lbf/ft3 (2,700 kN-m/m^3)), 2012.
- EN 13286-2:2012 Unbound and hydraulically bound mixtures—Part 2: Test methods for laboratory reference density and water content—Proctor compaction.
- NF P18-574 Granulats—Essai de fragmentation dynamique, French Standard (withdrawn).
- ASTM D6925-15, Standard Test Method for Preparation and Determination of the Relative Density of Asphalt Mix Specimens by Means of the Superpave Gyratory Compactor, 2015.
- EN 12697-31:2007 Bituminous mixtures—Test methods for hot mix asphalt—Part 31: Specimen preparation by gyratory compactor.

- EN 12697-30:2007 Bituminous mixtures—Test methods for hot mix asphalt—Part 30: Specimen preparation by impact compactor.
- ASTM D6926-10 Standard Practice for Preparation of Bituminous Specimens Using Marshall Apparatus (2010).

Tests on compacted asphalt specimens

- EN 12697-23:2003 Bituminous Mixtures. Test Methods for Hot Mix Asphalt. Determination of the Indirect Tensile Strength of Bituminous Specimens, 2003.
- ASTM D6931-12 Standard Test Method for Indirect Tensile (IDT) Strength of Bituminous Mixtures (2012).

Tests on mineral aggregates

- ASTM C136/C136M-14 Standard Test Method for Sieve Analysis of Fine and Coarse Aggregates, 2014.
- ASTM C127-15, Standard Test Method for Relative Density (Specific Gravity) and Absorption of Coarse Aggregate, 2015.
- ASTM C128-15, Standard Test Method for Relative Density (Specific Gravity) and Absorption of Fine Aggregate, 2015.
- EN 1097-6:2013 Tests for mechanical and physical properties of aggregates—Part 6: Determination of particle density and water absorption.
- EN 1097-7:2008 Tests for mechanical and physical properties of aggregates—Part 7: Determination of the particle density of filler—Pyknometer method.
- EN 933-3:2012 Tests for Geometrical Properties of Aggregates. Determination of particle shape. Flakiness index.
- EN 933-4:2008 Tests for Geometrical Properties of Aggregates. Determination of particle shape. Shape index.
- ASTM C702/C702M-11, Standard Practice for Reducing Samples of Aggregate to Testing Size, 2011.
- ASTM D3398-00 (2006) Standard Test Method for Index of Aggregate Particle Shape and Texture (Withdrawn 2014 and replaced by ASTM C1252-06).
- ASTM C1252-06 Standard Test Methods for Uncompacted Void Content of Fine Aggregate (as Influenced by Particle Shape, Surface Texture, and Grading) (Withdrawn 2015 NOT REPLACED).

Binder tests

- ASTM D5/D5M-13 Standard Test Method for Penetration of Bituminous Materials, 2013.
- EN 1426: 2007 Bitumen and bituminous binders—Determination of needle penetration.
- EN 1427:2007 Bitumen and bituminous binders—Determination of the softening point—Ring and Ball method.
- ASTM D36/D36M-14e1 Standard Test Method for Softening Point of Bitumen (Ring-and-Ball Apparatus), 2014.

References

AASHTO AGC–ARTBA Joint Committee (1997) Task Force no. 38, Report of Cold Recycling of Asphalt Pavements. Interim Report

Asphalt Academy (2009) Technical guideline: bitumen stabilised materials. A guideline for the design and construction of bitumen emulsion and foamed bitumen stabilised materials, TG2, 2nd edn. CSIR

Austroads Technical Report AP-T188-11 (2011) Review of structural design procedures for foamed bitumen pavements. Austroads Ltd.

Bocci M, Grilli A, Cardone F, Graziani A (2011) A study on the mechanical behaviour of cement-bitumen treated materials. Int J Constr Build Mater 25(2):773–778. ISSN: 0950-0618

Charmot S (2006) Central plant cold mix. ARRA meeting, Palm Springs

Cold Bitumen Stabilized Base Courses (1999) Norwegian Public Roads Administration, Guidelines to Standard 018 Road Construction, Manual 198-e

Cold Recycling (2010) Wirtgen cold recycling technology, 3rd edn. Wirtgen GmBH

Construction Specification for Cold In-Place Recycling (2010) Ontario provincial standard specification OPSS 333

Cross SA, Kearney ER, Justus HG, Chesner WH (2010) Cold in-place recycling in New York State. Final Summary Report, SPR Research Project No. C-06-21, NYSERDA-TORC Contract No. 6764F-2, New York State Department of Transportation, Albany, NY, July 2010, 248 p

CSIR Transportek (1998) Foamed asphalt mixes mix design procedure. CR-98/077, CSIR Transportek, Pretoria, South Africa

Dave EV (2011) Cold recycling of asphalt concrete: review of North American state of practice, RILEM TC-SIB: TG-6, Liverpool

De Bock L et al. Best Practise guide for the dismantling and recycling of other materials not commonly recycled in roads. DIRECT-MAT (DIsmantling and RECycling Techniques for road MATerials—sharing knowledge and practices)

Decker DS, Young TY (1996) Handling RAP in an HMA facility. In: Proceedings of the Canadian technical asphalt association, Edmonton, Alberta

Duval J (2008) Engineered emulsion cold in-place recycling. NW Pavement Management Association, Spring Conference, Richland, Washington, 9 Mar

EN 13108-8 (2005) Bituminous mixtures—material specifications—Part 8: reclaimed asphalt

EN 932-1 (1996) Tests for general properties of aggregates—Part 1: methods for sampling

Engineering Service Center (2005) Lab. Procedure no. 8, Method of test for determining the percent of emulsified recycling agent to use for cold recycling for asphalt concrete, State of California DoT, Business, Transportation and Housing Agency

Epps JA (1990) Cold-recycled bituminous concrete using bituminous materials. NCHRP Synthesis of Highway Practice 160. University of Nevada-Reno

Gray JE (1962) Characteristics of graded base course aggregates determined by triaxial tests. National Crushed Stone Association, Engineering Bulletin No. 12, National Crushed Stone Association, Washington, D.C.

Hefer AO, Scullion T (2002) Materials, specifications, and construction techniques for heavy duty flexible bases: literature review and status report on experimental sections. Texas Transportation Institute, The Texas A&M University System, College Station, Texas (Report 0-4358-1), October, 2002 (Resubmitted: July 2005)

Jahren CT, Ellsworth BJ, Cawley B, Bergeson K (1998) Review of cold in-place recycled asphalt concrete projects. Department of Civil and Construction Engineering lowa State University, lowa DOT Project HR-392, lowa Department of Transportation

Jones D, Fu P, Harvey JT (2009) Full-depth pavement reclamation with foamed asphalt in California: guidelines for project selection, design and construction, UCPRC-GL-2008-01, University of California Pavement Research Center Davis and Berkeley

Kleyn EG (1984) Aspects of pavement evaluation and design as determined with the aid of the dynamic cone penetrometer. M.Ing. Theses (in Afrikaans), Department of Civil Engineering, University of Pretoria, Pretoria

Maccarrone S, Holleran G, Leonard DJ, Dip SH (1994) Pavement recycling using foamed bitumen. In: 17th Australian road research board conference, Part 3, pp 349–365

Maintenance Technical Advisory Guide (MTAG) (2008) Volume I—flexible pavement preservation second edition. Chapter 13—In-place recycling, California department of Transportation (CALTRANS)

Mohammad LN, Abu-Farsakh MY,Wu Z, Abadie C (2003) Louisiana experience with foamed recycled asphalt pavement base materials. Transp Res Rec J Transp Res Board (1832):17–24

Murphy DT, Emery JJ (1996) Modified cold in-place asphalt recycling. Transp Res Rec 1545 (Ontario, Canada)

National Center for Asphalt Technology (1998) Alabama University, Alabama US DoT, FHWA and Office of Technology Application, Review of Pavement Recycling Guidelines for State and Local Governments, Washington D.C.

New York State DoT (2010) Item 405.02010004—Cold in-place Recycling Asphalt Concrete

Pavement recycling guidelines for state and local governments (1997) Chapter 14 cold-mix design asphalt recycling (material and mix design), Federal Highway Administration, FHWA-SA-98-042

Perraton D, Tebaldi G, Dave E, Bilodeau F, Giacomello G, Grilli A, Graziani A, Bocci M, Grenfell J, Muraya P, Pasetto M, Kuna K, Apeagyei A, Lo Presti D, Airey G, Jenkins K, Hajj E, Hugener M, Marsac P (2015) Tests campaign analysis to evaluate the capability of fragmentation test to characterize recycled asphalt pavement (RAP) material. In: 8th international RILEM symposium on testing and characterization of sustainable & innovative bituminous materials, Ancona, Italy, 7–9 Oct 2015

Queensland Department of Main Roads (2009) Pavement design manual. Supplement to Part 2, Pavement Structural Design of the Austroads Guide to Pavement Technology, Brisbane, Qld.

Ramanujam JM, Jones JD (2000) Characterisation of foamed bitumen stabilization. Road Sys Eng Technol Forum, pp 1–22

RAW 2010 (2011) Standaard RAW Bepalingen 2010, CROW—het nationale kennisplatform voor infrastructuur, verkeer, vervoer en openbare ruimte, 1264 p

"Reclaimed Asphalt Pavement: User Guideline", User guidelines for byproducts and secondary use of materials in pavement construction. Recycled Materials Resource Center, University of New Hampshire, website: http://www.rmrc.unh.edu/tools/uguidelines/rap133.asp

Recycling and reclamation of asphalt pavements using in-place methods—a synthesis of highway practice. NCHRP Synthesis 421, Transportation research board (2011)

Rogge DF et al (1992) Use of asphalt emulsions for in-place recycling: Oregon experience. Transportation research record 1342, TRB, National Research Council, Washington, D.C.

Saleh M (2004) Detailed experimental investigation for foamed bitumen stabilization, Transfund New Zealand Research Report, No. 258

Saleh MF, Herrington P (2003) Foamed bitumen stabilisation for New Zealand roads, Transfund New Zealand Research Report No. 250, p 88,

Santucci L (2007) Recycling asphalt pavements—a strategy revisited. Tech Topic no. 8, Technology Transfer Program, Institute of Transportation Studies, University of California Berkeley

Scholz T, Hicks RG, Allen D (1990) Mix-design practices for cold in-place recycled pavements. Asphalt Emulsions, ASTM STP 1079, Muncy ed. Philadelphia, pp 44–64

Standard Specifications for Highway and Bridge Construction (2011) Asphalt Emulsions, Minnesota Department of Transportation (MnDOT)

Tario JD, Rossi MA, Cross SA, Kearney ER, Justus HG, Chesner WH (2010) Cold in-place recycling in New York state. Final Summary Report, Contract No. 6764F-2, The NewYork State Energy Research and Development Authority, The New York State DoT, Chesner Engineering P.C. 2010

TC 237-SIB (2010) Testing and characterization of sustainable innovative bituminous materials and systems

Tebaldi G, Dave EV, Marsac P, Muraya P, Hugener M, Pasetto M, Graziani A, Grilli A, Bocci M, Marradi A, Wendling L, Gaudefroy V, Jenkins K, Loizos A, Canestrari F (2014) Synthesis of standards and procedures for specimen preparation and in-field evaluation of cold-recycled asphalt mixtures. Int J Road Mater Pavement Des 15(2):272–299

Thompson MR, Garcia L, Carpenter SH (2009) Cold in-place recycling and full-depth recycling with asphalt products (CIR&FDRWAP). Illinois Center for Transportation, University of Illinois, Research Report ICT-09-036

Index

M. N. Partl et al. (eds.), *Testing and Characterization of Sustainable Innovative Bituminous Materials and Systems*, RILEM State-of-the-Art Reports 24,
https://doi.org/10.1007/978-3-319-71023-5